Interactions of Ethylene Oxide-Propylene Oxide Block Copolymers with Lipid Bilayers

A DISSERTATION

SUBMITTED TO THE FACULTY OF

UNIVERSITY OF MINNESOTA

BY

Wenjia Zhang

IN PARTIAL FULFILLMENT OF THE REQUIREMENTS

FOR THE DEGREE OF

DOCTOR OF PHILOSOPHY

Advisors: Frank S. Bates, Timothy P. Lodge

August 2019

Acknowledgment

I would like to first thank Prof. Frank Bates and Prof. Timothy Lodge for their continuous guidance and support in the last 5 years. I was very impressed by their enthusiasm and vast and deep knowledge in polymer science when I first met with them, which aroused my curiosity in polymers and drove me to join their groups. Working with them over the past 5 years further made me believe that it is one of the best decisions I ever made so far. They gave me a lot of freedom that allowed me to explore what I am interested in at my own pace. At the meantime, they are highly approachable and responsive; they constantly gave me inspirational and forward-looking suggestions and provided many useful resources when I feel confused and frustrated by my research. Without them, the journey and the dissertation about my doctoral work would not have been possible. Besides research, I am very grateful for their positive impact on my personal growth. Their high standards have challenged me to hone my critical thinking ability and professional communication skills. My character was also influenced and reshaped by their diligence, perseverance, and conscientiousness at work. Additionally, I would like to thank my undergraduate research advisor Prof. Michael Solomon and undergraduate supervisor Dr. Susan Montgomery. Without their support and encouragement, I would not have decided to pursue a PhD degree.

It has been a pleasure to work on an interdisciplinary and collaborative project during graduate school, which gave me a chance to interact with so many talented professors, postdoctoral researchers, and graduate students with different backgrounds. Especially, I

would like to thank Prof. Joseph Metzger, Prof. Joseph Zasadzinski, Prof. Benjamin Hackel, Prof. Samira Azarin, Prof. Yuk Sham, Prof. DeWayne Townsend, Prof. Demetri Yannopoulos, and Prof. Jason Bartos for informative discussions and suggestions on this project. Dr. Mihee Kim and Hannah Seo have been close collaborators. I really enjoy and appreciate all the detailed conversations we had about our research, which always inspired me with new ideas. Also, our trips to the national lab to do neutron reflectivity experiments are memorable as we built our camaraderie by overcoming so many unexpected difficulties. Dr. Karen Haman and Dr. Evelyne Houang have been very helpful when I first joined this project. They never lost patience when answering my naive questions or teaching me to do some simple experiments. I am also glad to have the opportunity to work with younger graduate students Joseph Hassler and Adelyn Crabtree, who will continue the exciting work on this project.

I am thankful for National Institutes of Health (NIH) to fund this project and provide the opportunity for researchers with diversified expertise to collaborate across disciplines. Also, I would like to thank Dr. Letitia Yao at the NMR lab in the Department of Chemistry and Dr. Bing Luo at the Characterization Facility for their tremendous help with NMR and Raman spectroscopy, respectively. I would not be able to get access to these instruments and obtain high-quality data without all the training and troubleshooting during the experiments provided by these two dedicated scientists. Additionally, I went to National Institute of Standards and Technology (NIST) a few times during graduate school to do neutron experiments. I would like to thank Dr. Yimin Mao for his help with neutron

scattering experiments and Dr. Sushil Satija, Dr. Guangcui Yuan, and Dr. Frank Heinrich for neutron reflectivity experiments.

It has been an unforgettable experience to work in the Bates and Lodge groups with so many awesome coworkers and friends who are always willing to help. The collaborative culture in both groups promotes many insightful discussions. In particular, I would like to thank Dr. Karen Haman for getting me started in the lab; Dr. Tuoqi Li for teaching me to do the anionic polymerization; Dr. Mihee Kim for teaching me to do neutron experiments; McKenzie Coughlin for doing the cryo-TEM. Also, many thanks to Prof. Jennifer Laaser, Prof. Robert Hickey, Dr. Ralm Ricarte, Dr. Soonyong So, Dr. Yuanchi Ma, Dr. Boxin Tang, Dr. Yiming Zeng, Dr. Amanda Maxwell, Dr. Seyoung Jung, Dr. Yaming Jiang, Dr. Sujay Chopade, Dr. Jun Xu, Dr. Qile Chen, Dr. Cecilia Hall, Dr. Peter Schmidt, Dr. Dan Zhao, Dr. Svetlana Morozova, Dr. Piril Ertem, Dr. Jimin Shim, Dr. Jiuyang Zhang, Itaru Asano, Aakriti Kharel, En Wang, Ingrid Haugan, Shuyi Xie, Hannah Seo, Julia Early and many others for helpful discussions.

In addition, I am very grateful to my classmates. We have worked together to slog through coursework, pass the preliminary exam, find jobs, and prepare for graduation, which makes me feel I am not alone. In particular Huaiyu Yan, Hui-Min Chuang, Pin-Kuang Lai, Hwanhui Yun, En Wang, Aakriti Kharel, and many more to name – I am lucky to have met these friends in my class and I wish our friendship can last lifelong. Also, I would like to thank all the faculty members and staffs especially Julie Prince and Teresa Bredahl who have dedicated to make CEMS such a wonderful department and made me so proud to be a CEMSer.

In the end, none of my accomplishments in graduate school would be possible without the unconditional love, support, and sacrifice from my parents and my grandparents. They have prepared me into who I am today. Also, I must thank my husband Ziang Li, who has always been my biggest fan. He shares my joy when I am high and picks me up when I am low. I am so grateful that graduate school made us meet each other, and I look forward to a lifetime of understanding, respecting, and supporting each other and making each other a better person.

Dedication

To my husband, Ziang, and my parents, Huanran and Ying.

Abstract

Nonionic poly(propylene oxide)-*b*-poly(ethylene oxide) (PPO-PEO) block copolymers, known as Pluronics or poloxamers, have been widely studied for their great potential in cell membrane stabilization and permeabilization due to their amphiphilicity and biocompatibility. A hydrophilic dominant commercial poloxamer P188 shows a reasonable stabilization effect *in vivo* on dystrophic muscle cell membranes. Despite recent advances made in this field, the structure-function relationships and the underlying mechanism of polymer protection are not fully understood. The goals of this dissertation are to understand the fundamental mechanism of polymer-membrane association and to further design effective polymers to improve the therapeutic approach of cell membrane stabilization for Duchenne muscular dystrophy. Herein, we developed a simple yet powerful method that enables the quantification of the relatively weak interactions between the copolymers and vesicular lipid bilayers based on distinct diffusivity of free and bound polymers, using pulsed-field-gradient NMR (PFG-NMR). This is the first quantitative study that systematically investigated polymer binding to lipid membranes in the literature to our knowledge, which provides direct evidence regarding how polymer structure and membrane composition and curvature dictate their interactions. With lab-synthesized PPO-PEO diblock analogs as complements to the commercial triblock poloxamers, we found that polymers with larger molecular weight and higher hydrophobicity result in stronger polymer-membrane association. Also, the lipid bilayer composition plays a critical role. Notably, polymer binding drops 10-fold in a universal fashion as cholesterol concentration in the bilayer increases from 0 to 30 mol.%. Switching the lipid headgroup from choline to glycerol significantly enhanced polymer binding. Additionally, polymer protection efficacy on liposomes against induced lipid peroxidation was assessed and compared with their stabilization efficacy *in vitro* and *in vivo*.

Table of Contents

Acknowledgment i

Dedication v

Abstract vi

List of Tables xii

List of Figures xiv

Chapter 1 - Introduction 1

1.1 Overview of Poloxamers 1

1.1.1 Physical Properties 4

1.1.2 Micellization and Phase Behavior 7

1.1.3 Applications 12

1.2 Diblock Analogs to Poloxamers 15

1.2.1 Hydrophilic-Hydrophobic Balance 16

1.2.2. Overall Molecular Weight 19

1.3 Membranes 20

1.3.1 Cell Membranes 20

1.3.2 Lipid Monolayer Model Membranes 21

1.3.3 Lipid Bilayer Model Membranes 22

1.4 Development of the Mechanism of Polymer-Membrane Association 26

1.5 Overview of Thesis 34

Chapter 2 - Experimental Techniques 38

2.1 Polymer Synthesis 39
2.2 Polymer Characterization 41
2.3 Liposome Preparation 45
2.4. Liposome Characterization 47
2.4.1. Dynamic Light Scattering (DLS) 47
2.4.2 Cryogenic Transmission Electron Microscopy (Cryo-TEM) 49
2.4.3 Small-Angle Neutron Scattering (SANS) 50
2.5 Quantification of Polymer Binding 52
2.6 Screening of the Stabilization Efficacy of Block Copolymers 56
2.6.1 Liposome Peroxidation as a Model Stress 56
2.6.2 Polymer Stabilization Efficacy on Liposomes against Lipid Peroxidation 58
Chapter 3 - Influence of Polymer Structure on Polymer-Membrane Association 61
3.1 Introduction 61
3.2 Experimental Section 63
3.2.1 Materials 63
3.2.2 Polymer Synthesis and Characterization 64
3.2.3 Liposome Preparation and Characterization 64
3.2.4 PFG-NMR Measurements 65
3.3 Results and Discussion 65
3.3.1 Effect of Polymer Molecular Weight 74
3.3.2 Effect of Composition 78

3.3.3 Effect of Polymer Concentration 87
3.4 Conclusions 93
Chapter 4 - Influence of Cholesterol and Bilayer Curvature on Polymer-Membrane Association 94
4.1 Introduction 94
4.2 Experimental Section 97
4.2.1 Materials 97
4.2.2 Polymer Synthesis and Characterization 98
4.2.3 Liposome Preparation and Characterization 98
4.2.4 PFG-NMR Measurements 99
4.2.5 Cryogenic Transmission Electron Microscopy (cryo-TEM) 100
4.3 Results and Discussion 100
4.3.1 Liposome Size Characterization 100
4.3.2 Effect of Cholesterol 105
4.3.3 Bilayer Curvature Effect 116
4.4 Conclusions 125
Chapter 5 - Influence of Lipid Composition on Polymer-Membrane Association 127
5.1 Introduction 127
5.2 Experimental Section 130
5.2.1 Materials 130
5.2.2 Polymer Synthesis and Characterization 131

5.2.3 Liposome Preparation and Characterization 131
5.2.4 PFG-NMR Measurements 131
5.2.5 Raman Spectroscopy 132
5.3 Results and Discussion 132
5.3.1 Effect of Lipid Headgroup 132
5.3.2 Effect of the Degree of Unsaturation of Lipid Alkyl Chains 149
5.4 Conclusions 153
Chapter 6 - Screening of the Stabilization Efficacy of Block Copolymers 155
6.1 Introduction 155
6.2 Experimental Section 158
6.2.1 Materials 159
6.2.2 Polymer Synthesis and Characterization 159
6.2.3 Liposome Preparation 160
6.2.4 Polymer Stabilization Efficacy Measurement 160
6.3 Results and Discussion 161
6.3.1 The Effect of Polymer Architecture 166
6.3.2 The Effect of Relative Hydrophobic-Hydrophilic Composition 167
6.3.3 The Effect of Polymer Endgroup 169
6.3.4 The Effect of Polymer Molecular Weight 170
6.4 Conclusions 179
Chapter 7 - Bottlebrush Polymers 180

7.1 Introduction 180
7.2. Experimental Section 182
7.2.1 Polymer Synthesis 182
7.2.2 Polymer Characterization 184
7.3 Results and Discussion 189
7.3.1 POEGMA 189
7.3.2 POPGMA-*b*-POEGMA 195
7.4 Conclusions 198
Chapter 8 – Conclusions and Outlook 199
8.1 Project Summary 199
8.2 Project Outlook 203
8.2.1. Variation of Polymer Architecture, Structure, and Chemistry 204
8.2.2 Mechanistic Investigation of Polymer-Membrane Association 205
Bibliography 209

List of Tables

Table 1.1. Physical properties of Pluronics. 6

Table 2.1. Polymer characterization. 44

Table 2.2. Core radius and shell thickness of vesicular lipid bilayer. 52

Table 3.1. Summary of fitting results and related parameters. 67

Table 3.2. Summary of calculated radius of gyration of polymers. 71

Table 3.3. Summary of fitting results of 0.2 mg/mL P103, P104, P105 and F108 after no incubation and after 1-week incubation with liposomes at room temperature. 72

Table 3.4. Summary of fitting results of 3 replicates of 1 mg/mL P105 in 5 mM POPC liposome solution in D_2O at 27 °C. 73

Table 3.5. Summary of fitting results with corresponding errors by Kärger model. 82

Table 4.1. Liposome size characterization in D_2O by DLS. 103

Table 4.2. Summary of liposome radii and the percentage of liposome surface area within multilamellar liposomes measured from cryo-TEM. 104

Table 4.3. Summary of polymer binding to 5 mM POPC/cholesterol liposomes extruded through a polycarbonate membrane with 50 nm pore radius in D_2O at 27 °C at different cholesterol molar percentages. 107

Table 4.4. Summary of polymer binding to 5 mM POPC liposomes with different curvature in D_2O at 27 °C. 118

Table 4.5. Binding of F127 to 5 mM POPC/cholesterol liposomes extruded through a polycarbonate membrane with 25 nm pore radius in D_2O at 27 °C. 121

Table 4.6. Fitting results of the decay parameter *A*. 124

Table 5.1. Liposome size characterization by DLS. 133

Table 5.2. Summary of polymer binding to 5mM POPC liposomes in D_2O, to POPC liposomes in 150 mM NaCl D_2O solution, and to POPG liposomes in 150 mM NaCl D_2O solution at 27 °C. 138

Table 5.3. Summary of polymer binding of 0.2 mg/mL F127 to 5mM POPC/POPG liposomes at various POPG molar percentage in the lipid bilayer in 150 mM NaCl D_2O solution at 27 °C. 142

Table 5.4. Summary of binding of 1 mg/mL F108 to 5 mM POPG liposomes in different salt solutions..... 148

Table 5.5. Summary of polymer binding to 5mM POPC liposomes and to 5 mM POPG liposomes in D_2O at 27 °C. 151

Table 5.6. Summary of polymer binding of 0.2 mg/mL F127 to 5mM DPPC liposomes in D_2O at 27 °C. 153

Table 6.1. Summary of the commercial triblock and diblock polymers. 160

Table 6.2. R_h with dispersity of the liposomes with polymers before and after peroxidation. 163

Table 6.3. R_h with dispersity of liposomes with poloxamers before and after peroxidation. 174

Table 6.4. R_h with dispersity of the liposomes with P188 before and after peroxidation. 177

Table 7.1. Polymer characterization..... 186

Table 7.2. Summary of polymer binding with uncertainty and the diffusion coefficients used for fitting..... 192

List of Figures

Figure 1.1. Chemical structures of various PPO-PEO triblock and diblock copolymers .. 4

Figure 1.2. CMC of Pluronics. 10

Figure 1.3. DSC curves of various poloxamers in water (1% w/v) 11

Figure 1.4. Schematic of dystrophin that connects the cell membrane to actin. 13

Figure 1.5. (a) Surface pressure — area per lipid isotherms of poloxamer P338 with DPPC monolayers. 27

Figure 1.6. Schematic of different mechanisms of polymer-lipid bilayer association 30

Figure 1.7. Schematic of a two-state transition mechanism of the interactions between P181 and lipid bilayers 32

Figure 2.1. (a) Synthetic scheme of PPO-PEO diblock polymers. 41

Figure 2.2. Three side reactions during the anionic polymerization of PPO. 41

Figure 2.3. MALDI spectra and SEC traces of F68 and F127 43

Figure 2.4. Chemical structures of various components in lipid bilayers 46

Figure 2.5. Liposome characterization by DLS. 48

Figure 2.6. Cryo-TEM images of 10 mM POPC liposomes in D_2O extruded through a polycarbonate membrane with 50 nm pore radius. 50

Figure 2.7. Liposome characterization by SANS 51

Figure 2.8. ^1H NMR spectrum of 1 mg/mL P105 in 5 mM POPC liposome in D_2O. 54

Figure 2.9. Experimental and fitted echo decay curves of 1 mg/mL P105 in the presence of 5 mM POPC liposome in D_2O at 27 °C 56

Figure 2.10. Lipid peroxidation reactions 57

Figure 2.11. Experimental schematic of measuring polymer stabilization efficacy in a liposome peroxidation assay. 59

Figure 3.1. Schematic of interactions between block copolymers and liposomes..... 63

Figure 3.2. Experimental and fitted echo decay curves of the protons from the choline group of 5 mM POPC liposome solution in D_2O at 27 °C 66

Figure 3.3. Characterization of the diffusivity of 1 mg/mL F127 in D_2O at 27 °C by PFG-NMR and DLS 68

Figure 3.4. Experimental and fitted echo decay curves of 1 mg/mL P105 in 5 mM POPC liposome solution in D_2O at 27 °C and the corresponding schematic of surface coverage of a half liposome 70

Figure 3.5. Experimental and fitted echo decay curves of H_2O in the presence of 5 mM POPC liposome and 5 mM POPC liposome plus 1 mg/mL P105 in D_2O at 27 °C..... 73

Figure 3.6. Experimental and fitted echo decay curves of 1 mg/mL F127, F87, F108, F68, and PEO-8 in 5 mM POPC liposome solution in D_2O at 27 °C 76

Figure 3.7. Experimental and fitted echo decay curves of 1 mg/mL P65, L35, P104, and P84 in 5 mM POPC liposome solution in D_2O at 27 °C..... 77

Figure 3.8. Experimental and fitted echo decay curves of 0.2 mg/mL P103, P104, P105, and F108 in 5 mM POPC liposome solution in D_2O at 27 °C..... 80

Figure 3.9. Simulations of the Kärger model..... 83

Figure 3.10. Experimental and fitted echo decay curves of 1 mg/mL $tPPO_{14}$-PEO_{46}, $tPPO_{14}$-PEO_{78}, and $tPPO_{14}$-PEO_{159} in 5 mM POPC liposome solution in D_2O at 27 °C . 85

Figure 3.11. Experimental and fitted echo decay curves of 1 mg/mL $tPPO_{29}$-PEO_{68} and $tPPO_{14}$-PEO_{78} in 5 mM POPC liposome solution in D_2O at 27 °C 86

Figure 3.12. Experimental and fitted echo decay curves of 1 mg/mL $hPPO_{13}$-PEO_{43}m and $tPPO_{14}$-PEO_{46} in 5 mM POPC liposome solution in D_2O at 27 °C 87

Figure 3.13. Fraction of liposome surface area covered by polymer molecules as a function of polymer concentration of F127..... 88

Figure 3.14. Experimental and fitted echo decay curves of F127 at various concentrations in 5 mM POPC liposome solution in D_2O at 27 °C 89
Figure 3.15. Summary of polymer molecular weight, block length, endgroup and concentration effect on the interactions between polymer and liposome 92
Figure 3.16. Binding percentage as a function of the number of repeat units of PO in the polymer 92
Figure 4.1. Schematic of manipulating bilayer curvature by varying the liposome size . 99
Figure 4.2. Cryo-TEM images of 10 mM liposomes with various cholesterol concentration and the corresponding histograms of liposome radius. 104
Figure 4.3. Experimental and fitted echo decay curves of 0.2 mg/mL F127 in the presence of 5 mM POPC liposome in D_2O at 27 °C. 108
Figure 4.4. Experimental and fitted echo decay curves of 0.2 mg/mL F127 in the presence of 5 mM POPC/cholesterol liposome solution in D_2O at 27 °C. 109
Figure 4.5. Experimental and fitted echo decay curves of 0.2 mg/mL P103 in the presence of 5 mM POPC/cholesterol liposome solution in D_2O at 27 °C 110
Figure 4.6. Experimental and fitted echo decay curves of 1 mg/mL *t*PPO_{14}-PEO_{46} in the presence of 5 mM POPC/cholesterol liposome solution in D_2O at 27 °C. 111
Figure 4.7. Experimental and fitted echo decay curves of 1 mg/mL F68 in the presence of 5 mM POPC liposome solution in D_2O at 27 °C. 112
Figure 4.8. Binding percentage of various polymers as a function of cholesterol molar percentage in POPC/cholesterol lipid bilayers 113
Figure 4.9. (a) F127 binding with 5mM liposomes composed of DOPC/cholesterol and POPC/cholesterol in D_2O at 27 °C as a function of cholesterol molar percentage..... 115
Figure 4.10. Binding percentage of various polymers as a function of POPC lipid bilayer curvature. 117

Figure 4.11. Polymer binding percentage of 0.2 mg/mL F127 to POPC/cholesterol liposomes at two different curvatures as a function of cholesterol molar percentage. ... 120
Figure 4.12. The fittings of single exponential decay model 124
Figure 5.1. Chemical structures of POPC and POPG. 129
Figure 5.2. Echo decay curves of 5mM neat POPG liposomes, 5mM POPG liposomes in the presence of 0.2 mg/mL F127, and 0.2 mg/mL F127 in the presence of 5mM POPG liposome at 27 °C in D_2O and in 150 mM NaCl D_2O solution 135
Figure 5.3. Polymer binding with POPC liposomes in D_2O and in 150 mM NaCl D_2O solution, and with POPG liposomes in 150 mM NaCl D_2O solution 137
Figure 5.4. Echo decay curves of 0.2 mg/mL F127 in D_2O and in 150 mM NaCl D_2O solution 139
Figure 5.5. Polymer binding percentage of 0.2 mg/mL F127 as a function of POPG molar percentage in the POPC/POPG lipid bilayer in 150 mM NaCl D_2O solution. 141
Figure 5.6. Schematic of hydrogen bonding between a PEO block and glycerol headgroups of POPG in the lipid bilayers. 142
Figure 5.7. Raman spectra of F108, neat POPG liposomes, polymer-liposome mixture, and superposition of pure polymers and pure liposomes 144
Figure 5.8. Binding percentage of 1 mg/mL F108 to 5 mM POPG liposomes in different salt solutions 148
Figure 5.9. The binding percentage in logarithmic scale of various polymer species with 5 mM POPC liposomes and with 5 mM PLPC liposomes in D_2O at 27 °C. 150
Figure 5.10. Polymer binding percentage of 0.2 mg/mL F127 as a function of DPPC molar percentage in POPC/DPPC lipid bilayers at 27 °C. 152
Figure 6.1. Size distributions of liposomes before and after peroxidation strong and poor protection by polymers 156

Figure 6.2. Chemical structures of various PPO-PEO triblock and diblocks 158

Figure 6.3. Average scattered intensities of liposomes with different polymers at 5:1 and 10:1 polymer/lipid molar ratios before and after lipid peroxidation..... 162

Figure 6.4. R_h distributions at 90º of neat liposomes and liposomes with various polymers at 5:1 polymer/lipid molar ratio before and after lipid peroxidation. 164

Figure 6.5. R_h distributions at 90º of neat liposomes and liposomes with variosu polymers at 10:1 polymer/lipid molar ratio before and after lipid peroxidation. 165

Figure 6.6. Average scattered intensities of liposomes with commercial poloxamers at 5:1 polymer/lipid molar ratio before and after lipid peroxidation.. 172

Figure 6.7. R_h distributions at 90º of neat liposomes and liposomes with commercial poloxamers at 5:1 polymer/lipid molar ratio before and after lipid peroxidation..... 173

Figure 6.8. Average scattered intensities of liposomes with commercial poloxamers at same molar and same mass concentration before and after lipid peroxidation 175

Figure 6.9. Average scattered intensities of liposomes with commercial P188 from two different batches at 5:1 polymer/lipid molar ratio before and after lipid peroxidation .. 176

Figure 6.10. R_h distributions at 90º of neat liposomes and liposomes with old and new P188 at 5:1 and 10:1 polymer/lipid molar ratio before and after lipid peroxidation. 177

Figure 6.11. SEC traces and NMR spectra of old and new P188. 178

Figure 7.1. Schematics of bottlebrush polymers. 181

Figure 7.2. Synthetic schemes of bottlebrush polymers 184

Figure 7.3. SEC traces of the synthesized bottlebrush polymers 186

Figure 7.4. ^{1}H NMR spectra of a POEGMA before and after removing trithiocarbonate endgroup. 188

Figure 7.5. UV-vis spectra of two POEGMAs before and after removing trithiocarbonate endgroups. 188

Figure 7.6. Experimental and fitted echo decay curves of 10k POEGMAs with 5 mM POPC liposome in D_2O at 27 °C 190
Figure 7.7. Experimental and fitted echo decay curves of 30k POEGMAs with 5 mM POPC liposome in D_2O at 27 °C 191
Figure 7.8. Binding summary of POEGMAs and PEO8. 192
Figure 7.9. Average scattered intensities of POPC liposomes with E(500m)10 at 2.5:1, 5:1 and 10:1 polymer/lipid molar ratios before and after lipid peroxidation. and the corresponding R_h distributions at 90º..... 194
Figure 7.10. Average scattered intensities of POPC liposomes with different POEGMAs at 5:1 polymer/lipid molar ratio before and after lipid peroxidation. and the corresponding R_h distributions at 90º..... 195
Figure 7.11. Experimental and fitted echo decay curves of E(500m)10-P(375h)4-CTA at 0.2 mg/mL in D_2O at 27 °C 197
Figure 7.12. Experimental and fitted echo decay curves of E(500m)10-P(375h)4-CTA and F127 at 0.2 mg/mL in 5 mM POPC liposome solution in D_2O at 27 °C..... 197
Figure 7.13. Chemical structures of linear PPO with bottlebrush PEO and bottlebrush PPO with linear PEO..... 198
Figure 7.14. Synthetic scheme of PPO-POEGMA. 198
Figure 8.1. Schematics of a bottlebrush polymer, and two possible structures of mikto-arm star polymers..... 205
Figure 8.2. SANS profiles of liposome incubation with low polymer concentration at 37 °C in pure D_2O and 84% H_2O/16% D_2O 206

Chapter 1 - Introduction

1.1 Overview of Poloxamers

Poloxamers are one of the most widely used classes of commercial non-ionic surfactants, invented by Wyandotte Chemicals Corporation (acquired by BASF in 1969) in the early 1950s.[1–3] These compounds are symmetric triblock copolymers, composed of a central hydrophobic block of poly(propylene oxide) (PPO) flanked by two hydrophilic blocks of poly(ethylene oxide) (PEO), as shown in Figure 1.1a. Note that "hydrophobic" and "hydrophilic" are two relative terms. Within the temperature range of our interest (*i.e.*, from room temperature to body temperature), PPO is generally considered as a hydrophobic component while PEO as a hydrophilic component. Poloxamers are synthesized by first slowly adding propylene oxide (PO) monomers to propylene glycol in the presence of a trace amount of alkaline catalyst (*e.g.*, sodium or potassium hydroxide) at elevated temperature and pressure, followed by sequential addition of ethylene oxide

(EO) monomers until a desired molecular weight is obtained.[4,5] The alkaline catalyst is neutralized by phosphoric acid after polymerization and then removed, resulting in a final product of poloxamers with pH of 7 ± 1 and 0.05% residual neutral salt.[4]

Prior to the invention of poloxamers, detergent molecules typically consist of PEO as the most commonly used hydrophile and hydrocarbon units derived from fatty acids, fatty alcohols, or alkyl phenols as the hydrophobe.[2,3] Such detergents, however, have the following restrictions. (1) The overall molecular weight or the hydrophobic-hydrophilic balance of the surfactant molecules have limited variations due to the difficulty of modifying the hydrophobic chain length. Since the hydrophobic portion of the detergents are commonly derived from fatty alcohols, a large variety of fatty alcohols with different lengths is required, which is industrially infeasible in terms of storage and handling of many types of organic compounds and dealing with different reaction conditions corresponding to different fatty alcohols.[3] (2) Surfactants with high detergency are all in liquid or paste forms, which is less desirable and convenient for packaging and distribution compared to solids.[2,3] Increasing the weight percentage of PEO in the detergents can result in solid products, but at the expense of the detergency, which becomes less effective due to an overbalance in the hydrophilic part of the molecule.[2,6] The invention of poloxamers provided greater flexibility in modifying the molecular weight and hydrophobic-hydrophilic balance of nonionic surfactants and enabled the production of nonionic surfactants with high detergency in solid form.

In the nomenclature of the poloxamers (*e.g.*, P188 as shown in Figure 1.1b), the last digit (8 for P188) indicates the weight percentage of the hydrophilic PEO block (*i.e.*, 80

wt. % of PEO in P188). The first two digits (18 for P188) indicate the molecular weight of the hydrophobic chains (*i.e.*, 1800 g/mol). Poloxamers are also known by the trade name Pluronics (BASF). In the nomenclature of Pluronics (*e.g.*, F68, equivalent to P188), the last digit (8 for F68) indicates the weight percentage of the hydrophilic PEO block, which is same as that in the poloxamer designation. The first one or two digits (6 for F68) multiplied by three indicates the length of the hydrophobic chains (*i.e.*, 1800 g/mol). The letter before the numbers indicates the physical state of the polymers: L stands for liquid, P for paste, and F for flakes.

(a)

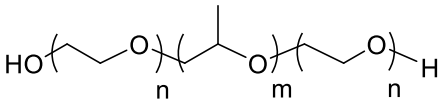

(b)

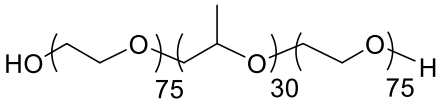

(c)

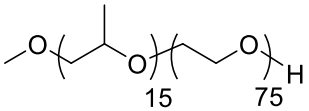

(d)

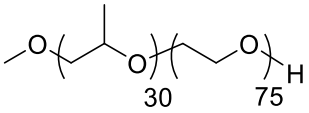

(e)

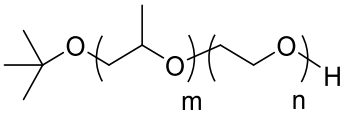

(f)

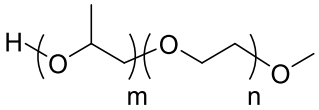

(g)

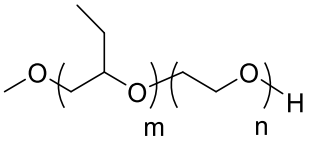

Figure 1.1. Chemical structures of (a) poloxamers, (b) poloxamer P188 (Pluronic F68), (c) diblock analog I of P188, (d) diblock analog II of P188, (e) diblock analog with a *tert*-butyl endgroup on the PPO block, (f) diblock analog with a hydroxyl endgroup on the PPO block, and (g) PBO-PEO diblock copolymer.

1.1.1 Physical Properties

Several physical properties of Pluronics are summarized in Table 1.1.[7,8] Hydrophilic-lipophilic balance (HLB) is a measure of the hydrophilicity of a surfactant molecule; a larger value of HLB indicates higher hydrophilicity. HLB is generally calculated from the molecular weight of the hydrophilic and hydrophobic portions of the molecule ($M_{\text{hydrophilic}}$ and $M_{\text{hydrophobic}}$, respectively) based on the following equation:[9]

$$\text{HLB} = 20 \cdot \frac{M_{\text{hydrophilic}}}{M_{\text{hydrophilic}} + M_{\text{hydrophobic}}} \tag{1.1}$$

HLB of Pluronic block copolymers provided by the manufacturer, however, don't follow the above standard definition. Instead, the following empirical equation has been used,[10]

$$\text{HLB} = -36.0 \cdot \frac{N_{\text{PO}}}{N_{\text{PO}} + N_{\text{EO}}} + 33.2 \tag{1.2}$$

where N_{PO} and N_{EO} represent the number of repeat units of EO and PO blocks, respectively. Equations 1.1 and 1.2 both indicate that the HLB of a surfactant molecule is dictated by the relative block length of PEO and PPO blocks. As shown in Table 1.1 the most hydrophilic polymers (*i.e.*, having a HLB of more than 24) contain at least 70 wt. % of PEO as indicated by the last digit of their designation, whereas the most hydrophobic polymers (*i.e.*, having a HLB of 1─7) consist of only 20 wt. % of PEO. The PPO and PEO contents in Pluronics also play a role in their melting point and cloud point (*i.e.*, the start of liquid-liquid phase separation in water). Pluronics with a high PEO content usually have a relatively high melting point and high cloud point compared to those with low PEO content, which can be attributed to the higher melting point of PEO (T_{m} ~ 66 ºC[11]) and higher solubility of PEO in water than PPO, respectively.[7]

Table 1.1. Physical properties of Pluronics.

Polymer	Molecular Weight[a] (kg/mol)	N_{PO}[a]	N_{EO}[a]	HLB[a]	Melting Point[a] (ºC)	Surface tension[a,c] (dynes /cm)	CMC at 37 ºC[b] (M)	Cloud point[a,d] (ºC)
L35	1.9	16	11	18─23	7	49	5.3×10^{-3}	73
F38	4.7	16	43	>24	48	52	-	>100
L42	1.63	22	4	7─12	−26	46	-	37
L43	1.85	22	6	7─12	−1	47	2.2×10^{-3}	42
L44	2.2	23	10	12─18	16	45	3.6×10^{-3}	65
L62	2.5	34	6	1─7	−4	43	4.0×10^{-4}	32
L63	2.65	32	9	7─12	10	43	-	34
L64	2.9	30	13	12─18	16	43	4.8×10^{-4}	58
P65	3.4	29	19	12─18	27	46	-	82
F68	8.4	29	76	>24	52	50	4.8×10^{-4}	>100
L72	2.75	38	6	1─7	−7	39	-	25
P75	4.15	36	24	12─18	27	43	-	82
F77	6.6	34	53	>24	48	47	-	>100
P84	4.2	43	19	12─18	34	42	7.1×10^{-5}	74
P85	4.6	40	26	12─18	34	42	6.5×10^{-5}	85
F87	7.7	40	61	>24	49	44	9.1×10^{-5}	>100
F88	11.4	39	104	>24	54	48	2.5×10^{-4}	>100
F98	13.0	45	118	>24	58	43	7.7×10^{-5}	>100
P103	4.95	60	17	7─12	30	34	6.1×10^{-6}	86
P104	5.9	61	27	12─18	32	33	3.4×10^{-6}	81
P105	6.5	56	37	12─18	35	39	-	91
F108	14.6	50	133	>24	57	41	2.2×10^{-5}	>100
L122	5.0	69	11	1─7	20	33	-	19
P123	5.75	69	20	7─12	31	34	4.4×10^{-6}	90
F127	12.6	65	100	18─23	56	41	2.8×10^{-6}	>100

[a]Specified by supplier.[7] N_{EO} represents the number of EO repeat units in one PEO block.
[b]Reported by Batrakova et al.[8]
[c]0.1% aqueous, 25 ºC.
[d]1% aqueous.

1.1.2 Micellization and Phase Behavior

The critical micellization concentration (CMC) and critical micellization temperature (CMT) are two important physical parameters of poloxamers. CMC and CMT are the concentration and temperature above which the poloxamers start to form micelles in water at a certain temperature or a certain concentration, respectively. Due to the amphiphilicity of poloxamers, the hydrophilic PEO blocks will form the micelle corona while the hydrophobic PPO blocks will form micelle cores to avoid interaction with water above the CMC or CMT.

The common techniques used to determine the CMC of poloxamers include light scattering, fluorescent dye solubilization, and surface tension measurements, where the CMC is reflected by a break in the curve of the data.[6,12–15] Polymer micellization detected by dynamic and static light scattering is indicated by a significant increase of both scattered intensity and particle size.[14] The dye solubilization method involves the use of a fluorescence probe, which has minimum fluorescence intensity in a hydrophilic environment (*e.g.*, water) and maximum in a hydrophobic environment (*e.g.*, micelle core).[13] In the case of surface tension measurements, the CMC is determined by the slope change of the surface tension as a function of polymer concentration.[12] The CMC of a poloxamer at a certain temperature reported in the literature may vary by up to an order of magnitude.[6] This can be due to: (1) different techniques used to measure the CMC, (2) different lots of the poloxamers provided by the manufacturer, and (3) coexistence of free polymers and micelles over a relatively wide range of temperature or concentration instead of a sharp transition.[16] Alexandridis and Hatton have demonstrated that the discrepancy in

the CMC values obtained by different techniques could be reduced by carefully selecting the criteria used to interpret CMC data.[7] The onset of increased light scattering intensity and increased fluorescence intensity (*i.e.*, the onset of solubilization of a hydrophobic dye) should be used to estimate CMC based on light scattering and dye solubilization methods, respectively; the second break in the surface tension curve should be used since the first break is possibly attributed to polymer rearrangement at the interface of air and water.[7,12] The CMC of poloxamers at 37 ºC as reported by Batrakova et al. using fluorescent probe solubilization technique are listed in Table 1.1.[8]

Poloxamer composition plays a critical role in setting the CMC. It was found that the CMC of poloxamers decreases exponentially as the PPO block length increases at constant PEO block length.[13,17] For example, Pluronic P65, P84, and P123 have the same PEO block length (ca. 19 repeat units per PEO block) and increasing PPO block lengths (ca. 29, 43, and 69 repeat units, respectively). As shown in Figure 1.2a, the CMC at 35 ºC increases by an order of magnitude when the PPO block length doubles (*i.e.*, P65 vs. P84), and by three orders of magnitude when the PPO block length triples (*i.e.*, P65 vs P123).[13] A previous study on diblock PPO-PEO copolymers came to the same conclusion.[18] On the other hand, the variation of PEO block length has a relatively weak effect on the CMC. As listed in Table 1.1, the CMC of Pluronics with similar PPO block length (*e.g.*, P84, P85, F87, and F88) slightly increases upon increasing the PEO block length.[8] Comparing P84 with F88, the CMC only increases by an order of magnitude with a five-fold increase of the PEO block length. In the case of P84 and P85, the CMC does not change as the PEO block length only varies by a few repeat units. Therefore, only large variation of PEO block length leads

to an appreciable change of the CMC. Also, the CMC depends on the overall molecular weight of the poloxamers. Both Table 1.1 and Figure 1.2b illustrate that the CMC of poloxamers with same relative PPO/PEO composition significantly decreases as the overall molecular weight increases, which is caused primarily by the longer PPO block.[8,13] These documented relationships indicate that the PPO block length has a more pronounced effect on the CMC compared to the PEO block length. Additionally, the CMC of Pluronics significantly decreases with increasing temperature, as shown in Figure 1.2. This is because both PPO and PEO have a lower critical solution temperature (LCST) in water, which means that water becomes a poorer solvent for both blocks as the temperature increases, attributable to the breaking of hydrogen bonding between the ether oxygen of the polymers and water molecules.[12,19–22] Note that PEO is soluble in water over a wide range of molecular weight and concentration at physiological temperature, whereas PPO with only 18 repeat units undergoes phase separation in water above 1 ºC.[22–25] The lower LCST associated with PPO relative to PEO makes the length and fraction of PPO a dominant factor in the micellization of poloxamers.

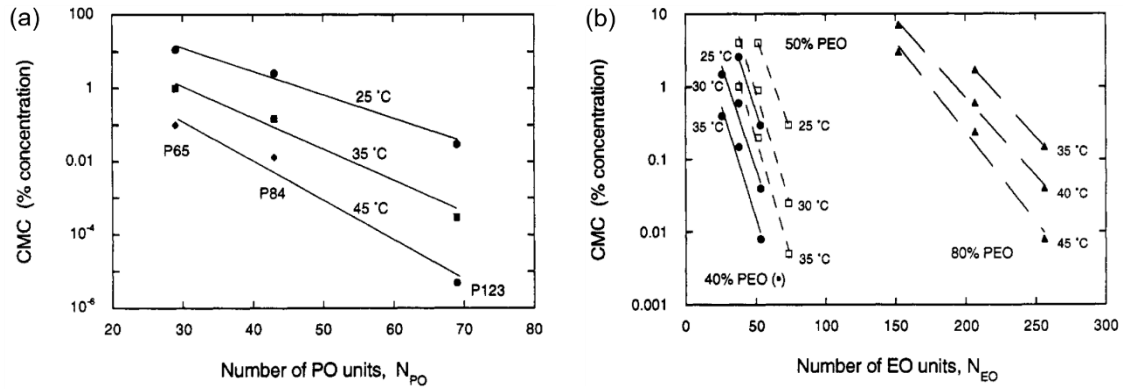

Figure 1.2. CMC of Pluronics with (a) the same PEO block length, and (b) the same PEO wt. % at various temperatures. Figure adapted with permission from Alexandridis, P; Holzwarth, J. F.; Hatton, T. A. *Macromolecules* **1994**, *27*, 2414–2425. Copyright 1994 American Chemical Society.

The thermodynamics of poloxamer micellization have been widely investigated by differential scanning calorimetry (DSC).[7,26–34] The enthalpy change during micellization is indicated by the endothermic peaks as shown in Figure 1.3.[29] An endothermic process means that the stand enthalpy of micellization, ΔH^{o}, is positive. Given that the standard free energy of micellization ΔG^{o} can be expressed as:

$$\Delta G^{\circ} = \Delta H^{\circ} - T\Delta S^{\circ} \tag{1.3}$$

where T is temperature and ΔS^{o} is the standard entropy of micellization, it can be inferred that ΔS^{o} must be positive in order to maintain a negative value of ΔG^{o} since the formation of thermodynamically stable micelles is spontaneous. Therefore, poloxamer micellization in water is an entropy-driven process.[35] An entropy increase during micellization could be explained by the hydrophobic interactions between the PPO blocks to form hydrophobic cores.[7,36–41] The aggregation of hydrophobes in aqueous solutions can significantly increase the entropy of water, which is much larger than the entropy loss caused by the

increasing ordering of the polymer molecules due to micelle structure formation.[7] As the temperature or concentration further increases, various lyotropic liquid crystalline phases (*e.g.*, cubic, hexagonal, and lamellar) can be formed.[7,16,19,42–47] Previous work by Ma et al. using ^{1}H NMR spectroscopy showed that the temperature-induced micellization of poloxamers is dominated by the PPO portion, while the PEO portion plays a more dominant role in the crystallization process.[48] Macroscopic phase separation of poloxamers from water will occur when the cloud point is reached.[19] Micellization and the phase behavior of poloxamers can be tuned by adding cosolvents (*e.g.*, methanol, ethylene glycol, ethanolamine, etc.),[19,49–51] cosolutes (*e.g.*, alkali-halide salts, sodium thiocyanate, urea, etc.),[30,32,47,52–60] and surfactants (*e.g.*, sodium dodecyl sulfate).[61–66]

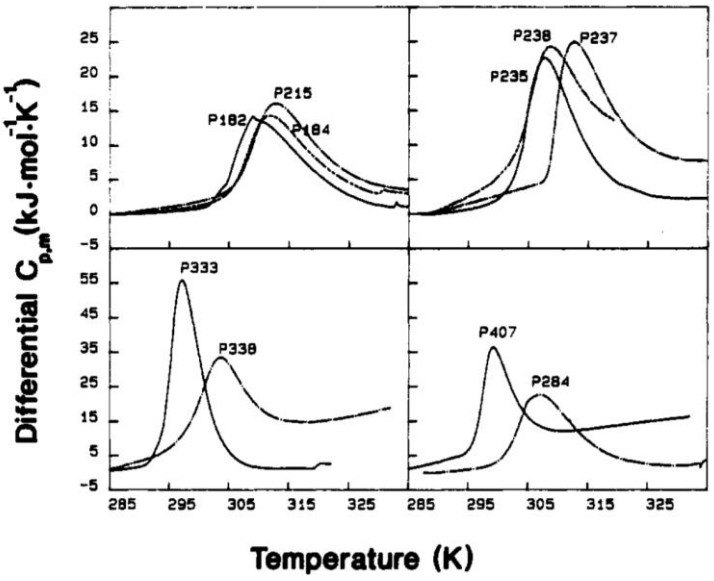

Figure 1.3. DSC curves of various poloxamers in water (1% w/v). Figure adapted with permission from Armstrong, J. K.; Parsonage, J.; Chowdhry, B.; Leharne, S.; Mitchell, J.; Beezer, A.; Loehner, K.; Laggner, P. *J. Phys. Chem.* **1993**, *97*, 3904–3909. Copyright 1993 American Chemical Society.

1.1.3 Applications

In addition to broad industrial applications as surfactants, poloxamers also have many biomedical applications, especially in the area of cell membrane stabilization and permeabilization, due to their amphiphilicity and biocompatibility. Hydrophilic dominant poloxamers such as P188 (or Pluronic F68), which contains 80 wt.% PEO (*ca*. 27 and 75 repeat units per PPO and PEO blocks, respectively) have been used as membrane stabilizers to block dystrophic heart failure,[67] protect dystrophic skeletal muscle,[68] prevent reperfusion injury after myocardial infarction,[69] and attenuate acute injury to the blood-brain barrier.[70–73] In contrast, poloxamers with longer hydrophobic PPO blocks such as F127 (*ca*. 64 and 108 repeat units per PPO and PEO blocks, respectively), or with lower PEO content such as L61 (*ca*. 10 wt.% PEO), have been applied to promote membrane permeability and to facilitate drug and gene delivery due to their facile incorporation into the cell membrane.[74–80]

Of particular interest in all these applications is membrane stabilization of dystrophic muscle cells by poloxamers. Dystrophin is a cytoskeletal protein that connects the myocyte membrane (sarcolemma) to the cytoskeleton (actin); the cell membrane is also linked to the extracellular matrix by the dystrophin-glycoprotein complex (including sarcospan, α- and β-dystroglycan (DG), dystrobrevins (DB), syntrophins (SYN), and α-, β-, γ-, δ-sarcoglycan complex (SGC)), as shown in Figure 1.4.[81–83] The dystrophin bridge regulates the stresses on the cell membrane imposed by muscle contraction and thus enables sarcolemma stability.[83,84] Dystrophin deficiency causes Duchenne muscular dystrophy (DMD), a fatal disease that leads to striated muscle deterioration including all skeletal,

respiratory and cardiac muscles in humans.[85] DMD patients cannot express dystrophin due to a generic mutation. The absence of the protein makes the sarcolemma extremely fragile and vulnerable to mechanical damage induced by muscle contraction. This damage is believed to give rise to the high permeability to Ca^{2+} through the cell membrane, leading to necrosis and muscle weakness.[86,87] DMD occurs in 1 in every 3,500 male births each year, and the patients are usually diagnosed during childhood.[68,88,89] The symptoms of DMD generally begin as progressive muscle decline and over-sized calf muscles, followed by loss of ambulation, along with the complications including curvature of the spine (scoliosis), respiratory difficulty, and cardiomyopathy.[6,89,90] Unfortunately, there is no cure to prevent striated muscle deterioration for DMD patients, and the patient's expected life span is approximately 30 years.[6]

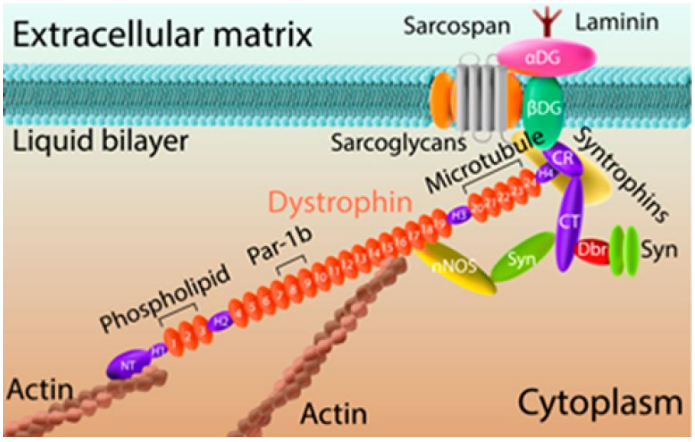

Figure 1.4. Schematic of dystrophin that connects the cell membrane to actin. Figure adapted with permission from Le, S.; Yu, M.; Hovan, L.; Zhao, Z.; Ervasti, J.; Yan, J. *ACS Nano* **2018**, *12*, 12140–12148. Copyright 2018 American Chemical Society.

Although experimental DMD therapeutics, such as gene therapy, have great potential, these novel techniques still face many challenges in human trials.[91–94] Existing symptomatic treatments of DMD, such as corticosteroids, have limited benefits, but adverse effects are significantly more common.[95–97] Most symptomatic treatments intend to improve the muscle strength and allow the patients to walk by retarding the muscle degeneration for a short period of time.[96] But, these treatments only show efficacy on the skeletal muscles and not the cardiac muscles, despite the fact that both muscles are affected by DMD.[67] Furthermore, the improvement of ambulation in DMD patients increases stress on the untreated diseased heart due to the increasing cardiac demands.[81,82] In fact, dystrophic heart failure is the second leading cause of fatalities in DMD.[85,98] Relative to skeletal myopathy, less attention has been paid to cardiomyopathy because (1) cardiac symptoms do not typically appear at early stages, and (2) the disease may be misdiagnosed as symptoms of fatigue and difficulty breathing due to progressive weakness of the skeletal and respiratory muscles.[6,81,89] The trade-off between the DMD cardiomyopathy and skeletal myopathy gives rise to the essential need of a therapeutic strategy that can simultaneously treat all striated muscles.[68] Previous work by Yasuda et al. and Houang et al. surprisingly showed that P188 not only has a significant stabilization effect on the dystrophic myocardium in animal models of DMD, but also confers significant protection to dystrophic limb skeletal muscles *in vivo* by subcutaneous P188 delivery.[67,68,99] Based on their work, the use of P188 is a novel therapeutic approach for stabilizing dystrophic cell membranes and temporarily correcting the defects caused by DMD.

1.2 Diblock Analogs to Poloxamers

Early work on cell membrane stabilization by block copolymers was limited to commercially available triblock poloxamers, especially P188. Recently, diblock analogs of Pluronics have been investigated in cellular assays by Kim and coworkers, which demonstrate the protective effect of the diblock architecture on cell membranes against hypo-osmotic stress *in vitro*.[100] Houang et al. and Lee et al. also found that PPO-PEO diblock copolymers can stabilize dystrophic muscle cell membranes and restore the integrity of blood-brain barrier *in vivo*, respectively.[70,101] These studies demonstrate that appropriately designed diblock copolymers interact with cell membranes as effectively as triblock poloxamers, and can potentially be used in many applications that have involved the use of triblock poloxamers. However, to date, only a few studies in the literature have investigated the role of diblock architectures in polymer-membrane association from a fundamental perspective, which leaves considerable room for further investigation on interaction mechanisms and polymer structure design to improve membrane stabilization efficacy.[102–104]

One benefit of the diblock architecture is that it presents a simpler compound from a synthetic standpoint. Another benefit is that the hydrophobic block has a free end instead of connecting to the second hydrophilic block, which provides additional control over the hydrophobicity of the PPO block through endgroup functionalization. This could give additional insight into how hydrophobicity affects the interactions with cell membranes. Therefore, various PPO-PEO diblock copolymers were synthesized as complements to the commercial triblock poloxamers as described in the following chapters.

1.2.1 Hydrophilic-Hydrophobic Balance

Hydrophilic-hydrophobic balance is a critical determinant to whether a polymer will enhance or disrupt cell membrane integrity.[105–107] A study by Cheng et al. only selected commercially available P181 and P188 as two representative models since they are the most hydrophobic and hydrophilic formulations in the poloxamer class, respectively.[106] Although the comparison between P181 and P188 gives us a qualitative understanding on how the hydrophilic–hydrophobic balance of the polymer affects the interactions with membranes, a quantitative and systematic study of the underlying mechanism has not been developed yet. The hydrophilic-hydrophobic balance of the polymer could be manipulated by modifying the lengths of the PPO and PEO blocks, the end group functionality on the hydrophobic block, and the chemical composition of the block copolymers. More details can be found in the following subsections.

Hydrophilic and Hydrophobic Block Length

To make a comparison between triblock poloxamers and PPO-PEO diblock copolymers, the diblock analogs needs to be carefully selected. Since P188 is the most widely studied poloxamer for membrane stabilization, we will first consider the diblock analogs of P188 as the initial model system, which will be further extended to include other PPO-PEO diblock copolymers with different block lengths.

Two possible diblock analogs can be obtained from P188, as shown in Figure 1.1c and Figure 1.1d. One is simply cleaving the P188 molecule in the middle so that the relative hydrophilic/hydrophobic composition of the PPO-PEO diblock copolymer remains the

same (Figure 1.1c, analog I). The other analog is simply removing an entire PEO block on one end from the P188 molecule; the length of PPO block remains unchanged, with one side flanked by a single PEO block (Figure 1.1d, analog II). In Chapter 3, we demonstrate that analog I (named as $tPPO_{14}$-PEO_{78}, where "t" stands for the *tert*-butyl endgroup originated from the initiator used in the synthesis) is a more appropriate diblock analog to P188 compared to analog II (named as $tPPO_{29}$-PEO_{68}) according to their binding to model membranes. Note that the two diblocks we synthesized contain an additional *tert*-butyl endgroup compared to the ideal diblock analogs to P188 as shown in Figure 1.1c and Figure 1.1d. At this point, we only focus on selecting the proper PPO/PEO composition for the analog without considering the endgroup effect. Analog II shows much stronger binding to the model membranes than analog I or P188 does, which is clearly attributable to the higher hydrophobic content of this compound. Hence, analog I has been adopted as the model diblock to study cell membrane stabilization *in vitro* and *in vivo*.[100,101] Moreover, the hydrophobic and hydrophilic blocks can be further tuned to other lengths beyond the basic diblock analog described above. Kim et al. synthesized a series of diblock copolymers and investigated the effect of polymer size, composition, and architecture on their protection efficacy on myoblasts based on hypo-osmotic stress *in vitro*.[100] Also, the effect of polymer hydrophilic-hydrophobic balance on the interactions with model membranes is elucidated in Chapter 3 using both triblock and diblock architectures.

Hydrophobic Block End Group Functionality

The main difference between the triblock and diblock architectures is the "exposed" hydrophobic block. By removing the second hydrophilic PEO block, the hydrophobic PPO

block is no longer constrained and thereby acts as a free end to interact with the surroundings. Compared with the triblock architecture, the free PPO block could embed itself into the interior of the lipid bilayer more easily, and facilitate stronger adsorption of the hydrophilic block onto the membrane surface.[102] This behavior of the hydrophobic block of a diblock copolymer has been previously termed "anchoring".[6,101,102] Previous work by SAXS revealed that the anchoring function of the hydrophobic block in the diblock architecture plays an important role in the phase transition of polymer-doped membrane systems.[102]

The anchoring strength can be further reinforced by altering the functional group at the end of the hydrophobic PPO block. Recent studies compared the membrane stabilization efficacy of diblocks with *tert*-butyl endgroups (Figure 1.1e) versus those with hydroxyl endgroups (Figure 1.1f) on the PPO blocks. *In vitro* and *in vivo* experiments led to the conclusion that diblock with the tert-butyl endgroup confers much more effective protection.[100,101] In this context, we have investigated how polymer endgroup chemistry influences their association with model membranes as detailed in Chapter 3. In Chapter 6, the protection efficacy of these polymers with different endgroups was evaluated based on a model system of damaged membranes, which could be potentially used as screening results before further cellular and animal studies.

Chemical Composition

In addition to block length and endgroup functionality, chemical composition of each block could also be modified. For example, poly(1,2-butylene oxide) (PBO) is also commonly used as the hydrophobic component in an amphiphilic diblock copolymers and

can be considered as a substitute for PPO. Leiske and coworkers showed that PBO-PEO diblock copolymers have similar insertion mechanisms into a phospholipid monolayer as poloxamers do.[103] The substitution of PBO enables the investigation on the effect of chemically changing the hydrophilic-hydrophobic balance. The synthetic strategy for PBO-PEO diblock copolymers is similar to the diblock poloxamer synthesis as described in Chapter 2. The only change is using 1,2-epoxybutane (BO) monomers instead of PO monomers. To further manipulate the hydrophilic-hydrophobic balance by tuning the composition chemically, statistical copolymers are an alternative to diblock copolymers. Instead of connecting homopolymer blocks, statistical copolymers consist of more than one type of monomer, the sequence of which depends on the relative reactivity of each monomer species.

1.2.2. Overall Molecular Weight

Recent work by Wang *et al.* using microcantilevers showed that Pluronic F98 exhibits greater inhibition of lipid diffusion than F68 does, indicating F98 has a greater extent of hydrophobic block insertion into the lipid bilayer.[108] F98 and F68 have the same composition (*i.e.*, 80 wt. % PEO), but the total molecular weight of F98 is larger than F68. Inspired by this study, we are interested in how differences in molecular weight affect the polymer-membrane association. If the composition of triblock poloxamers is fixed, the hydrophilic and hydrophobic blocks will get longer proportionally when increasing the total molecular weight. Based on previous mechanistic studies reported in the literature, it is believed that longer hydrophobic blocks help the entire polymer molecule approach to

the membrane and accelerate the insertion into the membrane, which also increases the risk of membrane disruption.[106–108] However, in the presence of the longer hydrophilic blocks adsorbed on the surface, deeper insertion of the hydrophobic block is constrained, which could eliminate the risk of membrane disruption. Therefore, we hypothesize that increasing the molecular weight of the poloxamers will improve the cell membrane stabilization effect. A series of commercial poloxamers with 80 wt. % PEO were employed to investigate the molecular weight effect on their protection efficacy on model membrane systems as described in Chapter 6.

1.3 Membranes

1.3.1 Cell Membranes

In eukaryotic cells, an intact cell membrane acts as a permeable barrier that controls transport of certain ions and small molecules into and out of the cell.[105] Regardless of the cell type, the primary composition of the cell membrane is an amphiphilic phospholipid bilayer (phosphatidylcholine, phosphatidylethanolamine, phosphatidylinositol, phosphatidylserine, sphingomyelin, etc.), cholesterol, and proteins. Plasma membranes The ionic transport between extra- and intracellular fluid is regulated by function-specific proteins embedded in the lipid bilayer that maintain the transmembrane ionic concentration gradients at affordable metabolic energy costs.[109] Cell membranes are vulnerable to many types of injury including thermal trauma,[110] frostbite,[111] free-radical mediated radiation,[112] barometric trauma,[113,114] electric shock,[115,116] and mechanical shear or crush forces.[117–119]

For minor injuries the cell membrane can be self-repaired by intracellular vesicle fusion, as a naturally occurring process which forms a “patch” to stabilize the porated membrane and seal pores.[120,121] Any severe damage, however, results in the irreversible loss of cell membrane integrity. The porated cell membrane quickly causes a disruption of ionic concentration gradients and eventually leads to necrosis of the cell due to the exhaustion of metabolic energy.[110] Due to the complexity of cell membranes, model membrane systems were widely used for the study of polymer-membrane association, as detailed in the following subsections.

1.3.2 Lipid Monolayer Model Membranes

Model membrane systems can be generally divided into two different types: monolayers and bilayers. The lipid monolayer model mimics the outer leaflet of cell membranes.[122] It is a two-dimensional film formed by a single layer of amphiphilic lipid molecules at the air-water interface, with the hydrophilic headgroups immersed in the liquid subphase (water) and the hydrophobic tails up in the air.[105,123,124] Langmuir troughs have been used to change the surface area of the monolayer film so that the lipid packing density could be adjusted. Damaged cell membranes can be simulated by lipid monolayers with reduced lipid packing density, corresponding to low surface pressure and high surface area of the lipid film.[123–125] Lipid monolayers are widely applied to study membrane phase behavior and the association with polymers and peptides using fluorescence microscopy,[103,104,122–126] surface pressure ─ area per lipid isotherms,[103,104,122–129] interfacial X-ray diffraction and reflectivity,[103,129–132] and shear rheology.[133,134]

Compared to bilayer systems, lipid monolayers provide greater control over membrane composition because the interactions between the opposing leaflets in the bilayers can lead to phase separation, change of lipid packing, and crystal formation (especially in the presence of high cholesterol content), whereas the lipid monolayers can maintain a single stable phase.[130,133,135] Despite the flexibility in tuning the membrane composition, there are several limitations that prevents the monolayer from being an ideal model membrane system. First, lipid monolayers lack the second leaflet of the bilayers that essentially have twice the thickness of the monolayers. Thus lipid monolayers are not appropriate models for the study of insertion dynamics of small molecules, polymers or proteins in the vertical dimension of real cell membranes. Additionally, lipid monolayers have flat configurations, which makes them unable to be used to study curvature effects. Previous studies showed that membrane curvature plays an important role in lipid packing and the association with proteins.[136,137] Based on these arguments, lipid bilayers with adjustable curvature (*e.g.*, unilamellar lipid vesicles) are better model membranes than monolayer systems.

1.3.3 Lipid Bilayer Model Membranes

Liposomes, or more specifically, unilamellar lipid vesicles, represent a close biophysical parallel to cell membranes. Vesicles can be classified into three categories: small (SUVs), large (LUVs), and giant unilamellar vesicles (GUVs), corresponding to a typical diameter of less than 50 nm, 50 – 1000 nm (commonly 100 – 200 nm), and more than a micron, respectively. SUVs and LUVs are widely used as model membranes to investigate the partitioning of polymers and peptides into membranes using fluorescence

spectroscopy,[138–141] circular dichroism spectroscopy,[141–143] zeta-potential measurements,[142,144] and isothermal titration calorimetry.[145–147] GUVs are commonly employed to visualize and monitor the phase separation and fluctuations of the membranes using optical microscopy, due to their large size.[148–154]

SUVs and LUVs are prepared by size reduction of multilamellar vesicles (MLVs), which are formed by hydration of dry lipid films followed by agitation.[155] Sonication and extrusion are two common techniques used to disrupt MLVs and reduce the liposome size, resulting in SUVs or LUVs depending on the sonication time and power as well as the extrusion pore size.[155–158] A few freeze-thaw cycles prior to sonication or extrusion were found to improve the unilamellarity and trapping efficiency of the vesicles formed, especially in the case of high lipid concentration.[159,160] Sonication is mostly used to prepare SUVs. However, the high curvature of SUVs makes them less stable compared to LUVs; fusion of SUVs to LUVs can be induced when stored below lipid phase transition temperature (*i.e.*, the temperature above which the lipid physical state changes from ordered gel phase to the disordered liquid crystalline phase) or subjected to a freeze-thaw cycle.[155,161–164] The mean size and distribution of SUVs prepared by sonication may have relatively large variation between batches since the sonication is usually terminated when the cloudy lipid suspension becomes visually transparent with slight haziness, which qualitatively indicates that the size of MLVs have been largely reduced.[155] Also, prolonged sonication and the heat accumulated during the sonication process, which can lead to lipid hydrolysis and peroxidation, makes sonication a less efficient method for liposome production.[161] In this context, LUVs prepared by extrusion with a pore diameter of 50 –

200 nm are more prevalent vesicular bilayer systems in the literature. Related studies using LUVs include investigating membrane bending rigidity,[165–167] drug permeation through membranes,[168–170] and the interactions between membranes and polymers, peptides, and proteins.[106,107,126,146,147,171]

In addition to SUVs and LUVs, GUVs are another class of unilamellar lipid vesicles. GUVs can be prepared by the spontaneous swelling method,[172–174] as well as the electroformation method.[135,175,176] The spontaneous swelling method is similar to the formation of MLVs, except for an additional step of pre-hydration and no agitation. The dry lipid thin film formed at the bottom of the sample vial needs to be pre-hydrated with water-saturated nitrogen, followed by gently adding extra water and incubating under nitrogen for a few more hours to allow the lipids to swell.[172–174] Agitation should be avoided during the swelling period to improve the vesicle unilamellarity.[172] In the case of electroformation, a lipid solution in organic solvent is spread on the surface of two parallel electrodes facing each other. The solvent is evaporated before applying an electric field, and water is then filled between the two electrodes.[135,175,176] Compared to spontaneous swelling of GUVs, the electroformation method provides more control over the size and size distribution of GUVs by tuning the electrical parameters.[177] Since the size of GUVs is on the order of a micrometer, it brings several advantages in comparison to SUVs and LUVs. (1) Lower bilayer curvature of the GUVs better mimics that of living cells, the size of which is also on the order of micrometer.[135] (2) More information about membrane phase behavior can be revealed due to the higher visibility of GUVs using optical microscopy;[178] GUVs have been extensively employed to investigate the phase diagrams of binary- and

ternary-component lipid bilayers using fluorescence microscopy.[148–154] (3) Cell membrane damage mimicked by an external model stress applied to a lipid bilayer is more easily observed with GUVs due to their large size. For example, the burst and reseal of the GUVs subjected to hypo-osmotic stress can be directly imaged by confocal microscopy.[179]

Additional types of lipid bilayer model membranes include supported lipid bilayers and free-standing lipid bilayers. Single supported lipid bilayers can be prepared by unilamellar lipid vesicle fusion or by sequential monolayer deposition using a Langmuir trough on silicon wafers.[130,180–184] Oriented stacks of bilayer arrays on a silicon wafer can be fabricated by the rock-and-roll method.[185] Supported lipid bilayers with curvature can be made by lipid vesicle adsorption onto silica beads; the bilayer curvature is manipulated by varying the diameter of the beads.[186] Similar to lipid monolayers, which present a large area, supported lipid bilayers are extensively employed to investigate membrane structure and the binding of polymers and proteins to the membranes, using surface-sensitive techniques such as surface plasmon resonance,[182] atomic force microscopy,[130,180] neutron reflectivity,[181,183] and grazing incidence X-ray diffraction.[130] Beltramo and coworkers recently developed a platform to generate free standing lipid bilayers with millimeter scale areas that allows for the dynamic control of the membrane tension and shows great potential for generating model membrane to study the association with polymers.[187]

1.4 Development of the Mechanism of Polymer-Membrane Association

The mechanism of polymer-membrane association has been widely studied in the last two decades. Inspired by the application of P188 as membrane stabilizers, Maskarinec and coworkers investigated the insertion of a series of hydrophilic dominant Pluronics into lipid monolayers using surface pressure-area isotherms coupled with fluorescence microscopy measurements.[105,123,124] The surface pressure-area isotherms indicated that the hydrophilic dominant Pluronics only incorporate into the lipid monolayer at reduced packing density. As shown in Figure 1.5a, significant insertion of polymers into the monolayer was not observed until the surface pressure was lowered to 22 mN/m. When the lipid packing density is restored to normal levels, P338 is "squeezed out" from the lipid monolayer as the isotherm of DPPC + P338 resembles that of pure DPPC when the surface pressure is greater than 35 mN/m (Figure 1.5b).[124] Molecular dynamics simulations also demonstrated that P188 can seal the pores on lipid bilayers, while little interaction was found with intact lipid bilayers.[188,189] Fluorescence microscopy measurements revealed that the insertion of Pluronics changes the morphology and phase behavior of the lipid monolayers. Grazing incidence X-ray diffraction and X-ray reflectivity experiments conducted by Wu *et al*. led to a similar conclusion; the authors also argued that polymer insertion gives rise to tighter lipid packing and induces polymer/lipid phase separation.[129,131] The morphological changes in the lipid monolayer induced by polymer insertion was further explored by atomic force microscopy (AFM).[190] It confirmed that there is a threshold of lipid packing density for polymer insertion, only below which the morphological changes in the

monolayer were observed, indicating polymer insertion. Other amphiphilic block copolymers, such as diblock copolymers of PBO and PEO and triblock copolymers of poly(glycerol monomethacrylate) and poly(propylene oxide) (PGMA-PPO-PGMA), showed similar influence on the morphology and phase behaviors of lipid monolayers upon their insertion.[103,191,192] These studies on lipid monolayers form the basis of understanding poloxamer interactions with the model membrane system.

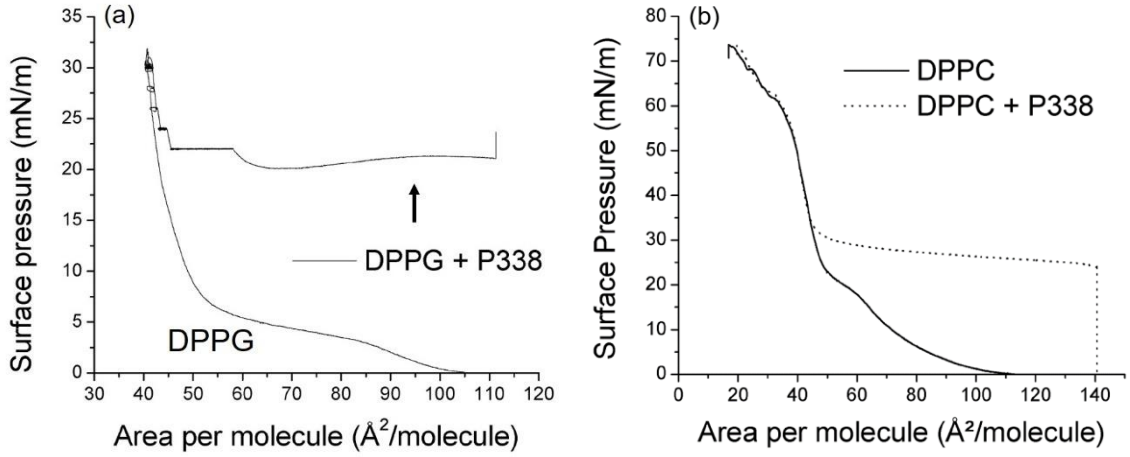

Figure 1.5. (a) Injection of P338 into the water subphase of a DPPG monolayer at 30 °C. (b) Lateral compression isotherms of DPPC and P338-pretreated DPPC on a water subphase at 30 °C. Figure adapted with permission from Maskarinec, S. A.; Lee, K. Y. C. *Langmuir* **2003**, *19*, 1809–1815. Copyright 2003 American Chemical Society.

In addition to lipid monolayers, bilayer systems have also been extensively employed for mechanistic studies of polymer-membrane association. In the late 1990s, Kostarelos *et al.* found that the interaction between poloxamers and lipid bilayers is much more extensive when the polymers are mixed with lipids before liposome formation, compared to when the polymers are added to pre-formed liposomes.[193,194] The incorporation of polymers into lipid bilayers in the former case was demonstrated by the change of bilayer

microenvironment and restricted molecular mobility in the bilayer, detected by hydrophobic dyes and ^{31}P and ^{13}C NMR, respectively.[195,196] The authors further investigated the size change of the liposomes in the presence of pre-added and post-added polymers.[193,194,197] Pre-added polymers caused a dramatic increase of vesicle size due to initial polymer incorporation, followed by a size decrease at high polymer concentration possibly due to solubilization and disruption of the lipid bilayer. On the other hand, the post-added polymers only slightly increase the vesicle size, suggesting modest polymer-bilayer association. Another separate experiment showed that the liposomes in the presence of pre-added polymers, but not post-added polymers, can significantly retard osmotic swelling, indicating modification of bilayer properties induced by pre-added polymers.[193] Johnsson *et al.* also showed that Pluronic F127 has a relatively weak interaction with pre-formed lipid vesicles.[198] According to these results, it has been proposed that the pre-added polymers can incorporate into the bilayer interior by spanning the lipid bilayer, while the post-added polymers may only weakly adsorb on the liposome surface. Recent molecular dynamics simulations also show that the final configuration of the polymer with respect to the lipid bilayer is determined by its initial configuration.[199,200] When the polymer was placed in the lipid-water interface (analogous to post-added polymers), the polymer was observed to partially insert into the bilayer with a U-shaped configuration. Conversely, when the polymer was placed in the center of the bilayer (analogous to pre-added polymers), a transmembrane configuration was obtained.

In the 2000s, small angle X-ray scattering (SAXS) experiments by Firestone and coworkers revealed that the configuration of poloxamers when interacting with lipid

bilayers not only depends on when the polymers are added, but the length of the PPO block.[102,201,202] Free lipid molecules of dimyristoyl-*sn*-glycero-3-phosphocholine (DMPC) were premixed with the polymers in water and measured by SAXS to obtain the phase structure. SAXS profiles show that a highly ordered swollen lamellar structure is formed when the PPO block length approximates the dimension of the acyl chains of the lipid bilayer, implying that the PPO block spans the lipid bilayer with two PEO blocks perpendicular to the membrane surface on each side (*i.e.*, brush-like), which increases the lattice spacing of the lamellar structure (Figure 1.6a). On the contrary, poloxamers with a shorter PPO block length yield a lamellar structure similar to that of a simple dispersion of DMPC without polymers in water, suggesting the PPO block may only partially insert into the lipid bilayer with two PEO blocks laterally dangling on the same side of the membrane (*i.e.*, mushroom-like), and thus the lattice spacing changes little compared to the lamellar structure of pure DMPC (Figure 1.6b). These results were further explored by molecular dynamics simulations.[203,204] In addition to the effects of the PPO block length, several studies elucidated that the PEO block length also plays a role, indicating that the absolute hydrophobic block length along with relative hydrophilic-hydrophobic balance of the polymer determines the polymer-membrane interaction.[104,197,205–207] Poloxamers with a longer PPO block or higher weight percentage of PPO enhance membrane permeability,[193,198,205,207–209] accelerate the flip-flop of lipids (transmembrane lipid translocation),[169,170,208,210–212] and increase membrane rigidity,[193,202,206] which could be attributed to stronger association with the membranes compared to less hydrophobic polymers.

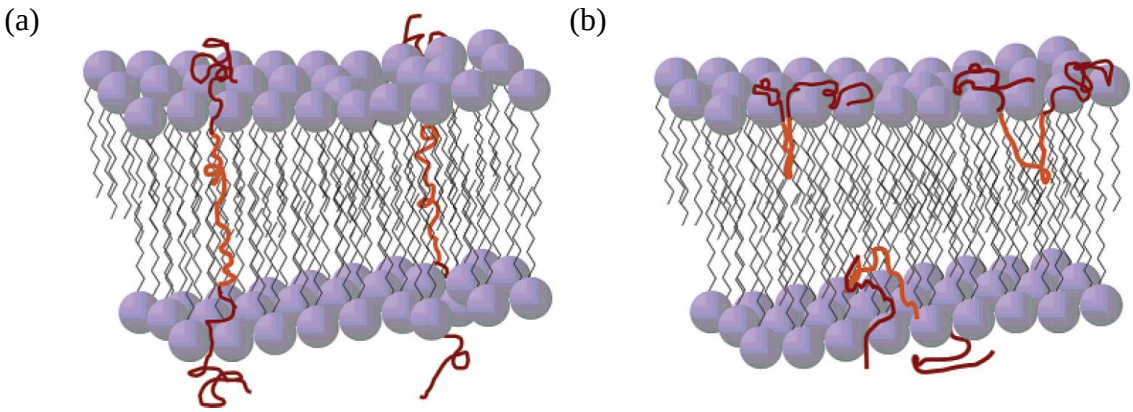

Figure 1.6. (a) Full insertion of PPO block by spanning the lipid bilayer. (b) Partial insertion of the PPO block. Figure adapted with permission from Firestone, M. A.; Wolf, A. C.; Seifert, S. *Biomacromolecules* **2003**, *4*, 1539–1549. Copyright 2003 American Chemical Society.

In addition to polymer hydrophobicity, temperature and polymer concentration also have significant impact on polymer-membrane association. The interaction between polymers and membranes becomes stronger at higher temperature, which could be attributed to enhanced membrane fluidity and higher hydrophobicity of the polymers due to their LCST behavior.[108,125,201] Wu *et al.* elucidated that poloxamers only partition into liposomes with a fluid phase, not a gel phase, based on isothermal titration calorimetry measurements.[146,147] As the temperature or polymer concentration increases, the integration of poloxamers into membranes could create pores in the lipid bilayer,[199] induce membrane phase transitions,[201] and change the liposome morphology (*e.g.*, disrupt the liposomes into micelles or flat discs).[147,190,213,214] It was found that polymer interactions with the membrane will compete with micellization at higher polymer concentrations.[194,203] Temperature and polymer concentration also affect the configuration of the polymers incorporated into the membrane.[102,183,201] The PEO blocks could switch from parallel (*i.e.*,

mushroom-like) to perpendicular (*i.e.*, brush-like) to the lipid bilayer as the temperature or polymer concentration increases.

In recent work, a two-state transition mechanism of the interactions between poloxamers and lipid bilayers has been proposed. According to this model, regardless of the hydrophobicity of poloxamers, they first adsorb onto the membrane surface, followed by insertion into the bilayer interior; the hydrophilic-hydrophobic balance of the polymers, however, determines the kinetics between the two states.[106,147,179] As shown in Figure 1.7a, a hydrophobic-dominant block copolymer (*e.g.*, P181) would quickly insert under the headgroup of the lipid bilayer right after adsorbing onto the membrane surface, because (1) the hydrophobic block prefers to interact with the lipid tails rather than the hydrophilic lipid headgroups, and (2) the hydrophilic blocks are too short to hold the entire polymer chain on the surface. Eventually, the entire polymer molecule would fully insert into the bilayer interior after 7 h, as shown in Figure 1.7b. In contrast, adsorption onto the membrane surface with little insertion was observed for a hydrophilic-dominant block copolymer (*e.g.*, P188) within the same time frame.[106] Nevertheless, insertion of P188 was observed at longer-time incubation with the bilayers (*i.e.*, more than a day), using fluorescence leakage from giant unilamellar vesicles as an indicator.[179] It was shown that several-hour incubation of P188 with the bilayer vesicles can retard fluorescence leakage under osmotic stress due to the protective effect by polymer adsorption, whereas incubation for more than a day led to significant leakage due to disruption of membrane integrity by polymer insertion. A recent work by Kim *et al.* using surface plasma resonance further confirmed that P188 and PEO homopolymers exhibit slow binding kinetics to lipid

bilayers.[182] An isothermal titration calorimetry study also demonstrated that P338 (a larger version of P188) partitioned into the outer leaflet of the lipid bilayer on a relatively short timescale (~200 min), and migrated to the inner leaflet on a longer timescale (38 h).[147] A liposome peroxidation assay developed by Wang *et al.* elucidated that only hydrophilic dominant poloxamers can provide effective protection to liposomes against induced lipid peroxidation due to their adsorption on the membrane surface. While the propensity of the short hydrophobic block to interact with the lipid tails facilitates the entire polymer molecule approaching the membrane surface, the long hydrophilic blocks form hydrogen bonding networks with the surface hydration layers of the lipid headgroups.[107] Several simulation studies demonstrated that the PPO block interacts with lipid tails while the PEO block interacts with the lipid headgroups.[188,189,204]

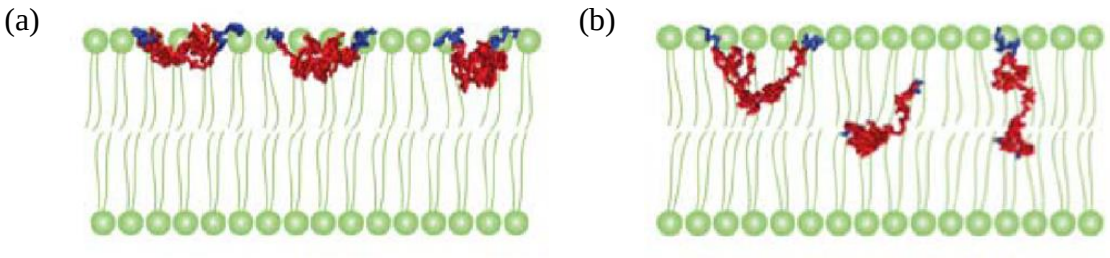

Figure 1.7. Schematic of a two-state transition mechanism of the interactions between P181 and lipid bilayers. (a) Adsorption happens immediately after introducing the polymers, and (b) insertion into the bilayer interior happens after 7 h incubation. Figure adapted with permission from Cheng, C.-Y.; Wang, J.-Y.; Kausik, R.; Lee, K. Y. C.; Han, S. *Biomacromolecules* **2012**, *13*, 2624–2633. Copyright 2012 American Chemical Society.

Although significant advances have been made in this field, there are many remaining unresolved puzzles. The previous studies as summarized above set up the basic

understanding of the mechanism of polymer-membrane association, but comprehensive conclusions cannot be drawn. One of the controversies is whether PEO blocks can insert into the bilayer interior. Despite most work in the literature suggesting that only PPO can interact with lipid tail region, a few studies proposed that PEO can overcome the energy barrier to move toward the bilayer center, which perturbs local lipid packing and induces water pores.[212,215,216] In this context, more direct experimental evidence of poloxamer configuration in the lipid bilayers is needed. There are two main challenges regarding the direct observation of the interaction between poloxamers and lipid bilayers. First, the polymer-membrane association is inherently weak, especially for hydrophilic dominant poloxamers that have great potential for cell membrane stabilization, such as P188. This presents extra challenges to understanding the molecular mechanism of membrane protection by such polymers. Second, the techniques used to probe the polymer-membrane association may change the polymer properties and thereby the experimental observations may not reflect the real mechanism in living tissue. For example, fluorescent dye labelling on polymers could efficiently track the location of polymers in cells or animals. However, the addition of the dye molecule to the polymer structure could alter the hydrophobic-hydrophilic balance of the polymers and affect the interaction with the membranes. Therefore, the chemistry of the dye needs to be carefully selected and evaluated using control experiments. Additionally, the gap between model membranes and real cell membranes needs to be filled. Most mechanistic studies in the literature are based on model membranes. However, some inconsistency of polymer behavior in model membrane systems and in cellular assays have been found. Grozdova and coworkers showed that the

poloxamer binding efficiency with cells increases as the PEO block length increases, whereas the partitioning into artificial lipid bilayers decreases upon increasing PEO block length.[217] In this context, more investigation is needed on how the composition of cell membranes versus simple lipid bilayers affects polymer-membrane association.

1.5 Overview of Thesis

This interdisciplinary work aims at developing a fundamental understanding of polymer-membrane association that could be applied to solve real-world challenges in DMD therapy. More specifically, the goals of this project are as follows: (1) to investigate the fundamental mechanism of the interactions between PPO-PEO block copolymers and lipid membranes; (2) to assess the membrane stabilization efficacy of the copolymers with various molecular weights, hydrophilic-hydrophobic balance, block architectures, and polymer solution concentrations to understand the structure-property relationship; and (3) to design improved polymers as membrane stabilizers to optimize the therapeutic approach of cell membrane stabilization for DMD based on (1) and (2). To accomplish these goals, we first synthesized PPO-PEO diblock copolymers as complements to the commercial triblock Pluronics so that the molecular parameters (*e.g.*, individual block length, endgroup chemistry, etc.) could be systematically tuned. Following the synthesis, the polymer-membrane association was studied by quantifying the polymer binding to vesicular lipid bilayers using the pulsed-field gradient NMR technique (PFG-NMR), which reveals how polymer structure dictates their interaction with the membranes. Large unilamellar vesicles were used as a simplified model for real cell membranes in our study due to the ease of

preparation and relative vesicle stability. Also, the model bilayer system enabled us to modify the membrane composition and curvature, which has not been well studied in the literature. The PFG-NMR technique is a simple yet powerful method to explore polymer binding to liposomes since it overcomes the two challenges as mentioned in the last section. First, the high resolution of PFG-NMR enables the characterization of extremely weak interactions as it can detect polymer binding as low as 0.1%. Second, no molecular modification of the polymers or membranes is required, which eliminates potential artifacts associated with other techniques as noted above. The protective effect of polymers was evaluated on model damaged membranes, which provides an alternative screening method for further *in vitro* and *in vivo* studies of polymer stabilization efficacy conducted by our collaborators. The effective polymer formulation *in vivo* was correlated with the polymer binding determined on model membranes, which could provide insights on the molecular mechanism of polymer protection and thereby further guide a rational design of polymer structure that can improve the stabilization efficacy for DMD.

Chapter 2 describes the experimental techniques used throughout this thesis, including polymer synthesis and characterization, liposome preparation and characterization, quantification of polymer binding to liposomes, and the screening method of polymer protection efficacy. Polymers were synthesized by anionic polymerization and characterized by matrix-assisted laser desorption/ionization (MALDI) mass spectroscopy, size exclusion chromatography (SEC), and ^{1}H nuclear magnetic resonance spectroscopy (NMR). Liposomes were prepared by the extrusion method and characterized by dynamic light scattering (DLS), cryogenic transmission electron microscopy (Cryo-TEM), and

small-angle neutron scattering (SANS). Polymer binding to liposomes was determined by PFG-NMR. The screening method of polymer protection efficacy used liposomes as the model membranes and lipid peroxidation as the model stress to introduce damage to the lipid bilayers. The molecular weight and dispersity of polymers and some representative results of liposome characterization are also included in this chapter.

In Chapter 3, the interactions between polymers and lipid bilayers are described from the polymer perspective. The polymer-membrane association was investigated by quantifying the polymer binding to unilamellar liposomes. The effect of polymer molecular weight, composition (*i.e.*, individual block length and endgroup chemistry), and concentration on their binding to membranes was investigated and it was found that polymers with larger molecular weight and higher hydrophobicity have stronger binding.

In Chapter 4, the polymer-membrane association was explored from the membrane perspective, where the concentration of cholesterol in the bilayer and the bilayer curvature were varied. Polymer binding significantly decreases as cholesterol concentration increases, whereas the binding was less affected by bilayer curvature. The results demonstrate that cholesterol plays a dominant role.

Chapter 5, an extension of Chapter 4, investigates how membrane composition affects binding with the block copolymers. The influence of lipid headgroup and the degree of unsaturation of lipid alkyl chains on polymer-membrane interaction were explored. We found that polymer binding is significantly enhanced as the lipid headgroup is switched from a choline to a glycerol group, possibly due to hydrogen bonding formation between the ether oxygen of the polymers and the glycerol groups of lipids. Additionally, varying

the degree of unsaturation of lipid alkyl chains revealed that the liposomes with two mono-unsaturated hydrocarbon chains have stronger binding with polymers, compared to those with one saturated chain and one mono- or poly-unsaturated chain.

Chapter 6 presents a screening method that can be applied to assess the protection efficacy of polymers on damaged membranes. The effect of polymer architecture, overall molecular weight, and hydrophilic-hydrophobic balance was investigated. The polymer protection efficacy was further compared with their performance in a cellular essay and in animal models, which were conducted by our collaborators.

Chapter 7 presents some preliminary results on the association of bottlebrush polymers with lipid bilayers, characterized by PFG-NMR and the lipid peroxidation assay. Polymer protection efficacy screened by the lipid peroxidation assay indicates that bottlebrush PEO can be potentially used as membrane stabilizers. The binding of a bottlebrush diblock PPO-PEO is significantly lower than that of a linear triblock poloxamer with similar molecular weight and PEO wt. %, which might be attributed to higher rigidity of the bottlebrush polymer due to its crowded side chains.

Chapter 8 summarizes the key findings shown in this thesis and discusses potential future directions for this project with some preliminary results.

Chapter 2 - Experimental Techniques

* Adapted with permission from Zhang, W.; Haman, K. J.; Metzger, J. M.; Hackel, B. J.; Bates, F. S.; Lodge, T. P. *Langmuir* **2017**, *33*, 12624–12634. Copyright © 2017 American Chemical Society, and from Zhang, W.; Coughlin, M. L; Metzger, J. M.; Hackel, B. J.; Bates, F. S.; Lodge, T. P. *Langmuir* **2019**, *35*, 7231−7241. Copyright © 2019 American Chemical Society.

This chapter describes the experimental techniques used in Chapters 3-7. The synthesis of linear diblock copolymers using anionic polymerization is introduced and the experimental procedures are included in Section 2.1. Polymer characterization including size exclusion chromatography (SEC) and matrix-assisted laser desorption/ionization mass spectroscopy (MALDI) are provided in Section 2.2. Liposomes were prepared by the extrusion method as described in Section 2.3. The resulting unilamellar liposomes were

characterized by various techniques including dynamic light scattering (DLS), cryogenic transmission electron microscopy (Cryo-TEM), and small-angle neutron scattering (SANS) as discussed in Section 2.4. Pulsed-field-gradient NMR (PFG-NMR, also known as diffusion-ordered spectroscopy (DOSY)) was employed to quantify polymer binding to liposomes as described in Section 2.5. A screening method of polymer stabilization efficacy on damaged lipid membranes using lipid peroxidation as a model stress is introduced in Section 2.6.

2.1 Polymer Synthesis

PPO-PEO diblock copolymers were synthesized by sequential anionic polymerization. Reaction setup and monomer purification followed procedures described elsewhere.[218–220] All reactions occurred in an air- and water-free environment, using tetrahydrofuran (THF) as the solvent. To synthesize diblock copolymers with a *tert*-butyl endgroup ($tPPO_{14}$-PEO_{46}, $tPPO_{14}$-PEO_{78}, $tPPO_{14}$-PEO_{159} and $tPPO_{29}$-PEO_{68}, where "t" stands for the *tert*-butyl endgroup and the subscripts denote the number average degrees of polymerization), PO monomer was first initiated with potassium *tert*-butoxide at room temperature, followed by successive addition of PO monomers in the presence of 18-crown-6 ether (freeze-dried, 2:1 molar ratio to *tert*-butoxide) to reduce side reactions. The three main side reactions are shown in Figure 2.2, which arise from the high acidity of the methyl protons of PO.[221] This leads to additional types of termination and chain transfer reactions, which would give a broad distribution of synthesized polymers. Ding *et al.* reported that in the presence of 18-crown-6 ether, the anionic polymerization of bulk PO prefers propagation rather than the

generation of unsaturation by the side reactions.[218,222,223] The potassium cation is complexed inside the ring structure of the crown ether to form ligand-separated ion pair aggregates that favor propagation steps.[222] Allgaier *et al.* also showed that with the help of crown ether, the reaction temperature can be reduced to −23 °C without significantly extending the reaction time of the polymerization.[221] Hence, another strategy to reduce the side reactions is to add an ice water bath for the reactor. The reaction was terminated by excess acidic methanol (1:10 37 w/w% hydrochloric acid:methanol) after 48 h. The synthetic scheme for the PPO block is shown in Figure 2.1a. The PPO block was recovered by filtering out the precipitates of potassium salts and crown ether complexes and evaporating all the THF solvent. To grow the second PEO block from the PPO block, the hydroxyl endgroup on the PPO block was reinitiated with freshly made potassium naphthalenide at 45 °C, followed by 24 h propagation and termination of the PEO block, as shown in Figure 2.1b. *Tert*-butyl PPO-PEO diblock copolymers were recovered by filtration and dialysis to remove potassium salts and naphthalene. The polymer was finally freeze-dried from benzene to obtain a fine white powder, which was subjected to molecular characterization.

To synthesize a PPO-PEO diblock copolymer with a hydroxyl endgroup on the PPO block ($hPPO_{13}$-$PEO_{43}m$, where "h" represents the hydroxyl endgroup on the PPO block and "m" represents the methyl endgroup on the PEO block), a commercial monomethoxy-PEO (2000 g/mol) was initiated with freshly made potassium naphthalenide at 45 °C, followed by propagation in the presence of 18-crown-6 ether to improve the conversion of the PPO block. The reaction was terminated after 36 h by the addition of acidic methanol.

The synthetic scheme is shown in Figure 2.1c. The final product was recovered by filtration, dialysis and freeze-drying.

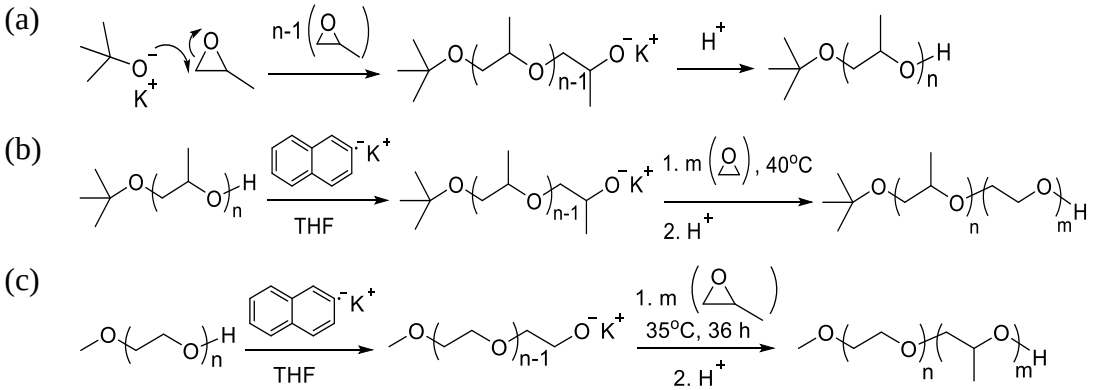

Figure 2.1. (a) Initiation, propagation and termination of PPO block by anionic polymerization. (b) Reinitiation of hydroxyl-terminated PPO block, followed by propagation and termination of the PEO block to form tPPO-PEO diblock copolymer. (c) Initiation of monohydroxyl-terminated PEO block, followed by propagation and termination of the PPO block to form hPPO-PEO diblock copolymer.

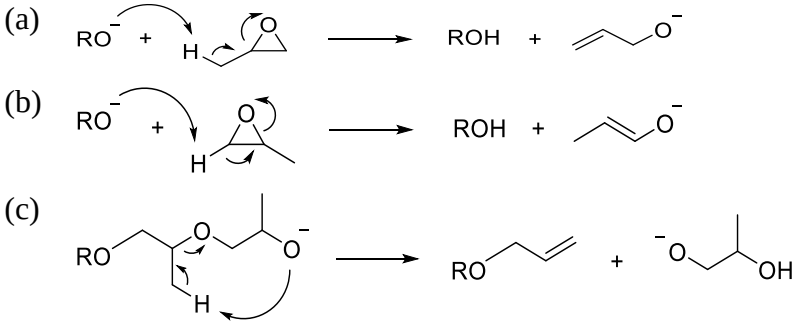

Figure 2.2. Three side reactions during the anionic polymerization of PPO.[221]

2.2 Polymer Characterization

The number-average molecular weight (M_n) and dispersity ($Đ$) of each polymer were determined by both MALDI mass spectrometry (AB SCIEX TOF/TOF 5800) SEC (Phenogel columns, Phenomenex) with a multi-angle laser light scattering detector (Wyatt

DAWN) and THF as the mobile phase. MALDI samples were prepared by mixing 0.2 mL of a matrix solution (20 mg/mL α-cyano-4-hydroxycinnamicacid in THF), 5 µL of a salt solution (1 mg/mL silver trifluoroacetate in THF), and 0.1 mL of a polymer solution (1 mg/mL in THF). Note that MALDI shows a bimodal distribution for commercial triblock copolymers due to diblock contamination, as shown in Figure 2.3. The small peak with lower molecular weight of F68 in Figure 2.3a due to diblock contaminant was not clearly resolved in Figure 2.3b. The large peak with lower molecular weight of F127 in Figure 2.3c corresponds to the shoulder of the SEC trace in Figure 2.3d. An estimate of the diblock contaminant in commercial F127 is 30 wt.% based on the integration of the area under the shoulder in Figure 2.3d. An estimate of the diblock contaminant in F68 is 7.7 wt.%, which is calculated from the ratio of the integration of the area of the small peak in Figure 2.3a to that in Figure 2.3c and the estimated diblock contaminant in F127 from SEC. The intensity of the peak with smaller molecular weight is greater than the one with larger molecular weight for F127, since MALDI preferentially samples lower molecular weights. Thus M_n and $Đ$ values of the commercial triblock copolymers as characterized by MALDI are based on the larger molecular weight peaks only. SEC samples were prepared as 10 mg/mL polymer solution in THF. The refractive index increment (dn/dc) for each polymer was estimated as the weight average of PPO (dn/dc = 0.087 mL/g) and PEO (dn/dc = 0.068 mL/g).[224,225] Polymer compositions (w_{PEO}) were calculated from the molar ratios characterized by ^{1}H NMR spectroscopy (Bruker AV-500) in $CDCl_3$. Table 2.1 summarizes M_n, $Đ$, w_{PEO}, and the corresponding average number of repeat units of PO (N_{PO}) and EO (N_{EO}).

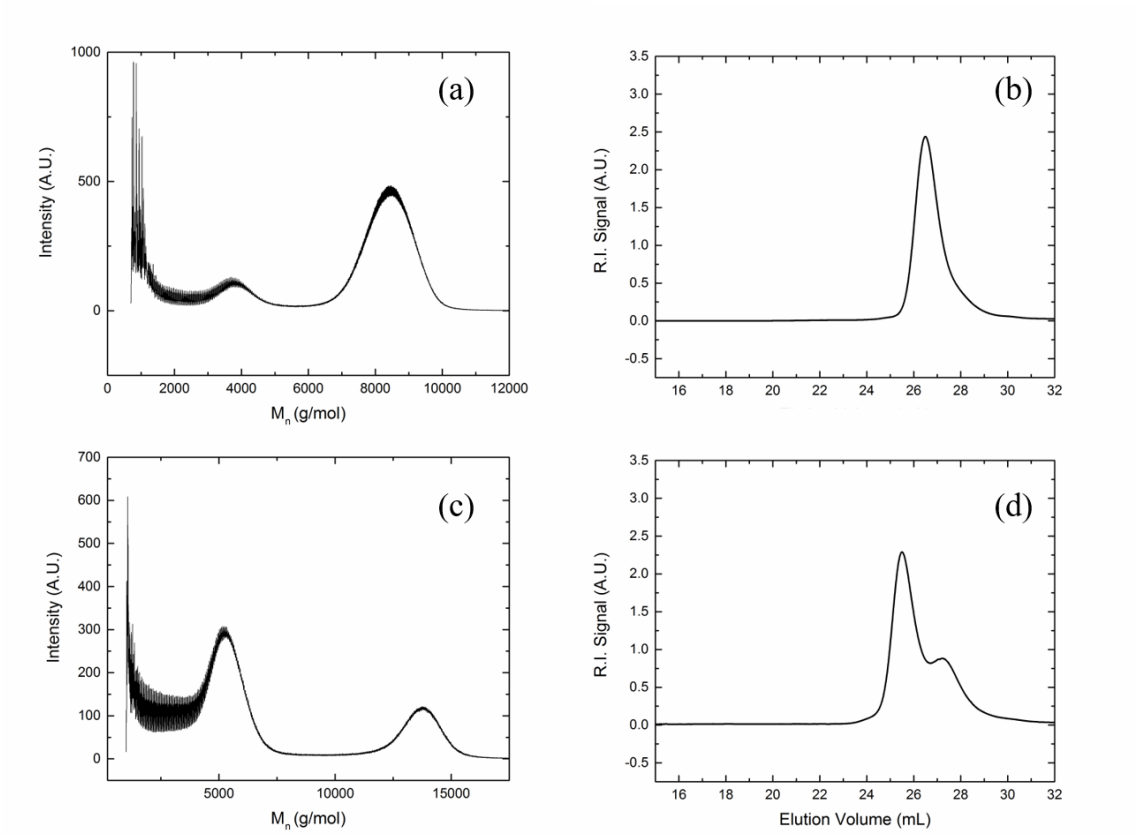

Figure 2.3. MALDI spectra of (a) F68 and (c) F127, using CHCA as the matrix and AgTFA as the salt. SEC traces of (b) F68 and (d) F127 in THF at a flow rate of 1 mL/min.

Table 2.1. Polymer Characterization.

	$M_{n,1}$[a] (g/mol)	$M_{n,2}$[b] (g/mol)	$M_{n,3}$[c] (g/mol)	$Đ$[b]	$Đ$[c]	$w_{PEO,1}$[a]	$w_{PEO,2}$[d]	N_{PO}[e]	N_{EO}[e]
F68	8,400	8,200	7,900	1.01	1.04	0.80	0.81	27	75
F108	14,600	15,900	14,700	1.01	1.04	0.80	0.82	49	148
F87	7,700	7,700	8,000	1.01	1.15	0.70	0.70	40	61
F127	12,600	13,200	10,800	1.01	1.07	0.70	0.72	64	108
P103	4,950	5,200	4,600	1.02	1.14	0.30	0.33	60	19
P104	5,900	5,700	5,300	1.02	1.18	0.40	0.42	57	27
P105	6,500	6,500	5,700	1.02	1.12	0.50	0.50	56	37
L35	1,900	1,900	2,100	1.04	1.13	0.50	0.48	17	10
P65	3,400	3,400	3,200	1.03	1.16	0.50	0.49	30	19
P84	4,200	4,200	3,600	1.03	1.05	0.40	0.42	42	20
$hPPO_{13}$-$PEO_{43}m$	-	2,600	2,700	1.02	1.08	-	0.72	13	43
$tPPO_{14}$-PEO_{46}*	-	2,900	3,000	1.03	1.07	-	0.70	14	46
$tPPO_{14}$-PEO_{78}	-	4,300	3,900	1.03	1.08	-	0.80	14	78
$tPPO_{14}$-PEO_{159}*	-	7,900	7,500	1.01	1.05	-	0.89	14	159
$tPPO_{29}$-PEO_{68}*	-	4,700	4,900	1.04	1.10	-	0.63	29	68
PEO-8	8,000	8,600	8,700	1.01	1.03	1	1	0	195

[a]Specified by supplier.

[b]Determined by MALDI mass spectroscopy.

[c]Determined by SEC. Weight-average *dn*/*dc* was used with *dn*/*dc* = 0.068 for PEO and 0.087 for PPO.

[d]Determined from molar ratios by ^{1}H NMR spectroscopy.

[e]Calculated from number-average molecular weight ($M_{n,2}$) and weight fraction of PEO ($w_{PEO,2}$). For triblock Pluronics, N_{EO} represents the number of repeat units of EO in one PEO block.

*Synthesized by Dr. Karen Haman.

2.3 Liposome Preparation

The procedure to prepare liposomes was adapted and modified from methods detailed elsewhere.[107,156,157,226] First, phospholipids in chloroform were dried with argon to form a thin film of lipid on the wall of the glass vial. Trace amounts of chloroform were further removed under vacuum for 30 min. The phospholipids were then hydrated with water or salt solution and heated above the lipid phase transition temperature for 30 min. The lipid solution was vortexed every 5 min during the hydration process until the lipids were fully emulsified. The final liposome solution was obtained by extruding the lipid solution back and forth 27 times through a polycarbonate membrane with a specific pore size using an Avanti Mini-Extruder. The chemical structures of the liposome components used in this work are summarized in Figure 2.4.

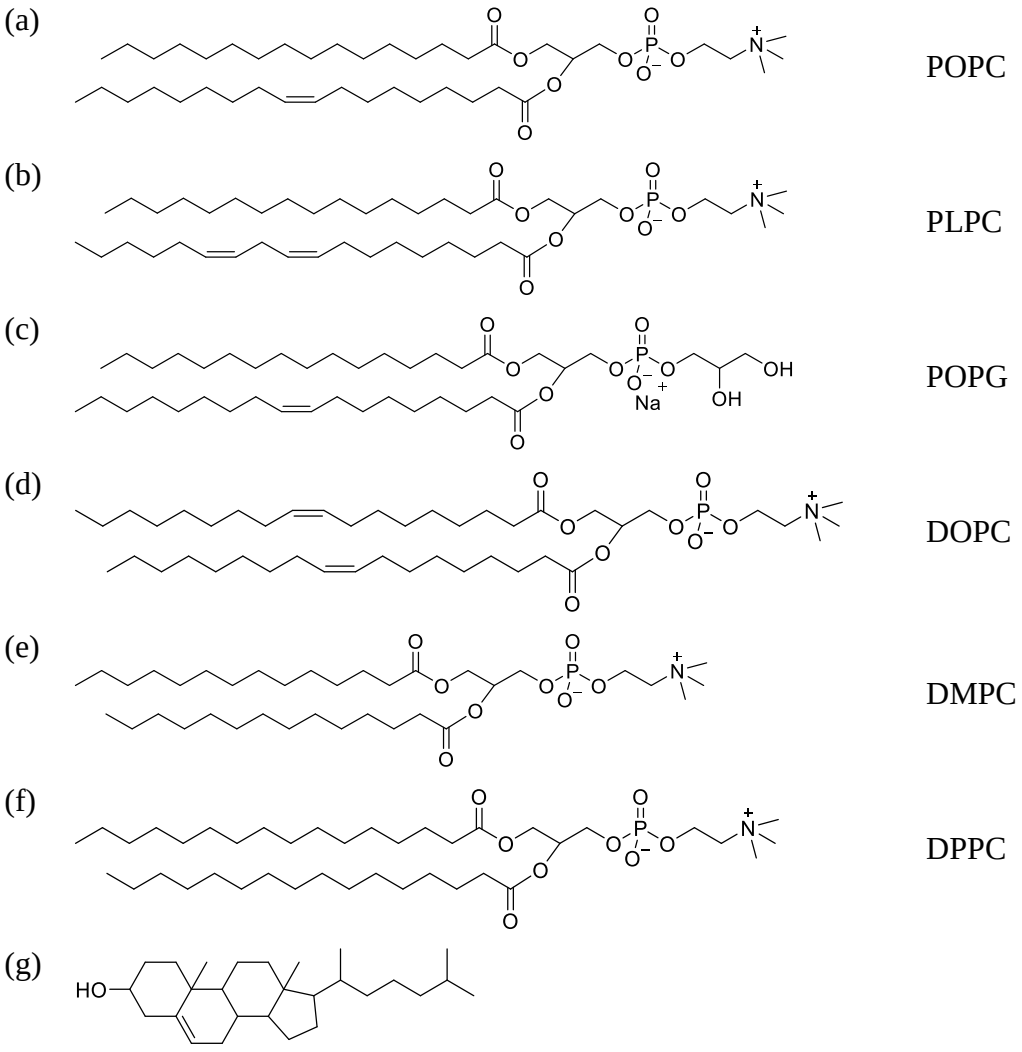

Figure 2.4. Chemical structures of (a) 1-palmitoyl-2-oleoyl-glycero-3-phosphocholine (POPC), (b) 1-palmitoyl-2-linoleoyl-sn-glycero-3-phosphocholine (PLPC), (c) 1-palmitoyl-2-oleoyl-sn-glycero-3-phospho-(1'-rac-glycerol) (POPG), (d) 1,2-dioleoyl-sn-glycero-3-phosphocholine (DOPC), (e) 1,2-dimyristoyl-sn-glycero-3-phosphocholine (DMPC), (f) 1,2-dipalmitoyl-sn-glycero-3-phosphocholine (DPPC), and (g) cholesterol.

2.4. Liposome Characterization

2.4.1. Dynamic Light Scattering (DLS)

Multi-angle DLS measurements were performed on a Brookhaven BI-200SM system with a laser wavelength of 637 nm at 27 °C. Each sample was measured at 5 scattering angles ranging from 60° to 120° in 15° increments in a temperature-controlled decalin bath that matches the refractive index of the sample cell. The resulting intensity autocorrelation functions were fit to a second-order cumulant expansion to acquire the mean decay rate Γ and dispersity, represented by the reduced second cumulant μ_2/Γ^2, at each angle. The mutual diffusion coefficient D_m was obtained from the linear fit of Γ vs. q^2, where q is the scattering factor (eq 2.1). The average hydrodynamic radius R_h was further calculated from D_m through the Stokes−Einstein relationship (eq 2.2). Liposome samples were diluted to 100 μM from the original stock solution for DLS measurements. All samples were filtered through 0.2 μm filters before measurements. An example of liposome size characterization by DLS was shown in Figure 2.5, using POPC liposomes extruded with 50 nm pore radius in D_2O as the sample solution.

$$\Gamma = D_m q^2 \tag{2.1}$$

$$D_m = \frac{k_B T}{6\pi\eta R_h} \tag{2.2}$$

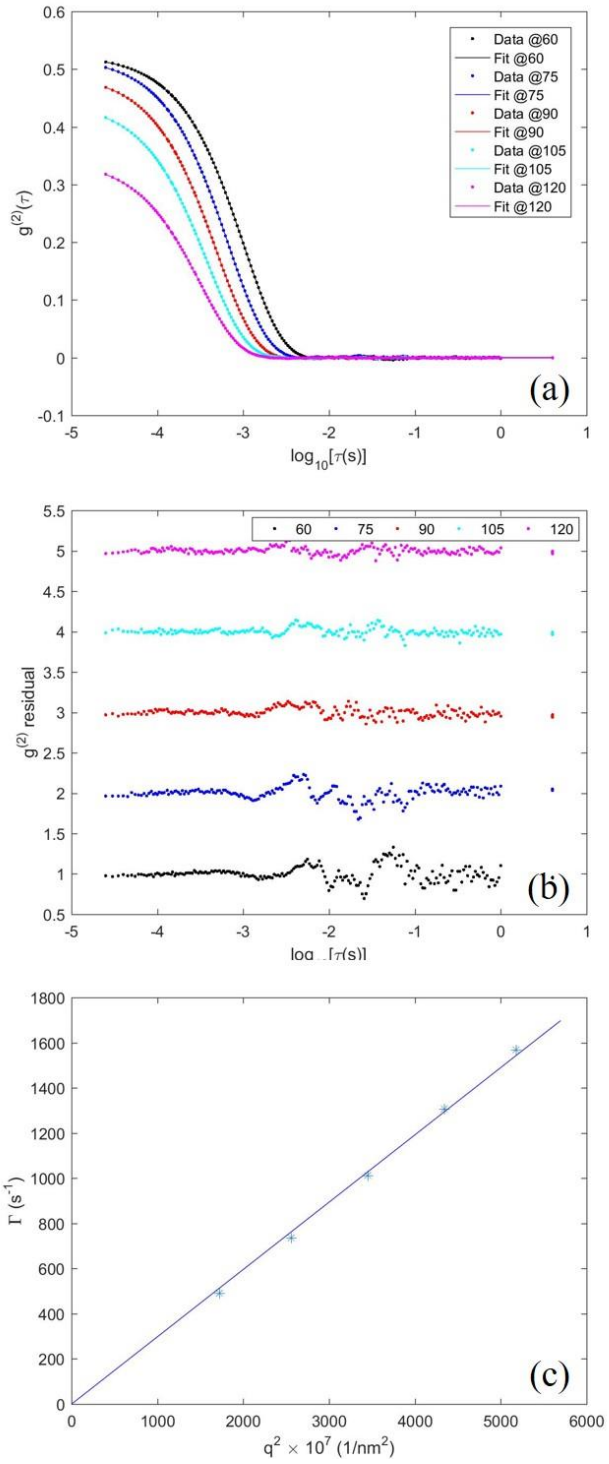

Figure 2.5. (a) DLS intensity autocorrelation functions fit to a second-order cumulant expansion, (b) the corresponding residuals, and (c) Γ versus q^2 plot of POPC liposomes extruded with 50 nm pore radius in D_2O measured at 27 °C. R_h was obtained as 70 nm with $Đ = 1 + \mu_2/\Gamma^2 = 1.04$.

2.4.2 Cryogenic Transmission Electron Microscopy (Cryo-TEM)

Solution samples were prepared for imaging using a FEI Vitrobot Mark IV vitrification system with the climate control chamber set to 27 °C and 100% humidity. 5 μL of the sample was pipetted onto a lacy carbon/Formvar grid (Ted Pella, 200 mesh) that was previously cleaned and hydrophilized using a PELCO easiGlow glow discharge cleaning system. The sample was annealed in the chamber for 1 s before the grid was blotted for 7 s with the instrument defined blot force set to –2, equilibrated for 3 s, and plunged into liquid ethane cooled by liquid nitrogen. The grids were then transferred into liquid nitrogen for storage prior to imaging. The vitrified sample grids were transferred to a Gatan-626 single tilt cryo-holder and imaged using a FEI Techni G2 Spirit Bio-Twin microscope operated at 120 kV coupled with a FEI Eagle CCD camera (2048 × 2048 pixels). A representative cryo-TEM image of liposomes was shown in Figure 2.6, using POPC liposomes extruded with 50 nm pore radius in D_2O as the sample solution.

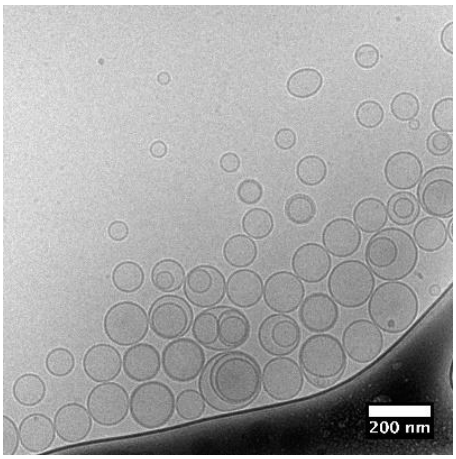

Figure 2.6. Cryo-TEM images of 10 mM POPC liposomes in D_2O extruded through a polycarbonate membrane with 50 nm pore radius.

2.4.3 Small-Angle Neutron Scattering (SANS)

SANS experiments were conducted on the NG-7 30m SANS beamline at the National Institute of Standards and Technology (NIST) Center for Neutron Research (Gaithersburg, MD). This instrument employed a wavelength of 8 Å, a wavelength spread ($\Delta\lambda/\lambda$) of 0.11, and sample-to-detector distances of 1, 4, and 15 m were used to collect scattering data. The corresponding q range is approximately 0.0007─0.4 A^{-1}, where the magnitude of the scattering vector q is defined $q = 4\pi\lambda^{-1} \sin(\theta/2)$ and θ is the scattering angle. The sample cells (0.1 cm thickness) were placed in a heating block to ensure the measurement at a temperature higher than the lipid phase transition temperature. The acquired 2D scattering patterns were reduced and azimuthally averaged to generate 1D plots of scattering intensity $I(q)$ versus q. Igor Pro package provided by NIST was used for data reduction that corrects for empty cell scattering, detector efficiency, background noise, and sample transmission. SasView software was used for fitting.

A representative SANS profile of neat liposomes is shown in Figure 2.7a. The Liposomes were prepared by tail deuterated lipids d54-DMPC in D_2O at 10 mg/mL lipid concentration, using an extrusion membrane of 50 nm pore radius. The sample was prepared and measured at 37 °C. The data profile was fit to a core multi-shell model. Table 2.2 summarizes the fitting results of core radius and thickness of each shell, according to the schematic of the lipid bilayer illustrated in Figure 2.7b. The thickness of shell 1 and 3 are assumed to be equal since they both represent the headgroups of lipids. A nonsymmetrical Schultz distribution with $\sigma/\mu = 0.28$ was applied to account for the polydispersity, where σ is the mean of the distribution and μ is standard deviation.

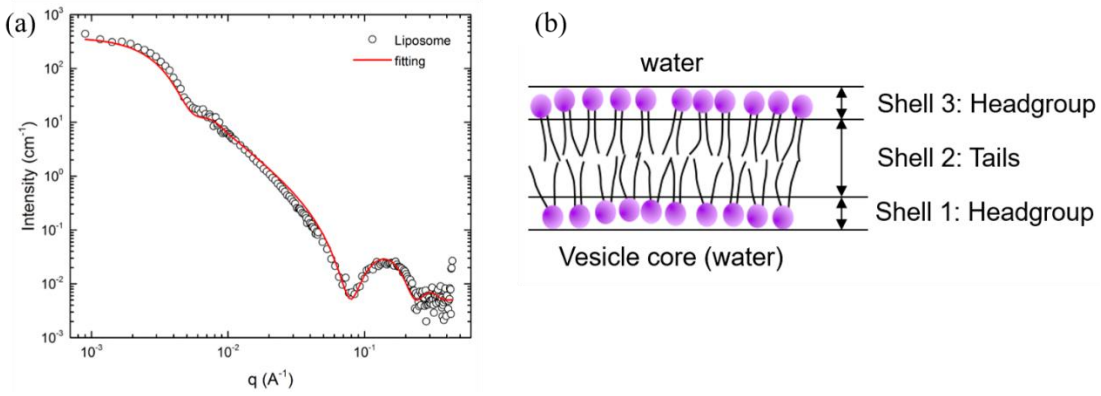

Figure 2.7. (a) SANS data and fitting of neat DMPC liposomes at 10 mg/mL in D_2O at 37 °C. Data were collected and analyzed in collaboration with Dr. Mihee Kim. (b) Schematic of the lipid bilayer corresponding to the spherical core-shell model.

Table 2.2. Core radius and shell thickness of vesicular lipid bilayer according to the core-shell model.

	Thickness (Å)	**Scattering length density (10^{-6} Å^{-2})**
Shell 3	13	4.40
Shell 2	25	6.90
Shell 1	13	4.40
Core	430	6.39

2.5 Quantification of Polymer Binding

A Bruker Avance III 500 MHz NMR instrument with a 5 mm broadband fluorine observe (BBFO) probe was employed for pulsed-field-gradient NMR (PFG-NMR) measurements, using the "ledbpgp2s" stimulated pulse sequence (longitudinal eddy current delay experiment using bipolar gradients acquired in 2D).[227] The echo-attenuated intensity I was recorded from each 1D ^{1}H spectrum corresponding to increasing gradient strengths G (from 2% to 95% of the maximum gradient strength). The translational diffusivity (D) of the samples was extracted from the linear fit based on the following relationship:

$$\ln\left(\frac{I}{I_0}\right) = -\gamma^2 G^2 \delta^2 D\left(\Delta - \frac{\delta}{3}\right) \tag{2.3}$$

where I_0 is the intensity with respect to zero gradient strength and γ is the gyromagnetic ratio of ^{1}H (42.6 MHz/T). The length of the gradient pulse δ was set to 5 ms, and the diffusion time Δ set to 300, 500, and 700 ms for polymer-liposome mixtures, and 700 ms for pure polymer solutions. Data were analyzed by the Topspin 3.5 software package.

Polymer-liposome mixtures were prepared by combining 0.25 mL of 10 mM liposome stock solution with 0.25 mL of polymer stock solution (polymer concentration is specified

in Chapter 3, 4, and 5). Pure polymer and pure liposome samples were prepared as controls by adding 0.25 mL of the solvent (D_2O with or without salt added) to 0.25 mL of the polymer and liposome stock solutions, respectively. All samples were measured at 27 °C with a temperature fluctuation less than ± 0.3 °C (indicated by the temperature monitor inside the NMR equipment). We found that the incubation time of polymers with liposomes prior to measurements has little influence on polymer binding (see Table 3.3). Therefore, all the freshly made samples were measured with no further incubation. Also, the binding of each polymer was only measured once due to high reproducibility (see Table 3.4).

Figure 2.8 shows the ^1H NMR spectrum of a 5 mM POPC liposome solution in D_2O containing 1 mg/mL P105 as a representative polymer. The proton peaks of PEO (labeled "a") and choline head groups (labeled "c") were selected to probe the diffusion of polymer and liposome, respectively. Note that the signal intensity of the alkyl chains (labelled "e") is weaker than that of choline head groups, despite of more protons in the alkyl chains. It could due to poor solubility of the alkyl chains. The interactions between polymers and lipid bilayers were investigated by comparing the diffusion of polymers with and without liposomes. Taking P105 as an example in Figure 2.9, the logarithmic normalized echo-attenuated intensity $\ln(I/I_0)$ of the polymer in the absence of liposomes (open circles) decreases linearly with the quantity $\gamma^2G^2\delta^2(\Delta-\delta/3)$ according to eq 2.3, indicating that polymer molecules undergo simple translational diffusion in water and that there is no micelle formation.

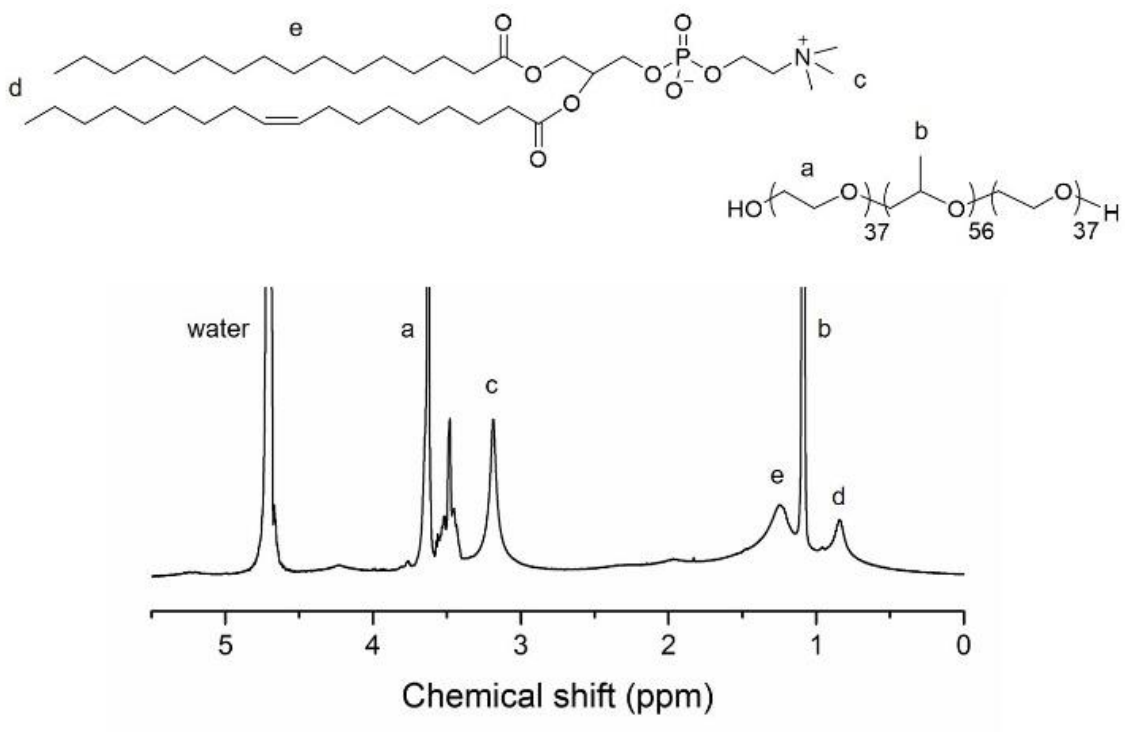

Figure 2.8. ^{1}H NMR spectrum of 1 mg/mL P105 in 5 mM POPC liposome in D_2O.

For polymers in the presence of liposomes, however, the echo decay curves (filled symbols in Figure 2.9) are no longer linear, which means that the diffusion of the polymers cannot be described by eq 2.3. In the mixed solution, a certain amount of polymer interacts with the lipid bilayers, whereas the remaining polymers are still free coils. The diffusion of the bound polymer is hindered by the liposome, so that it is reasonable to assume that the bound polymers have the same diffusivity as that of the liposome, which is at least one order of magnitude slower than that of free polymers. The difference in polymer mobility gives rise to two decay processes: a rapid decay corresponding to free polymers in the mixture, and a slower decay corresponding to the polymers associated with the lipid membranes. The initial slope of the echo decay curves, D_{free}, coincides with that in the

absence of liposomes because the echo-attenuated intensity is dominated by the signal from free polymers at low $\gamma^2G^2\delta^2(\Delta-\delta/3)$. The intensity from rapid diffusion is completely attenuated at high $\gamma^2G^2\delta^2(\Delta-\delta/3)$, where the slope represents the diffusion coefficient of the polymers associated with the lipid bilayers, D_{bound}. The three echo decay curves of the polymers in the presence of liposomes measured at fixed δ (5 ms) and various Δ (300, 500 and 700 ms) almost overlap, which implies that the molecular exchange rate between the free polymers and the polymers bound to liposomes is very slow on the time scale of the diffusion experiments. Thus we can quantify the interaction of polymers with lipid bilayers by fitting the echo decay curves with a simple biexponential model, as shown in eq 2.4,[228] assuming that molecular exchange between bound and free states is negligible.

$$\frac{I}{I_0} = f_{\text{bound}} \cdot \exp\left(-\gamma^2 G^2 \delta^2 D_{\text{bound}} \left(\Delta - \frac{\delta}{3}\right)\right) + (1-f_{\text{bound}}) \cdot \exp\left(-\gamma^2 G^2 \delta^2 D_{\text{free}} \left(\Delta - \frac{\delta}{3}\right)\right) \quad (2.4)$$

D_{free} was obtained from the slope of the echo decay curves of the polymer in the absence of liposomes, whereas D_{bound} was obtained from the final slope of the curves of the polymer in the presence of liposomes. The diffusion coefficient of the liposome in the mixture was also used to estimate D_{bound} if the interaction between the polymers and lipid membranes is too weak to give a reliable slope of the final plateau. In all cases the extracted values of D_{bound} were within 20% of the diffusion coefficient of free liposomes. The only fitting parameter in eq 2.4 is f_{bound}, which represents the molar percentage of the polymer molecules bound to the liposomes.

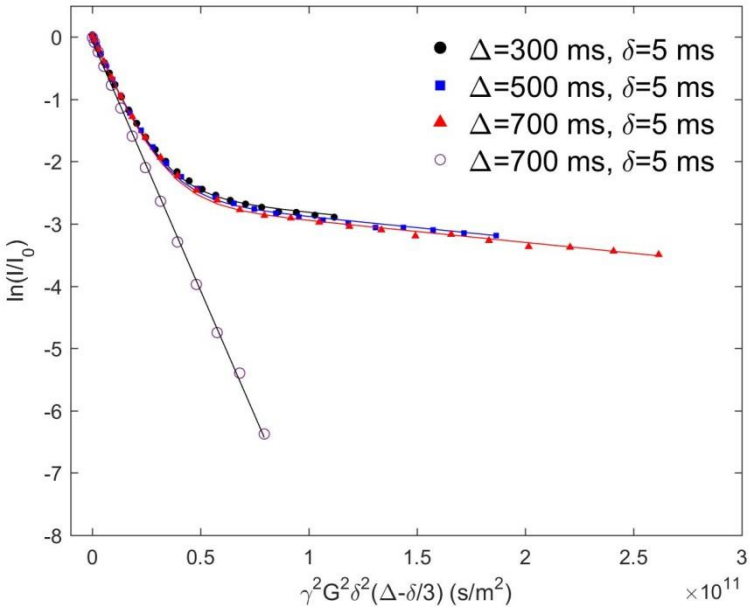

Figure 2.9. Experimental and fitted echo decay curves of the protons from PEO of 1 mg/mL P105 in the presence of 5 mM POPC liposome in D_2O at 27 °C with Δ = 300, 500, 700 ms (filled circles, filled squares, and filled triangles, respectively) and with fixed δ = 5 ms. The data were fit to eq 2.4. The open circles denote the proton signal from PEO of 1 mg/mL P105 in the absence of liposomes; these data were fit to eq 2.3.

2.6 Screening of the Stabilization Efficacy of Block Copolymers

2.6.1 Liposome Peroxidation as a Model Stress

Lipid peroxidation is a type of naturally occurring damage that occurs with cell membranes.[229–233] The process can be initiated by short-lived activated chemical species known as reactive oxygen species (ROS), which are generated during the normal respiration process.[234] This type of oxidative damage to lipid-based cell membranes can be mimicked by liposome peroxidation induced by free radicals in a controlled fashion. Compared to other model stresses that can be applied to liposomes, such as mechanical force or osmotic pressure, lipid peroxidation is simpler to apply and more straightforward

to detect, which makes it ideal to mimic the damage for screening tests. One of the free radical generators that can be used for liposome peroxidation is 2,2-azobis(2-amidinopropane) dihydrochloride (AAPH).[235–238] It has good solubility in water and has steady rate of degradation under thermal/UV irradiation, which produces two peroxyl radicals per cleavage event, as shown in Figure 2.10a.[236,239]

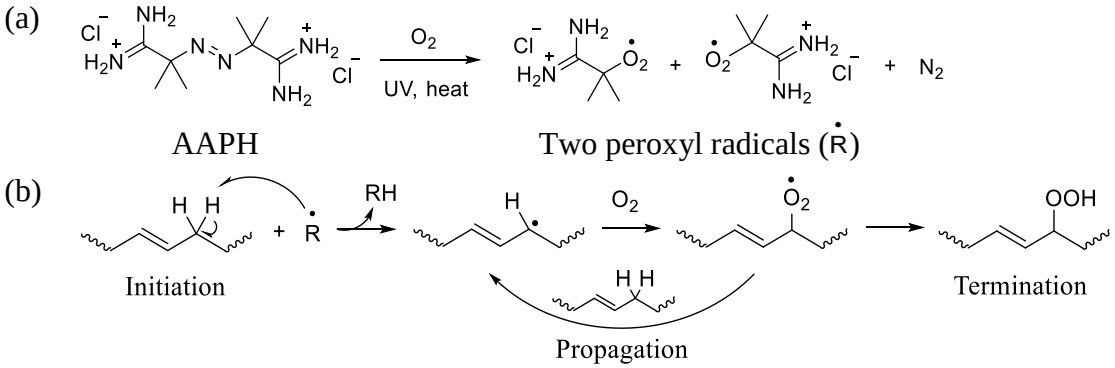

Figure 2.10. (a) Generation of peroxyl radicals from decomposition of AAPH.[236,239] (b) Mechanism of lipid peroxidation on unsaturated lipid tails.[234]

Following the initiation of free radicals, polyunsaturated fatty acid (PUFA) tails can be peroxidized on the carbon atoms next to the double bonds, since the hydrogen atoms become very reactive, as shown in Figure 2.10b.[234] The resulting hydroperoxyl group induces hydrophilicity in the lipid tails, which drives the alkyl chain to move towards the water/membrane interface and thereby significantly change the cross-section area and solubility of the lipid tails.[234] Moreover, cleaved lipids can be formed from hydroperoxide degradation as secondary products, which further affects the size and structural integrity of the liposome.[234,240,241] The propagation of lipid peroxidation eventually results in partial or full disruption of the liposome.

2.6.2 Polymer Stabilization Efficacy on Liposomes against Lipid Peroxidation

Polymer stabilization efficacy on cell membranes can be estimated using a liposome peroxidation assay.[6,107] The experimental schematic is shown in Figure 2.11. DLS was employed to measure the liposome size distribution and scattered intensity at each step. First, neat liposomes were prepared, which gives a narrow dispersity and a relatively high scattered intensity as shown in Figure 2.11 step 1. Second, free radicals were added to the liposome solution. Without the protection from polymers, liposomes were fully disrupted into single lipid molecules or small aggregates, resulting in extremely low scattered intensity (Figure 2.11 step 2). Also, the disrupted liposomes were unable to show a clear and narrow size distribution due to the extremely low intensity, on the same order of magnitude as background scattering. In this context, the scattered intensity and size distribution of neat liposomes at step 1 and negative control at step 2 (*i.e.*, bare liposomes followed by peroxidation) can be considered as two limits corresponding to full population and full rupture of the liposomes, respectively. The scattered intensity in between can be used to differentiate the level of liposome survival due to polymer protection. Note that an important assumption for this screening method is that the addition of polymers has little influence on the scattered intensity and the size distribution of liposomes, as polymers have negligible contribution to the scattered intensity compared to that of liposomes due to their much smaller size. Therefore, liposomes in the presence of polymers were measured to confirm that polymer addition has little effect (Figure 2.11 step 3). A similar level of scattered intensity and a similar size distribution to those at step 1 indicate that introducing

polymers into the system has no significant effect. Eventually, by introducing free radicals into the system as shown in Figure 2.11 step 4, liposomes were stabilized by polymers against lipid peroxidation to some extent since the association of the polymers with the lipid bilayers can slow down or block the diffusion of the free radicals into the lipid bilayer. Such a protective effect can be quantified based on the scattered intensity. Liposome size distribution can also qualitatively indicate polymer stabilization efficacy. If the polymers have poor protection, the liposome size distribution will become broader since the liposomes are partially disrupted. Altogether, the liposome scattered intensity along with the size distribution reveals the efficacy of polymer stabilization against lipid peroxidation. Higher scattered intensity and narrower size distribution of the liposomes indicate more effective protection of polymers.

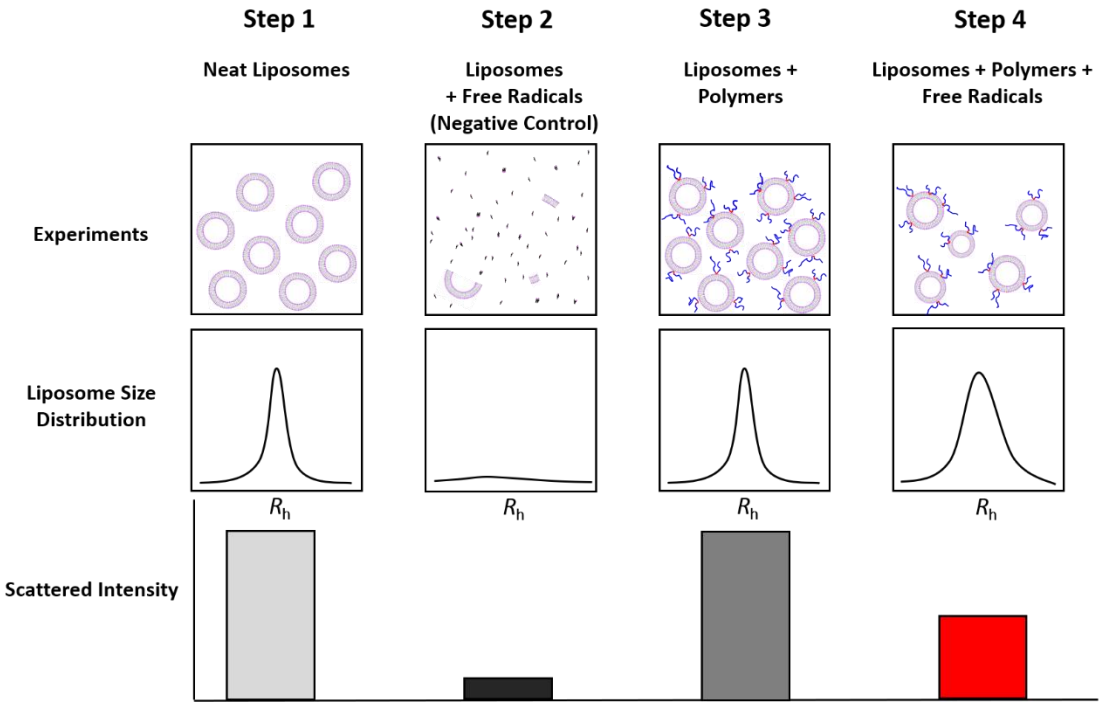

Figure 2.11. Experimental schematic of measuring polymer stabilization efficacy in a liposome peroxidation assay.

The liposomes were prepared following the procedures described in Section 2.3 to obtain a stock concentration of 100 μM. Polymer stock solutions were prepared at 5:1 and 10:1 molar ratio to the liposome stock solution (*i.e.*, 500 μM and 1000 μM, respectively). AAPH stock solution was prepared at 60 mM. At step 1, the neat liposome solution was prepared by diluting 0.25 mL of the liposome stock solution with 0.75 mL water to reach a final concentration of 25 μM liposomes for the DLS measurement. The samples at step 2 and 3 were prepared by adding 0.25 mL of AAPH stock solution and 0.25 mL of polymer stock solution to a mixture of 0.25 mL of liposome stock solution and 0.5 mL of water, respectively. The samples at step 4 were prepared by mixing 0.25 mL of liposome stock solution, polymer stock solution, AAPH stock solution and water. The peroxidation reaction was induced by AAPH under 30 min UV irradiation ((λ=254 nm) at 37 °C. The R_h and the scattered intensity of the samples were determined by multi-angle DLS at 25 °C.

Chapter 3 - Influence of Polymer Structure on Polymer-Membrane Association

3.1 Introduction

The effect of PPO-PEO block polymer structure on polymer-membrane association has been studied over the recent two decades. It has been shown that the hydrophobic PPO block length is a key determinant of the interaction mechanism with lipid bilayers according to both experimental and computational results.[102,106,108,201–203,205] Recently, on

the basis of an *in-vitro* cellular assay, it was found that the protection efficacy of PPO-PEO block copolymers on cell membranes is highly influenced by the polymer composition as well as the overall molecular weight.[100] In this context, the polymer structure plays a critical role in the interactions between PPO-PEO block copolymers and lipid membranes, which therefore determines the performance of polymers in both membrane stabilization and permeabilization. However, few studies have been able to quantify the association between polymer and membranes directly.

In this study, we investigate how polymer structure dictates the polymer-lipid membrane association systematically by quantitative measurements via pulsed-field-gradient NMR (PFG-NMR). Liposomes, or more specifically, large unilamellar vesicles (LUVs), were used as the model membrane system. The polymer species involved in this work all belong to the family of PPO-PEO block copolymers, as shown in Figure 1.1. In addition to commercial Pluronics (Figure 1.1a), diblock analogs with *tert*-butyl endgroups or hydroxyl endgroups on the PPO block were also synthesized as complements to the triblock architecture (Figure 1.1b and Figure 1.1c). Most relevant studies in the literature have been restricted to commercially available triblock copolymers. The inclusion of the diblock architecture expands the array of available structures within this chemical family, and thereby provides greater flexibility to manipulate molecular parameters systematically, such as the overall molecular weight, the hydrophobic and hydrophilic block lengths, and the endgroups. The interactions between polymers and lipid bilayers are quantified by PFG-NMR. After mixing a polymer solution with the liposome solution, a fraction of the polymer molecules associate with the lipid bilayers, while the majority remain as free coils

in the solution, as shown schematically in Figure 3.1. Since the polymers bound to the liposome move much more slowly than free polymers, two distinct polymer diffusivities (*i.e.*, free and bound) in the presence of liposomes can be characterized, and therefore the amount of polymer attached to the liposomes can be determined, assuming the exchange rate between the free and bound polymers is low.

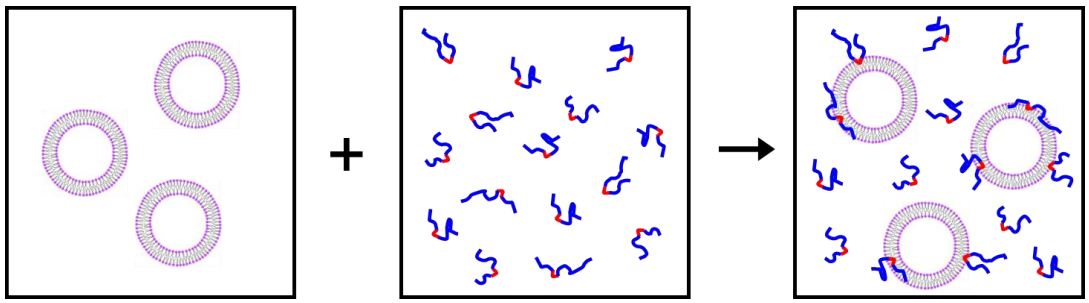

Figure 3.1. Schematic of interactions between block copolymers and liposomes. After mixing a liposome solution with a polymer solution, a fraction of the polymer molecules associates with the liposomes, whereas the others remain as free chains.

3.2 Experimental Section

Details of the experimental techniques used in this chapter were described in Chapter 2. The materials, sample preparation, and experimental procedures that are specific to this chapter are summarized below.

3.2.1 Materials

Pluronics F68, F108, F87, F127, P103, P104, P105, L35, P65, and P84 were provided by BASF. Ethylene oxide (EO, ≥ 99.5%), propylene oxide (PO, ≥ 99%), methoxy-terminated polyethylene glycol (methoxy-PEO, 2000 g/mol), potassium *tert*-butoxide, n-

butyllithium, potassium, naphthalene, and 18-crown-6 ether for anionic polymerization were purchased from Sigma-Aldrich and used as received, unless otherwise noted. PEO-8 (8000 g/mol) was purchased from EMD Millipore (Billerica, MA). 1-palmitoyl-2-oleoyl-*sn*-glycero-3-phosphocholine (POPC) in chloroform was purchased from Avanti Polar Lipids (Alabaster, AL) and used as received. Silver trifluoroacetate (AgTFA) and α-cyano-4-hydroxycinnamic acid (CHCA, ≥ 98%) for matrix-assisted laser desorption/ionization mass spectrometry (MALDI) characterization were also purchased from Sigma-Aldrich. Deuterium oxide (D_2O, 99.9 atom % D) and chloroform-d ($CDCl_3$, 99.8 atom % D + 0.05% V/V TMS) were purchased from Cambridge Isotope Laboratories, Inc.

3.2.2 Polymer Synthesis and Characterization

The diblock polymers used in this chapter were synthesized by anionic polymerization. The number-average molecular weight, dispersity, and composition of the polymers were summarized in Table 2.1.

3.2.3 Liposome Preparation and Characterization

POPC phospholipids in chloroform were first completely dried with argon to form a thin lipid film on the wall of the glass vial. The dry lipid film was then hydrated with D_2O to 10 mM and heated to 37 °C for 30 min, with vortex applied every 5 min to fully emulsify the lipids. Unilamellar liposomes (with a small amount of multilamellar liposome residuals)

were obtained by extruding the lipid solution through a polycarbonate membrane of 50 nm pore radius. The liposome size was characterized by DLS and PFG-NMR.

3.2.4 PFG-NMR Measurements

The NMR samples were prepared by mixing 0.25 mL of freshly made 10 mM liposome stock solution with 0.25 mL of polymer stock solution in D_2O at room temperature. Pure polymer and pure liposome solution were prepared as controls by adding 0.25 mL of D_2O to 0.25 mL of stock solutions of polymer and liposome at room temperature. The final liposome concentration in the samples is 5 mM, and the final polymer concentrations are listed in Table 3.1. All the samples were measured in D_2O at 27 °C without incubation.

3.3 Results and Discussion

The liposome solution was characterized by DLS (Figure 2.5) and PFG-NMR (Figure 3.2) to determine the mean hydrodynamic radius R_h. The R_h obtained from DLS is 70 nm with a dispersity $\mu_2/\Gamma^2 = 0.04$, whereas the R_h obtained from PFG-NMR is 41 ± 2 nm. We suspect that the difference between R_h measured by PFG-NMR and DLS is due to: (1) the probing time window of PFG-NMR is much smaller than that of DLS, which measures the full decay of liposomes, and (2) the DLS signal is weighted to larger structures. The self-diffusion coefficients of the free polymers measured by PFG-NMR are summarized in Table 3.1, indicating free chains at the concentration listed in the table. A representative PFG-NMR data profile for free polymers is shown by the open circles in Figure 3.4a. A

representative polymer F127, which has the lowest critical micelle concentration (CMC) among all the Pluronics employed in this study, was measured by DLS to determine the mean hydrodynamic radius R_h.[8] The echo decay curve of F127 along with the DLS measurements (Figure 3.3) confirmed that F127 are free coils in D_2O at 1 mg/mL at 27 °C.

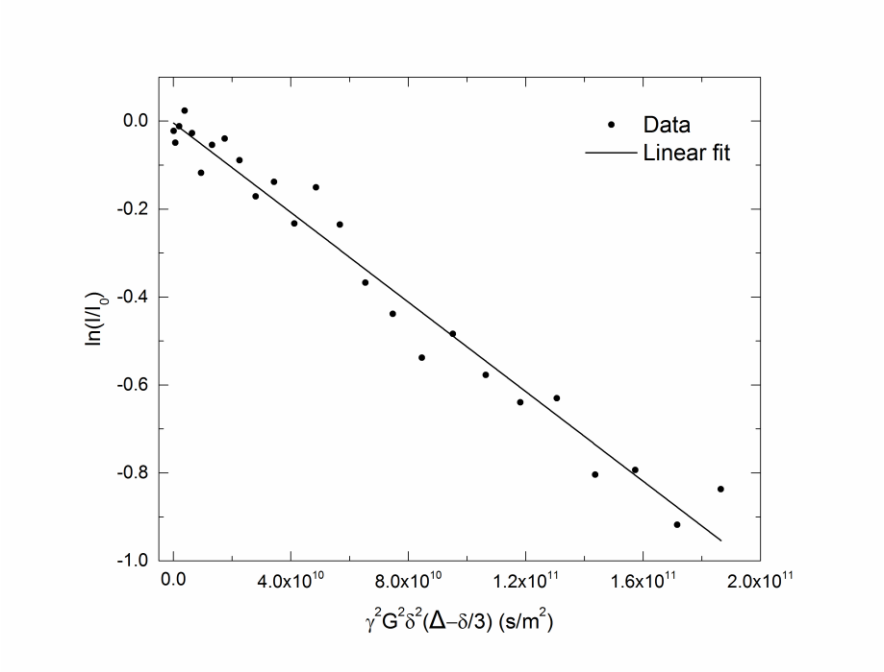

Figure 3.2. Experimental and fitted echo decay curves of the protons from the choline group of 5 mM POPC liposome solution in D_2O at 27 °C with Δ = 500 ms and δ = 5 ms. The data were fit to eq 2.3. The diffusion coefficient of the liposome $D_{lipo} = 5.1\times10^{-12} \pm 0.2\times10^{-12}$ m^2/s. The corresponding R_h is 41 ± 2 nm.

Table 3.1. Summary of fitting results and related parameters with corresponding errors.

	c (mg/mL)	D_{bound} [a] (10^{-11} m^2/s)	D_{free} [b] (10^{-11} m^2/s)	f_{bound} [c] (%)	N [d]	θ [e] (%)
F68	1	0.5*	6.8	0.10 ± 0.02	1 ± 1	0.2 ± 0.1
F108	0.2	0.5*	5.4	1.8 ± 0.2	2 ± 1	0.8 ± 0.2
F108	1	0.5*	4.9	0.9 ± 0.3	6 ± 2	1.8 ± 0.8
F87	1	0.6*	7.2	0.2 ± 0.1	2 ± 1	0.3 ± 0.1
F127	0.2	0.5	5.9	18.2 ± 0.7	30 ± 4	7.5 ± 1.4
F127	0.5	0.5	5.9	16.0 ± 0.7	66 ± 9	17 ± 3
F127	1	0.4	5.9	12.6 ± 0.6	104 ± 15	26 ± 5
L35	1	0.4	14.4	0.75 ± 0.02	43 ± 6	1.5 ± 0.3
P65	1	0.5	11.0	0.87 ± 0.02	28 ± 4	1.7 ± 0.3
P105	0.2	0.4	8.7	9.4 ± 0.6	32 ± 5	3.7 ± 0.7
P105	1	0.4	8.3	7.9 ± 0.4	132 ± 19	15 ± 3
P84	1	0.4	10.2	1.0 ± 0.1	26 ± 4	1.9 ± 0.4
P104	0.2	0.5*	9.2	8.5 ± 0.7	32 ± 5	3.2 ± 0.7
P104	1	0.4	8.6	6.3 ± 0.5	119 ± 19	12 ± 2
P103	0.2	0.5*	9.7	12.5 ± 1.3	53 ± 9	4.6 ± 1.0
$hPPO_{13}$-$PEO_{43}m$	1	0.6*	12.6	0.17 ± 0.03	7 ± 2	0.4 ± 0.1
$tPPO_{14}$-PEO_{46}	1	0.5*	11.7	0.5 ± 0.1	20 ± 4	1.0 ± 0.2
$tPPO_{14}$-PEO_{78}	1	0.5*	9.9	0.15 ± 0.04	4 ± 1	0.3 ± 0.1
$tPPO_{14}$-PEO_{159}	1	0.5*	6.7	0.14 ± 0.04	2 ± 1	0.3 ± 0.1
$tPPO_{29}$-PEO_{68}	1	0.6	9.2	1.9 ± 0.1	43 ± 6	3.7 ± 0.7
PEO-8	1	0.5*	6.5	0.1 ± 0.1	1 ± 1	0.2 ± 0.1

[a] Obtained from the final slope of the echo decay curves of the polymer in the presence of liposomes. *Estimated from the diffusion coefficients of liposome in the polymer-liposome mixture measured by PFG-NMR due to noisy data at the final slope.

[b] Obtained from the linear fit of the echo decay curves of polymer without the presence of liposome. Only the data points before 5.0×10^{10} s/m^2 $\gamma^2G^2\delta^2(\Delta-\delta/3)$ were used for the linear fit to ensure a strong signal since the signal of polymer decays very rapidly.

[c] Obtained from the average and standard deviation of the fitting results at Δ = 300, 500, and 700 ms based on eq 2.4.

[d] Calculated from eq 3.1. Error was propagated from that of f_{bound}.

[e] Calculated from eq 3.3. Error was propagated from that of f_{bound}.

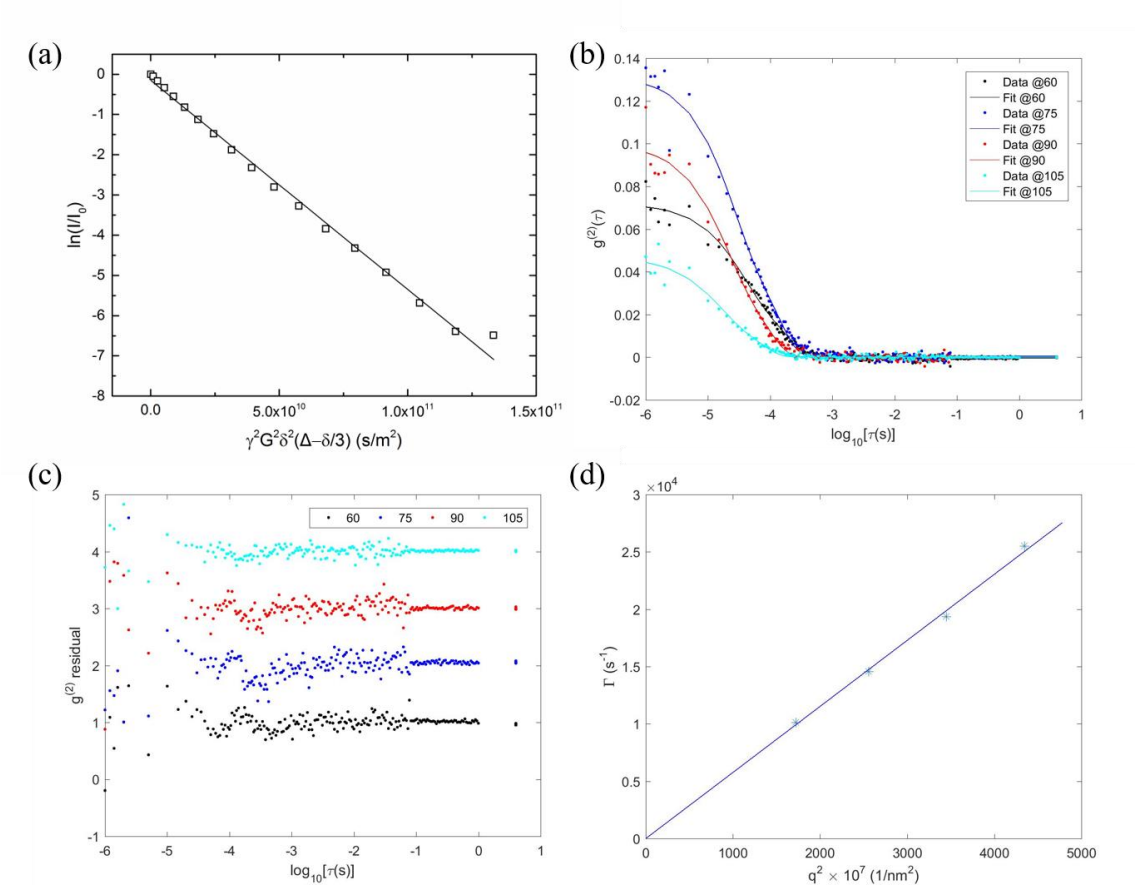

Figure 3.3. (a) Experimental and fitted echo decay curves of the protons from PEO of 1 mg/mL F127 in D_2O at 27 °C in the absence of liposome with Δ = 700 ms and δ = 5 ms. The data were fit to eq 2.3. The diffusion coefficient is D_{F127} = 5.9×10^{-11} m^2/s. The corresponding R_h is 4 nm. (b) DLS intensity autocorrelation functions and (c) the corresponding residuals of 1 mg/mL F127 in D_2O at 27 °C, using a second-order cumulant expansion fit. (d) Γ versus q^2 plot for 1 mg/mL F127 in D_2O. R_h was obtained as 4 nm, indicating free chains.

The binding percentage f_{bound} of various polymer species was obtained by fitting the echo decay curves of polymers in the presence of liposomes to a biexponential decay model (eq 2.4). An example of the fitting is shown in Figure 3.4a (filled symbols). The average number of bound polymer molecules per liposome, N, was further calculated by:

$$N = \frac{c}{M_n} \cdot \frac{f_{bound}}{\frac{n_{lipo}}{N_{tot}}} \tag{3.1}$$

where c is the mass concentration of polymer and n_{lipid} is the molar concentration of lipid molecules (5 mM) in the mixture solution. The number of POPC lipid molecules per liposome, N_{tot}, was estimated by:[242]

$$N_{tot} = \frac{4\pi R_{lipo}^2}{A} + \frac{4\pi\left(R_{lipo}\text{-}t\right)^2}{A} \tag{3.2}$$

where t is the thickness of POPC lipid bilayer (52 ± 2 Å),[243,244] A is the area per lipid (68 ± 2 Å^2),[245] and R_{lipo} is the radius of the liposome, approximated as R_h (41 ± 2 nm). The fraction of liposome surface area covered by bound polymer molecules, θ, was further estimated from N by:

$$\theta = N \cdot \frac{\pi R_g^2}{4\pi R_{lipo}^2} \tag{3.3}$$

where R_g is the radius of gyration of the polymer, as summarized in Table 3.2. This analysis assumes that the bound polymer occupies an area corresponding to the coil size in free solution. To visualize the polymer-lipid bilayer association, a schematic of surface coverage of half a liposome by 1 mg/mL P105 as a representative polymer is shown in Figure 3.4b. The zoom-in view depicts a possible mechanism of interaction between polymer and lipid bilayer: the hydrophobic PPO block inserts into the lipid bilayer interior, whereas the hydrophilic PEO blocks adsorb onto the head group of the lipid bilayer.[106]

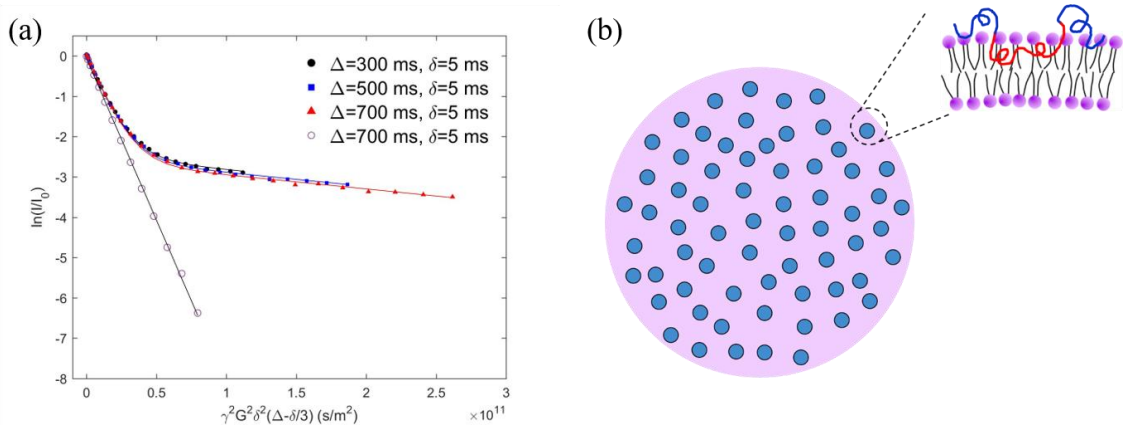

Figure 3.4. (a) Experimental and fitted echo decay curves of the protons from PEO of 1 mg/mL P105 in 5 mM POPC liposome solution in D_2O at 27 °C with Δ = 300, 500, 700 ms (filled circles, filled squares, and filled triangles, respectively) and with fixed δ = 5 ms. The data were fit to eq 2.3. The open circles denote the proton signal from PEO of 1 mg/mL P105 in the absence of liposomes; these data were fit to eq 2.4. (b) Schematic of surface coverage of a half liposome by P105. The pink circle represents the surface area of a half liposome, and the small particles represent the estimated cross sectional area of polymer molecules associated with the lipid bilayer, using R_g in a theta solvent as the estimated polymer radius. The zoomed-in view shows one possible interaction between a polymer and the lipid bilayer.

Table 3.2. Summary of calculated radius of gyration of polymers.

Polymer	R_g (nm)[a]
F68	3.3
F108	4.6
F87	3.1
F127	4.1
P103	2.4
P104	2.6
P105	2.8
L35	1.5
P65	2.0
P84	2.2
$hPPO_{13}$-$PEO_{43}m$	1.8
$tPPO_{14}$-PEO_{46}	1.9
$tPPO_{14}$-PEO_{78}	2.4
$tPPO_{14}$-PEO_{159}	3.2
$tPPO_{29}$-PEO_{68}	2.4
PEO-8	3.4

[a]Calculated from the number of repeat units of the polymer and statistical segment length of PEO (6 Å), assuming theta solvent conditions.

Note that the incubation time of polymers with liposomes prior to measurement apparently has little effect on polymer binding, as Table 3.3 shows that the binding percentage f_{bound} does not change appreciably from no incubation to 1-week incubation at room temperature, for all four selected polymers (P103, P104, P105 and F108 at 0.2 mg/mL). Also, three replicates of 1 mg/mL P105 in 5 mM POPC liposome solution were measured and the corresponding fitting results show that they all have approximately 8% of polymers bound to the lipid bilayers (Table 3.4). Due to the high reproducibility of the polymer binding, the remaining polymers were measured only once. Table 3.1 summarizes the fitting results and the estimates of the error for f_{bound}, and the resulting parameters N and θ for the interactions of the liposome with each polymer species at given mass

concentration. D_{bound} and D_{free} are also summarized in Table 3.1. The analysis of the water signal is shown in Figure 3.5. The diffusion coefficient is 1.7×10^{-9} m^2/s in both cases: water in the presence of liposome and water in the presence of liposome plus polymer (*e.g.*, 1 mg/mL P105). Note that despite the coexistence of free and encapsulated states of water, the decay curve only has a single slope instead of two distinct slopes, because the exchange rate of water molecules is too rapid to allow observation of two different decays. Leson *et al*. also demonstrated that two different decays cannot be observed even at 50 ms.[246] In such case, PFG-NMR measures an average diffusivity of the water molecules in the free states and encapsulated states (~2 wt.%). Due to the high diffusivity of water, we conclude that the membrane has high permeability to water with and without polymer addition. The following subsections will discuss how polymer structure as well as polymer concentration affect the interactions with lipid bilayers.

Table 3.3. Summary of fitting results of 0.2 mg/mL P103, P104, P105 and F108 after no incubation and after 1-week incubation with liposomes at room temperature.

	f_{bound}[a] (%) (no incubation)	f_{bound}[a] (%) (1-week incubation)
P103	14.3 ± 2.0	13.1 ± 2.2
P104	8.5 ± 1.3	8.2 ± 1.1
P105	8.9 ± 2.5	10.3 ± 1.0
F108	1.8 ± 0.2	1.4 ± 0.5

[a] Obtained from the average and standard deviation of the fitting results at Δ = 300, 500, and 700 ms based on eq 2.4.

Table 3.4. Summary of fitting results of 3 replicates of 1 mg/mL P105 in 5 mM POPC liposome solution in D_2O at 27 °C.

Replicate No.	D_{bound} [a] (10^{-11} m^2/s)	D_{free} [b] (10^{-11} m^2/s)	f_{bound} [c] (%)	N [d]	θ [e] (%)
1	0.4	8.3	7.9 ± 0.4	132 ± 19	15 ± 3
2	0.4	8.3	8.1 ± 0.7	135 ± 22	16 ± 3
3	0.4	8.2	8.4 ± 0.3	140 ± 20	16 ± 3

[a] Obtained from the final slope of the echo decay curves of the polymer in the presence of liposomes.

[b] Obtained from the linear fit of the echo decay curves of polymer without the presence of liposome. Only the data points before 5.0×10^{10} s/m^2 $\gamma^2G^2\delta^2(\Delta-\delta/3)$ were used for the linear fit to ensure a strong signal since the signal of polymer decays very rapidly.

[c] Obtained from the average and standard deviation of the fitting results at Δ = 300, 500, and 700 ms based on eq 2.4.

[d] Calculated from eq 3.1. Error was propagated from that of f_{bound}.

[e] Calculated from eq 3.3. Error was propagated from that of f_{bound}.

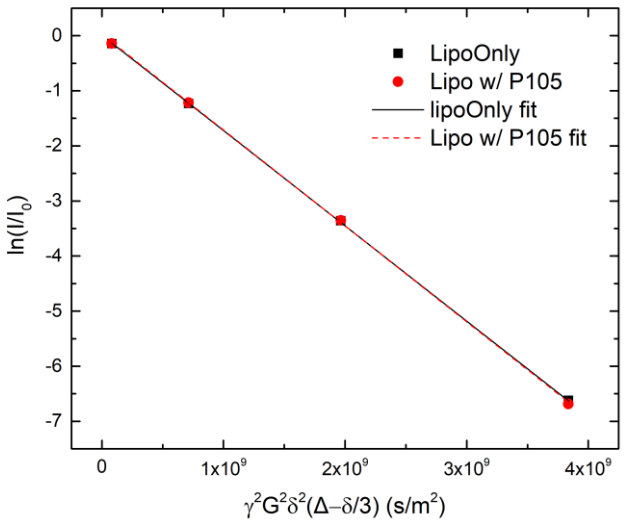

Figure 3.5. Experimental and fitted echo decay curves of the protons from H_2O in the presence of 5 mM POPC liposome and 5 mM POPC liposome plus 1 mg/mL P105 in D_2O at 27 °C with Δ = 500 ms and δ = 5 ms. The data were fit to eq 2.3.

3.3.1 Effect of Polymer Molecular Weight

The effect of molecular weight was studied by comparing four sets of commercial polymers: F127 vs. F87, P105 vs. P65 and L35, P104 vs. P84, and F108 vs. F68. In each set the polymers have the same w_{PEO}, as reflected by the last digit of the designation. The only varying parameter in each set is the total molecular weight, which is proportional to the first or first two digits of the designation for a given composition. Among all four sets, F127 (M_n =13,200 g/mol) vs. F87 (M_n = 7,700 g/mol) shows the most significant molecular weight effect. As shown in Figure 3.6a, the echo decay curves of F127 in the presence of liposome give strong signals at large $\gamma^2G^2\delta^2(\Delta-\delta/3)$, providing a reliable slope for the final plateau that demonstrates a significant number of F127 molecules have attached to the liposomes. In contrast, the echo decay curves of F87 in Figure 3.6b show a weaker signal as the intensity is more attenuated, and barely displays a final plateau, which indicates less interaction between F87 and the lipid membranes. The parameter f_{bound} in Table 3.1 enables quantitative comparison of the binding percentage of F127 and F87 to the liposomes. The binding percentage increases from 0.2 % of F87 to 12.6 % of F127, indicating a remarkable increase upon increasing the molecular weight by 70%. The insets of Figure 3.6a and Figure 3.6b illustrate the liposome surface coverage by F127 and F87, respectively. Clearly, there are many more F127 molecules on the liposome surface than F87. Also, F127 molecules have a larger radius of gyration than F87, since F127 has higher molecular weight, and thus larger particles with higher binding percentage result in much greater areal density on the liposome surface. Additionally, another pair of hydrophilic polymers F108 (M_n = 15,900 g/mol) vs. F68 (M_n = 8,200 g/mol) was investigated. The two polymer species

with $w_{PEO} \approx 0.80$ have less association with the lipid bilayers than the ones with $w_{PEO} \approx 0.70$. In Figure 3.6c, whereas the echo decay curves of F108 in the polymer-liposome mixture show a hint of a nonlinear relation, the signal is too weak at high $\gamma^2G^2\delta^2(\Delta-\delta/3)$. In Figure 3.6d, the data for F68 are as linear as for free polymers in the absence of liposome, because the signal of the final plateau is completely lost. These two figures illustrate that polymer-lipid bilayer association is reduced when the polymer is very hydrophilic. Nevertheless, F108 vs. F68 shows the same trend as F127 vs. F87, in that increasing molecular weight can enhance the polymer binding to the lipid bilayers despite more uncertainty for F108 vs. F68 due to the reduced signal. PEO-8 was measured as a control (Figure 3.6e), which has little interaction with the lipid bilayers.

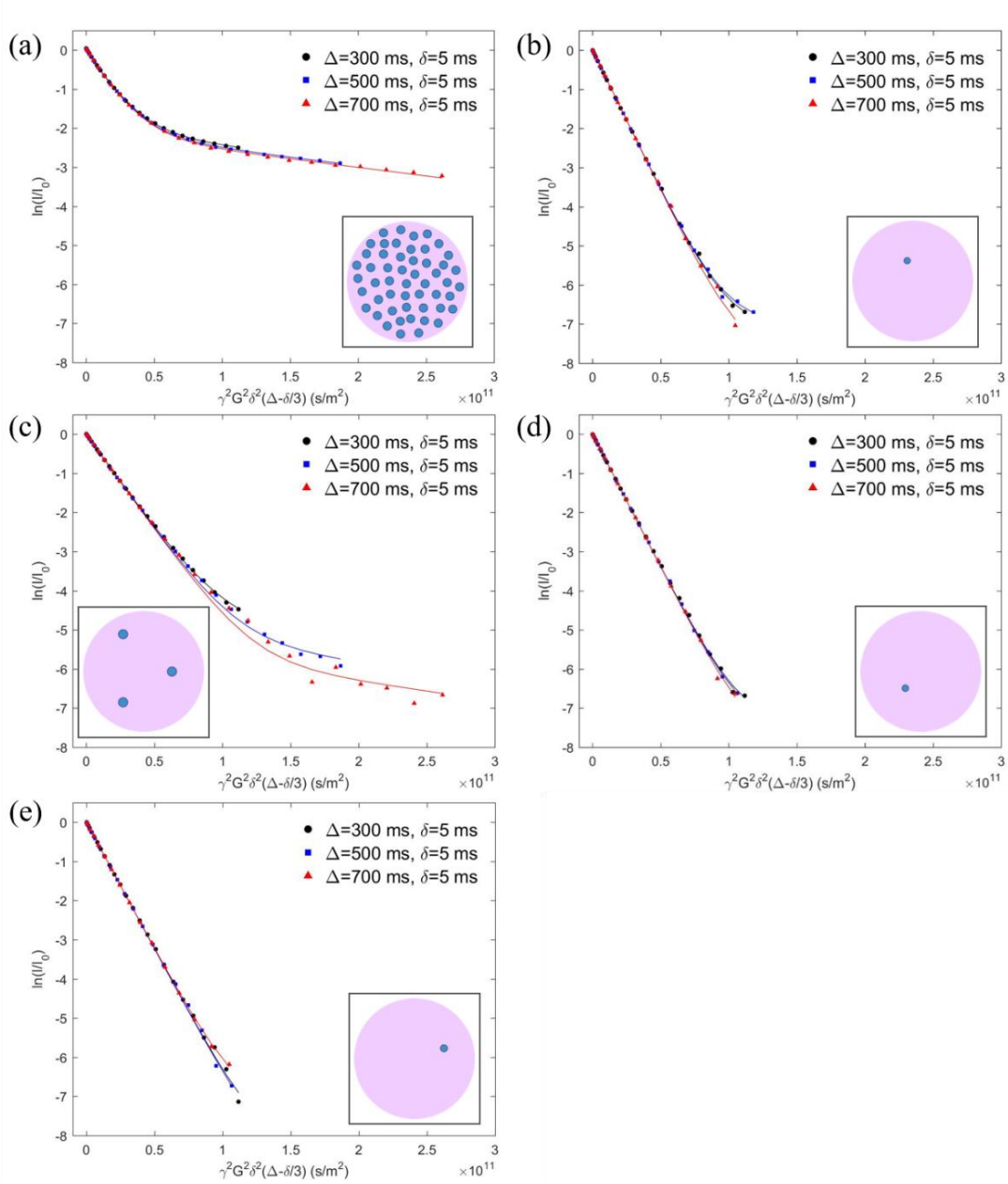

Figure 3.6. Experimental and fitted echo decay curves of the protons from PEO of 1 mg/mL (a) F127, (b) F87, (c) F108, (d) F68, and (e) PEO-8 in 5 mM POPC liposome solution in D_2O at 27 °C with Δ = 300, 500, 700 ms and fixed δ = 5 ms. The data were fit to eq 2.4. The insets show schematics of the surface coverage of half a liposome by polymer.

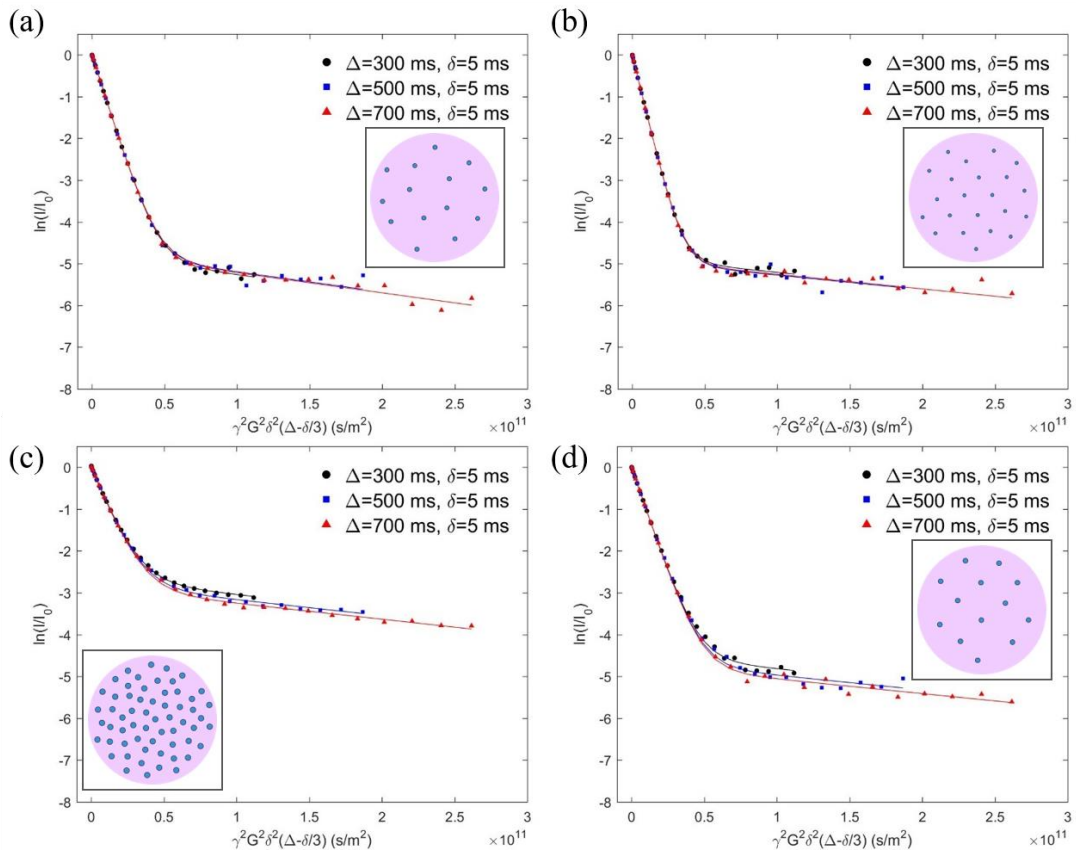

Figure 3.7. Experimental and fitted echo decay curves of the protons from PEO of 1 mg/mL (a) P65, (b) L35, (c) P104, and (d) P84 in 5 mM POPC liposome solution in D_2O at 27 °C with Δ = 300, 500, 700 ms and fixed δ = 5 ms. The data were fit to eq 2.4. The insets show schematics of surface coverage.

In addition to hydrophilic polymers, two sets of more hydrophobic polymers were tested: one with $w_{PEO} \approx 0.50$, including P105 (M_n = 6,500 g/mol), P65 (M_n = 3,400 g/mol) and L35 (M_n = 1,900 g/mol), and one with $w_{PEO} \approx 0.40$, including P104 (M_n = 5,700 g/mol) and P84 (M_n = 4,200 g/mol). For the former set, the echo decay curves of P65 and L35 (Figure 3.7a and Figure 3.7b, respectively) show two distinct slopes despite the noisy data in the final plateau, corresponding to two different diffusivities of the polymers in the presence of liposomes. Compared to F87 and F68, which barely show the sign of the final

plateau, the existence of the plateau suggests that P65 and L35 have stronger interactions with lipid membranes. Nevertheless, the signal fluctuations in the final plateau of P65 and L35 indicate that the amount of polymer associated with the membranes is not sufficient to provide a strong signal. In contrast, the echo curves of P105 in Figure 3.4a have stronger intensity at the final plateau, which suggests that there are more polymer molecules associated with the membranes than those of P65 or L35. Similarly, as shown in Table 3.1 and Figure 3.7c and Figure 3.7d, P104 has stronger binding ability to lipid membranes than P84, since P104 has higher molecular weight. It can be seen that increasing the molecular weight doesn't enhance the polymer-liposome interaction for L35 to P65 as significantly as for P65 to P105. We hypothesize that there is a favorable range of molecular weight, beyond which further increase in molecular weight induces no noticeable increase in the interaction with lipid bilayers. Based on these four sets of polymers, the binding percentage to the liposomes as well as the liposome surface coverage increase more than 5 times by simply doubling the molecular weight. Note that (1) when the polymer is very hydrophilic (*e.g.*, F68 vs. F108), the comparison of molecular weight effects has higher uncertainty due to weaker binding, and (2) when the molecular weight is too small (*e.g.*, L35 vs. P65), the molecular weight sensitivity of the association with lipid bilayers is reduced.

3.3.2 Effect of Composition

The effect of polymer composition is attributable to the hydrophilic-lipophilic balance (HLB), which can be manipulated by varying the PEO and PPO block lengths, as well as the endgroups. The effect of PEO length was studied by selecting the four commercial

triblock copolymers P103, P104, P105 and F108, which have a fixed PPO length (as indicated by the same first two digits of their designations). The PEO length increases from P103 to F108 such that the compositions are $w_{PEO} \approx 0.30$, 0.40, 0.50 and 0.80, respectively. Note that these four polymers were measured at 0.2 mg/mL instead of 1 mg/mL because P103, the most hydrophobic polymer among these four, forms micelles at 1 mg/mL. The fluctuation of the echo-attenuated intensity of the final plateaus in Figure 3.8 is attributable to the more dilute polymer concentration. Since F108 is the only polymer among these four that lost the signal of the final plateau (Figure 3.8d), it is clear that the more hydrophobic polymers P103, P104, and P105 have stronger interactions with the lipid membranes than the hydrophilic F108. Comparing the binding degree as well as the liposome surface coverage of these four polymers listed in Table 3.1, the most hydrophobic polymer P103 binds the most, whereas the most hydrophilic polymer F108 binds the least, despite its higher molecular weight. This also underscores the fact that molecular weight has a limited effect for very hydrophilic polymers. P104 and P105 have similar levels of association, which could be explained by the trade-off between total molecular weight and HLB as the PEO length increases. The polymer becomes less hydrophobic from P104 to P105, while the total molecular weight also increases with increasing PEO block length. Thus, the hydrophobicity effect is compensated by the molecular weight effect.

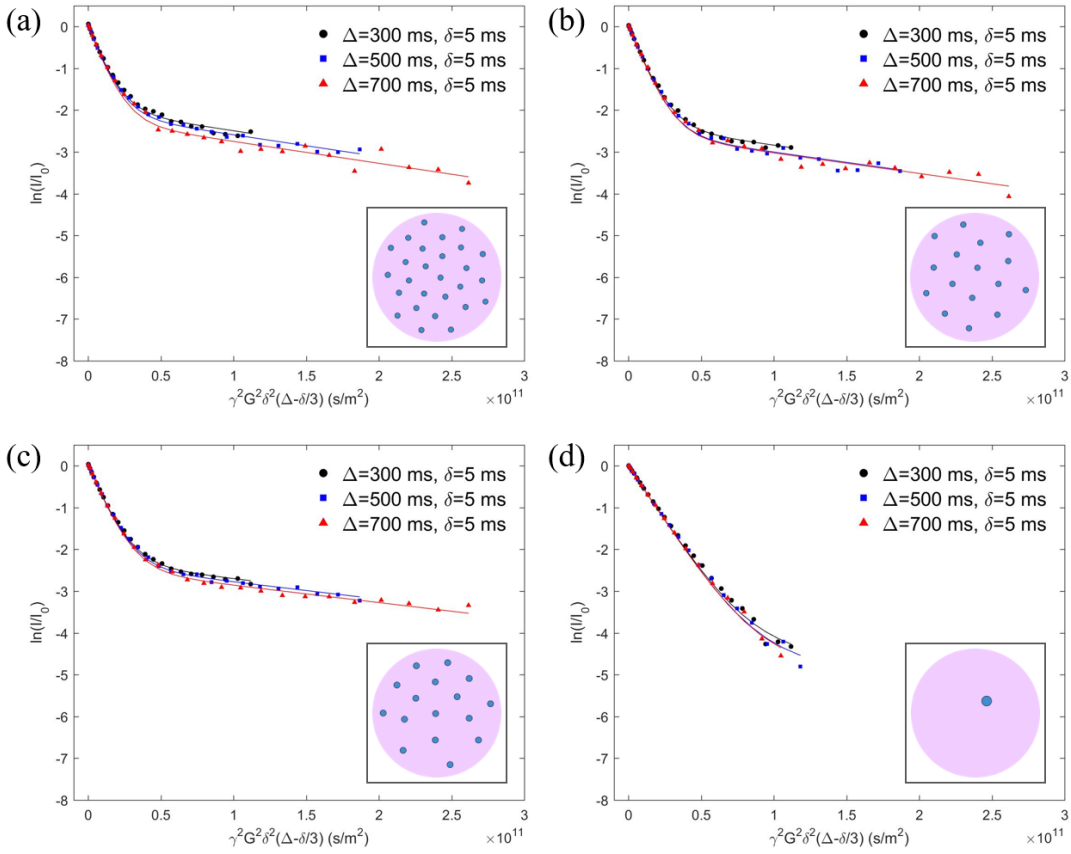

Figure 3.8. Experimental and fitted echo decay curves of the protons from PEO of 0.2 mg/mL (a) P103, (b) P104, (c) P105, and (d) F108 in 5 mM POPC liposome solution in D_2O at 27 °C with Δ = 300, 500, 700 ms and fixed δ = 5 ms. The data were fit to eq 2.4. The insets show schematics of surface coverage.

Note that there is some suggestion of exchange between bound and unbound states, in the lack of perfect superposition of the curves for different Δ in Figure 3.6, Figure 3.7, and Figure 3.8. These curves were fit to the Kärger model as summarized in Table 3.5.[247] The Kärger model is described by eq 3.4-3.13.[247] Here, k_{bound} and k_{free} are rate constants defined by eq 3.4 and 3.5. The parameters Q_1 and Q_2 are defined by eq 3.6 and 3.7, where τ_{bound} and τ_{free} represent the residence times of bound and free polymers, respectively. The

apparent rate constants k_a and k_b are defined by eq 3.9 and the apparent populations N_a and N_b are defined by eq 3.9 and 3.10. The Kärger model can be described by a biexponential decay using apparent rate constants and populations, as shown in eq 3.13. Compared to the biexponential model, the Kärger model adds one more fitting parameter, τ_{bound}, to account for the molecular exchange rate between bound and unbound states.[246,248,249] The smaller τ_{bound}, the more rapid the exchange. The binding percentages obtained from the Kärger model shows the same trends as that from biexponential model, but the absolute values of the binding fraction are systematically higher than those from the biexponential model by ~30% for most polymers. The binding of F108 and P84 shows a large discrepancy between the two models, attributable to the large uncertainty of f_{bound} due to their relatively weak interactions with liposomes. Note that the uncertainty in τ_{bound} is large due to two factors: (1) the signal at high $\gamma^2G^2\delta^2(\Delta-\delta/3)$ is noisy, and (2) the differences between the final plateaus are too small to give precise exchange rates, indicating that the residence time of bound polymers is longer than the current applied diffusion time. Simulations of the Kärger model at different τ_{bound} are shown in Figure 3.9, which demonstrate that τ_{bound} needs to be less than 1 s to render the exchange between free and bound states observable within the applied diffusion time scale. In our case, however, τ_{bound} of most polymers exceeds 1 s. Based on the relatively slow exchange rate between free and bound states, we consider the biexponential model to be a valid simplification to fit the data.

Table 3.5. Summary of fitting results with corresponding errors by Kärger model.

	c (mg/mL)	D_{bound} [a] (10^{-11} m^2/s)	D_{free} [b] (10^{-11} m^2/s)	τ_{bound} [c] (s)	f_{bound} [c] (%)
F108	1	0.5*	4.9	0.27 ± 0.02	2.7 ± 0.4
P105	0.2	0.4	8.7	3.2 ± 2.8	11.3 ± 1.4
P105	1	0.4	8.3	1.8 ± 0.6	9.7 ± 0.4
P84	1	0.4	10.2	1.1 ± 0.9	1.8 ± 0.5
P104	0.2	0.5*	9.2	1.2 ± 0.4	11.4 ± 0.5
P104	1	0.4	8.6	2.3 ± 0.8	7.3 ± 0.5
P103	0.2	0.5*	9.7	1.5 ± 0.7	16.1 ± 2.1

[a] Obtained from the final slope of the echo decay curves of the polymer in the presence of liposomes. *Estimated from the diffusion coefficients of liposome in the polymer-liposome mixture measured by PFG-NMR due to noisy data at the final slope.

[b] Obtained from the linear fit of the echo decay curves of polymer without the presence of liposome. Only the data points before 5.0×10^{10} s/m^2 $\gamma^2G^2\delta^2(\Delta-\delta/3)$ were used for the linear fit to ensure a strong signal since the signal of polymer decays very rapidly.

[c] Obtained from the average and standard deviation of the fitting results at Δ = 300, 500, and 700 ms based on the Kärger model described below.

$$k_{bound} = \gamma^2\delta^2G^2D_{bound} \tag{3.4}$$

$$k_{free} = \gamma^2\delta^2G^2D_{free} \tag{3.5}$$

$$Q_1 = \frac{1}{2}(k_{free} + k_{bound} + \frac{1}{\tau_{bound}} + \frac{1}{\tau_{free}}) \tag{3.6}$$

$$Q_2 = \frac{1}{2}\sqrt{\left(k_{free} - k_{bound} - \frac{1}{\tau_{bound}} + \frac{1}{\tau_{free}}\right)^2 + \frac{4}{\tau_{bound}\tau_{free}}} \tag{3.7}$$

$$k_{a,b} = Q_1 \mp Q_2 \tag{3.8}$$

$$N_b = \frac{1}{2} - \frac{\frac{1}{4}\left((f_{bound} - f_{free})(k_{free} - k_{bound}) + \frac{1}{\tau_{bound}} + \frac{1}{\tau_{free}}\right)}{Q_2} \tag{3.9}$$

$$N_a = 1 - N_b \tag{3.10}$$

$$\frac{f_{\text{free}}}{f_{\text{bound}}} = \frac{\tau_{\text{free}}}{\tau_{\text{bound}}} \tag{3.11}$$

$$f_{\text{free}} + f_{\text{bound}} = 1 \tag{3.12}$$

$$\frac{I}{I_0} = N_{\text{a}} \cdot \exp\left(-k_{\text{a}}\left(\Delta - \frac{\delta}{3}\right)\right) + N_{\text{b}} \cdot \exp\left(-k_{\text{b}}\left(\Delta - \frac{\delta}{3}\right)\right) \tag{3.13}$$

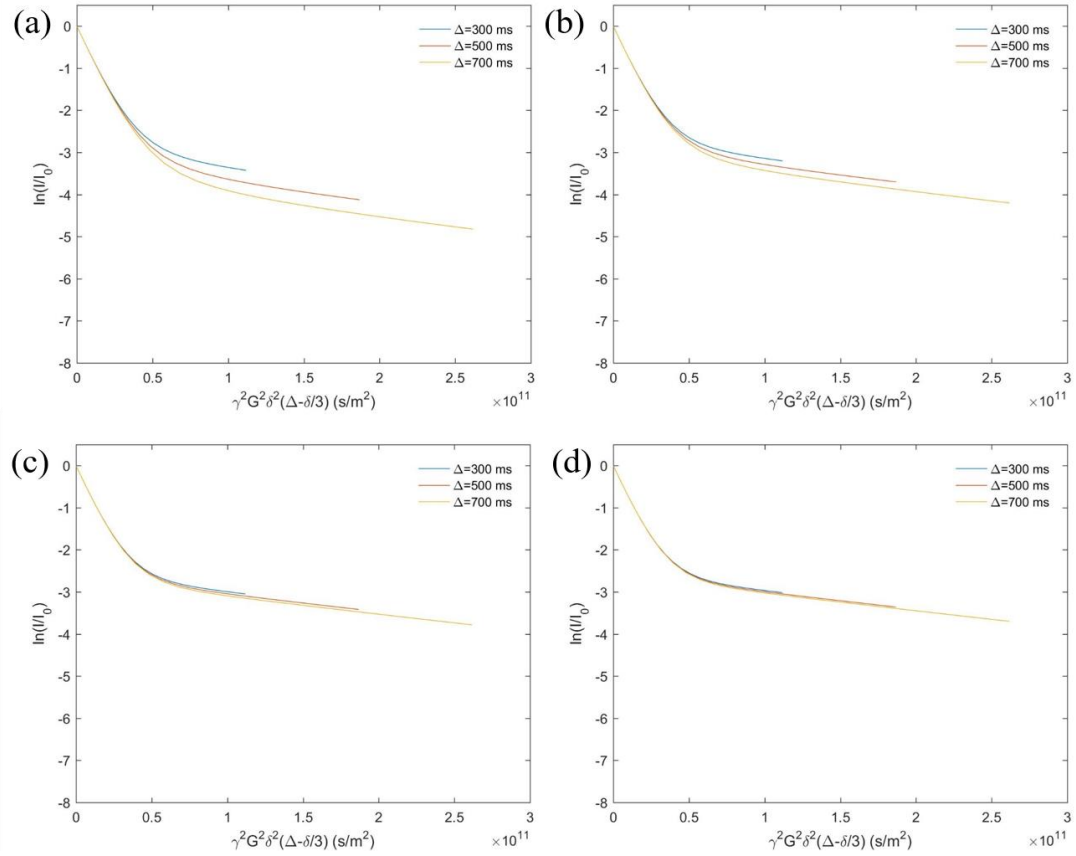

Figure 3.9. Simulations of the Kärger model at τ_{bound} = (a) 0.5 s, (b) 1 s, (c) 3 s, and (d) 5 s with Δ = 300, 500 and 700 ms and δ = 5 ms, assuming $D_{\text{free}} = 0.4 \times 10^{-11}$ m^2/s, $D_{\text{bound}} = 8.3 \times 10^{-11}$ m^2/s and $f_{\text{bound}} = 0.08$ based on experimental data of 1 mg/mL P105 in 5 mM POPC liposome solution.

A set of three diblock copolymers $tPPO_{14}$-PEO_{46}, $tPPO_{14}$-PEO_{78}, and $tPPO_{14}$-PEO_{159} was also tested by PFG-NMR (Figure 3.10). As implied by their nomenclature, they contain a constant PPO block length and an increasing PEO block length, with $w_{PEO} \approx 0.7$, 0.8 and 0.9. The signal quality of the echo decay curves illustrates that $tPPO_{14}$-PEO_{46} has the strongest interaction with the lipid membranes, as a final plateau region was no longer observed for the other two polymers. This follows the trend that the binding percentage decreases with increasing PEO block length, as shown in Table 3.1. However, the binding percentage of these three polymers in general is much lower than that of P103, P104, and P105, which could be attributed to the higher hydrophilicity of $tPPO_{14}$-PEO_{46}, $tPPO_{14}$-PEO_{78}, and $tPPO_{14}$-PEO_{159}.

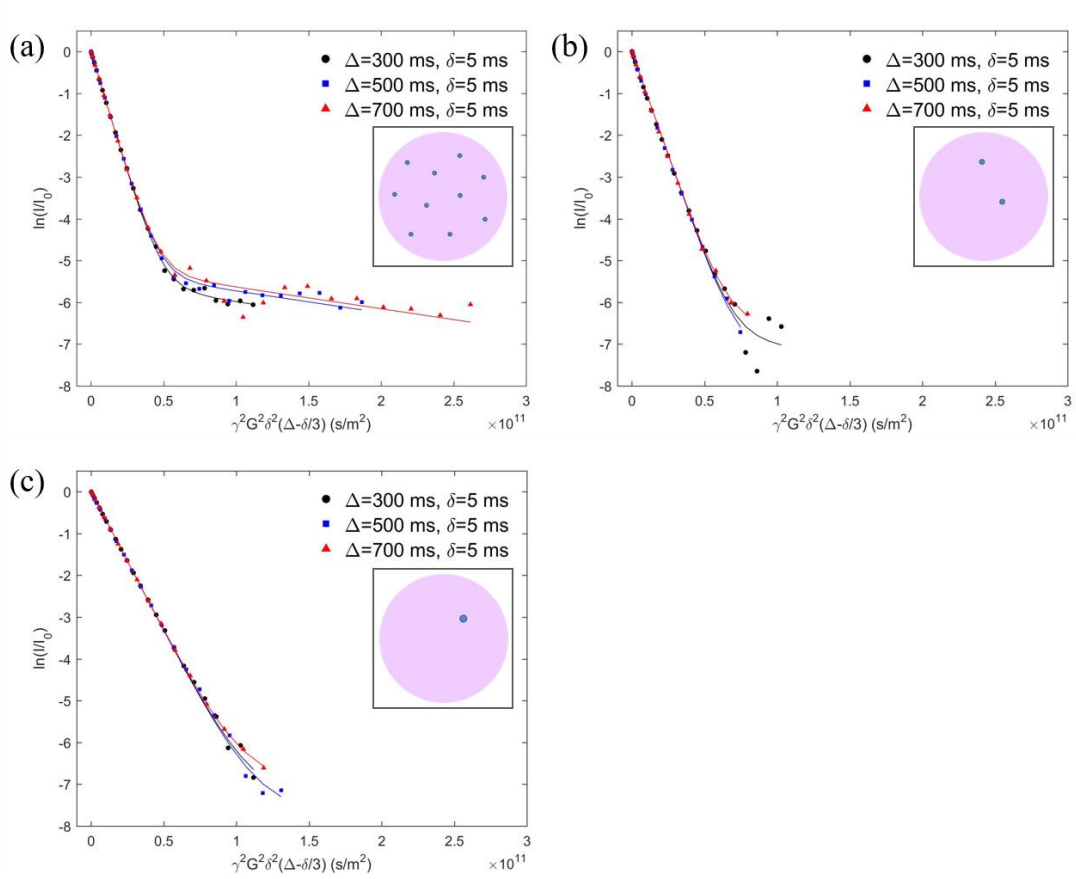

Figure 3.10. Experimental and fitted echo decay curves of the protons from PEO of 1 mg/mL (a) $tPPO_{14}$-PEO_{46}, (b) $tPPO_{14}$-PEO_{78}, and (c) $tPPO_{14}$-PEO_{159} in 5 mM POPC liposome solution in D_2O at 27 °C with Δ = 300, 500, 700 ms and fixed δ = 5 ms. The data were fit to eq 2.4. The insets show schematics of surface coverage.

An alternative way to change the HLB is to modify the PPO block length, while keeping the PEO block length fixed. A pair of synthesized diblock copolymers $tPPO_{29}$-PEO_{68} and $tPPO_{14}$-PEO_{78} were employed to study this. Although there is a small discrepancy in PEO block length, the PPO block length of $tPPO_{29}$-PEO_{68} is twice of that of $tPPO_{14}$-PEO_{78}. The echo decay curves of these two polymers in Figure 3.11 look quite different: $tPPO_{29}$-PEO_{68} reveals two distinct slopes in the probing window, and the strength of the plateau is

moderately high (Figure 3.11a); $tPPO_{14}$-PEO_{78}, on the other hand, only shows a single exponential decay, reflecting little interaction with the lipid bilayers (Figure 3.11b). As quantified in Table 3.1, $tPPO_{29}$-PEO_{68} has approximately 10 times higher binding, as well as the number of bound polymers per liposome and surface coverage, than $tPPO_{14}$-PEO_{78}. This indicates that as the PPO block length increases, the polymer becomes more hydrophobic and more polymer molecules associate with the lipid membrane.

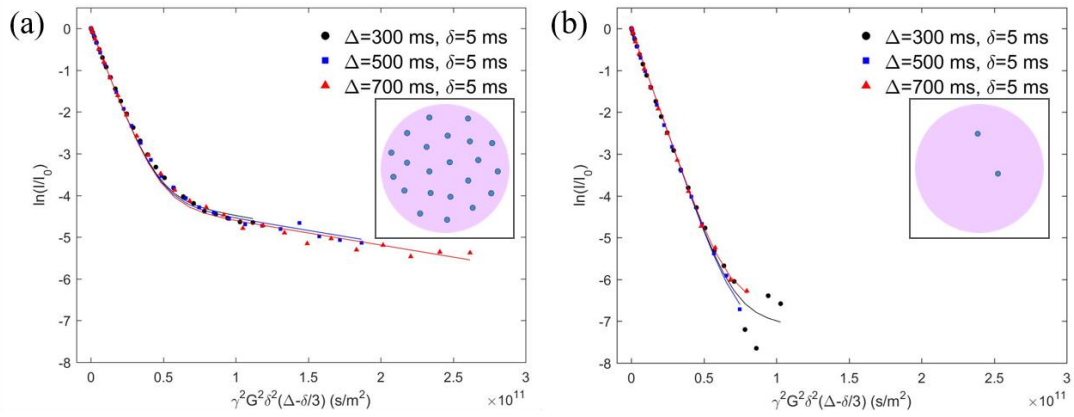

Figure 3.11. Experimental and fitted echo decay curves of the protons from PEO of 1 mg/mL (a) $tPPO_{29}$-PEO_{68} and (b) $tPPO_{14}$-PEO_{78} in 5 mM POPC liposome solution in D_2O at 27 °C with Δ = 300, 500, 700 ms and fixed δ = 5 ms. The data were fit to eq 2.4. The insets show schematics of surface coverage.

Endgroup chemistry is also an important contributor to the composition effect. Two synthesized diblock copolymers with different endgroups on the PPO block were investigated: $hPPO_{13}$-PEO_{43}m, with a hydrophilic hydroxyl endgroup, and $tPPO_{14}$-PEO_{46} with a hydrophobic *tert*-butyl endgroup. While ideally the endgroup on the other PEO terminus would be the same for the two polymers, we assume that the variation from a normal hydroxyl endgroup of $tPPO_{14}$-PEO_{46} to a methyl endgroup of $hPPO_{13}$-PEO_{43}m has

little effect on the hydrophobicity of the polymer, especially given that the PEO block is relatively long. Based on the echo decay curves in Figure 3.12a, $hPPO_{13}$-$PEO_{43}m$ barely interacts with the lipid bilayers. Its counterpart $tPPO_{14}$-PEO_{46} has stronger associations with the liposomes as the decay curves in Figure 3.12b are clearly biexponential. Therefore, the more hydrophobic endgroup on the PPO block drives a stronger attraction of the polymers to the lipid bilayers. Note that the endgroup exerts a relatively minor influence compared to molecular weight and block length. A bulkier hydrophobic endgroup might be required to observe a more noticeable difference.

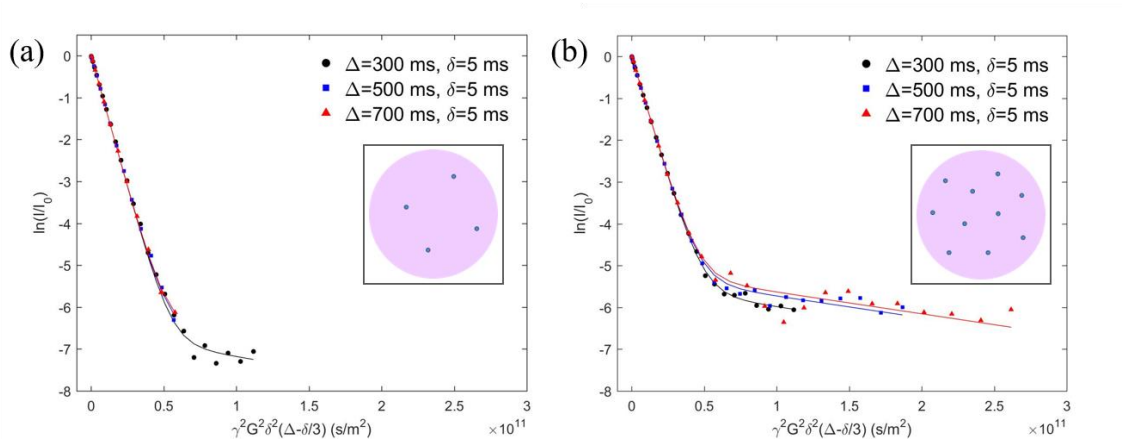

Figure 3.12. Experimental and fitted echo decay curves of the protons from PEO of 1 mg/mL (a) $hPPO_{13}$-$PEO_{43}m$ and (b) $tPPO_{14}$-PEO_{46} in 5 mM POPC liposome solution in D_2O at 27 °C with Δ = 300, 500, 700 ms and fixed δ = 5 ms. The data were fit to eq 2.4. The insets show schematics of surface coverage.

3.3.3 Effect of Polymer Concentration

Finally, the effect of concentration was investigated by adjusting the concentration of F127 from 0.2 to 1 mg/mL. As concentration increases, the liposome surface coverage also increases, while the binding percentage decreases, as summarized in Table 3.1 and shown

in Figure 3.13. (The echo decay curves of F127 at 0.2, 0.5, and 1 mg/mL in the presence of liposomes can be found in Figure 3.14). The latter trend can be attributed to approaching the limit of liposome surface coverage at high polymer concentration. As can be seen in Figure 3.13, the liposome surface coverage appears to approach a maximum as the concentration increases. We speculate that at certain high polymer concentration, the liposome surface coverage would saturate because the membrane surface would become too crowded. It is also conceivable that the liposome would be disrupted by concentrated polymer due to the resulting osmotic stress, prior to achieving maximum surface coverage, especially for those polymers that have weak interactions or insufficient binding with the liposomes. Concentrations of F127 beyond 1 mg/mL were not tested due to micelle formation.

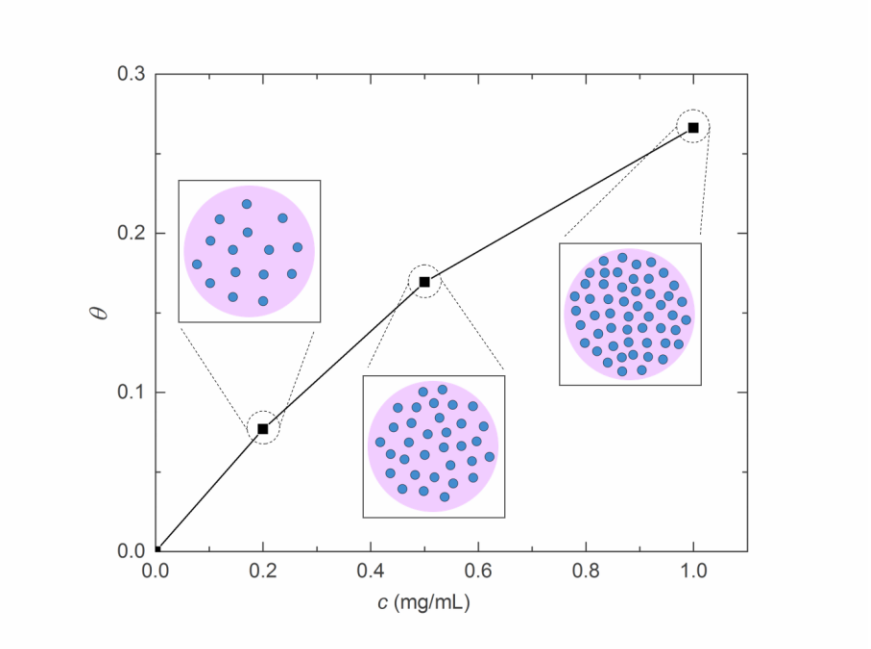

Figure 3.13. Fraction of liposome surface area covered by polymer molecules as a function of polymer concentration of F127. The insets show schematics of surface coverage by polymers at different concentration.

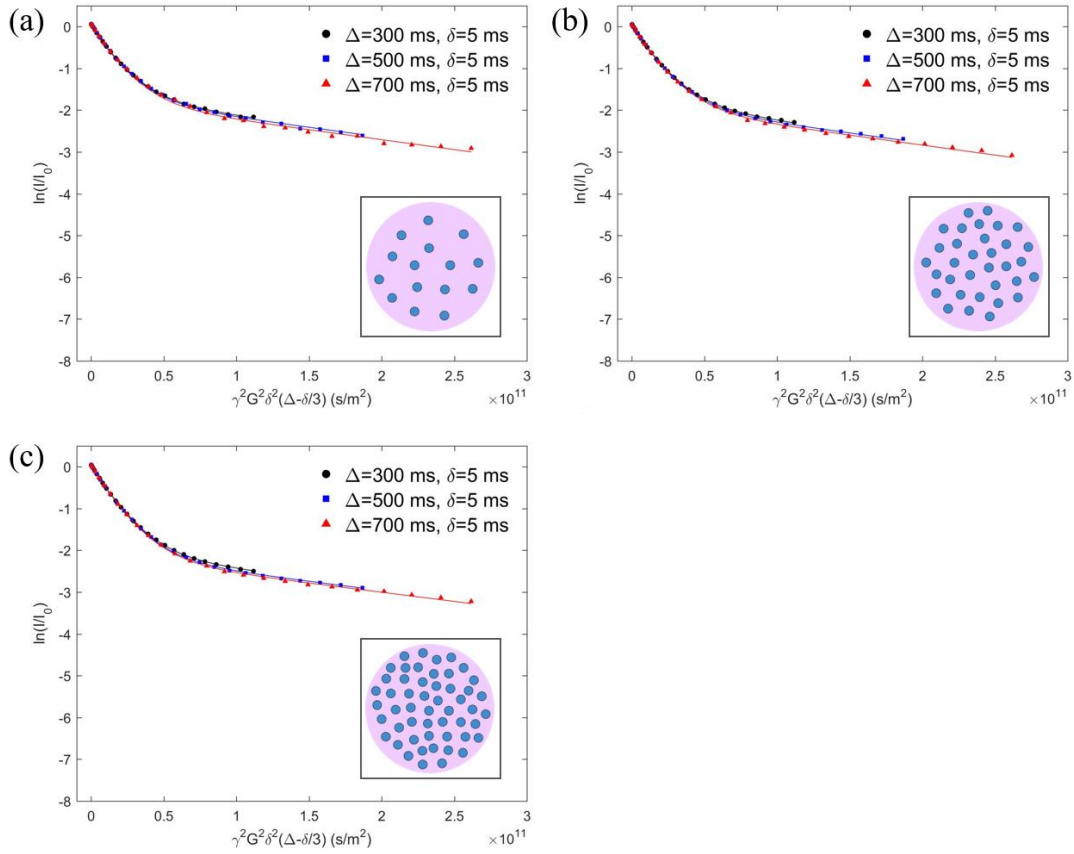

Figure 3.14. Experimental and fitted echo decay curves of the protons from PEO of F127 at (a) 0.2 mg/mL, (b) 0.5 mg/mL, and (c) 1 mg/mL in 5 mM POPC liposome solution in D_2O at 27 °C with Δ = 300, 500, 700 ms and fixed δ = 5 ms. The data were fit to eqn 2. The insets show schematics of surface coverage.

To summarize the effects of all three variables described above, a 3-D plot of liposome surface coverage by the various polymers is shown in Figure 3.15. The three axes represent the total molecular weight, w_{PEO}, and concentration, corresponding to the three factors investigated. The volume of the spheres is proportional to the fractional surface coverage of the liposomes. Thus, the larger the sphere, the more polymer binding and thus stronger

interactions. When looking at the effect of concentration, the spheres become larger along each vertical dashed line as concentration increases. Examining the plane of w_{PEO} vs. the total molecular weight, the upper corner within the thick dashed line contains relatively large spheres, indicating strong interactions of the polymers with the liposomes. Higher molecular weight and higher hydrophobicity of the polymer both enhance the polymer-lipid bilayer association. By extension, when looking at the binding percentage as a function of the PPO block length (Figure 3.16), an appreciably large PPO block is necessary for strong interactions. The small spheres on the other side of the dashed line in Figure 3.15 reflect weaker interactions between the polymers and liposomes, either because the hydrophobicity is not sufficient or the molecular weight is not high enough, or both.

Given that the exchange between the free and bound polymers is not significant on the timescale of the diffusion experiments, we infer that the hydrophobic block at least partly inserts into the lipid bilayer, which makes it harder for the bound polymers to escape from the liposome. If the polymer only adsorbed onto the membrane surface, there should be relatively facile molecular exchange due to weak binding. The experiments here would not detect any weak binding, assuming that each polymer only spent a small fraction of time associated with a liposome. Previously, Cheng *et al.* investigated the interactions between Pluronics and lipid bilayers through the measurement of local hydration dynamics in the membrane by ^{1}H Overhauser dynamic nuclear polarization NMR spectroscopy (ODNP). The results showed that the intrabilayer water diffusivity was enhanced by hydrophobic Pluronics, which indicates that the polymer molecules inserted into the bilayer interior and increased the membrane permeability.[106] This result is consistent with our inference that

Pluronics insert into the lipid bilayers. That polymers with higher molecular weight exhibit stronger interactions with the lipid bilayers is consistent with the observation that polymers with higher molecular weight have a lower CMC,[13] which reflects the drive for polymer molecules to insert into hydrophobic bilayers or micellar interiors, rather than remaining as free chains. The effect of composition is also intuitively reasonable, as the HLB determines whether it is energetically more favorable for polymers to stay in water or associate with the liposomes. Earlier work on cellular assays by Kim *et al*. and on liposome protection against peroxidation by Wang *et al*. both showed that only hydrophilic dominant PPO-PEO block copolymers can protect the integrity of the lipid membranes.[100,107] Given that the more hydrophobic polymers have stronger interactions with the lipid bilayers, there is a higher possibility of hydrophobic polymers to disturb or even disrupt the membrane, which may account for the lack of membrane protection. The cellular system has additional differences to the system studied here, including mixed lipid content, cholesterol, and transmembrane proteins. Besides tuning the block length, adding a hydrophobic endgroup to the PPO block can help anchor the PPO block into the bilayer interior, since it further reinforces the hydrophobicity of the polymer. A previous *in vivo* study of membrane stabilization by block copolymers by Houang *et al*. demonstrated that the replacement of a hydroxyl endgroup by a *tert*-butyl endgroup on the PPO block of a diblock analog to F68 could significantly enhance the stabilization efficacy of polymers on the dystrophic membrane.[101] This result also confirmed the importance of the endgroup, despite the fact that it is less significant in the case considered here.

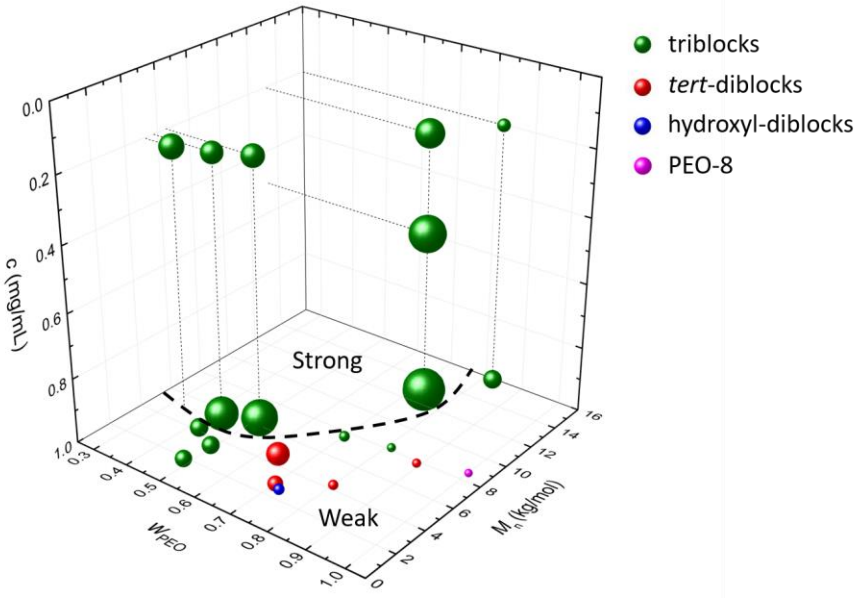

Figure 3.15. Summary of polymer molecular weight, block length, endgroup and concentration effect on the interactions between polymer and liposome. The volume of the spheres is proportional to θ.

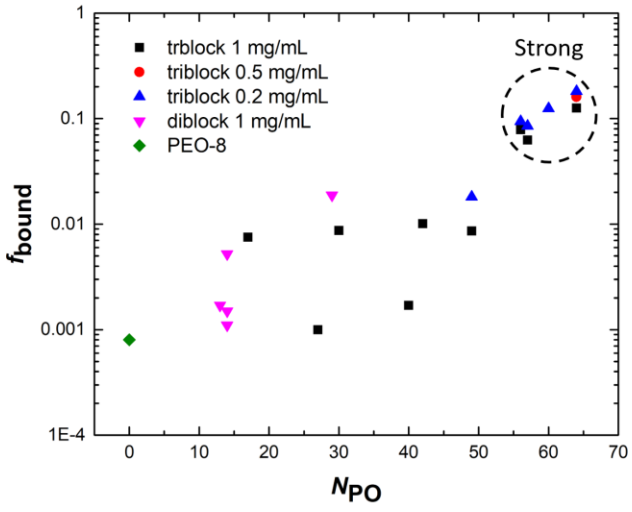

Figure 3.16. Binding percentage as a function of the number of repeat units of PO in the polymer.

3.4 Conclusions

We have investigated the effect of polymer structure and concentration on the molecular interactions between PPO-PEO block copolymers and POPC unilamellar liposomes as model lipid bilayers. The polymer structure was tuned by modifying the total molecular weight and the composition, including the PPO and PEO block lengths and the endgroup on the PPO block. The binding of the polymers with lipid membranes was determined by PFG-NMR, which quantified polymer diffusion in the absence and presence of liposomes. The logarithmic normalized echo-attenuated intensity $\ln(I/I_0)$ of the free polymer showed a linear relationship with the parameter $\gamma^2G^2\delta^2(\Delta-\delta/3)$, implying simple translational diffusion in the absence of liposomes. In the polymer-liposome mixture, the non-linear relationship reflects interactions with lipid bilayers. The binding percentage of polymers to the liposomes was quantified by applying a biexponential model to the echo decay curves. The fitting results showed that larger molecular weight and higher hydrophobicity of the polymers give rise to higher binding percentage, as well as liposome surface coverage, and thereby stronger associations with lipid bilayers. As polymer concentration increases, the binding percentage decreases while the liposome surface coverage increases. This is attributable to the saturation of the liposome surface coverage at certain high concentration. Additionally, it has been shown that the binding percentage is independent of incubation time, indicating that the polymer-lipid bilayer association reaches equilibrium very quickly. These results demonstrate that PFG-NMR is a straightforward and useful tool to quantify the binding of block copolymers with lipid bilayers, and should bring new insights into the mechanistic studies of polymer-membrane association.

Chapter 4 - Influence of Cholesterol and Bilayer Curvature on Polymer-Membrane Association

4.1 Introduction

In Chapter 3, we systematically investigated how polymer structure dictates the polymer interaction with lipid bilayers by quantifying the binding of both triblocks and diblocks to unilamellar liposomes. Larger molecular weight and more hydrophobic PPO-PEO block polymers were found to have stronger interactions with lipid bilayers. In this

chapter, we aimed at understanding how cholesterol content and lipid bilayer curvature influence the interactions between lipid bilayers and amphiphilic polymers, as few studies in the literature have explored the mechanism of polymer-membrane association from the membrane perspective.[168,207,250] Composition has a significant impact on multiple membrane properties. Cholesterol, for example, is one of the most common molecules found in eukaryotic cell membranes, and can make up as much as 50 mol% of plasma membranes.[251] It is a predominantly hydrophobic molecule, composed of steroid rings and one hydroxyl group. The moderate amphiphilicity due to the presence of the hydroxyl group tends to orient the cholesterol molecule such that the hydroxyl group is located at the interface between the membrane interior and aqueous medium via hydrogen bonding with lipid headgroups and water molecules, while the steroid rings sit in the membrane interior, approximately parallel to the hydrocarbon chains.[252–255] Cholesterol is a vital component to maintain membrane integrity, to control lipid packing, and to regulate membrane fluidity.[252,255–258] Earlier work suggested that the addition of cholesterol into a lipid bilayer could increase the ordering of the alkyl chains of the lipids,[259,260] increase membrane density,[261–264] decrease membrane permeability,[255] decrease membrane fluidity,[265,266] increase mechanical strength of the membrane,[258] and induce the formation of liquid domains enriched with particular lipid species.[151,267,268] Johnsson et al. found that inclusion of cholesterol in liposomal preparations reduces the incorporation of copolymers in the lipid bilayer and thus reduces the liposomal morphological changes due to the presence of copolymers, observed in the absence of cholesterol.[207] Zhirnov and coworkers also showed that cholesterol decreased binding of Pluronic L61 to liposomes, possibly due

to increasing microviscosity of the membrane.[168] Additionally, membrane curvature could also play a role in the interactions with polymers. Work by Ahmed, et al. using Raman spectroscopy indicated that the curvature of nanoparticle-supported lipid bilayers also has a significant effect on conformational order and alkyl chain packing.[186] By investigating the effect of cholesterol and bilayer curvature on the interactions between PPO-PEO type block copolymers and membranes, we aim to develop a deeper understanding of the mechanism of polymer-membrane association and bring the model membrane systems one step closer to real cell membranes.

In this chapter we quantify the copolymer interactions with model membranes at various cholesterol concentrations and bilayer curvatures, using pulsed-field-gradient NMR (PFG-NMR). PPO-PEO block copolymers examined include three commercial Pluronics (*i.e.*, F127, P103, and F68) and a lab synthesized diblock analogue containing a tertiary butyl group attached to the end of the PPO block (*i.e.*, *t*PPO_{14}-PEO_{46}). Unilamellar liposomes were used as model membranes due to the ease of tuning composition and curvature. Phosphatidylcholine, one of the most common lipids found in plasma membranes, has been widely used as a major component of model systems.[107,108,179] Herein, the lipid bilayer composition was manipulated by mixing cholesterol at various concentrations with 1-palmitoyl-2-oleoyl-sn-glycero-3-phosphocholine (POPC). Pure POPC bilayers were prepared as controls. The chemical structures of corresponding polymers and membrane components can be found in Figure 1.1 and Figure 2.4, respectively. Bilayer curvature was manipulated by varying the liposome size. Polymer binding to liposomes was quantified by PFG-NMR. This technique has been applied to

determine self-diffusion coefficients of small molecules,[269] to assess drug partitioning to polymer,[270–272] and to quantify the molecular exchange rate through membranes of polymersomes.[248,249,246] In the case of polymers mixed with liposomes, the diffusivity of polymers bound to liposomes can be distinguished from that of free polymers by PFG-NMR, from which the polymer binding can be quantified. Our results demonstrate that the cholesterol concentration has a significant effect on polymer-membrane association, while bilayer curvature plays a diminishing role with increasing liposome size.

4.2 Experimental Section

Details of the experimental techniques used in this chapter were described in Chapter 2. The materials, sample preparation, and experimental procedures that are specific to this chapter are summarized below.

4.2.1 Materials

Pluronics F68, F127, and P103 were provided by BASF. The materials used for anionic polymerization, including ethylene oxide (EO, ≥ 99.5%), propylene oxide (PO, ≥ 99%), potassium *tert*-butoxide, n-butyllithium, naphthalene, potassium, and 18-crown-6 ether, were purchased from Sigma-Aldrich and used as received. 1-palmitoyl-2-oleoyl-sn-glycero-3-phosphocholine (POPC) and 1,2-dioleoyl-sn-glycero-3-phosphocholine (DOPC) in chloroform were purchased from Avanti Polar Lipids (Alabaster, AL) and used as received. Cholesterol (≥ 99%) and the chemicals used for MALDI characterization

including silver trifluoroacetate (AgTFA) and α-cyano-4-hydroxycinnamic acid (CHCA, ≥ 98%), were also purchased from Sigma-Aldrich. Deuterium oxide (D_2O, 99.9 atom % D) and chloroform-d ($CDCl_3$, 99.8 atom % D + 0.05% V/V TMS) were purchased from Cambridge Isotope Laboratories, Inc.

4.2.2 Polymer Synthesis and Characterization

The diblock polymer *t*PPO_{14}-PEO_{46} used in this chapter was synthesized by anionic polymerization. The number-average molecular weight, dispersity, and composition of the polymers were summarized in Table 2.1.

4.2.3 Liposome Preparation and Characterization

The organic solvent present in the commercial phospholipid solution (*e.g.*, 10 mg/mL POPC in chloroform) was first evaporated under nitrogen followed by vacuum for 30 min to yield a thin lipid film on the wall of a glass vial. Next, the dried lipid film was hydrated with D_2O, which gave a final lipid concentration of 10 mM. During the hydration process, the sample vial was kept in a water bath at 37 °C for 1 h, with vortex applied every 5 min to the lipid suspension to facilitate the formation of large multilamellar lipid vesicles. Lastly, the lipid suspension was extruded through a polycarbonate membrane back and forth 27 times to obtain the final liposome solution. The hydrodynamic radius R_h of the liposomes was characterized by DLS.

The curvature κ of the lipid bilayer was manipulated by varying the liposome size (Figure 4.1), as $\kappa = 1/R$, where R is the liposome radius. This was accomplished by using polycarbonate membranes with 25, 50, and 100 nm radius pores. The R_h of the liposomes obtained from DLS was used to calculate κ. In the case of bicomponent liposome preparation (*i.e.*, POPC/cholesterol), POPC lipids were mixed with cholesterol in chloroform at a specific ratio calculated from the desired composition, followed by the same procedures described above.

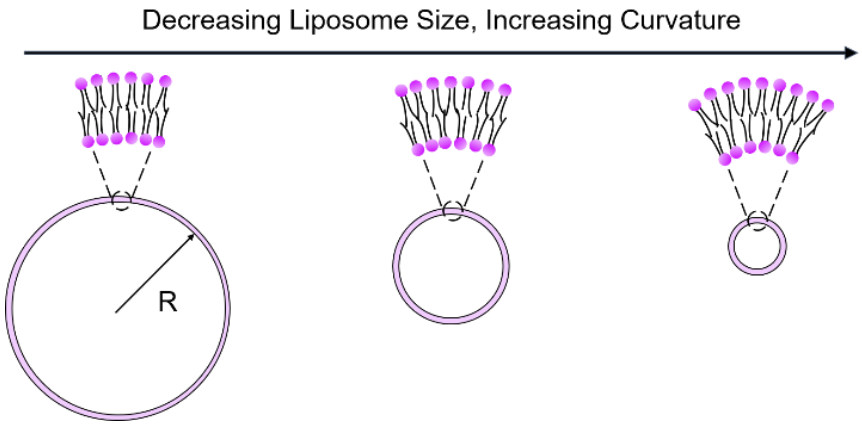

Figure 4.1. Schematic of manipulating bilayer curvature by varying the liposome size.

4.2.4 PFG-NMR Measurements

PFG-NMR was employed to quantify polymer binding. The polymer-liposome mixtures were prepared by combining 0.25 mL of 10 mM liposome stock solution with 0.25 mL of polymer stock solution (0.4 mg/mL for P103 and F127 and 2 mg/mL for F68 and tPPO$_{14}$-PEO$_{46}$ in D_2O). Note that the polymers P103 and F127 were dissolved at a

lower concentration due to their relatively low critical micelle concentrations (CMC).[8,13] Pure polymer and pure liposome samples were prepared as controls by adding 0.25 mL of D_2O to 0.25 mL of the polymer and liposome stock solutions, respectively. All the samples were measured in D_2O at 27 °C without incubation.

4.2.5 Cryogenic Transmission Electron Microscopy (cryo-TEM)

10 mM liposomes with various cholesterol molar percentage in D_2O at 27 °C were used for cryo-TEM imaging (details outlined in Chapter 2).

4.3 Results and Discussion

4.3.1 Liposome Size Characterization

Table 4.1 summarizes the mean R_h and dispersity (μ_2/Γ^2) values for the liposomes prepared using the three pore sizes, as characterized by DLS. When extruded through a polycarbonate membrane with a 25 nm pore radius, the R_h of POPC/cholesterol liposomes increase from 42 nm to 57 nm as the molar percentage of cholesterol in the bilayer increases from zero to 30 mol%. On the other hand, the R_h of the liposomes at intermediate size (*i.e.*, extruded through a polycarbonate membrane with 50 nm pore radius) fluctuates slightly between 65 nm and 70 nm with cholesterol composition. This variation in R_h is within experimental uncertainty. These results indicate that the effect of cholesterol on liposome R_h is more significant for smaller liposomes. Previous work found a remarkable increase of liposome R_h upon increasing the cholesterol molar percentage in liposomes extruded

with a 50 nm pore radius, which could be attributed to increasing membrane stiffness.[166] Such an increase in liposome R_h, however, was only observed in the liposomes extruded with 25 nm pore radius in our case. The dispersity of liposomes was not significantly affected by the presence of cholesterol or the extrusion pore radius, as the values of μ_2/Γ^2 are all less than 0.1. Note that the variations in liposome size don't affect the quantification of polymer binding, since the liposome diffusion is still one order of magnitude slower than for the free polymer molecules, and accordingly the diffusion coefficients of bound and free polymers can still be readily distinguished by PFG-NMR.

Additionally, cryo-TEM was employed to characterize the size and morphology of liposomes with selected compositions. Liposomes with 0, 10, and 30 mol% cholesterol extruded through a polycarbonate membrane with 50 nm pore radius were selected as representative for cryo-TEM imaging, as shown in Figure 4.2a, Figure 4.2b, and Figure 4.2c, respectively. Liposome morphology shows little change as cholesterol molar percentage increases. A small number of multilamellar liposomes are present at all three cholesterol concentrations. The estimated percentages of liposome surface area within multilamellar liposomes are summarized in Table 4.2; at all three cholesterol concentrations, a similar small percentage of surface area is sequestered in the multilamellar liposomes (*i.e.*, less than 20%). The sequestered surface area of liposomes could be potentially reduced by increasing the times of extrusion.[156] Histograms of liposome radius measured from cryo-TEM are plotted in Figure 4.2d - Figure 4.2f. The mean and standard deviation of the liposome radius calculated from the histograms are summarized in Table 4.2 (*i.e.*, 49 ± 17 nm, 50 ± 19 nm, and 46 ± 21 nm at 0, 10, and 30

mol% cholesterol, respectively). The mean radius of the liposomes at all three cholesterol concentrations is close to the extrusion pore radius (*i.e.*, 50 nm). The mean radius is apparently constant, but the standard deviation is relatively large. This suggests that increasing cholesterol molar percentage in the lipid bilayer results in little change of liposome size in the case of a 50 nm extrusion pore radius, which agrees with the conclusion obtained from DLS. The histograms are reasonably well represented by a normal distribution based on the mean and the standard deviation obtained from the histograms as shown in Figure 4.2. The liposome radii measured by cryo-TEM were found to be smaller than the R_h measured by DLS. We interpret this difference to be due to: (1) R_h includes the thickness of the hydration layer of the lipid headgroups, and (2) DLS is skewed towards large size particles, since it measures intensity-averaged size and the scattered intensity of vesicles is proportional to R^2, whereas cryo-TEM measures the number-averaged size.[273]

Table 4.1. Liposome Size Characterization in D_2O by DLS.

Cholesterol Molar Percentage (%)	**Extrusion Pore Radius (nm)**	R_h* **(nm)**	μ_2/Γ^2 **at 90°**
0	25	42	0.06
1	"	48	0.06
2	"	47	0.07
5	"	48	0.07
10	"	51	0.06
20	"	55	0.06
30	"	57	0.05
0	50	70	0.04
1	"	70	0.03
2	"	70	0.04
5	"	65	0.06
10	"	67	0.04
20	"	68	0.03
30	"	69	0.05
0	100	109	0.07

*R_h measured by DLS has approximately 5% uncertainty.

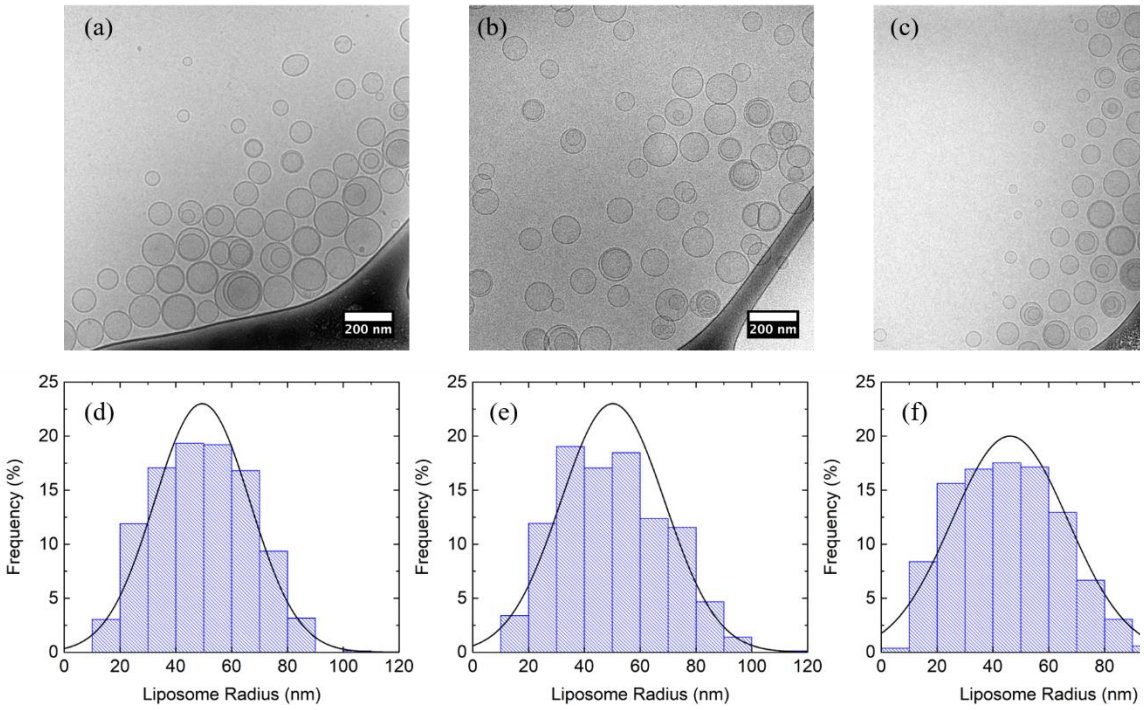

Figure 4.2. Cryo-TEM images of 10 mM liposomes in D_2O composed of (a) POPC, (b) 90 mol% POPC +10 mol% cholesterol, and (c) 70 mol% POPC +30 mol% cholesterol extruded through a polycarbonate membrane with 50 nm pore radius. (d), (e), and (f) are corresponding histograms of liposome radius measured from cryo-TEM compared with normal distribution based on the mean and the standard deviation of the population. Non-spherical liposomes were excluded. The radius of a multilamellar liposome was measured at the outermost vesicle.

Table 4.2. Summary of liposome radii and the percentage of liposome surface area within multilamellar liposomes measured from cryo-TEM.

Cholesterol Molar Percentage (%)	Total Counts[a]	Mean (nm)[b]	Standard Deviation (nm)	% of Liposome Surface Area within Multilamellar Liposomes
0	791	49	17	17
10	856	50	19	17
30	525	46	21	19

[a] The liposomes were extruded through a polycarbonate membrane with 50 nm pore radius. Non-spherical liposomes were excluded.

[b] The radius of a multilamellar liposome was measured at the outermost layer.

4.3.2 Effect of Cholesterol

The role of cholesterol was investigated by quantifying the binding of four representative PPO-PEO block copolymers (*i.e.*, F127, P103, *t*PPO_{14}-PEO_{46}, and F68) to the POPC liposomes containing various molar ratios of cholesterol using the intermediate size liposomes (*i.e.*, extruded through a polycarbonate membrane with 50 nm pore radius). F127 and P103 have relatively strong interactions with lipid bilayers compared to F68 and *t*PPO_{14}-PEO_{46}. More than 10 mol% of F127 and P103 bind to neat POPC liposomes, whereas less than 1 mol% of *t*PPO_{14}-PEO_{46} and F68 associated with the same bilayer particles (Table 4.3). Echo decay curves of F127 in the presence of liposomes with increasing cholesterol concentration are shown in Figure 4.4. In the control case of F127 interacting with neat POPC liposomes (Figure 4.3), the strong signal intensity of the echo decay curves retained at the final slope illustrates that a substantial fraction of polymer is bound to liposomes. In contrast, the polymer signal at the final slope becomes weaker upon increasing the cholesterol concentration in the lipid bilayer, indicating diminished polymer binding (Figure 4.4). When the cholesterol content reaches 10 mol%, the final slope of the polymer decay curves becomes noisy and less reliable, due to a lack of bound polymer. The decay curves barely display a final slope when the lipid bilayer contains more than 20 mol% cholesterol; the decay curve closely resembles a single-exponential decay of free polymers, thereby indicating little interaction between the polymers and lipid bilayers. The binding of P103 and *t*PPO_{14}-PEO_{46} show similar trends as F127 does upon increasing cholesterol content, as shown in Figure 4.5 and Figure 4.6, respectively. Binding of F68

was only measured with neat POPC liposomes (Figure 4.7); due to the low extent of association there was inadequate signal to noise to quantify the extent of binding in the presence of cholesterol, indicative of little interaction.

Table 4.3. Summary of polymer binding to 5 mM POPC/cholesterol liposomes extruded through a polycarbonate membrane with 50 nm pore radius in D_2O at 27 °C at different cholesterol molar percentages.

Cholesterol Molar Percentage (%)	D_{bound}[a] (10^{-11} m^2/s)	D_{free}[b] (10^{-11} m^2/s)	f_{bound}[c] (%)
F127 0.2 mg/mL			
0	0.5	5.9	18.2±0.7
1	0.4	6.0	17.5±0.9
2	0.4	6.0	15.4±0.7
5	0.5	5.9	10.3±0.7
10	0.5	5.9	5.5±0.6
20	0.6*	5.9	1.4±0.3
30	0.6*	5.9	0.7±0.1
P103 0.2 mg/mL			
0	0.5*	9.7	12.5±1.3
1	0.5*	9.8	11.3±1.4
2	0.5*	9.8	10.9±1.3
5	0.5*	9.8	5.5±0.7
10	0.5*	9.8	2.4±0.4
20	0.5*	9.8	1.4±0.2
30	0.5*	9.8	1.1±0.1
tPPO$_{14}$-PEO$_{46}$ 1 mg/mL			
0	0.5*	11.7	0.52±0.07
1	0.5*	11.6	0.30±0.01
2	0.5*	11.6	0.32±0.05
5	0.5*	11.6	0.20±0.03
10	0.5*	11.6	0.10±0.03
20	0.5*	11.6	0.11±0.03
30	0.5*	11.6	0.03±0.04
F68 1 mg/mL			
0	0.5*	6.8	0.10±0.02

[a] Obtained from the final slope of the echo decay curves of the polymer in the presence of liposomes.

*Estimated from the liposome diffusion coefficients measured by PFG-NMR using the ^{1}H signal of the three methyl groups from the choline group of POPC as the characterization peak, due to noise in the final slope of the polymer echo decay curves.

[b] Obtained from the linear fit of the echo decay curves of polymer without liposome. Only the data points before 5.0×10^{10} s/m^2 $\gamma^2G^2\delta^2(\Delta-\delta/3)$ were used for the linear fit to ensure a strong signal, since the signal of polymer decays very rapidly.

[c] Obtained from the average and standard deviation of the fitting results at Δ = 300, 500, and 700 ms based on eq 2.4.

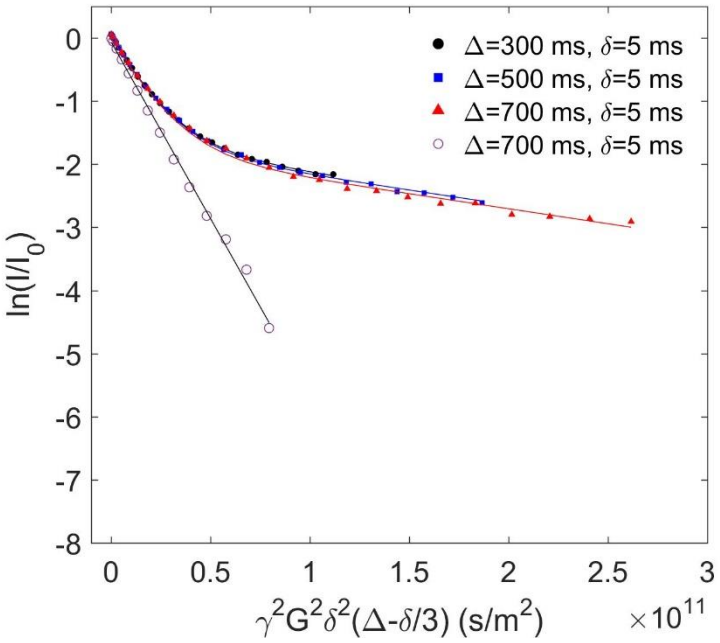

Figure 4.3. Experimental and fitted echo decay curves of the protons from PEO of 0.2 mg/mL F127 in the presence of 5 mM POPC liposome in D_2O at 27 °C with Δ = 300, 500, 700 ms (filled circles, filled squares, and filled triangles, respectively) and with fixed δ = 5 ms. The data were fit to eq 2.4. The open circles denote the proton signal from PEO of 0.2 mg/mL F127 in the absence of liposomes; these data were fit to eq 2.3.

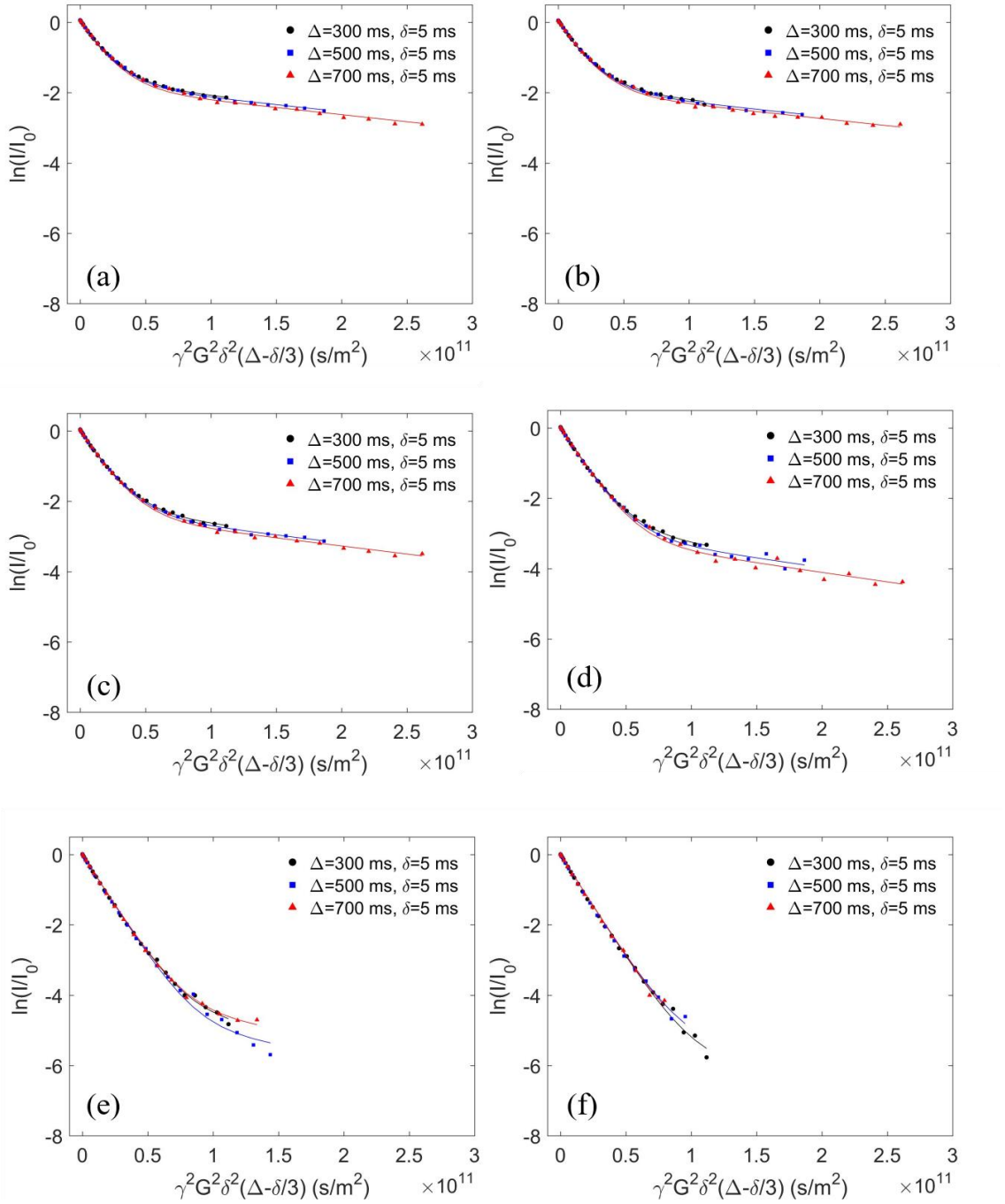

Figure 4.4. Experimental and fitted echo decay curves of the protons from PEO of 0.2 mg/mL F127 in the presence of 5 mM POPC/cholesterol liposome solution in D_2O at 27 °C with (a) 1 mol%, (b) 2 mol%, (c) 5 mol%, (d) 10 mol%, (e) 20 mol%, and (f) 30 mol% cholesterol.

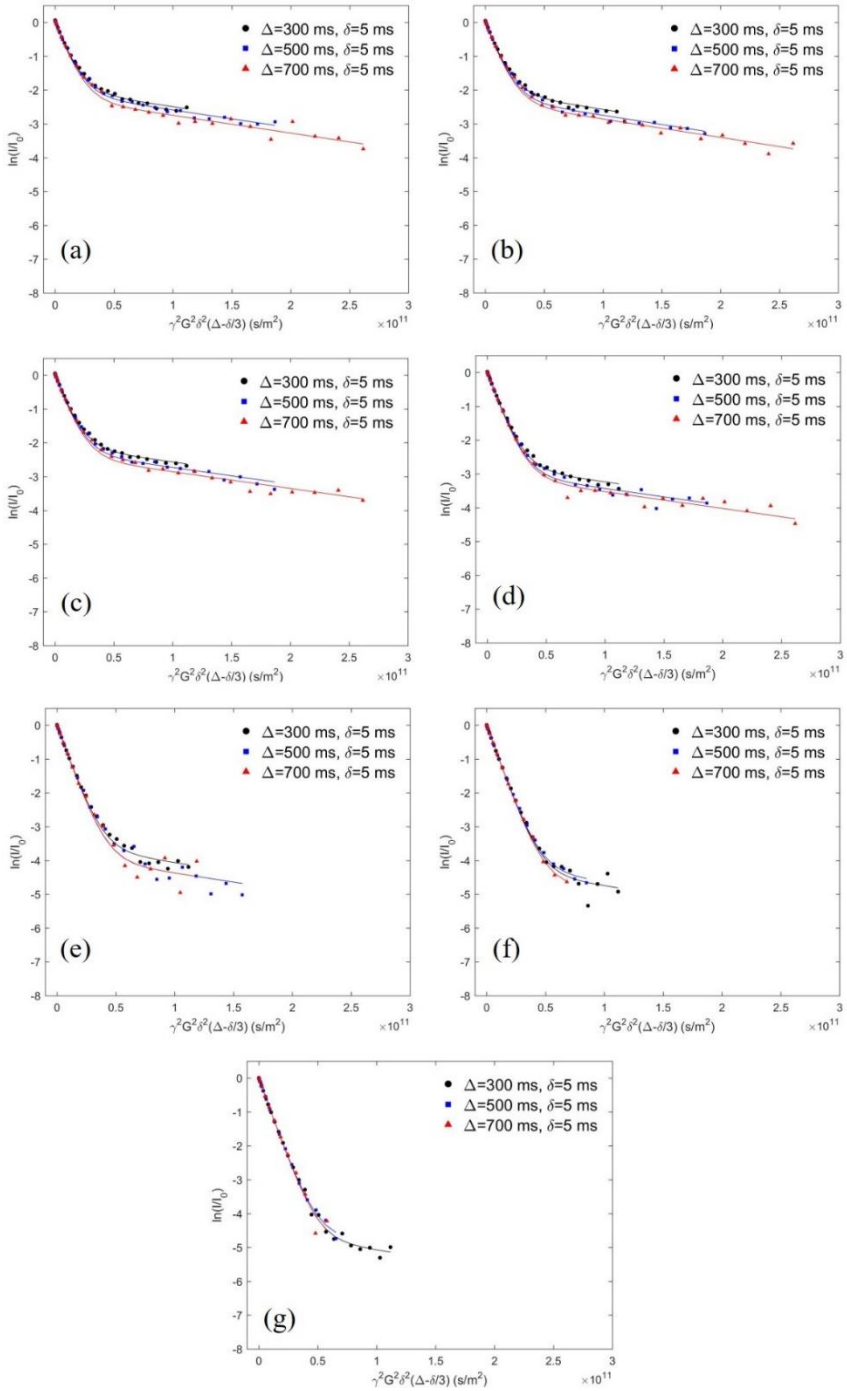

Figure 4.5. Experimental and fitted echo decay curves of the protons from PEO of 0.2 mg/mL P103 in the presence of 5 mM POPC/cholesterol liposome solution in D_2O at 27 °C with (a) 0 mol%, (b) 1 mol%, (c) 2 mol%, (d) 5 mol%, (e) 10 mol%, (f) 20 mol%, and (g) 30 mol% cholesterol.

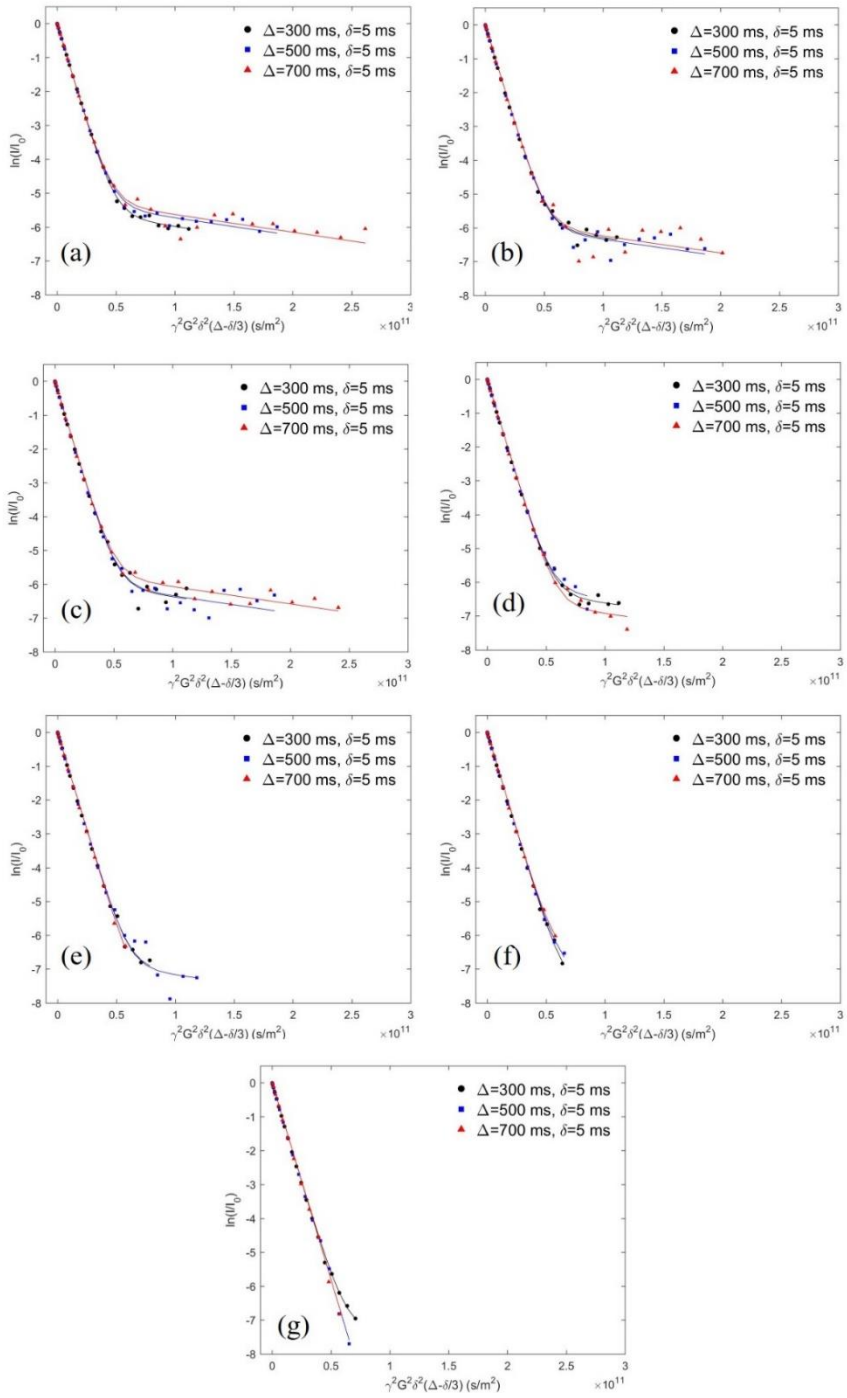

Figure 4.6. Experimental and fitted echo decay curves of the protons from PEO of 1 mg/mL *t*PPO_{14}-PEO_{46} in the presence of 5 mM POPC/cholesterol liposome solution in D_2O at 27 °C with (a) 0 mol%, (b) 1 mol%, (c) 2 mol%, (d) 5 mol%, (e) 10 mol%, (f) 20 mol%, and (g) 30 mol% cholesterol.

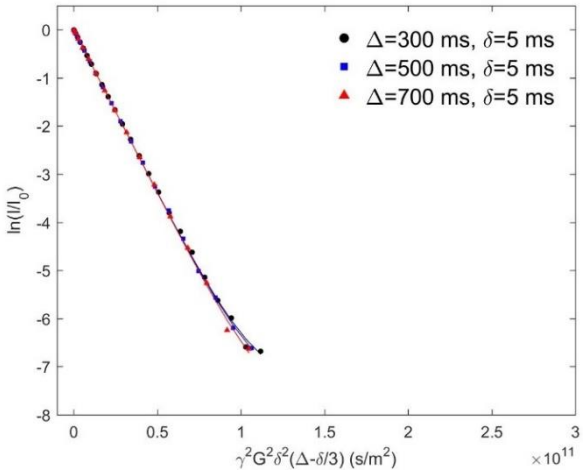

Figure 4.7. Experimental and fitted echo decay curves of the protons from PEO of 1 mg/mL F68 in the presence of 5 mM POPC liposome solution in D_2O at 27 °C.

The binding percentages of all four polymers (F127, P103, *t*PPO_{14}-PEO_{46}, and F68) extracted from the NMR data are plotted as a function of cholesterol molar percentage in the POPC/cholesterol lipid bilayers in Figure 4.8a and Figure 4.8b. The trends found for F127, P103, and *t*PPO_{14}-PEO_{46} are similar, where polymer binding decreases as cholesterol concentration increases, despite much weaker interactions between *t*PPO_{14}-PEO_{46} and the liposomes. These results are broadly consistent with earlier studies, which suggested that the addition of cholesterol decreases the polymer association with liposomes.[168,207] In order to compare the cholesterol effect on F127, P103, and *t*PPO_{14}-PEO_{46}, the polymer binding at various cholesterol concentrations was normalized to the binding with neat POPC liposomes (*i.e.*, no cholesterol addition) so that the binding trend of the three polymer species can be plotted on the same scale, as shown in Figure 4.8c. It can be seen that all three polymers exhibit a universal trend, with a remarkable ten-fold decrease in binding as the cholesterol concentration increases to 30 mol%. This cholesterol weakening effect on

polymer binding has little relative dependence on polymer species across a wide range of relative hydrophobicities, an observation that will be rationalized subsequently. The diffusion coefficients of free and bound polymers used for fitting and the resulting binding percentage of polymers to POPC liposomes at increasing cholesterol concentration are summarized in Table 4.3.

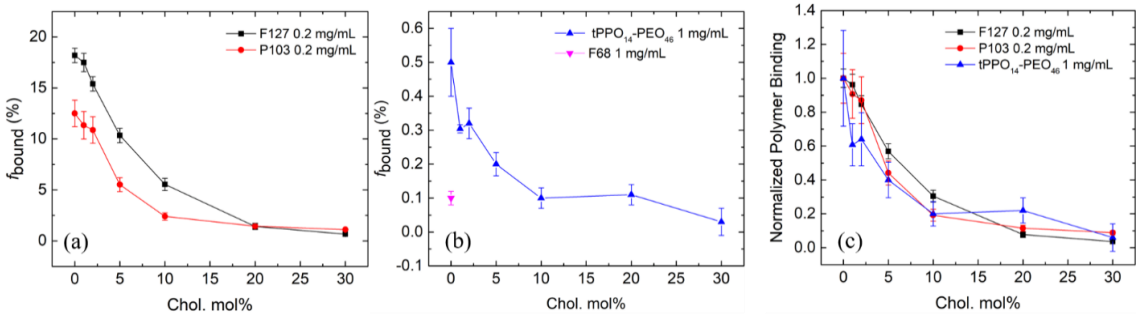

Figure 4.8. Polymer binding percentage of (a) two strongly bound polymer species, and (b) two weakly bound polymer species as a function of cholesterol molar percentage in POPC/cholesterol lipid bilayers. (c) Binding trend of three polymer species as a function of cholesterol molar percentage in the lipid bilayer, normalized to their binding with pure POPC lipid bilayers.

Significantly reduced polymer binding to liposomes could result from the change of membrane properties due to the presence of cholesterol. Membrane stiffness is a likely candidate, since the addition of cholesterol can induce ordering in lipid hydrocarbon chains, leading to membrane structural condensation and thereby increasing the bending modulus of the membrane.[166,274] Previous work of Arriaga and coworkers demonstrated that the bending modulus of POPC lipid bilayers significantly increases with added cholesterol.[166] Pan, et al. also investigated the effect of cholesterol on the membrane bending modulus, and reported that the stiffening effect of cholesterol on lipid bilayers is largely reduced when the phospholipids contain two mono-unsaturated hydrocarbon chains, compared to

one or none.[274] In order to test if the weakening effect of cholesterol on polymer binding depends on the degree of unsaturation of lipids, we compared the polymer binding to POPC liposomes with that to DOPC liposomes at increasing cholesterol molar percentage in the membrane. Since DOPC contains two mono-unsaturated hydrocarbon chains (Figure 2.4), while POPC only contains one, DOPC lipid bilayers remain more flexible (*i.e.*, lower bending modulus) than POPC bilayers when cholesterol is present, based on the study of Pan and coworkers. Note that despite the fact that the saturated chain of POPC only contains 16 carbons, which is two carbons shorter than the mono-unsaturated chains of DOPC (i.e., 18 carbons), we assume that this has little effect compared to the number of monosaturated chains of lipids on polymer binding and membrane bending modulus. As shown in Figure 4.9a, the polymer binding to DOPC liposomes is always greater than with POPC, despite the same overall trend that the binding decreases as the cholesterol molar percentage increases. After normalizing to the binding in the absence of cholesterol (Figure 4.9b), it can be seen that the polymer binding to DOPC liposomes decays more slowly than for POPC with increasing cholesterol. This indicates that cholesterol is less effective in reducing polymer binding to the lipid bilayers containing more mono-unsaturated hydrocarbon chains, which indirectly supports the hypothesis that the lipid bilayers with lower stiffness (*i.e.*, lower bending modulus) favor more polymer binding. Note that phospholipids with fully saturated hydrocarbon chains (e.g., DMPC) were not selected for this comparison because fully saturated lipids have relatively high phase transition temperatures, which would require temperatures above 27 °C used for the NMR measurements in order to access the fluid phase of the lipid membranes.

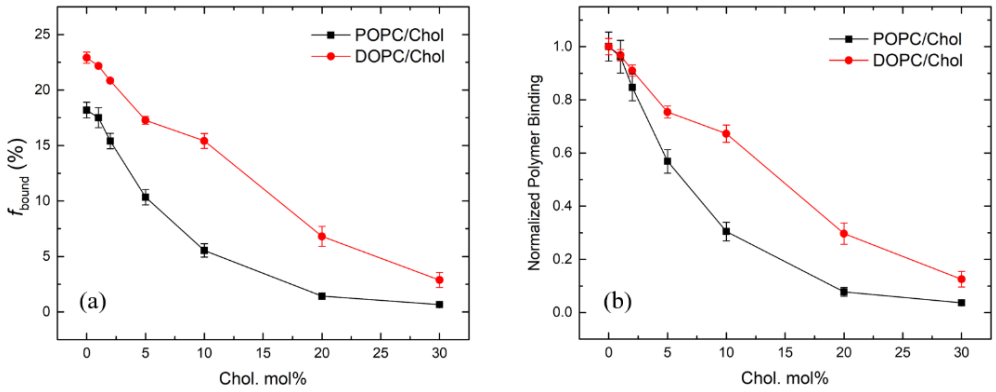

Figure 4.9. (a) Polymer binding percentage and (b) normalized polymer binding of 0.2 mg/mL F127 to 5 mM DOPC/cholesterol liposomes (red) and POPC/cholesterol liposomes (black) in D_2O at 27 °C as a function of cholesterol molar percentage.

Additionally, the hydrophobicity of the membrane alkyl chain region may also play an important role, as the hydrophobic interaction between the lipid bilayer interior and the PPO block of the polymers is a key determinant of the amount of polymer binding.[275] The addition of cholesterol may disturb such interactions since the steroid rings of cholesterol sitting in the bilayer interior are much more hydrophobic than lipid alkyl chains or the PPO blocks. We suspect that it is less favorable for the PPO blocks to associate with a much more hydrophobic component in the bilayer interior. It is also possible that the copolymer interacts less favorably with a more ordered lipid, or that increased membrane organization retards the initial stages of polymer association.

4.3.3 Bilayer Curvature Effect

Lipid bilayer curvature can be simply manipulated by altering the liposome size. Our work on quantifying polymer binding to lipid bilayers in Chapter 3 was based on liposomes with an intermediate extrusion pore radius of 50 nm.[275] Herein, two additional sizes of extrusion pore radius (25 nm and 100 nm) were used in order to obtain liposomes with three different curvatures, corresponding to κ = 0.009, 0.014, and 0.024 nm^{-1}, calculated as $\kappa = 1/R_h$. F127 and P103 were selected as representative strongly binding polymers, whereas *t*PPO_{14}-PEO_{46} and F68 were weakly binding polymers.[275] The binding percentages of the strongly and weakly interacting polymers with increasing lipid bilayer curvature are shown in Figure 4.10a and Figure 4.10b, respectively. The bilayer curvature, the diffusion coefficients of free and bound polymers used for fitting, and the resulting polymer binding percentage are summarized in Table 4.4. The binding of all four polymers increases as the lipid bilayer curvature increases. These results have also been normalized to the binding at the smallest curvature, as shown in Figure 4.10c. It can be seen that the normalized binding as a function of curvature for all polymer species except F68 collapse onto a consistent increasing trend with κ, *i.e.*, higher curvature results in greater polymer binding. When the bilayer curvature is less than 0.014 nm^{-1} (corresponding to an extrusion pore radius of 50 nm or more), polymer binding (except F68) is almost independent of the curvature. This finding validates the rationale for using liposomes with an extrusion pore radius of at least 50 nm as models to mimic the flat configuration of real cell membranes, as assumed in previous studies of polymer-membrane association.[14,15,24,169] The inconsistent binding trend of F68 can be attributed to its extremely weak interactions with liposomes, as the

binding percentage at highest curvature is only 0.2%; the inherently weak association of F68 with liposomes gives rise to large uncertainty in quantifying the polymer binding. We speculate that the higher polymer binding at higher bilayer curvature may be associated with the existence of greater space in the outer leaflet of the lipid bilayer with higher curvature. Interaction with polymers could mitigate the thermodynamic penalty associated with such inferior packing.

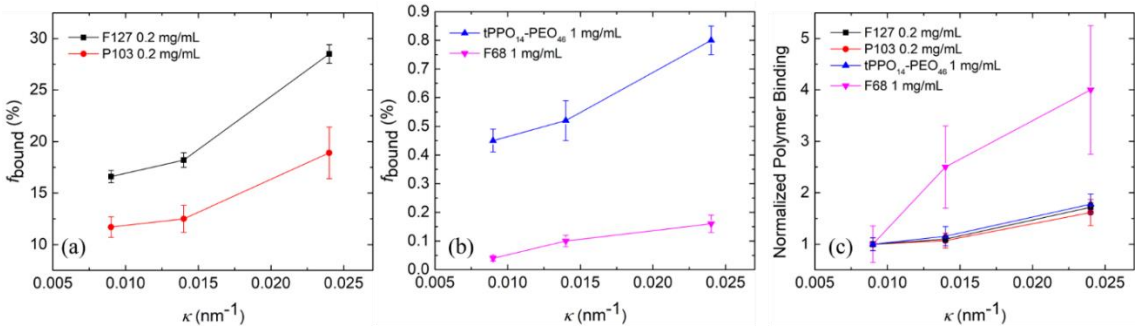

Figure 4.10. Polymer binding percentage of (a) two strongly bound polymer species, and (b) two weakly bound polymer species as a function of POPC lipid bilayer curvature. (c) Binding trend of four polymer species as a function of POPC lipid bilayer curvature, normalized to their binding to the liposome with the smallest curvature.

Table 4.4. Summary of polymer binding to 5 mM POPC liposomes with different curvature in D_2O at 27 °C.

Extrusion Pore Radius (nm)	R_h[a] (nm)	κ[b] (nm^{-1})	D_{bound}[c] (10^{-11} m^2/s)	D_{free}[d] (10^{-11} m^2/s)	f_{bound}[e] (%)
F127 0.2 mg/mL					
25	42	0.024	0.6	5.9	28.5±0.9
50	69	0.014	0.5	5.9	18.2±0.7
100	109	0.009	0.4	5.9	16.6±0.6
P103 0.2 mg/mL					
25	42	0.024	0.6	9.5	18.9±2.5
50	69	0.014	0.5*	9.7	12.5±1.3
100	109	0.009	0.5*	9.7	11.7±1.0
$tPPO_{14}$-PEO_{46} 1 mg/mL					
25	42	0.024	0.6*	11.7	0.8±0.1
50	69	0.014	0.5*	11.7	0.5±0.1
100	109	0.009	0.5*	11.6	0.45±0.04
F68 1 mg/mL					
25	42	0.024	0.6*	6.8	0.16±0.03
50	69	0.014	0.5*	6.8	0.10±0.02
100	109	0.009	0.5*	6.8	0.04±0.01

[a] Obtained from DLS.

[b] Calculated from R_h obtained from DLS ($\kappa = 1/R$, using R_h for R).

[c] Obtained from the final slope of the echo decay curves of the polymer in the presence of liposomes.

*Estimated from the liposome diffusion coefficients measured by PFG-NMR using the ^1H signal of the three methyl groups from the choline group of POPC as the characterization peak due to noise in the final slope of the polymer echo decay curves.

[d] Obtained from the linear fit of the echo decay curves of polymer without liposome. Only the data points before 5.0×10^{10} s/m^2 $\gamma^2G^2\delta^2(\Delta-\delta/3)$ were used for the linear fit to ensure a strong signal, since the signal of polymer decays very rapidly.

[e] Obtained from the average and standard deviation of the fitting results at Δ = 300, 500, and 700 ms based on eq 2.4.

We have demonstrated that higher cholesterol molar percentage in the lipid bilayer results in less polymer binding, whereas higher bilayer curvature results in more polymer binding. In order to investigate whether the cholesterol weakening effect on polymer binding can be mitigated by higher curvature of the lipid bilayers, we further measured the binding of F127 to lipid bilayers with a higher curvature (*i.e.*, extruded through a pore radius of 25 nm) as a function of cholesterol molar percentage (Figure 4.11a). Compared with its binding to the bilayer with an intermediate curvature (*i.e.*, extruded through a pore radius of 50 nm), F127 shows significantly more binding at higher curvature until the cholesterol molar percentage reaches 20 mol%. At 20 mol% and 30 mol% cholesterol, the binding percentage at both curvatures drop below 2% and shows no significant difference. Note that the liposomes at these high cholesterol levels exhibit more similar curvature (κ = 0.018 nm^{-1} and 0.014 nm^{-1}) because the curvature of the liposomes extruded through the 25 nm pores decreased with increased cholesterol (Table 4.1). For brevity, the average curvature of the liposomes extruded through the same pore radius is shown in Figure 4.11 (*i.e.*, 0.015 nm^{-1} for liposomes extruded through 50 nm pore radius and 0.020 nm^{-1} for 25 nm pore radius). Polymer binding at both curvatures as a function of cholesterol molar percentage was further normalized to their original binding with neat POPC liposomes (*i.e.*, no cholesterol addition). As shown in Figure 4.11b, the two curves overlap with each other and follow the same decreasing trend as cholesterol molar percentage increases. This indicates that the cholesterol weakening effect on polymer binding has little dependence on lipid bilayer curvature. The diffusion coefficients of free and bound polymers used for

fitting and the resulting polymer binding percentage at higher curvature (*i.e.*, 0.020 nm^{-1}) are summarized in Table 4.5.

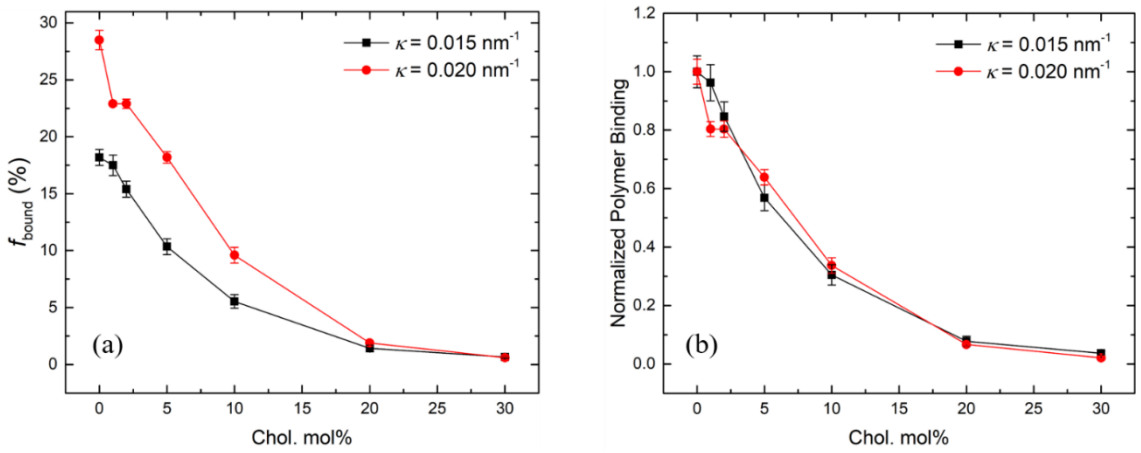

Figure 4.11. (a) Polymer binding percentage and (b) normalized polymer binding of 0.2 mg/mL F127 to POPC/cholesterol liposomes with κ = 0.015 nm^{-1} (black) and κ = 0.020 nm^{-1} (red) as a function of cholesterol molar percentage.

Table 4.5. Binding of F127 to 5 mM POPC/cholesterol liposomes extruded through a polycarbonate membrane with 25 nm pore radius in D_2O at 27 °C.

Cholesterol Molar Percentage (%)	D_{bound}[a] (10^{-11} m^2/s)	D_{free}[b] (10^{-11} m^2/s)	f_{bound}[c] (%)
0	0.6	5.9	28.5±0.9
1	0.7	5.9	22.9±0.2
2	0.7	5.9	22.9±0.4
5	0.7	5.9	18.2±0.5
10	0.7	5.9	9.6±0.7
20	0.6*	5.9	1.9±0.1
30	0.6*	5.9	0.6±0.2

[a] Obtained from the final slope of the echo decay curves of the polymer in the presence of liposomes.

*Estimated from the liposome diffusion coefficients measured by PFG-NMR using the ^{1}H signal of the three methyl groups from the choline group of POPC as the characterization peak due to noisy data at the final slope of polymer echo decay curves.

[b] Obtained from the linear fit of the echo decay curves of polymer without the presence of liposome. Only the data points before 5.0×10^{10} s/m^2 $\gamma^2G^2\delta^2(\Delta-\delta/3)$ were used for the linear fit to ensure a strong signal since the signal of polymer decays very rapidly.

[c] Obtained from the average and standard deviation of the fitting results at Δ = 300, 500, and 700 ms based on eq 2.4.

Figure 4.8c and Figure 4.11b reveal similar trends for relative polymer binding with increasing cholesterol molar percentage, independent of polymer species and lipid bilayer curvature. A straightforward argument can rationalize both the exponential form of the decay, and the fact that the normalized curves for quite different polymers collapse onto a single curve. The polymer binding percentage, f_{bound}, can be converted to an equilibrium binding constant K as follows:

$$K = \frac{[\text{bound}]}{[\text{free}]} = \frac{f_{\text{bound}}}{100 - f_{\text{bound}}} = \exp\left(-\frac{\Delta G^{\circ}}{RT}\right) \quad (4.1)$$

K is defined as the ratio of the concentration of bound polymers ([bound]) to that of free polymers ([free]), assuming that the concentration of lipid binding sites remains unchanged and thereby is incorporated into *K*. *K* is related to the standard free energy change of the binding process, ΔG^{o}, where *R* is the gas constant and *T* is the temperature. For a given polymer, we can define three free energies, corresponding to three possible states: G°_{free} as the free energy of a polymer in water (*i.e.*, unbound state), $G^{\circ}_{bound,lipid}$ as the free energy of a polymer bound to a liposome composed of 100 mol% POPC, and $G^{\circ}_{bound,chol}$ as the free energy of a polymer bound to a liposome composed of 100 mol% cholesterol (a hypothetical limit). If the binding to a mixed lipid/cholesterol layer is linear in the cholesterol composition *x* (*i.e.*, eq 4.2), analogous to an assumption of "ideal mixing" in the layer, then ΔG^{o} will vary linearly with the cholesterol molar percentage, as shown by eq 4.3 which is obtained by simply rearranging eq 4.2.

$$\Delta G^{\circ} = (1 - x) \cdot G^{\circ}_{bound,lipid} + x \cdot G^{\circ}_{bound,chol} - G^{\circ}_{free} \tag{4.2}$$

$$\Delta G^{\circ} = \left(G^{\circ}_{bound,chol} - G^{\circ}_{bound,lipid}\right) \cdot x + G^{\circ}_{bound,lipid} - G^{\circ}_{free} \tag{4.3}$$

Therefore, *K* can be written as:

$$K = e^{-\frac{G^{\circ}bound,lipid - G^{\circ}free}{RT}} \cdot e^{-\frac{\left(G^{\circ}bound,chol - G^{\circ}bound,lipid\right)}{RT} \cdot x} \tag{4.4}$$

Since $e^{-\frac{G^{\circ}bound,lipid - G^{\circ}free}{RT}}$ is a constant, *K* after normalization can be written as:

$$\frac{K(x)}{K(0)} = e^{-\frac{\left(G^{\circ}bound,chol - G^{\circ}bound,lipid\right)}{RT} \cdot x} \tag{4.5}$$

Therefore, $\frac{K(x)}{K(0)}$ can be fitted to a single exponential decay model $y = e^{-Ax}$, where

$$A = \frac{\left(G^{\circ}_{bound,chol} - G^{\circ}_{bound,lipid}\right)}{RT} \tag{4.6}$$

According to the derivations above, the assumption of "ideal mixing" in the lipid bilayer is therefore sufficient to explain the single exponential decay observed. Then, if we make the further assumption that the incremental free energy cost to bind a more hydrophilic polymer compared to a more hydrophobic polymer is the same for pure lipid and for pure cholesterol, then the exponential decay constant *A* is independent of polymer. *K* for the various polymer species interacting with liposomes with different curvatures is plotted as a function of *x* in Figure 4.12. Each curve is fit to the single exponential decay model as described above. The fitted values of parameter *A* are summarized in Table 4.6. Within the uncertainty of these fits all the data can be accounted for by a single value of *A*. This confirms the assumption that the difference of the standard free energy of a polymer bound to a liposome composed of 100 mol% POPC compared to a hypothetical liposome composed of 100 mol% cholesterol changes little with the variation of polymer species or bilayer curvature. Similarly, we can assume that for a specific polymer interacting with two different lipid bilayer curvatures, the extra cost of binding due to the curvature change is the same for the polymer bound to pure lipid and to pure cholesterol, and thereby *A* is the same for two different curvatures.

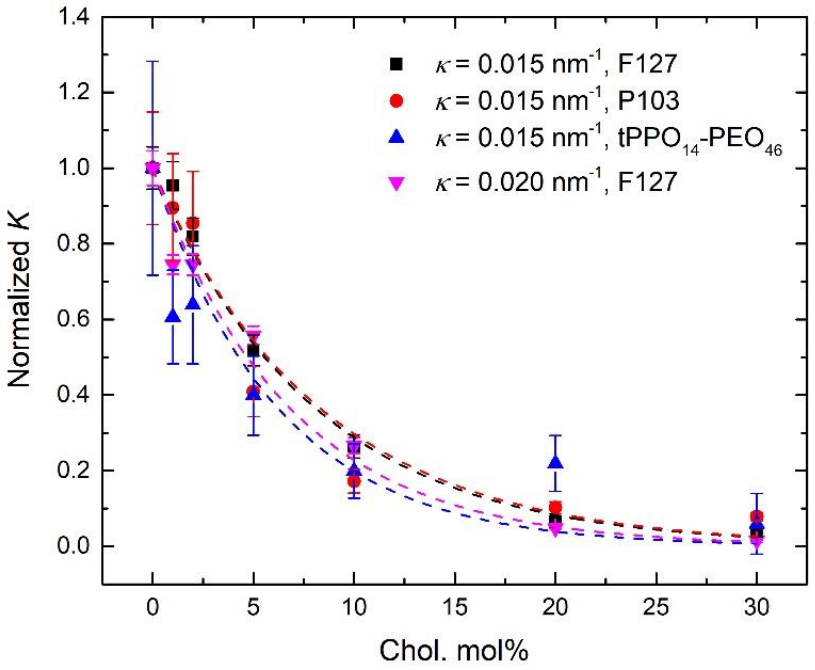

Figure 4.12. Single exponential decay model fitted to the normalized *K* of various polymer species bound to POPC/cholesterol liposomes with different curvatures as a function of cholesterol molar percentage.

Table 4.6. Fitting results of the decay parameter *A*.

Polymer Species	**Bilayer Curvature (κ, nm^{-1})**	**Parameter *A****
F127	0.015	0.13±0.01
F127	0.020	0.15±0.01
P103	0.015	0.12±0.02
$tPPO_{14}$-PEO_{46}	0.015	0.16±0.03

* A single exponential decay was applied to fit the data. Errors of the data points (as shown by the error bars in Figure 4.12) were taken into account by weighting the fitting, using $w_i = \frac{1}{\sigma_i^2}$, where σ_i is the error of each data point.

4.4 Conclusions

We have investigated how cholesterol concentration and lipid bilayer curvature affect the interaction of both strongly and weakly binding PPO-PEO block copolymers with POPC and DOPC liposomes. Copolymer binding to liposomes was probed by PFG-NMR, which can resolve the relative amounts of free and liposome-bound polymers. The role of cholesterol was studied by quantifying polymer binding at various cholesterol molar percentages. For POPC, the copolymer binding decays exponentially with cholesterol composition, by a factor of 10 at 30 mol% cholesterol relative to the pure lipid bilayer. This could be due to an increase in membrane bending modulus and/or hydrophobicity. Polymer binding also decreases as the bilayer curvature decreases, most notably between liposomes with extrusion radii of 25 and 50 nm, with less variation as the size increases to 100 nm. This may be due to the creation of greater void space in the outer leaflet of the lipid bilayer with higher curvature, which is mitigated by the presence of the hydrophobic PPO blocks. All the data obtained with the weakly and strongly associating PPO-PEO block copolymers at different bilayer curvatures and with varying cholesterol content, can be reduced to a single exponential curve of normalized equilibrium binding constant K versus cholesterol content. This superposition can be rationalized with only two plausible assumptions, that the free energy change of binding is linear in cholesterol content, and that the increment in free energy to bind a more hydrophilic polymer than a more hydrophobic one is independent of the membrane composition. In summary, these results demonstrate that cholesterol in the lipid bilayer plays a dominant role in controlling the interactions of liposomes with both weakly and strongly adsorbing PPO-PEO block

polymers. This finding establishes a key factor in understanding how Pluronics/poloxamers impact cellular activity in living systems.

Chapter 5 - Influence of Lipid Composition on Polymer-Membrane Association

5.1 Introduction

In Chapter 4, we investigated the role of cholesterol in polymer-membrane association. The major components of plasma membranes are phospholipids, which form the bilayer scaffold of membranes.[252,276] Phospholipids are amphiphilic molecules generally comprising two hydrocarbon chains and a polar headgroup consisting of a phosphate group and a functional group (e.g., choline, ethanolamine, serine, glycerol, and inositol).[276] Headgroup species and their charges can strongly affect the phospholipid membrane dipole potential,[277] headgroup conformations,[278] phase transition,[279–281] raft formation,[282,283] and their interactions with drug molecules, polymers, peptides, and proteins.[137,171,284–289] The

degree of unsaturation and the length of the hydrocarbon chains dictate the lipid phase transition temperature and the conformational order of the hydrocarbon chains that involves trans-gauche isomerizations, which further affects other bilayer parameters (e.g., bilayer thickness and area per lipid) as well as phase behavior.[151,260,290] Exploring the influence of lipid composition on their interactions with polymers will enable us to develop a more comprehensive understanding of the mechanism of polymer-membrane association from a membrane perspective and help improve the design of model membrane systems.

Herein, the effect of lipid composition on polymer-membrane association was investigated by quantifying the polymer binding to liposomes composed of various phospholipids with different headgroups and degree of unsaturation of the hydrocarbon chains. Large unilamellar liposomes were selected as model membranes, the preparation of which gives precise control over the lipid bilayer composition. Polymers involved in this study include commercial triblock poloxamers and lab-synthesized diblock analogs; their chemical structures are shown in Figure 1.1. Polymer binding to liposomes was determined by PFG-NMR based on the distinctly different diffusivities of free and bound polymers. Lipid headgroup composition was manipulated by mixing 1-palmitoyl-2-oleoyl-sn-glycero-3-phospho-(1'-rac-glycerol) sodium salt (POPG; Figure 5.1b) with 1-palmitoyl-2-oleoyl-sn-glycero-3-phosphocholine (POPC, Figure 5.1a) at various molar ratios to compare the effect of glycerol headgroups with choline headgroups. Pure POPC liposomes were used as controls since phosphatidylcholine is one of the major components found in eukaryotic cell membranes and is widely used as the basic constituent in model membranes.[107,108,179] Phosphatidylglycerol, on the other hand, is a relatively minor

component in eukaryotic cell membranes and is mostly found in bacterial cell membranes.[291] Nevertheless, given that POPG has the same phase transition temperature and almost the same chemical structure except the headgroup as POPC, it can be considered as a simple model to study how the presence of net charges and hydroxyl groups in the lipid headgroups affect their interactions with polymers from a fundamental perspective. It has been reported that the net charge and hydroxyl groups carried by the headgroup of POPG play important roles in headgroup-headgroup interactions, which could change the orientation and conformation of the headgroups, as well as the area per lipid.[292–295] Additionally, the degree of unsaturation of lipid hydrocarbon chains was manipulated by tuning the content of saturated and unsaturated lipids in the liposomes. The results obtained from this study demonstrate the critical role that lipid composition plays on polymer-membrane association and provides guidance to future studies using more complicated membrane compositions than a two-component membrane system.

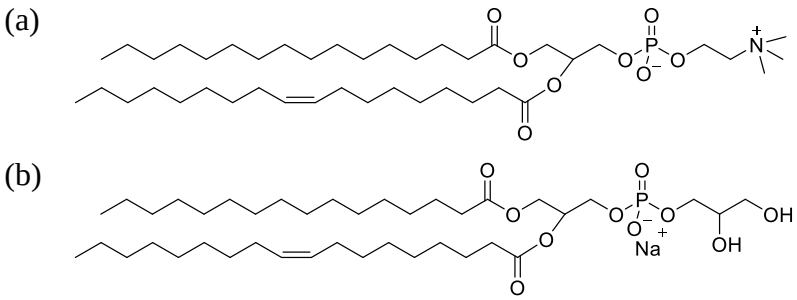

Figure 5.1. Chemical structures of (a) 1-palmitoyl-2-oleoyl-glycero-3-phosphocholine (POPC), and (b) 1-palmitoyl-2-oleoyl-sn-glycero-3-phospho-(1'-rac-glycerol) (POPG).

5.2 Experimental Section

Details of the experimental techniques used in this chapter are described in Chapter 2. The materials, sample preparation, and experimental procedures that are specific to this chapter are summarized below.

5.2.1 Materials

Pluronics F68, P84, P103, P104, P105, F108, and F127 were provided by BASF. Ethylene oxide (EO, ≥ 99.5%), propylene oxide (PO, ≥ 99%), potassium, naphthalene, potassium *tert*-butoxide, n-butyllithium, 18-crown-6 ether, sodium chloride (NaCl, ≥ 99.0%), silver trifluoroacetate (AgTFA), and α-cyano-4-hydroxycinnamic acid (CHCA, ≥ 98%), were purchased from Sigma-Aldrich and used as received. 1-palmitoyl-2-oleoyl-sn-glycero-3-phosphocholine (POPC, 16:0-18:1 PC), 1-palmitoyl-2-oleoyl-sn-glycero-3-phospho-(1'-rac-glycerol) sodium salt (POPG, 16:0-18:1 PG), 1,2-dioleoyl-sn-glycero-3-phosphocholine (DOPC, 18:1(Δ9-Cis) PC), 1-palmitoyl-2-linoleoyl-sn-glycero-3-phosphocholine (PLPC, 16:0-18:2 PC), and 1,2-dipalmitoyl-sn-glycero-3-phosphocholine (DPPC, 16:0 PC) in chloroform were purchased from Avanti Polar Lipids (Alabaster, AL) and used as received. Deuterium oxide (D_2O, 99.9 atom % D) and chloroform-d ($CDCl_3$, 99.8 atom % D + 0.05% V/V TMS) were purchased from Cambridge Isotope Laboratories, Inc. Ultrapure water with resistivity of 18.2 MΩ × cm was obtained from a Millipore Direct Q-3 water system (EMD Millipore, Billerica, MA).

5.2.2 Polymer Synthesis and Characterization

The diblock polymers *t*PPO_{14}-PEO_{46}, *t*PPO_{14}-PEO_{78}, and *t*PPO_{29}-PEO_{68} used in this chapter were synthesized by anionic polymerization as described in Chapter 2.1. The number-average molecular weight, dispersity, and composition of the polymers are summarized in Table 2.1.

5.2.3 Liposome Preparation and Characterization

Liposomes were prepared by the extrusion method as described in Chapter 2.3. The bicomponent liposomes (*i.e.*, POPC/POPG and POPC/DPPC) were prepared by mixing POPC lipids with POPG and DPPC lipids at a specific ratio. The dry lipid films of various lipid composition were hydrated at 37 ºC, except for the ones containing DPPC, which were hydrated at 50 ºC due to a higher lipid phase transition temperature of DPPC. The liposomes used for PFG-NMR experiments were prepared in D_2O or 150 mM NaCl salt solution in D_2O, while those used for Raman measurements were prepared in ultrapure H_2O. The hydrodynamic radius R_h and size dispersity of the liposomes was characterized by DLS as described in Chapter 2.4.1.

5.2.4 PFG-NMR Measurements

Polymer-lipid bilayer association was evaluated by quantifying the polymer binding to the liposomes via PFG-NMR as described in Chapter 2.5.

5.2.5 Raman Spectroscopy

Raman spectroscopy measurements were performed on a WITec alpha300 R confocal Raman microscope equipped with a UHTS300 spectrometer (1800 g/mm grating), a DV401 CCD detector, and a 60× water immersion objective (Nikon Fluor 60× W, NA = 1.00). An Omnichrome Argon ion laser with 514.5 nm excitation and 50 mW maximum output power was used as the laser beam source. The laser power was adjusted to acquire stable Raman spectra with the highest possible signal intensity. Raman scattering was performed in a backscattering geometry and collected with an integration time of 90 s. WITec Control software was used for data acquisition and analysis.

Polymer-liposome samples were prepared by combining equal volume of 60 mM liposome stock solution and 40 mg/mL polymer stock solution (both prepared with 150 mM NaCl in H_2O), leading to a final concentration of 30 mM liposomes and 20 mg/mL polymers in the mixture used for Raman measurements. Pure liposome solution at 30 mM and pure polymer solution at 20 mg/mL were prepared as controls by diluting the liposome and polymer stock solutions with 150 mM NaCl solution. All the samples were measured at room temperature.

5.3 Results and Discussion

5.3.1 Effect of Lipid Headgroup

The size and dispersity of the liposomes composed of POPC and POPG are summarized in Table 5.1. The NaCl solution at physiologic concentration (150 mM) was used as the

solvent instead of pure D_2O in order to screen electrostatic interactions between anionic POPG lipids, which will be discussed in more details in the following paragraphs. The size of neat POPC liposomes remained the same when switching the solvent from D_2O to the salt solution. The liposome size slightly decreases as the molar percentage of POPG increases in the POPC/POPG lipid bilayer, whereas the dispersity of liposomes was not affected as the values of μ_2/Γ^2 determined by DLS all remain around 0.1. Note that the liposome diffusivity remains one order of magnitude slower than that of free polymers despite the moderate size decrease of the liposome. Therefore, the polymer binding to the liposomes can still be quantified by PFG-NMR due to the mobility difference between free polymers and liposomes.

Table 5.1. POPC/POPG Liposome Size Characterization by DLS.

POPG Molar Percentage (%)	R_h[a] **(nm)**	μ_2/Γ^2 **at 90°**
0*	70	0.04
0	70	0.08
20	66	0.08
40	66	0.11
60	61	0.07
80	62	0.08
100	62	0.10

[a] R_h measured by DLS has approximately 5% uncertainty.

*measured in D_2O as a control. All the other samples were measured in 150 mM NaCl solution in D_2O.

The headgroup effect was investigated by comparing polymer binding to POPC liposomes containing a choline group and POPG liposomes with a glycerol group. 150 mM

NaCl D_2O solution was used as the solvent instead of D_2O to stabilize the liposomes by screening the electrostatic interactions between negatively charged headgroups of POPG. The repulsive force between POPG headgroups was suspected to disrupt the liposomes after mixing with polymers, as shown in Figure 5.2. When using D_2O as the solvent (Figure 5.2a), the PFG-NMR data profile of the POPG liposomes after mixing with polymers (red circles) decays much faster than that of neat liposome (black squares) despite the noisy signal of neat liposomes. Faster diffusion and a nonlinear profile of the liposomes in the presence of polymers suggest that the liposomes were disrupted into smaller vesicles or aggregates with high dispersity. In the absence of salt, the repulsive interactions between POPG headgroups become significant, which make the liposomes unstable and vulnerable to disturbances induced by polymer association. The highly disperse diffusivity of polymers in the presence of liposomes illustrated by the nonlinearity of the profile (blue triangles) is attributed to the polymer binding to the disrupted polydisperse liposomes. In contrast, as shown in Figure 5.2b, the biexponential characteristics of the polymer decay curves (blue triangles) in the presence of liposomes were recovered when 150 mM NaCl D_2O solution was used. The linear plateau region (i.e., final slope of the polymer biexponential decay) indirectly indicates that the integrity of the liposome structure was retained, even though the liposome diffusion after mixing with polymers (red circles) was unable to be clearly resolved due to a noisy signal. Note that the decay curves of POPG liposomes were obtained using the ^1H signal of POPG alkyl chains since the ^1H signal of the headgroup can be barely observed. The noisy signal of liposomes can be attributed to

the broad signal peak due to liposome size dispersity and the poor solubility of alkyl chains in water, which significantly decreased the signal-to-noise ratios.

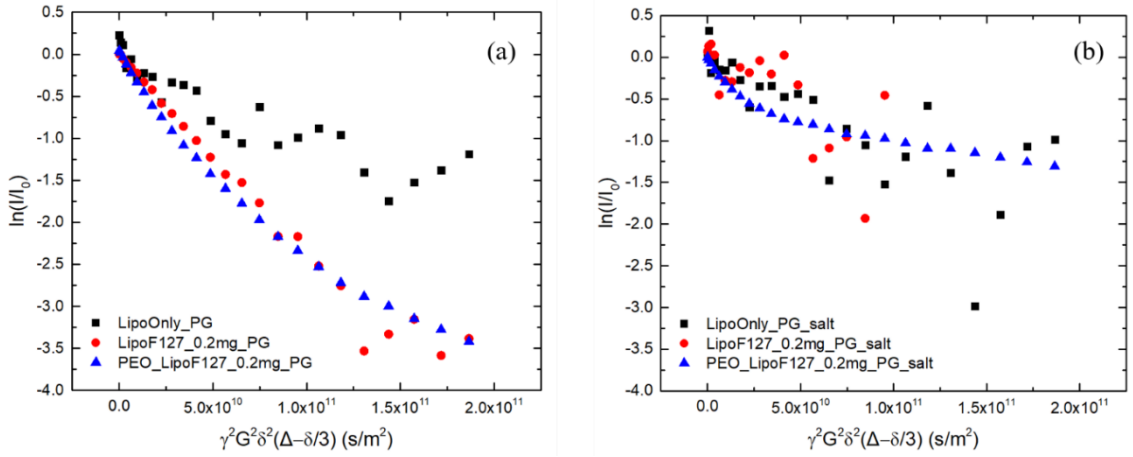

Figure 5.2. Echo decay curves of 5mM neat POPG liposomes (black square), 5mM POPG liposomes in the presence of 0.2 mg/mL F127 (red circle), and 0.2 mg/mL F127 in the presence of 5mM POPG liposome (blue triangle) at 27 °C in (a) D_2O and (b) 150 mM NaCl D_2O solution. The decay curves of POPG liposomes were obtained using the ^1H signal of POPG alkyl chains since the ^1H signal of the headgroup can be barely observed. The noisy signal of liposomes is attributed to the broad signal peak due to liposome dispersity and the poor solubility of alkyl chains in water, which significantly decreased the signal-to-noise ratios.

Polymer binding to POPC liposomes in D_2O, to POPC liposomes in 150 mM NaCl D_2O solution, and to POPG liposomes in 150 mM NaCl D_2O solution is displayed in Figure 5.3a. The binding plotted on a logarithmic scale is shown in Figure 5.3b. The values of binding percentage and related parameters used in the fitting are summarized in Table 5.2. In order to assess whether switching the solvent from water to salt solution makes any difference, the polymer binding to POPC liposomes in D_2O (gray bars) and that in 150 mM NaCl D_2O solution (red bars) were first compared. Some polymers show slightly more binding with POPC lipid bilayers in salt solution than in D_2O. This could be caused by a

slight decrease of the CMC of the polymers due to the presence of salt.[30,56,57,59] A lower CMC gives rise to a stronger drive for the hydrophobic block of the polymers to form a micellar core or insert into the hydrophobic bilayer interior, rather than interacting with water molecules.[275] Note that the physiologic salt concentration used in our study is not high enough to induce micellization, so the polymers still remain as free coils, despite the polymer concentration moving slightly closer to the CMC.[30,57,59] This is also verified by the linearity of the PFG-NMR profiles of free polymers in salt solution. Figure 5.4 shows an example of the echo decay curves of F127 in D_2O and in 150 mM NaCl D_2O solution. The two linear fits gave almost identical diffusivity of this polymer in water and in salt solution, indicating that the presence of 150 mM NaCl in D_2O doesn't induce polymer micellization. Therefore, changing the solvent from D_2O to 150 mM NaCl D_2O solution slightly increases the polymer binding to POPC lipid bilayers, but the effect is not significant, especially considering the error bars associated with the measurement of polymer binding.

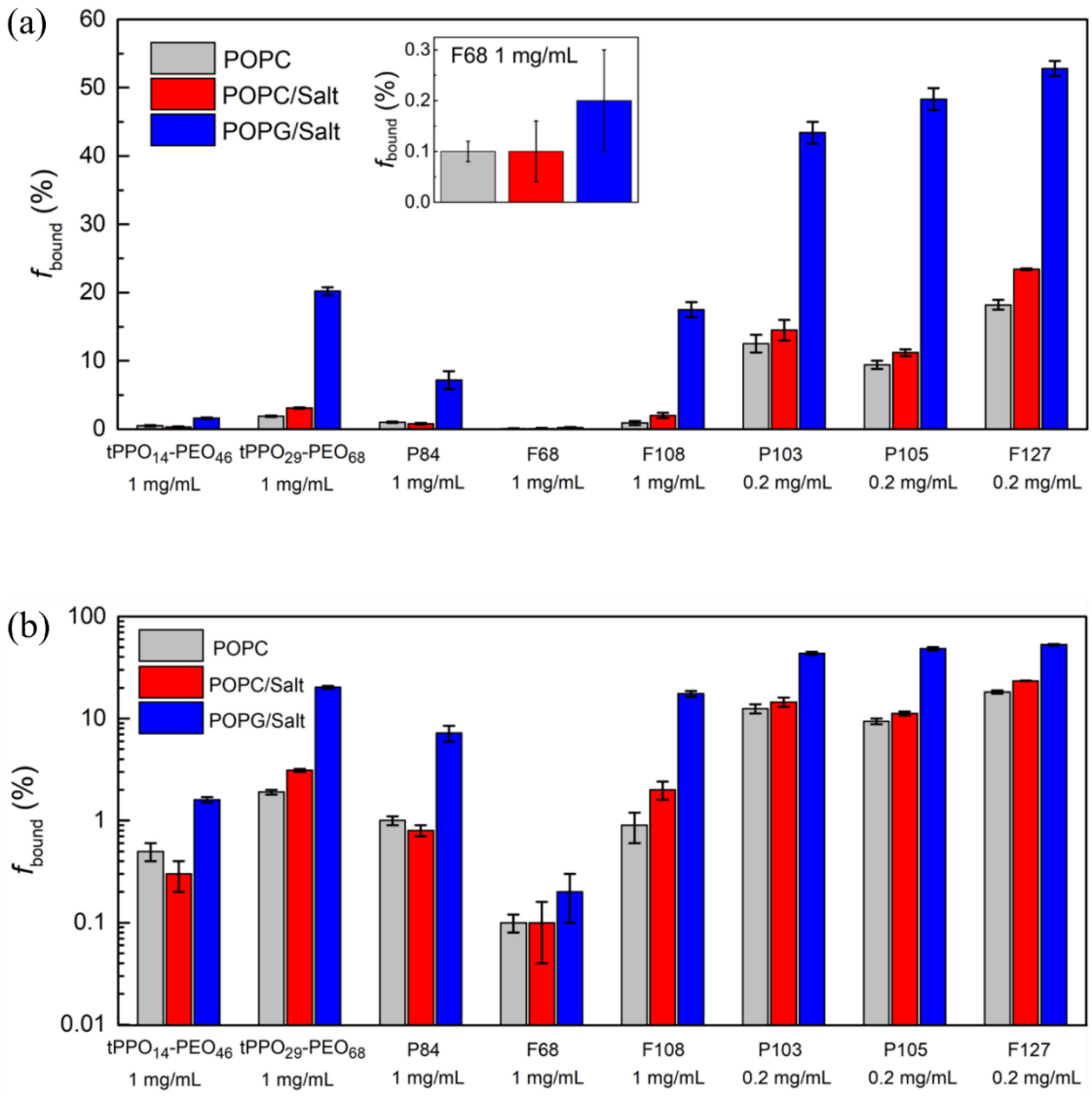

Figure 5.3. (a) Polymer binding with POPC liposomes in D_2O (gray), with POPC liposomes in 150 mM NaCl D_2O solution (red), and with POPG liposomes in 150 mM NaCl D_2O solution (blue). The inset shows a zoom-in view of the binding of F68. (b) Data replotted on a logarithmic scale.

Table 5.2. Summary of polymer binding to 5mM POPC liposomes in D_2O, to POPC liposomes in 150 mM NaCl D_2O solution, and to POPG liposomes in 150 mM NaCl D_2O solution at 27 °C.

Polymer	Concentration (mg/mL)	D_{bound}[a] (10^{-11} m^2/s)	D_{free}[b] (10^{-11} m^2/s)	f_{bound}[c] (%)
POPC liposomes in D_2O				
$tPPO_{14}$-PEO_{46}	1	0.5*	11.7	0.5±0.1
$tPPO_{29}$-PEO_{68}	1	0.6	9.2	1.9±0.1
P84	1	0.4	10.2	1.0±0.1
F68	1	0.5*	6.8	0.10±0.02
P103	0.2	0.5*	9.7	12.5±1.3
P105	0.2	0.4	8.7	9.4±0.6
F127	0.2	0.5	5.9	18.2±0.7
F108	1	0.5*	4.9	0.9±0.3
POPC liposomes in 150mM NaCl D_2O solution				
$tPPO_{14}$-PEO_{46}	1	0.5*	11.7	0.3±0.1
$tPPO_{29}$-PEO_{68}	1	0.6	9.3	3.1±0.1
P84	1	0.5*	10.1	0.8±0.1
F68	1	0.5*	7.2	0.12±0.06
P103	0.2	0.5*	10.1	14.5±1.5
P105	0.2	0.5*	8.6	11.2±0.5
F127	0.2	0.4	6.1	23.4±0.1
F108	1	0.5*	4.9	2.0±0.4
POPG liposomes in 150mM NaCl D_2O solution				
$tPPO_{14}$-PEO_{46}	1	0.5	11.4	1.6±0.1
$tPPO_{29}$-PEO_{68}	1	0.5	9.3	20.2±0.6
P84	1	0.5	9.8	7.2±1.3
F68	1	0.5*	7.3	0.2±0.1
P103	0.2	0.4	10.1	43.4±1.6
P105	0.2	0.4	8.7	48.3±1.6
F127	0.2	0.4	5.8	52.8±1.1
F108	1	0.4	4.9	17.5±1.1

[a] Obtained from the final slope of the echo decay curves of the polymer in the presence of liposomes. *Estimated from the liposome diffusion coefficients measured by PFG-NMR due to noisy data at the final slope of polymer echo decay curves.

[b] Obtained from the linear fit of the echo decay curves of polymer without the presence of liposome. Only the data points before 5.0×10^{10} s/m^2 $\gamma^2G^2\delta^2(\Delta-\delta/3)$ were used for the linear fit to ensure a strong signal since the signal of polymer decays very rapidly.

[c] Obtained from the average and standard deviation of the fitting results at Δ = 300, 500, and 700 ms based on eq 2.4.

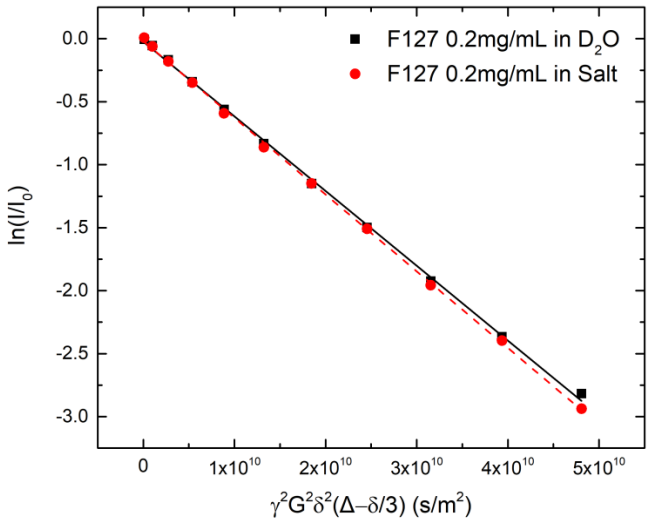

Figure 5.4. Echo decay curves of 0.2 mg/mL F127 in D_2O (black squares) and in 150 mM NaCl D_2O solution (red circle). The black and red lines are linear fits to the data, which give $D = 5.9\times10^{-11}$ m^2/s for the polymer in water, and 6.1×10^{-11} m^2/s for the polymer in the salt solution.

The effect of a choline headgroup versus a glycerol headgroup was studied by quantifying the polymer binding to POPC liposomes (red bars) and to POPG liposomes (blue bars) in 150 mM NaCl D_2O solution, as shown in Figure 5.3a. By switching the lipid from POPC to POPG, all the selected polymer species except F68 show significantly higher binding, as the blue bars are much taller than the red bars. In the case of F68, both POPG and POPC lipid bilayers show very low binding and there is no statistically significant difference in the binding percentage. This weak association between F68 and lipid bilayers can be explained based on the relatively short hydrophobic PPO blocks and large content of hydrophilic PEO blocks (ca. 80 wt.%).[275] Also, according to a study by Kim and

coworkers on polymer binding to flat supported lipid bilayers using surface plasmon resonance, the binding kinetics of F68 are very slow, taking as much as several weeks to observe evident binding of F68 to lipid bilayers,[182] while the binding of F68 to liposomes determined by PFG-NMR was measured with no incubation.

Next, we investigated how polymer binding varies with increasing POPG content in the lipid bilayer. F127 was selected as the representative polymer to illustrate polymer binding as a function of the molar percentage of POPG in the POPC/POPG bicomponent liposomes in 150 mM NaCl D_2O solution (Figure 5.5). Polymer binding of F127 at each POPG molar percentage is summarized in Table 5.3. Binding of F127 at 0 mol% and 100 mol% of POPG in the lipid bilayers (i.e., pure POPC and pure POPG) in the presence of salt, are shown by the red and blue bars, respectively, in Figure 5.3. Figure 5.5 shows that the binding of F127 increases as the POPG contents increases, with the headgroup effect becoming very significant when the bicomponent lipid bilayer contains more than 20 mol% POPG. A possible reason that the glycerol group of POPG enhances polymer binding is hydrogen bonding. Earlier work in the literature demonstrated that POPG lipid bilayers can form strong intermolecular hydrogen bonding within the hydrophilic headgroup layer due to the existence of the hydroxyl groups.[292–294] It was also found that POPG can form hydrogen bonds with the headgroup-specific sites on some proteins, resulting in tight binding between the lipid headgroup and the protein.[296] Additionally, it was suggested that the ether oxygen in PEO favors hydrogen bonding with the hydroxyl groups surrounding it.[128,297–300] In this context, we suggest that the headgroup of POPG could form hydrogen bonds with PPO-PEO block polymers, where the hydroxyl groups could function as

potential hydrogen bonding donors, while the ether oxygen of the PEO or PPO blocks could be potential hydrogen bonding acceptors. A schematic of proposed mechanism is shown in Figure 5.6. That the headgroup effect is not significant until more than 20 mol% POPG is present in the lipid bilayer could be because multiple hydrogen bonds need to be formed between one polymer molecule and two or more glycerol groups in order to observe enhanced polymer binding. We speculate that there is a threshold POPG content in the lipid bilayer, below which the lipid bilayer is unable to form enough hydrogen bonds with the polymers due to the lack of glycerol groups, and thereby, shows little increase of polymer binding.

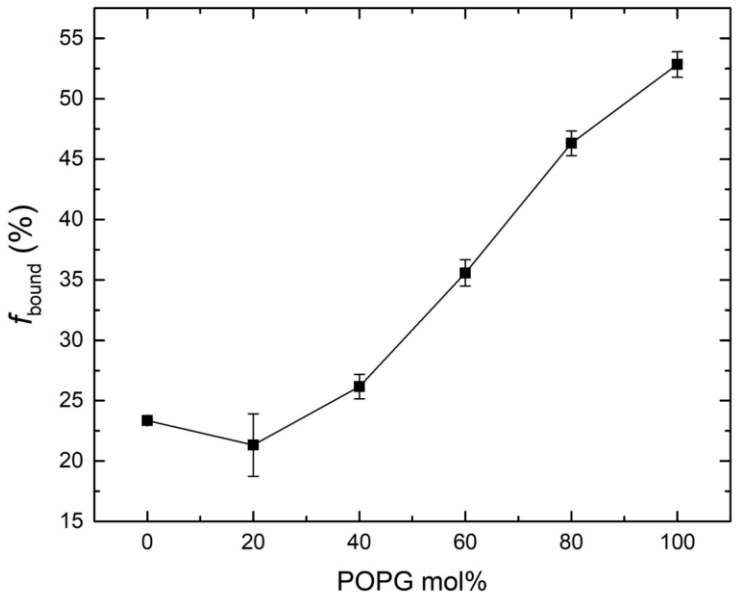

Figure 5.5. Polymer binding percentage of 0.2 mg/mL F127 as a function of POPG molar percentage in the POPC/POPG lipid bilayer in 150 mM NaCl D_2O solution.

Table 5.3. Summary of polymer binding of 0.2 mg/mL F127 to 5mM POPC/POPG liposomes at various POPG molar percentage in the lipid bilayer in 150 mM NaCl D_2O solution at 27 °C.

POPG mol%	D_{bound}[a] (10^{-11} m^2/s)	D_{free}[b] (10^{-11} m^2/s)	f_{bound}[c] (%)
0	0.4	6.1	23.4±0.1
20	0.5	5.9	21.3±2.6
40	0.4	5.9	26.2±1.0
60	0.4	5.9	35.6±1.1
80	0.4	5.9	46.3±1.0
100	0.4	5.8	52.8±1.1

[a] Obtained from the final slope of the echo decay curves of the polymer in the presence of liposomes.

[b] Obtained from the linear fit of the echo decay curves of polymer without the presence of liposome. Only the data points before 5.0×10^{10} s/m^2 $\gamma^2G^2\delta^2(\Delta-\delta/3)$ were used for the linear fit to ensure a strong signal since the signal of polymer decays very rapidly.

[c] Obtained from the average and standard deviation of the fitting results at Δ = 300, 500, and 700 ms based on eq 2.4.

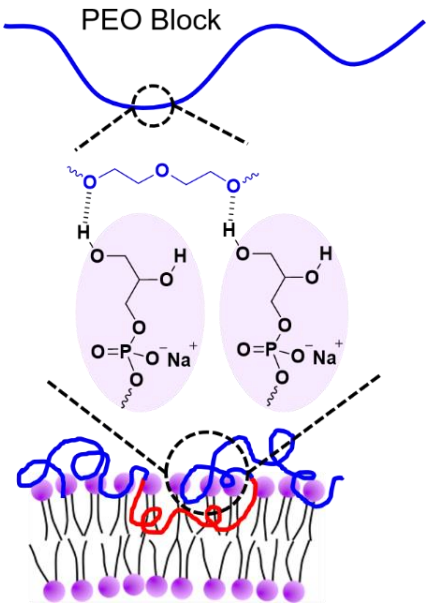

Figure 5.6. Schematic of hydrogen bonding between a PEO block and glycerol headgroups of POPG in the lipid bilayers.

In an attempt to verify our proposed mechanism, Raman spectroscopy was employed to probe possible hydrogen bonding between polymers and the POPG headgroups. The spectra of pure polymer F68 and pure liposome samples in the region of 750 – 1750 cm^{-1} are shown in Figure 5.7a and Figure 5.7b, respectively. The intensity of these two spectra were adjusted to keep the maximum intensity of the peak due to water bending vibrations to be the same. The peaks were assigned to different vibrational modes of the various bonds.[301–309] In Figure 5.7a, the strongest peak appears at ~1550 – 1750 cm^{-1}, which is due to the bending vibration (δ) of water molecules. The peaks at 1400 – 1500 cm^{-1} and at 1200 – 1350 cm^{-1} are attributed to the bending and twisting (*t*) vibrations of methylene groups in the polymer backbone, respectively. The peak observed at ~ 1140 cm^{-1} originates from the superposition of C-O-C asymmetric stretching (ν_a), C-C stretching, and CH_2 wagging (*w*). The shoulder to its left (lower wavenumber) is due to combined C-O-C symmetric stretching (ν_s) and CH_2 rocking (*r*). The broad peak from 800 to 1000 cm^{-1} is due to coupled C-O-C symmetric stretching with CH_2 rocking. In Figure 5.7b, two strong peaks evident in the region of 1200 - 1500 cm^{-1} correspond to CH_2 twisting and bending vibrations as POPG lipids contain relatively long alkyl chains. The broad peak from 1000 to 1200 cm^{-1} is attributed to the superposition of symmetric stretching of O-P-O with C-C stretching. Note that the concentration of polymers and liposomes for Raman measurements is much higher than that used in PFG-NMR measurements because Raman scattering produces weak signals, especially in aqueous solution.

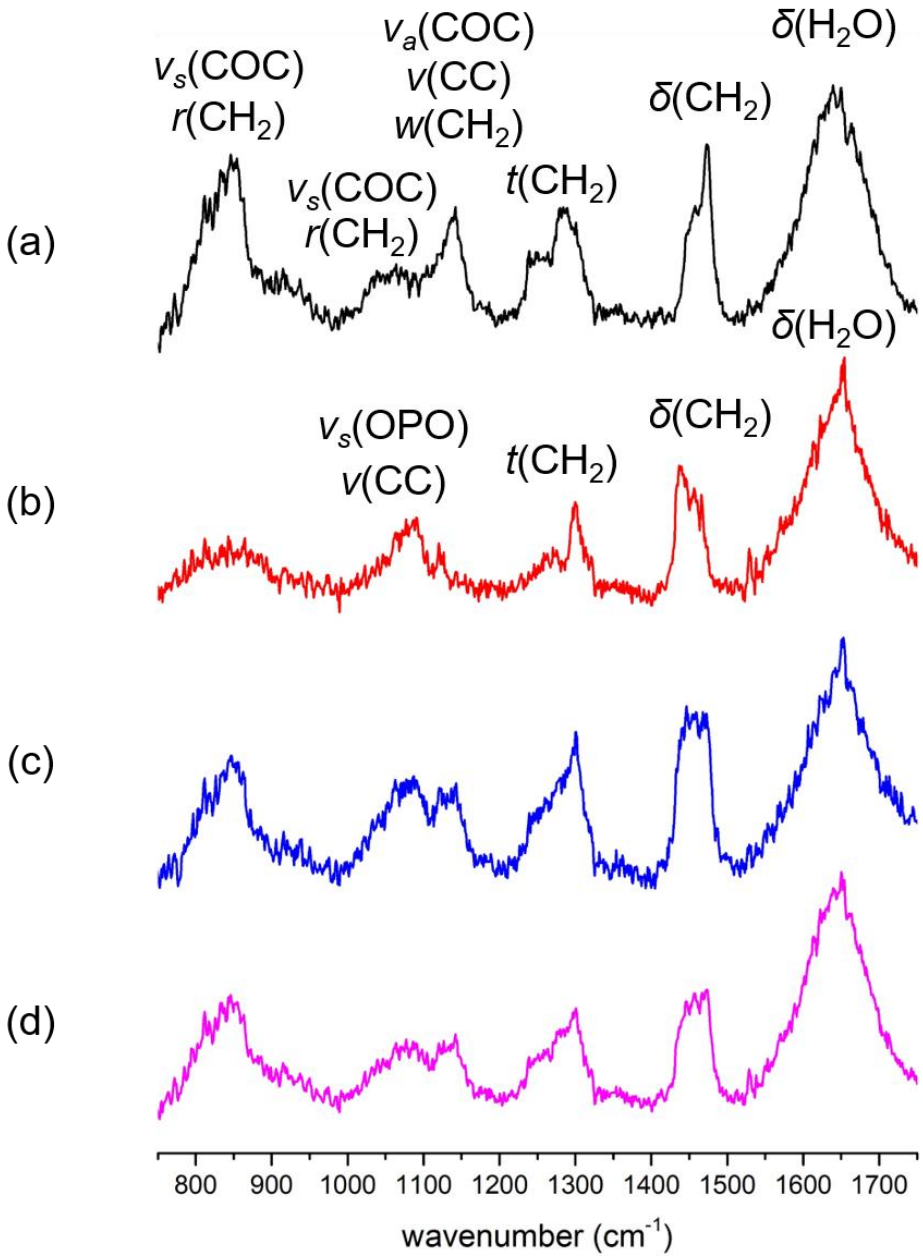

Figure 5.7. Raman spectra of (a) 20 mg/mL F108, (b) 30 mM POPG liposomes, and (c) polymer-liposome mixture of 20 mg/mL F108 and 30 mM POPG liposomes in H_2O. (d) Superposition of pure polymers and pure liposomes. δ: bending; *v*: stretching; *t*: twisting; *r*: rocking; *w*: wagging. The subscripts "s" and "*a*" stands for "symmetric" and "asymmetric", respectively.

To probe potential hydrogen bonding formed between POPG headgroups and polymers, the peak containing C-O-C asymmetric stretching vibrations at ~ 1140 cm^{-1} was monitored as an indicator since it is anticipated that hydrogen bonding would affect the ether oxygen of C-O vibrations of the polymers. Appreciable peak shift or intensity change indicates significant amount of hydrogen bond formation. Note that the stretching vibrations of the O-H bonds in the POPG headgroups could also be affected by hydrogen bond formation. However, it is not feasible to use this peak as an indicator because it is covered by the extremely strong peak of stretching vibrations of water molecules in the solution, which is at ~3400 cm^{-1} (not shown in the spectra). The spectrum of a polymer-liposome mixture is shown in Figure 5.7c and a direct superposition of the spectra of pure polymers (Figure 5.7a) and pure liposomes (Figure 5.7b) is shown in Figure 5.7d as a control, which represents the case of no polymer-liposome interactions. The intensity of the two spectra were also adjusted to keep maximum intensity of the water bending peak the same as that in Figure 5.7a and Figure 5.7b. Comparing Figure 5.7c and Figure 5.7d, no significant peak shift or intensity change was observed for the C-O-C asymmetric stretching vibrations at ~ 1140 cm^{-1} or even the full range of the spectra. This suggests there is not a significant amount of hydrogen bond formation between the POPG headgroups and polymers. However, the resolution of the Raman measurements may not be adequate to resolve the delicate hydrogen bonding for the following two reasons. First, the peak associated with the C-O-C asymmetric stretching vibrations (*i.e.*, the indicator of hydrogen bonding) is not well resolved due to overlap with the peaks of other vibrations (*i.e.*, C-C stretching and CH_2 wagging). Second, the maximum percentage of the ether oxygen atoms of the

polymers in solution bound to POPG liposomes is estimated to be approximately 14%. This means at most 14% of the C-O-C stretching signal can contribute to a peak shift or intensity change due to hydrogen bonding. This estimate is based on the assumptions that (1) all ether oxygen from both PPO and PEO in the bound polymers form hydrogen bonds with lipid headgroups, and (2) all hydroxyl groups in lipid headgroups can potentially participate in hydrogen bonding. In all likelihood the 14% estimate is considerably higher than the actual level of hydrogen bonding, and accordingly the associated Raman signal may not be detectable.

In addition to hydrogen bonding, bridging between the ether oxygen of polymers and POPG headgroups via salt cations represents another possible mechanism for stronger binding to POPG relative to POPC. Both experiments and simulations in the literature show that anionic lipid membranes are sensitive to interactions with cations.[310–312] Also, PEO has been recognized for several decades to complex with salt-based cations.[313] In this context, we speculate that the polymer binding can be enhanced by salt-cation bridging between the PEO blocks and the anionic surface of the POPG liposomes. This bridging effect was investigated by varying the cations and the salt concentration. If the bridging effect plays a significant role, polymer binding is anticipated to vary appreciably upon switching the type of cations. Figure 5.8 exhibits the binding of F108 to POPG liposomes in different salt solutions. The diffusivity of free and bound polymers used for fitting and the resulting binding percentage are summarized in Table 5.4. It can be seen that within experimental uncertainty polymer binding is unaffected by switching from sodium to potassium at a constant concentration of 150 mM. Polymer binding was not measured in

the presence of divalent cations such as Ca^{2+} and Mg^{2+} because it was found that during the lipid hydration process, the anionic POPG lipids aggregated and precipitated out of the aqueous solutions with 150 mM $CaCl_2$ or $MgCl_2$ instead of forming multilamellar liposomes. It could be because the divalent cations have strong bridging effect on the monovalent lipid headgroups, resulting in a precipitation of lipid-salt complex. Polymer binding to POPG liposomes was also measured at two salt concentrations. Again, there is little change of polymer binding in 150 mM vs. 300 mM NaCl. Note that the polymer binding only can be tested at intermediate salt concentration because the anionic POPG lipids cannot form stable liposomes in low or high salt concentration due to electrostatic interactions. At very low salt concentration (*e.g.*, 0 or 10 mM NaCl), the repulsive force between anionic POPG headgroups is strong so that the liposomes are not stable and are easily disrupted upon introducing polymers, as discussed previously. On the other hand, at high salt concentration (*e.g.*, 1000 mM NaCl), the repulsive forces between the lipid headgroups are nearly completely screened by the high ion concentration. Under this condition hydrogen bonding between the glycerol headgroups significantly increases attraction between liposomes and the liposomes loose colloidal stability and form large flocculates. These results indicate that salt cation bridging is not the main factor to account for the significant increase of polymer binding to POPG bilayers.

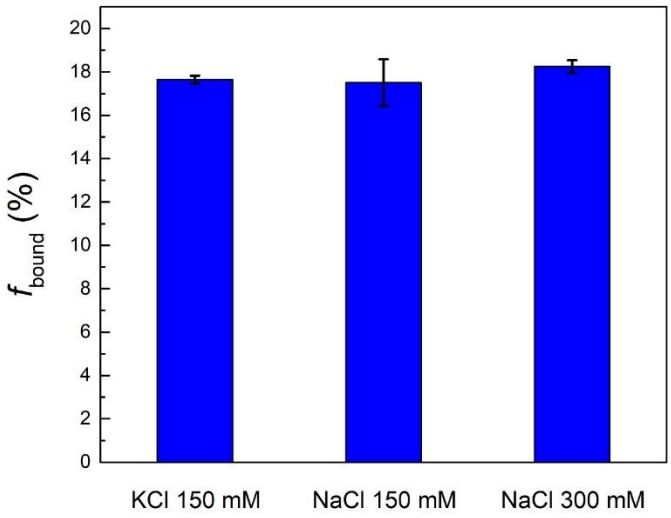

Figure 5.8. Binding percentage of 1 mg/mL F108 to 5 mM POPG liposomes in different salt solutions.

Table 5.4. Summary of binding of 1 mg/mL F108 to 5 mM POPG liposomes in different salt solutions.

Salt	Concentration (mM)	D_{bound}[a] (10^{-11} m^2/s)	D_{free}[b] (10^{-11} m^2/s)	f_{bound}[c] (%)
KCl	150	0.4	5.0	17.7 ± 0.2
NaCl	150	0.4	4.9	17.5 ± 1.1
NaCl	300	0.4	5.0	18.3 ± 0.3

[a] Obtained from the final slope of the echo decay curves of the polymer in the presence of liposomes.

[b] Obtained from the linear fit of the echo decay curves of polymer without the presence of liposome. Only the data points before 5.0×10^{10} s/m^2 $\gamma^2G^2\delta^2(\Delta-\delta/3)$ were used for the linear fit to ensure a strong signal since the signal of polymer decays very rapidly.

[c] Obtained from the average and standard deviation of the fitting results at Δ = 300, 500, and 700 ms based on eq 2.4.

5.3.2 Effect of the Degree of Unsaturation of Lipid Alkyl Chains

In Chapter 4.3.2, the binding of 0.2 mg/mL F127 to DOPC was compared with that to POPC. DOPC contains two mono-unsaturated hydrocarbon chains, whereas POPC only contains one. A slightly higher binding percentage with DOPC (22.9% ± 0.5%) versus POPC (18.2% ± 0.7%) indicates that the lipid alkyl chains with a higher degree of unsaturation favors more polymer binding. This is possibly due to a lower bending modulus of the DOPC bilayers.[274] Here, we examined more lipids with different degree of unsaturation in the alkyl chains. Comparisons of polymer binding to POPC and PLPC are shown in Figure 5.9. The diffusivity of the free and bound polymers used for fitting and the resulting binding percentage are summarized in Table 5.5. Unlike DOPC which contains one double bond in each of the hydrocarbon tails, the two double bonds of PLPC are in one hydrocarbon tail and the other hydrocarbon tail is saturated. It can be seen from Figure 5.9 that the percentage of polymer binding to POPC and to PLPC are the same within experimental error. Along with the comparison between polymer binding to DOPC and to POPC, these results indicate that the liposomes composed of lipids with two mono-unsaturated hydrocarbon chains tend to have higher binding with polymers, compared to the liposomes composed of lipids with one saturated chain and one mono- or poly-unsaturated chain.

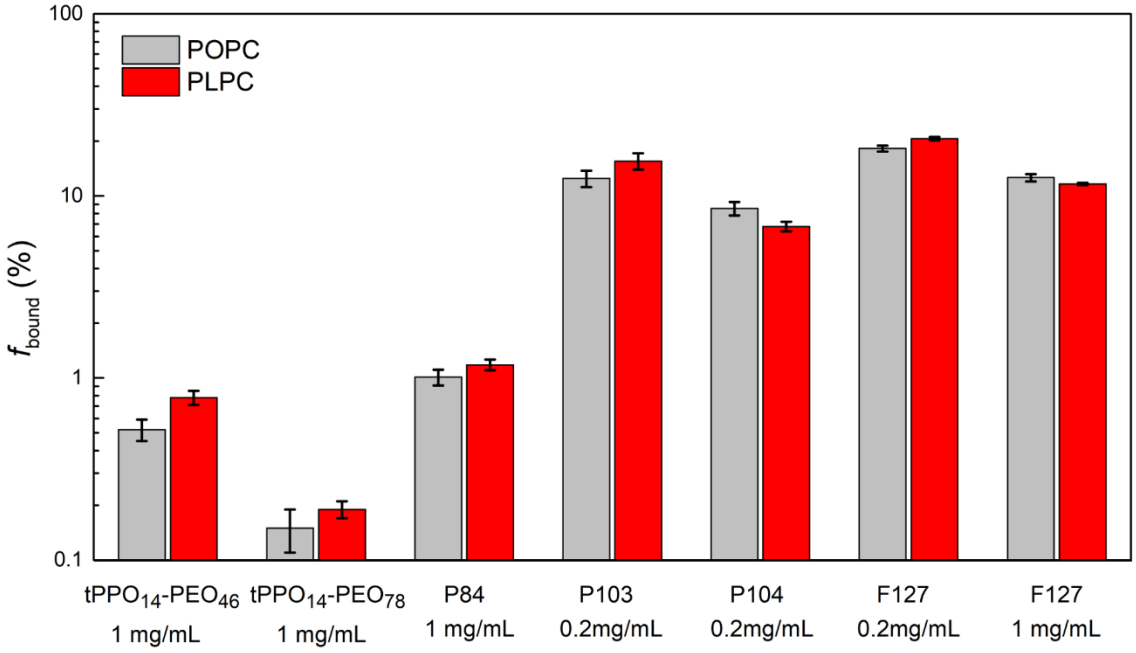

Figure 5.9. The binding percentage in logarithmic scale of various polymer species with 5 mM POPC liposomes (gray) and with 5 mM PLPC liposomes (red) in D_2O at 27 °C.

Table 5.5. Summary of polymer binding to 5mM POPC liposomes and to 5 mM POPG liposomes in D_2O at 27 °C.

Polymer	Concentration (mg/mL)	D_{bound}[a] (10^{-11} m^2/s)	D_{free}[b] (10^{-11} m^2/s)	f_{bound}[c] (%)
POPC liposomes				
$tPPO_{14}$-PEO_{46}	1	0.5*	11.7	0.5±0.1
$tPPO_{14}$-PEO_{78}	1	0.5*	9.9	0.15±0.04
P84	1	0.4	10.2	1.0±0.1
P103	0.2	0.5*	9.7	12.5±1.3
P104	0.2	0.5*	9.2	8.5±0.7
F127	0.2	0.5	5.9	18.2±0.7
F127	1	0.4	5.9	12.6±0.6
PLPC liposomes				
$tPPO_{14}$-PEO_{46}	1	0.4*	11.4	0.8±0.1
$tPPO_{14}$-PEO_{78}	1	0.4*	9.7	0.19±0.02
P84	1	0.5*	10.1	1.2±0.1
P103	0.2	0.5	9.5	15.5±1.6
P104	0.2	0.4	9.2	6.8±0.4
F127	0.2	0.5	6.0	20.6±0.5
F127	1	0.4	5.7	11.6±0.2

[a] Obtained from the final slope of the echo decay curves of the polymer in the presence of liposomes. *Estimated from the liposome diffusion coefficients measured by PFG-NMR due to noisy data at the final slope of polymer echo decay curves.

[b] Obtained from the linear fit of the echo decay curves of polymer without the presence of liposome. Only the data points before 5.0×10^{10} s/m^2 $\gamma^2G^2\delta^2(\Delta-\delta/3)$ were used for the linear fit to ensure a strong signal since the signal of polymer decays very rapidly.

[c] Obtained from the average and standard deviation of the fitting results at Δ = 300, 500, and 700 ms based on eq 2.4.

Additionally, the effect of the degree of unsaturation of lipid alkyl chains on polymer binding was investigated by varying the molar percentage of saturated lipid DPPC in POPC/DPPC bicomponent lipid bilayers. F127 was selected as a representative polymer for the binding measurements. The binding percentage of F127 as a function of DPPC molar percentage is shown in Figure 5.10. The diffusivity of free and bound polymers used

for fitting and the resulting binding percentage are summarized in Table 5.6. As shown in Figure 5.10, within uncertainty the amount of bound polymer is unaffected by the percent DPPC up to 30 mol%. As the molar percentage of DPPC increases further, polymer binding first slightly increases and then decreases. Polymer binding with pure DPPC liposomes was not measured because pure DPPC liposomes do not form a stable colloidal state in water, possibly due to the solid-ordered gel phase (L_β) of such lipid bilayers at 27 °C; the phase transition temperature of DPPC is 41 °C.[148,314,315] The increase in polymer binding at 30 mol% DPPC could be related to the phase transition of the POPC/DPPC lipid bilayer from liquid-disordered fluid phase (L_α) to coexisting fluid and gel phases ($L_\alpha + L_\beta$).[148,149,314–316]

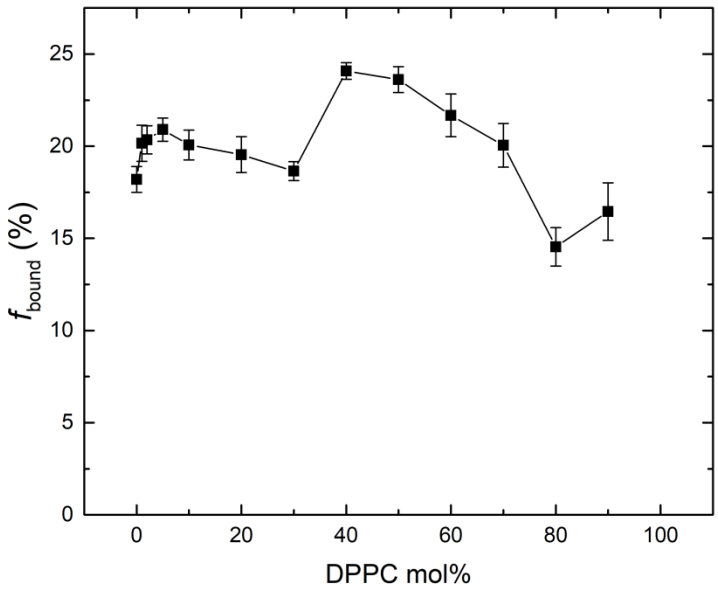

Figure 5.10. Polymer binding percentage of 0.2 mg/mL F127 as a function of DPPC molar percentage in POPC/DPPC lipid bilayers at 27 °C.

Table 5.6. Summary of polymer binding of 0.2 mg/mL F127 to 5mM DPPC liposomes in D_2O at 27 °C.

DPPC molar percentage (mol%)	D_{bound}[a] (10^{-11} m^2/s)	D_{free}[b] (10^{-11} m^2/s)	f_{bound}[c] (%)
0	5.9	0.5	18.2±0.7
1	6.0	0.5	20.2±1.0
2	6.0	0.5	20.3±0.8
5	6.0	0.5	20.9±0.6
10	6.0	0.5	20.1±0.8
20	6.0	0.4	19.5±1.0
30	6.0	0.4	18.7±0.5
40	6.0	0.4	24.1±0.5
50	6.0	0.4	23.6±0.7
60	6.0	0.4	21.7±1.2
70	6.0	0.4	20.1±1.2
80	6.0	0.4	14.5±1.0
90	6.0	0.7	16.5±1.6

[a] Obtained from the final slope of the echo decay curves of the polymer in the presence of liposomes.

[b] Obtained from the linear fit of the echo decay curves of polymer without the presence of liposome. Only the data points before 5.0×10^{10} s/m^2 $\gamma^2G^2\delta^2(\Delta-\delta/3)$ were used for the linear fit to ensure a strong signal since the signal of polymer decays very rapidly.

[c] Obtained from the average and standard deviation of the fitting results at Δ = 300, 500, and 700 ms based on eq 2.4.

5.4 Conclusions

We have investigated the influence of headgroup composition and the degree of unsaturation of lipid alkyl chains on polymer-lipid bilayer association. The interactions between polymers and lipid bilayers were probed by quantifying polymer binding to liposomes using PFG-NMR. Lipid headgroup composition in the bilayer was varied by

tuning the molar ratio of POPG to POPC. As POPG molar percentage in the bilayer increases, polymer binding significantly increases. We speculatively attribute this effect to hydrogen bonding between the glycerol headgroup of POPG and the ether oxygen of the polymers. Hydrogen bonding was not detected by Raman spectroscopy, although this is most likely due to an inherently weak signal. The addition of salt at physiological concentration in POPG liposome solutions prevents liposomes disruption due to electrostatic repulsion between POPG headgroups; modest variation of cation type and concentration has little effect on polymer binding to POPG liposomes. The role of degree of unsaturation of lipid alkyl chains was studied by comparing polymer binding to POPC, DOPC, PLPC, and DPPC/POPC bi-component liposomes. It was found that DOPC liposomes (i.e., lipids with two mono-unsaturated alkyl chains) exhibited the highest polymer binding percentage. Our results demonstrate that lipid composition plays a significant role on membrane interactions with amphiphilic block copolymers.

Chapter 6 - Screening of the Stabilization Efficacy of Block Copolymers

6.1 Introduction

A screening test is necessary to quickly assess a polymer's efficacy as a membrane stabilizer before applying the polymer for further mechanistic or *in vivo* studies. An important reason is that the *in vivo* studies are costly and time consuming, making unrealistic the testing of all of the relevant polymer species. In this context, a fast and low-cost screening test can efficiently examine all of the polymer species in a portfolio. Based on the screening results, the most interesting and promising polymer species can be selected to study the protection mechanisms *in vivo* and evaluate the potential for medical applications.

Wang *et al.* developed a screening method for block copolymer protection of liposomes using lipid peroxidation as a model stress.[107] In their study, a variety of commercially available poloxamer species were added to the liposome solution before initiating the peroxidation reaction by 2,2-azobis(2-amidinopropane) dihydrochloride (AAPH). The adsorption of polymers onto the liposome surface slows down the diffusion of the free radicals into the lipid bilayer, which protects the liposome from lipid peroxidation induced by the free radicals. The protective ability of the poloxamers was evaluated from the changes in liposome size and size distribution in the presence of polymers, before and after lipid peroxidation. From the liposome size distribution, the efficacy of protection by different poloxamer species can be compared. It has been shown that the liposome size and its distribution change little if the polymer has a strong protective effect against peroxidation (Figure 6.1a).[107] On the other hand, if the polymer shows poor protection, the liposomes would be partially or fully disrupted by lipid peroxidation, which results in a broader distribution and the peak position may shift to the left, corresponding to lower average R_h (Figure 6.1b).[107]

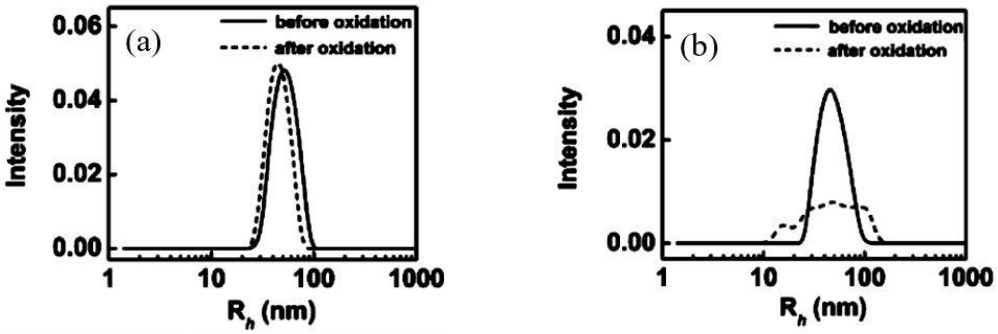

Figure 6.1. Size distributions of liposomes before and after peroxidation with (a) strong protection by polymers and (b) poor protection by polymers. Figure adapted with permission from Wang, J.-Y.; Marks, J.; Lee, K. Y. C. *Biomacromolecules* **2012**, *13*, 2616–2623. Copyright 2012 American Chemical Society.[107]

Although this approach provides a qualitative indication of the protective effect of the polymers, it does not offer a quantitative measure of the protection efficacy. Hence, we monitor the total scattered intensity of liposomes along with the size and distribution as a relatively comprehensive interpretation of the damage incurred.[6] The scattered intensity of neat liposomes and negative control (*i.e.*, bare liposomes followed by peroxidation), can be considered as two limits corresponding to full survival and full rupture of the liposomes, respectively. The scattered intensity in between can be used to differentiate the level of liposome survival due to polymer protection (see Chapter 2.6 for more details).[6]

Based on this simple but useful screening method, we are able to compare the protective effect of the diblock analog DP188 (Figure 6.2a) to that of the conventional triblock P188 (Figure 6.2b), and thereby investigate the role that polymer architecture plays on cell membrane stabilization. Also, we investigate the effect of the relative hydrophobic-hydrophilic composition of polymers on lipid membrane protection by varying the hydrophilic block length while keeping the hydrophobic block length unchanged. Three lab-synthesized *tert*-butyl ended diblock copolymers *t*PPO_{14}-PEO_{46} (70 wt.% PEO), *t*PPO_{14}-PEO_{78} (80 wt.% PEO), and *t*PPO_{14}-PEO_{159} (90 wt.% PEO) with increasing PEO block length were used (Figure 6.2c-e). The *tert*-butyl ended diblock *t*PPO_{14}-PEO_{78} in Figure 6.2d was also used to compare with the commercial diblock analog DP188 which contains a methyl endgroup, to isolate the endgroup effect, as they have similar PPO and PEO block lengths. Additionally, we study how the overall molecular weight of the copolymers influences protection efficacy based on five commercial Pluronics with the same relative hydrophobic-hydrophilic composition (*i.e.*, 80 wt.% PEO). The reliability of

the screening method was assessed by comparing the consistency with the polymer stabilization effects *in vitro* and *in vivo* for dystrophic cell membranes.

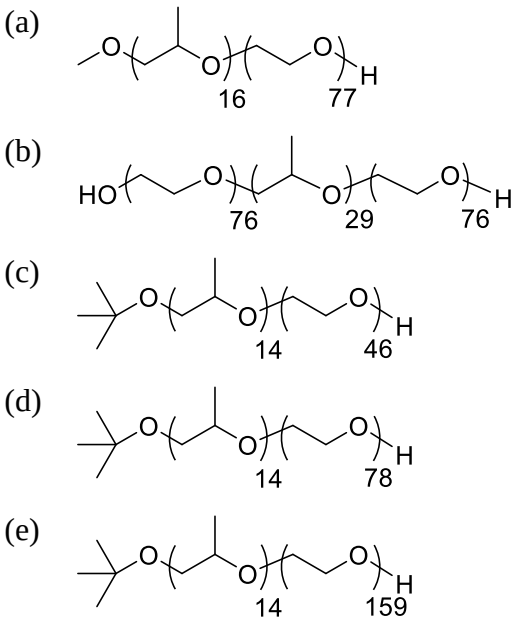

Figure 6.2. Chemical structures of a) methyl ended diblock analog DP188, b) P188, c) *tert*-butyl ended diblock copolymer with 70 wt.% PEO (*t*PPO_{14}-PEO_{46}), d) *tert*-butyl ended diblock copolymer with 80 wt.% PEO (*t*PPO_{14}-PEO_{78}), and e) *tert*-butyl ended diblock copolymer with 90 wt.% PEO (*t*PPO_{14}-PEO_{159}).

6.2 Experimental Section

Details of the experimental techniques used in this chapter are described in Chapter 2. The materials, sample preparation, and experimental procedures that are specific to this chapter are summarized below.

6.2.1 Materials

Pluronic F38, F68 (also known as P188), F88, F98, and F108 were generously provided by BASF. The diblock analog of P188, DP188 (P1862-EOPO), was purchased from Polymer Source (Montreal, Quebec). Ethylene oxide (EO, ≥ 99.5%), propylene oxide (PO, ≥ 99%), potassium *tert*-butoxide, n-butyllithium, potassium, naphthalene, and 18-crown-6 ether for anionic polymerization were purchased from Sigma-Aldrich and used as received, unless otherwise noted. 1-palmitoyl-2-oleoyl-*sn*-glycero-3-phosphocholine (POPC, PC (16:0-18:1)), 1-palmitoyl-2-oleoyl-*sn*-glycero-3-[phosphor-rac-(1-glycerol)] sodium salt (POPG, PG (16:0-18:1)), and 1-palmitoyl-2-linoeloyl-*sn*-glycero-3-phosphocholine (PLPC, PC (16:0-18:2)) in chloroform were purchased from Avanti Polar Lipids (Alabaster, AL) and used without further purification. The free radical generator 2,2'-azobis(2-amidinopropane) hydrochloride (AAPH) was also purchased from Sigma-Aldrich and used as received. Ultrapure water with resistivity of 18.2 MΩ × cm was obtained from a Millipore Direct Q-3 water system (EMD Millipore, Billerica, MA).

6.2.2 Polymer Synthesis and Characterization

The *tert*-butyl ended diblock polymers used in this chapter were synthesized by anionic polymerization. The number-average molecular weight, dispersity, and composition of the polymers are summarized in Table 2.1. The number-average molecular weight M_n and the average number of repeat units of PO (N_{PO}) and EO (N_{EO}) of the commercial triblock and diblock polymers with 80 wt. % PEO (specified by supplier) are summarized in Table 6.1.

Table 6.1. Summary of the commercial triblock and diblock polymers.

	M_n[a] (g/mol)	N_{PO}[b]	N_{EO}[b]
F38	4,700	16	43
F68 (P188)	8,400	29	76
F88	11,400	39	104
F98	13,000	45	118
F108	14,600	50	133
DP188	4,300	16	77

[a]Specified by supplier.

[b]Calculated from M_n and weight fraction of PEO (i.e., 80 wt.%). For triblock Pluronics, N_{EO} represents the number of repeat units of EO in one PEO block.

6.2.3 Liposome Preparation

POPC, PLPC, and POPG in chloroform (10 mg/mL) were mixed in a 6:3:1 molar ratio and then completely dried with argon to form a thin lipid film on the wall of the glass vial. The dry lipid film was then hydrated with Milli-Q water to 10 mM and heated to 37 °C for 30 min, with vortex applied every 5 min to fully emulsify the lipids. Unilamellar liposomes were obtained by extruding the lipid solution 19 times through a polycarbonate membrane of 50 nm pore radius.

6.2.4 Polymer Stabilization Efficacy Measurement

The stabilization efficacy of the copolymers on lipid membranes was estimated by the scattered intensity and the R_h of the liposomes using DLS. The R_h of the samples were determined from the DLS measurements at 5 angles. The scattered intensity, the dispersity,

and the size distribution plots of the samples are reported at 90°. The details of the assay are outlined in Chapter 2.

6.3 Results and Discussion

Figure 6.3 and Table 6.2 show the scattered intensities, R_h, and size dispersity of liposomes with polymers before and after lipid peroxidation. Higher scattered intensity of the liposomes with polymers after peroxidation indicates higher stabilization efficacy of the polymers. Figure 6.4 and Figure 6.5 show the R_h distributions of liposomes in the presence of different polymer species at polymer/lipid molar ratios of 5:1 and 10:1, respectively. Black curves in each plot represent the distribution of neat liposomes, while blue and red curves represent the distribution of liposomes with polymers before and after induced lipid peroxidation, respectively. Note that a red curve is not shown in some plots because the liposomes were highly disrupted by lipid peroxidation and thus the scattered intensity of the liposomes was too low to obtain a good fitting of size distributions, indicating little protection by the polymers. Broader distribution and smaller average R_h of the liposomes after peroxidation indicate worse protection by the polymers. These results can be considered as complements to the scattered intensity as criteria to determine the stabilization efficacy of polymers. In the pre-peroxidation stage, no significant changes were detected in scattered intensities or liposome size distributions in all polymer cases except for $tPPO_{14}$-PEO_{78}. This confirms that added polymers did not affect liposome behavior as the sizes of polymers are relatively small (R_g < 5 nm) and the concentration of added polymer is below the critical micelle concentration (CMC).

In the post-peroxidation stage, the stabilization efficacy of each polymer species is enhanced by doubling the polymer/lipid molar ratio. P188, DP188, and $tPPO_{14}$-PEO_{78} especially favor the higher polymer concentration, as the scattered intensity of survived liposomes at 10:1 is much higher than that at 5:1. Although we hypothesize that protection efficacy is improved by increasing polymer concentration, this concentration effect is surprisingly significant.

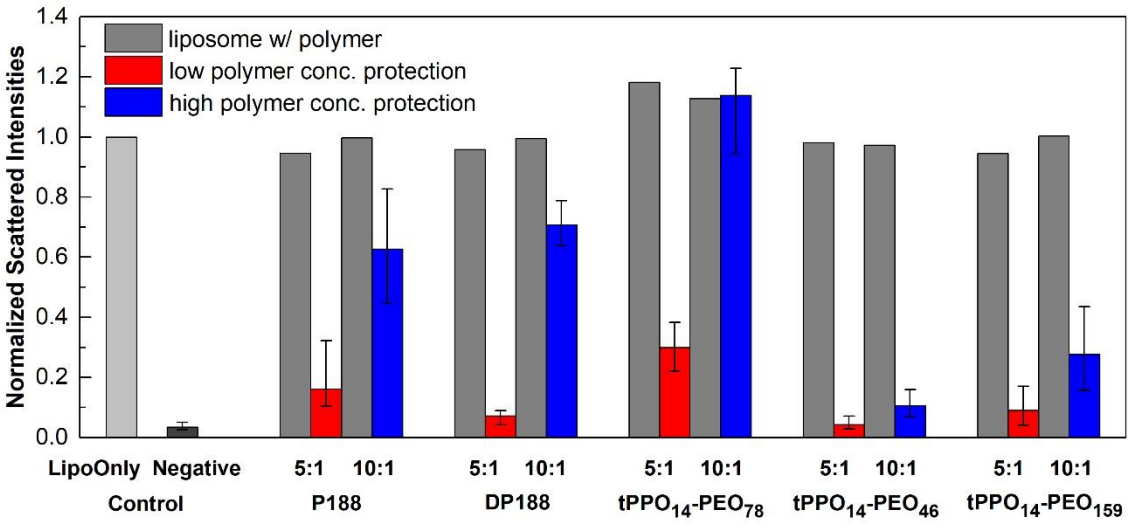

Figure 6.3. Average scattered intensities of liposomes with different polymers at 5:1 and 10:1 polymer/lipid molar ratios before and after lipid peroxidation. Error bars represent the data range for N = 6 replicates.

Table 6.2. R_h with dispersity of the liposomes with polymers before and after peroxidation.

Sample	**R_h (nm), Dispersity (μ/Γ^2)**							
Polymer/lipid molar ratio	5:1				10:1			
	before peroxidation		after peroxidation		before peroxidation		after peroxidation	
P188	68	0.02	49	0.24	69	0.06	57	0.14
DP188	66	0.04	-	-	66	0.04	63	0.05
$tPPO_{14}$-PEO_{78}	67	0.04	49	0.14	63	0.14	62	0.08
$tPPO_{14}$-PEO_{46}	66	0.06	-	-	66	0.04	41	0.30
$tPPO_{14}$-PEO_{159}	68	0.04	-	-	68	0.05	45	0.24
Neat liposome	67	0.04						

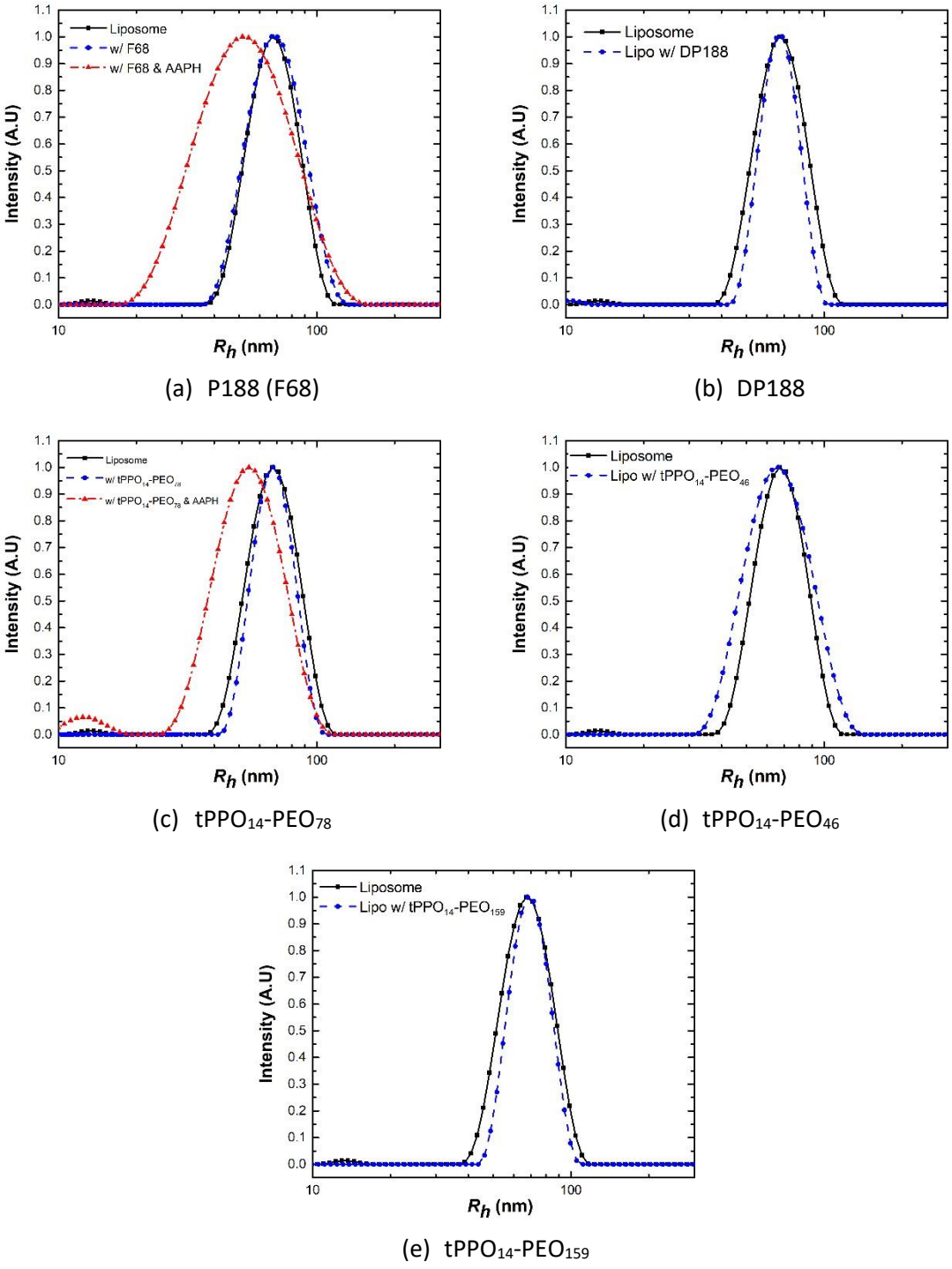

Figure 6.4. R_h distributions at 90° of neat liposomes (black), liposomes with (a) P188, (b) DP188, (c) $tPPO_{14}$-PEO_{78}, (d) $tPPO_{14}$-PEO_{46}, and (e) $tPPO_{14}$-PEO_{159} at 5:1 polymer/lipid molar ratio before (blue) and after (red) lipid peroxidation.

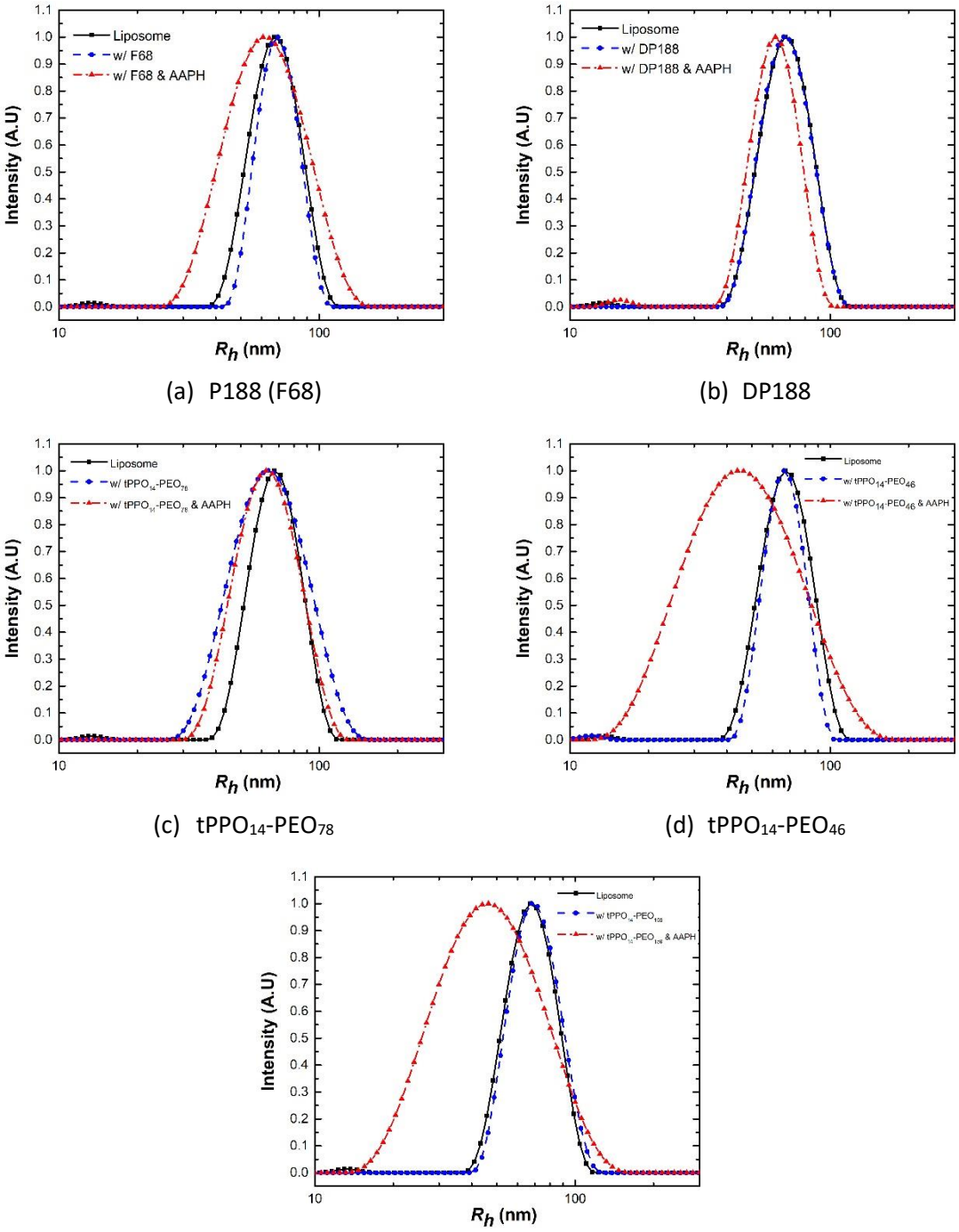

Figure 6.5. R_h distributions at 90º of neat liposomes (black), liposomes with (a) P188, (b) DP188, (c) $tPPO_{14}$-PEO_{78}, (d) $tPPO_{14}$-PEO_{46}, and (e) $tPPO_{14}$-PEO_{159} at 10:1 polymer/lipid molar ratio before (blue) and after (red) lipid peroxidation.

6.3.1 The Effect of Polymer Architecture

The effect of polymer architecture was investigated by comparing the commercial triblock P188 and its diblock analog DP188, which is equivalent to half of the P188 molecule. The scattered intensity along with the size distribution of the liposomes in the presence of these two polymer species indicate that both polymers have little protective effect at low concentration and intermediate protective effect at high concentration; the stabilization efficacy between these two polymer species have no significant difference within the error. These results demonstrate that the diblock architecture has similar protective function as the triblock in the lipid peroxidation assay, and can therefore also be used as a promising polymer model for the study of cell membrane stabilization. Additionally, the diblock architecture is easier to make delicate modifications on polymer structure such as individual block length and end group chemistry, which could potentially have significant impact on the stabilization efficacy of the polymers. For example, as discussed in the next section, the small change from a methyl to *tert*-butyl end group causes remarkable reinforcement in stabilization efficacy, even compared with the original P188.

The effect of polymer architecture was also investigated *in vitro* and *in vivo* by our collaborators Dr. Mihee Kim and Dr. Evelyne Houang, respectively.[99,100] The *in vitro* stabilization efficacy of the polymers was evaluated from the enzyme (lactate dehydrogenase (LDH)) release after cellular hypotonic stress and isotonic recovery applied to cultured murine myoblasts. Less LDH release indicates more efficient stabilization efficacy. Diblock analog DP188 and triblock P188 exhibited comparably effective protection against hypo-osmotic stress in the myoblast cellular assays. In the case of

protection during isotonic recovery, the diblock analog can only protect at high polymer concentration (150 μM), while the triblock P188 retains its protection efficacy at reduced concentration (14 μM).[100] The higher protection efficacy of triblock P188 at lower polymer concentration could be due to a longer hydrophobic PPO block or a higher mass concentration compared to that of the diblock analog. The *in vivo* studies on dystrophic animal models elucidate that the polymer architecture effect on their stabilization efficacy is highly dependent on the route of polymer delivery, due to different pharmacodynamics.[99] Subcutaneous delivery of P188 results in dramatic improvement in force maintenance based on the *in vivo* lengthening contraction force loss protocol, whereas the diblock analog showed little protection against force loss. As for intraperitoneal delivery, however, the diblock analog exhibited slightly higher stabilization efficacy than that of the triblock P188. Together with the *in vitro* studies, the diblock architecture can be considered as an alternative polymer model for cell membrane stabilization, despite evidence of reduced stabilization efficacy under some conditions.

6.3.2 The Effect of Relative Hydrophobic-Hydrophilic Composition

Membrane protection efficacy is strongly affected by the relative hydrophobic-hydrophilic composition of block copolymers, which is studied here by varying the PEO block length. $tPPO_{14}$-PEO_{46}, $tPPO_{14}$-PEO_{78} and $tPPO_{14}$-PEO_{159} have the same PPO block length with increasing PEO block lengths (*i.e.*, 70, 80 and 90 wt. % PEO). In the post-peroxidation scattered intensities shown in Figure 6.3, liposomes incubated with $tPPO_{14}$-PEO_{78} (80 wt. % PEO) resulted in much higher average scattered intensity than those

incubated with either of the other two polymers, with more pronounced effects at the higher 10:1 polymer/lipid molar ratio. No size distributions are shown for post-peroxidation liposomes incubated with $tPPO_{14}$-PEO_{46} (70 wt. % PEO) or $tPPO_{14}$-PEO_{159} (90 wt. % PEO) at the 5:1 polymer/lipid molar ratio, due to insufficient scattered intensities resulting from liposome disruption. As shown in Figure 6.5d and Figure 6.5e, the broadening of size distributions at the 10:1 polymer/lipid molar ratio also demonstrates poor protection by these two polymers. Hence, $tPPO_{14}$-PEO_{78} (80 wt. % PEO) is the most protective polymer among these three, indicating that 80 wt. % PEO is near the optimal composition for membrane protection against lipid peroxidation.

These three diblock copolymers were tested in an *in vitro* cellular assay by our collaborator Dr. Mihee Kim.[100] All three diblock copolymers show effective protection against enzyme release at a polymer concentration of 150 μM. However, at a much lower polymer concentration (*i.e.*, 14 μM), the polymer stabilization efficacy decreases as the PEO block length decreases. Compared to our results that the diblock with intermediate PEO length shows the most protective effect, the cellular assay, on the other hand, does not show strong evidence of hydrophobic-hydrophilic composition dependence at high polymer concentration; while the most hydrophilic diblock among the three conferred the most remarkable protection at low polymer concentration. Such inconsistency between the screening method and the *in vitro* cellular assay could be attributed to the differences between model lipid bilayers and real cell membranes such as the membrane composition and curvature.

6.3.3 The Effect of Polymer Endgroup

To study the endgroup effect, commercial diblock DP188 with a methyl group and $tPPO_{14}$-PEO_{78} with a *tert*-butyl group on the PPO end were compared as they have similar block lengths of PPO and PEO, as shown in Figure 6.2. Liposomes with $tPPO_{14}$-PEO_{78} after peroxidation again showed higher intensity at both 5:1 and 10:1 polymer/lipid molar ratios, indicating that the presence of a more hydrophobic *tert*-butyl endgroup can significantly enhance polymer stabilization efficacy. The post-peroxidation liposomes in the presence of DP188 at 5:1 polymer/lipid molar ratio were unable to reveal a clear size distribution due to liposome disruption, which also indicates that DP188 has little protection while $tPPO_{14}$-PEO_{78} has moderate protection at low concentration. A possible reason for the endgroup effect is that the *tert*-butyl endgroup increases the hydrophobicity of the polymers which facilitates the anchoring of PPO block into the hydrophobic lipid bilayer interior, and thereby helps the PEO block approach the bilayer surface to protect the liposomes.

The screening results of the endgroup effect were compared with that in the cellular assay and in the animal model.[100,101] In the cellular assay, the *tert*-butyl ended diblock gave rise to less LDH release from the myoblasts after isotonic recovery compared to its counterparts with methyl or hydroxyl endgroups. Remarkably, the *tert*-butyl endgroup retained its protective function at reduced polymer concentration (14 μM) after isotonic recovery whereas the counterparts showed lack of protection.[100] Also, the endgroup effect was studied on a Duchenne muscular dystrophy (DMD) model. The polymer stabilization efficacy was determined using an *in vivo* lengthening contraction force loss protocol.[101]

Similarly, it was found that the *tert*-butyl terminated diblock exhibited significant stabilization function against lengthening contraction-induced force loss in diseased mice *in vivo*. In contrast, neither of the methyl and hydroxyl terminated counterparts exhibited effective protection. The *in vitro* and *in vivo* results are consistent with our findings based on the screening method. Additionally, molecular dynamics simulations of the interactions between POPC lipid bilayers and diblock copolymers with *tert*-butyl and hydroxyl endgroups revealed distinct configurations of these two polymers associating with the bilayer: the *tert*-butyl ended PPO block inserts much deeper into the hydrophobic bilayer interior whereas the hydroxyl ended PPO block preferentially stayed at the hydrophilic lipid headgroup region.[101]

6.3.4 The Effect of Polymer Molecular Weight

We studied the effect of molecular weight of the polymer on membrane stabilization by comparing the protection efficacy of a series of commercial poloxamers from F38 to F108 that have the same PEO composition (80 wt. %) but increasing molecular weight, as shown in Table 6.1. The polymer/lipid molar ratio was 5:1 for all of the samples (*i.e.*, 125 μM polymer concentration). The scattered intensities of the liposomes in the presence of polymers before and after peroxidation are summarized in Figure 6.6. The corresponding size distributions of the liposomes with each polymer species are summarized in Figure 6.7. The pre-peroxidation scattered intensities and the size distribution of the liposomes in the presence of polymers are similar to those of neat liposomes, which again validates our assumption that the addition of polymers alone has little effect on liposome size. In the

post-peroxidation stage, the liposome scattered intensity gradually increases as the molecular weight of polymer increases from F38 to F108. Comparing F38 and F108, the stabilization efficacy dramatically changes from none to full protection as the molecular weight increases three times. This demonstrates that the stabilization efficacy can be significantly enhanced by increasing polymer molecular weight. The liposome size distributions included in Figure 6.7 also show consistent results. It can be seen that in the presence of F38 (*i.e.*, the smallest molecular weight), the liposomes were fully disrupted as no post-peroxidation size distribution is shown (Figure 6.7a). As the molecular weight of the polymers increases, the liposomes show broad size distributions in the case of F68 and F88, corresponding to intermediate stabilization efficacy (Figure 6.7b and Figure 6.7c). As the polymer molecular weight further increases, the liposomes were almost fully protected by F98 and F108, as the size distributions are narrow and similar to that of pre-peroxidation (Figure 6.7d and Figure 6.7e); the post-peroxidation scattered intensities were also approximately the same as those of the neat liposomes. The liposome R_h with dispersity in the presence of polymers before and after lipid peroxidation are summarized in Table 6.3.

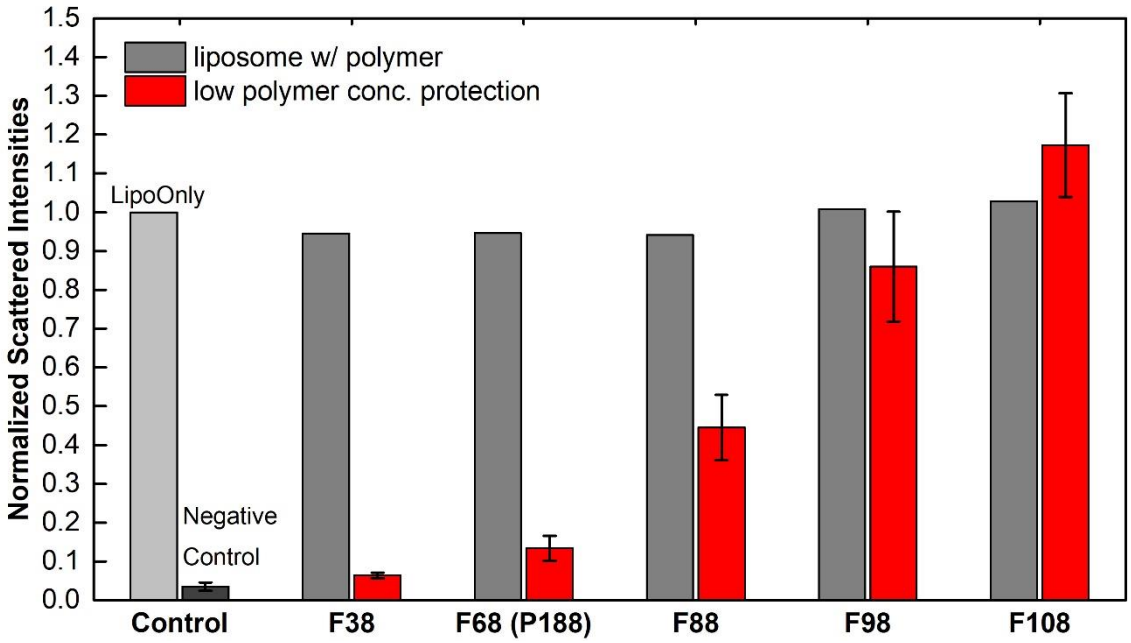

Figure 6.6. Average scattered intensities of liposomes with commercial poloxamers at 5:1 polymer/lipid molar ratio before and after lipid peroxidation. Error bars represent the data range for N = 3 replicates.

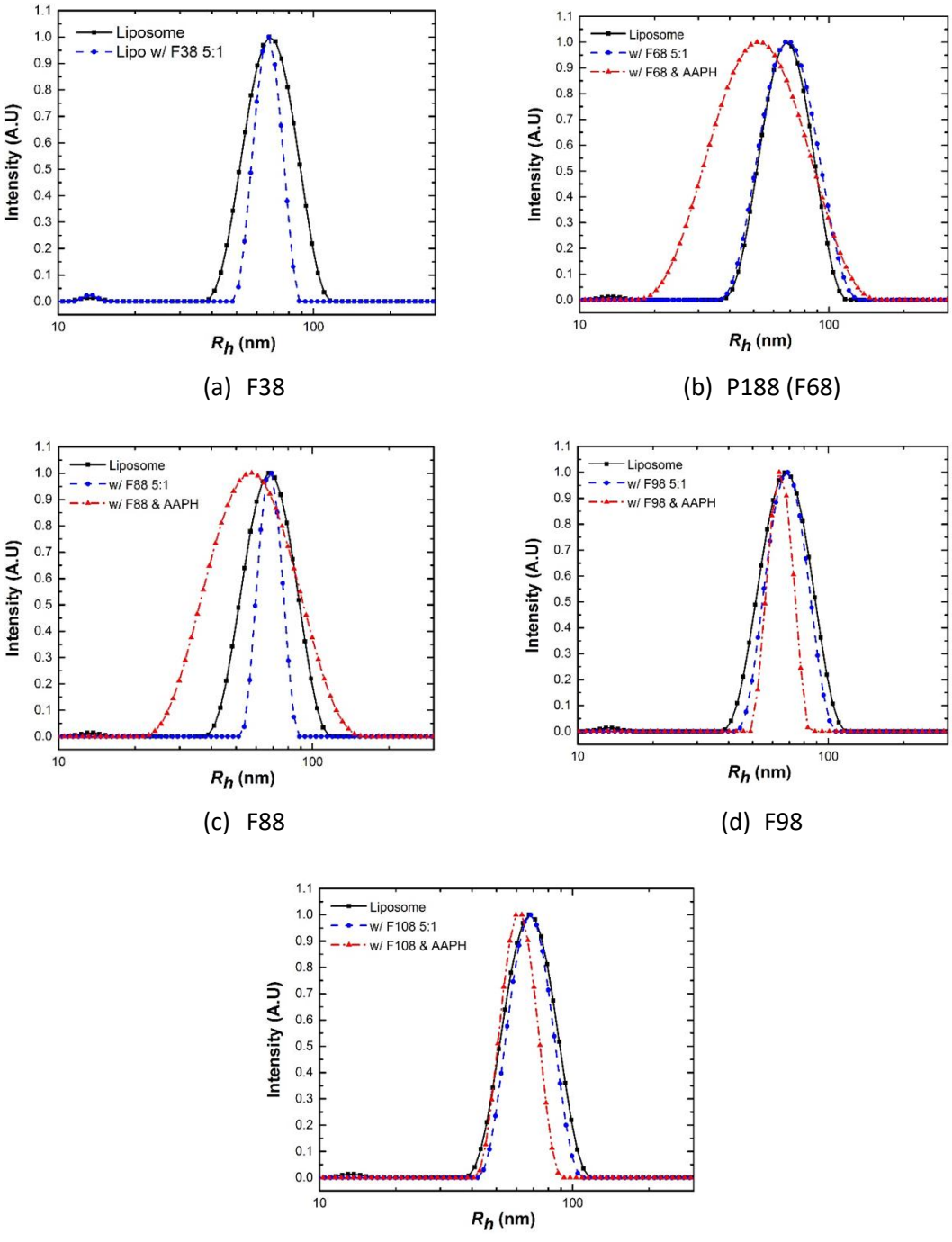

Figure 6.7. R_h distributions at 90º of neat liposomes (black), liposomes with (a) F38, (b) P188 (F68), (c) F88, (d) F98, and (e) F108 at 5:1 polymer/lipid molar ratio before (blue) and after (red) lipid peroxidation.

Table 6.3. R_h with dispersity of liposomes with poloxamers before and after peroxidation.

Sample	**R_h (nm), Dispersity (μ/Γ^2)**			
Polymer/lipid molar ratio	5:1			
	before peroxidation		after peroxidation	
F38	67	0.03	-	-
F68(P188)	68	0.02	49	0.24
F88	69	0.04	53	0.13
F98	68	0.07	64	0.16
F108	67	0.10	62	0.07
Neat liposome	67	0.04		

It should be noted that even though the molar concentration is kept the same for all polymers, the mass concentration of F108 is more than three times of that of F38 since the molecular weight of F108 is much larger than that of F38. To further demonstrate that the improvement of protection efficacy is not due to a mass effect, we performed the liposome protection against peroxidation by added polymers at the same mass concentration (*i.e.*, 1.05 mg/mL), as shown in Figure 6.8. It was observed that the stabilization efficacy increases as the molecular weight increases from F38 to F108, which agrees with the trend obtained by the same molar concentration. Additionally, both *in vitro* cellular assays and *in vivo* studies found that F108 is as effective as F68 (P188) at low concentration, while at high concentration, F108 partially lost its stabilization efficacy.[99,100] A possible explanation is that micelle formation occurs in F108 at high concentrations.

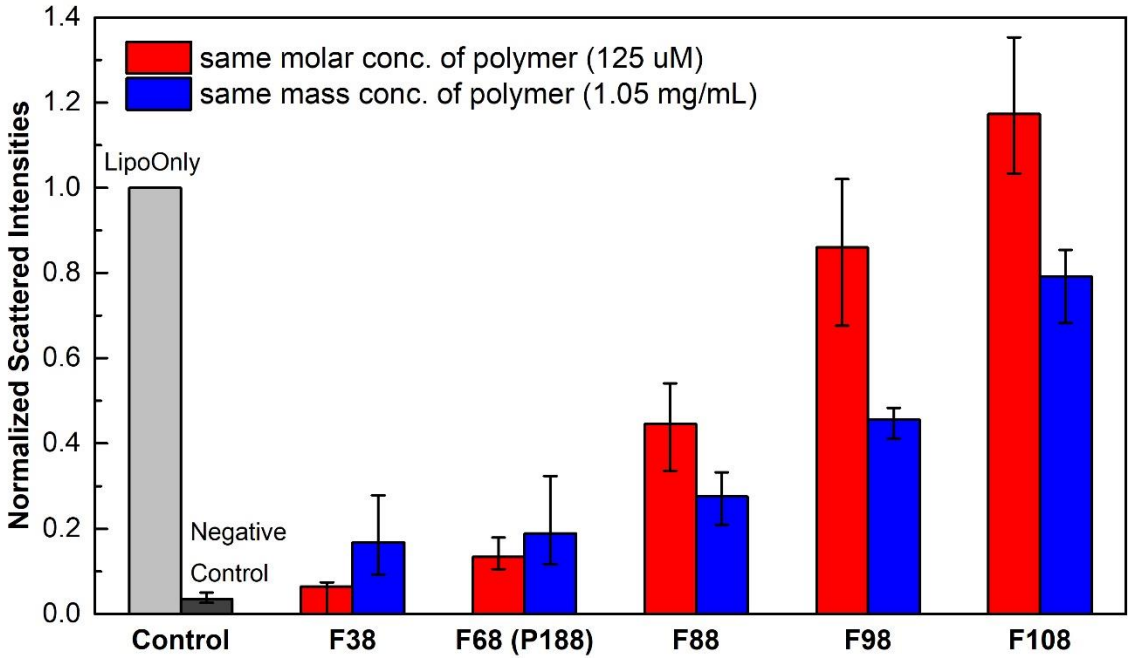

Figure 6.8. Average scattered intensities of liposomes with commercial poloxamers at same molar concentration (polymer/lipid molar ratio = 5:1) compared with those at same mass concentration (1.05 mg/mL) before and after lipid peroxidation. Error bars represent the data range for N = 3 replicates.

One problem we noticed is that the polymer protection efficacy obtained from this lipid peroxidation assay is not highly consistent across different batches of commercial Pluronics. For example, we measured the stabilization efficacy of P188 from a previous batch and a recent batch provided by BASF, as shown in Figure 6.9 (labelled as "old" and "new"). The scattered intensities indicate that P188 from the new batch has significantly higher protection efficacy than that of the old batch. The liposome size distributions included in Figure 6.10 also point to the same conclusion as the liposomes protected by the P188 from the recent batch shows narrower size distribution after induced peroxidation. The liposome R_h with dispersity in the presence of polymers before and after lipid peroxidation are summarized in Table 6.4. However, the characterization of P188 from

these two different batches by ^{1}H NMR and SEC indicate that they have similar molecular weight distribution and chemical structure (Figure 6.11). So far the reason that causes this problem is unclear; further investigation will be needed.

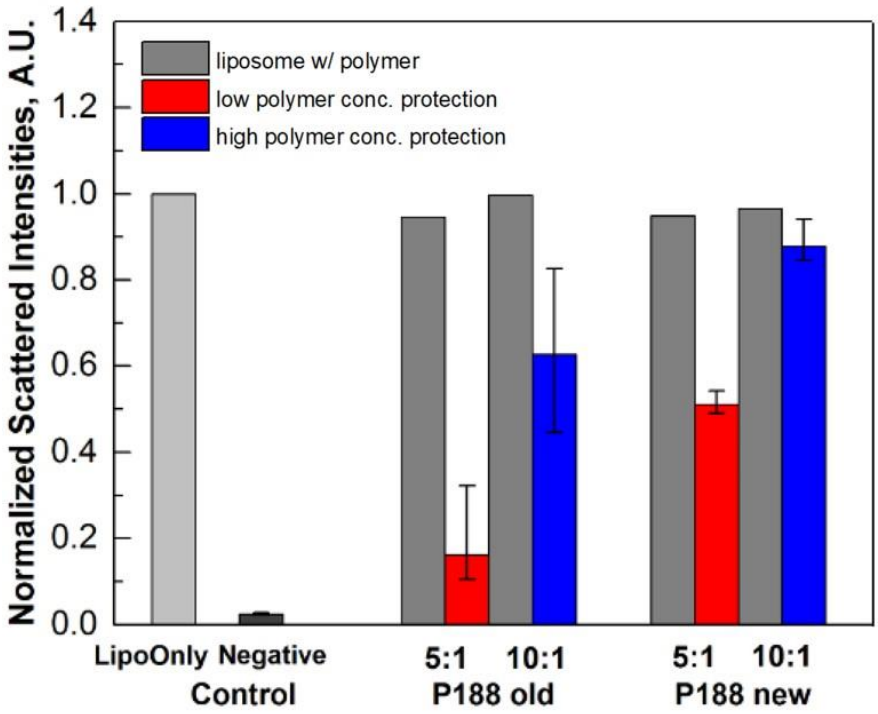

Figure 6.9. Average scattered intensities of liposomes with commercial P188 from two different batches at 5:1 polymer/lipid molar ratio before and after lipid peroxidation. Error bars represent the data range for $N \geq 3$ replicates.

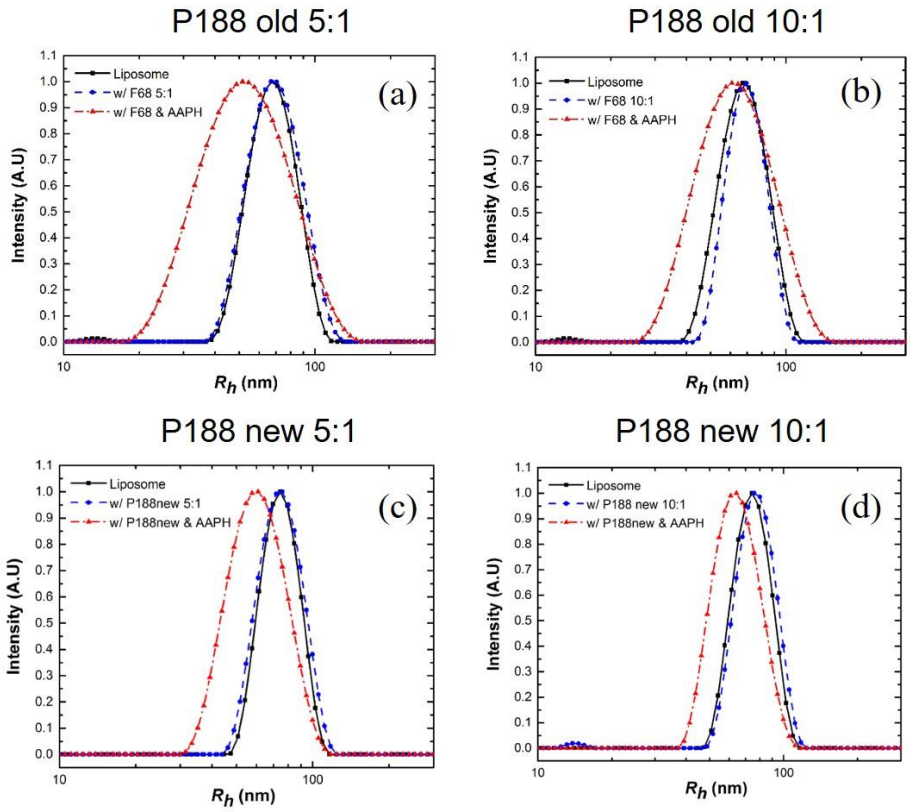

Figure 6.10. R_h distributions at 90º of neat liposomes (black), liposomes with (a) old P188 at 5:1, (b) old P188 at 10:1, (c) new P188 at 5:1, and (d) new P188 at 10:1 polymer/lipid molar ratio before (blue) and after (red) lipid peroxidation.

Table 6.4. R_h with dispersity of the liposomes with P188 before and after peroxidation.

Sample	**R_h (nm), Dispersity (μ/Γ^2)**							
Polymer/lipid molar ratio	5:1				10:1			
	before peroxidation		after peroxidation		before peroxidation		after peroxidation	
Old P188	68	0.02	49	0.24	69	0.06	57	0.14
New P188	72	0.05	65	0.09	73	0.07	62	0.08
Neat liposome	67	0.04	(for old P188)					
	72	0.05	(for new P188)					

(a)

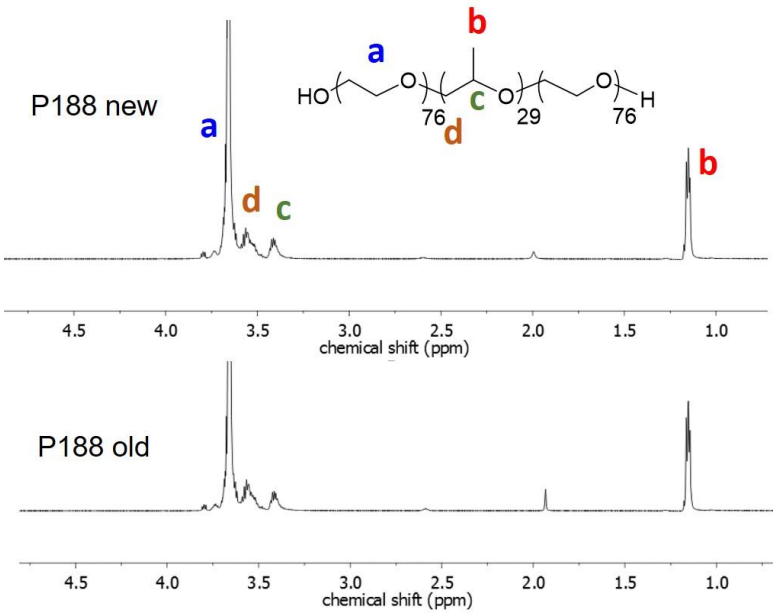

(b)

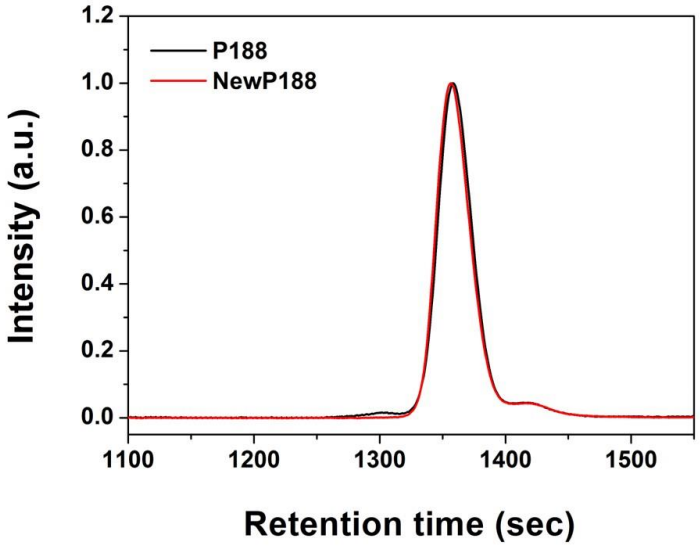

Figure 6.11. (a) SEC traces and (b) NMR spectra of old and new P188.

6.4 Conclusions

We have investigated the stabilization efficacy of block copolymers on liposomes against induced lipid peroxidation. A variety of triblock and diblock copolymers were tested in order to study the impact of polymer design on cell membrane stabilization, including relative hydrophobic-hydrophilic composition, endgroup chemistry, polymer architecture, and the overall molecular weight of the polymers. Our results show that the diblock analog of P188 is as effective as triblock P188 to protect the lipid bilayers against peroxidation, which validates the use of diblock architecture as an alternative polymer model for cell membrane stabilization. Also, the hydrophobic-hydrophilic composition of the polymers was investigated using three diblocks with the same PPO block length and increasing PEO block length (corresponding to 70, 80, and 90 wt. % PEO). The diblock with 80 wt. % PEO was found to have the highest stabilization efficacy among the three compositions. Endgroup effects were studied by comparing the stabilization efficacy of the *tert*-butyl ended diblock with that of the methyl ended diblock at the same PPO/PEO composition. The *tert*-butyl endgroup led to more effective protection, possibly due to its higher hydrophobicity which reinforces the anchoring of the PPO block into lipid bilayers. Additionally, it was shown that the stabilization efficacy against lipid peroxidation increases as the polymer molecular weight increases. Polymer stabilization efficacy obtained from the lipid peroxidation assay was compared with that from *in vitro* cellular assay and from *in vivo* study using dystrophic animal models; most of the results are consistent. This demonstrates that the lipid peroxidation assay can be potentially be used as a fast and simple screening of polymer stabilization efficacy.

Chapter 7 - Bottlebrush Polymers

7.1 Introduction

From Chapter 3, we learned that molecular structure has a remarkable influence on the interactions between block copolymers and lipid bilayers. Since we only investigated commercial linear triblock poloxamers and their diblock analogues, there is much room left to explore other polymer architectures and chemistries. One of the architectures we are interested in is the bottlebrush polymer (a linear backbone with dense brush-like polymeric side chains). It would be worth investigating whether the bottlebrush architecture leads to stronger polymer binding to the lipid membranes, since the crowded PEO side chains may increase polymer adsorption onto the hydration layer of the membrane surface, while the dense PPO side chains could possibly reinforce the anchoring of the hydrophobic portion of the macromolecule. Several molecular parameters could be manipulated in the bottlebrush architecture, such as polymer backbone length, side chain length and graft density, and the endgroup chemistry on the backbone.

Herein, we first investigated bottlebrush PEO (Figure 7.1a). Since linear PEO only showed appreciable interactions with lipid membranes at high concentration, the bottlebrush architecture is hypothesized to enhance polymer binding due to the crowding effect of the PEO side chains. Next, a bottlebrush PEO and PPO diblock polymer (Figure 7.1b) was synthesized and its binding to lipid bilayers was studied. The bottlebrush PEO is poly(oligo(ethylene glycol)) methyl ether methacrylate (POEGMA), composed of methyl methacrylate backbone and short PEO side chains. Similarly, the bottlebrush diblock is labelled POPGMA-*b*-POEGMA, where POPGMA stands for poly(oligo(propylene glycol)) methacrylate. Note that the monomer used to synthesize POEGMA (*i.e.*, OEGMA) contains a methyl group at the end of each OEG chain, while OPGMA monomer contains hydroxyl endgroups on the OPG chains. Since the results described below showed that the presence of the methyl groups in POEGMA had little improvement on polymer binding to the lipid bilayers, it is assumed that the endgroup difference between POEGMA and POPGMA is negligible.

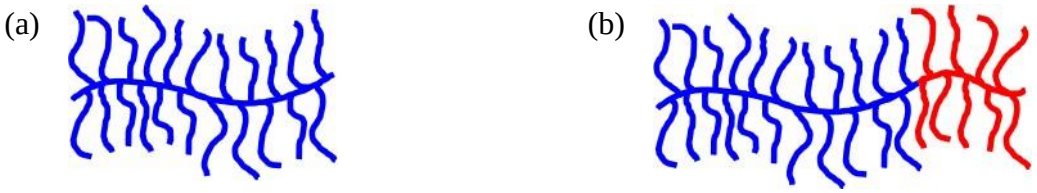

Figure 7.1. Schematics of (a) POEGMA, and (b) POPGMA-*b*-POEGMA. The hydrophobic PPO blocks are shown in red, while the hydrophilic PEO blocks are shown in blue.

7.2. Experimental Section

Details of quantifying polymer binding by PFG-NMR and screening polymer protection efficacy by the lipid peroxidation assay were described in Chapter 2. The synthesis and characterization of bottlebrush polymers are summarized below.

7.2.1 Polymer Synthesis

POEGMA was prepared by reversible addition−fragmentation chain-transfer polymerization (RAFT) as described elsewhere and shown in Figure 7.2a.[317,318] Briefly, OEGMA (Sigma, M_n = 500), the chain transfer agent (CTA) 4-cyano-4-[(dodecylsulfanylthiocarbonyl)sulfanyl]pentanoic acid (Sigma), and the initiator 4,4′-azobis(4- cyanopentanoic acid) (V-501, Sigma) were mixed at a desired molar ratio, where V-501:CTA is 1:10 and monomer:CTA is calculated from the targeted molecular weight, assuming 100% monomer conversion. The mixture was dissolved in anhydrous toluene to make the monomer concentration around 1 M. The solution was purged with argon for 30 min at room temperature, followed by polymerization under an argon atmosphere with stirring at 70 ºC for 24 h. The reaction was terminated by cooling in an ice bath and exposing to air. The resulting solution was diluted with tetrahydrofuran (THF) to make the polymer concentration around 0.25 g/mL and then precipitated in a large volume of cold hexane. The precipitation process was repeated two more times following dissolution of the polymer in THF. The final polymer product is a yellow viscous liquid.

The trithiocarbonate end groups of POEGMA could be removed by aminolysis and Michael addition, as shown in Figure 7.2b.[319,320] First, equimolar POEGMA and tris(2-carboxyethyl)phosphine hydrochloride (TCEP, Sigma) were dissolved in THF with a polymer concentration of 2 mM. The mixture was purged with argon for 15 min before adding *n*-propylamine (Sigma) to the solution with a molar ratio of *n*-propylamine/POEGMA = 50 and stirring for 5 h or until the reaction mixture turned from yellow to colorless at room temperature under an argon atmosphere. Methyl methacrylate (Sigma) with at least 100-fold molar excess with respect to POEGMA was then added and the solution was stirred at room temperature for 36 h. The final product was obtained by precipitation in cold hexane three times.

POPGMA-*b*-POEGMA was synthesized by growing POPGMA from POEGMA by RAFT, using POEGMA as a macro-CTA. The synthetic scheme is shown in Figure 7.2c and the experimental procedure is similar to that of POEGMA synthesis. The only modification is that excess OPGMA monomer was present initially and the reaction was conducted for 1.5 h with 30% monomer conversion. This modified procedure gives a narrower polymer dispersity and better control over the overall molecular weight since the desired POPGMA only has a few repeat units.

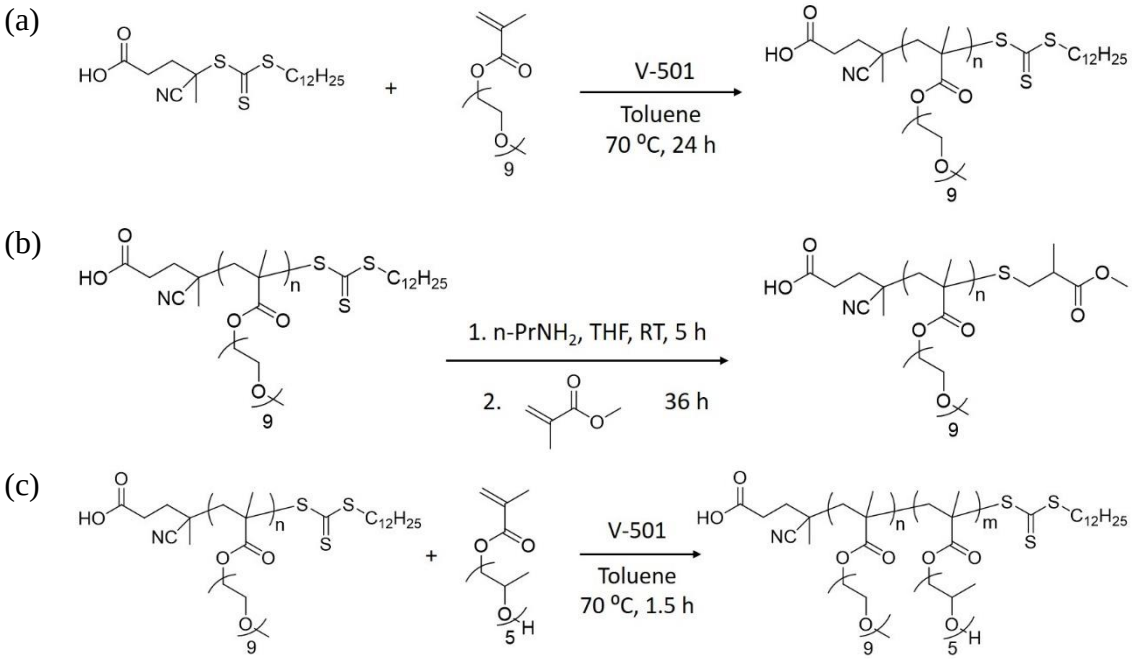

Figure 7.2. Synthetic schemes of (a) POEGMA by RAFT, (b) cleavage of trithiocarbonate end groups, and (c) POPGMA-*b*-POEGMA by RAFT.

7.2.2 Polymer Characterization

Polymers were characterized by both ^{1}H NMR and SEC equipped with a multiangle laser light scattering detector using dimethylformamide (DMF) containing 0.05 M lithium bromide (LiBr) as the mobile phase. The SEC traces are shown in Figure 7.3. The number-average molecular weight (M_n), dispersity ($Đ$), and the average number of repeat units of OPGMA (N_{OPGMA}) and OEGMA (N_{OEGMA}) are summarized in Table 7.1. As for nomenclature, the capital letter in front of the parenthesis represents the monomer type, with "E" for OEGMA and "P" for OPGMA. The number and the letter in the parenthesis represent the monomer molecular weight (in g/mol) and the endgroup of OEG or OPG ("m" means methyl and "h" means hydroxyl), respectively. The number following the

parenthesis represents polymer molecular weight (in kg/mol). “CTA” indicates whether the trithiocarbonate end group was cleaved or not. N_{OEGMA} obtained from NMR was estimated from the integrated intensity of the OEG peak with respect to that of the dodecyl group. N_{OPGMA} could not be estimated from NMR as none of the OPG characteristic peaks is well resolved from the OEG peak or the dodecyl peak. The molecular weight measured by SEC used d*n*/d*c* = 0.0505 mL/g for POEGMA.[321] The same d*n*/d*c* was used to estimate the molecular weight of the diblock since POEGMA is the major component (~70 wt. %) in the diblock. Note that 20% error of N_{OEGMA} was observed between NMR and SEC, possibly due to the discrepancy between the real d*n*/d*c* of the synthesized polymer and that obtained from the literature. A d*n*/d*c* measurement of POEGMA and POPGMA could be employed in the future to obtain more accurate molecular weight of bottlebrush polymers.

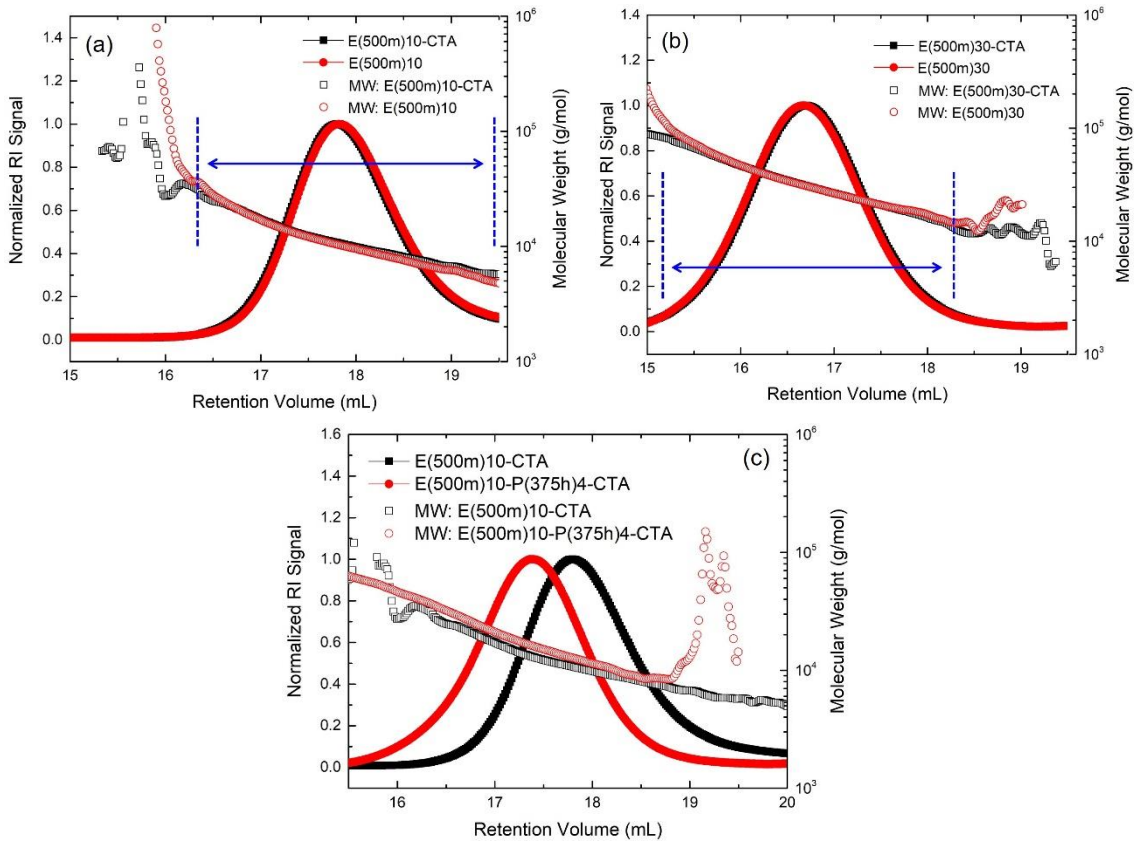

Figure 7.3. SEC traces of (a) E(500m)10 and (b) E(500m)30 with and without trithiocarbonate endgroups, and (c) E(500m)10-P(375h)4-CTA before and after growing the second POPGMA block.

Table 7.1. Polymer Characterization.

	M_n[a] (kg/mol)	$Đ$[a]	N_{OEGMA}[a]	N_{OPGMA}[a]	N_{OEGMA}[b]
E(500m)10-CTA	10.1	1.09	20	-	16
E(500m)10*	9.5	1.09	19	-	-
E(500m)30-CTA	29.3	1.14	60	-	49
E(500m)30	30.1	1.14	62	-	-
E(500m)10-P(375h)4-CTA	14.4	1.18	20	12	16

[a]Obtained from SEC. [b]Obtained from ^{1}H NMR. *backbone capped with methyl acrylate after CTA cleavage.

The SEC traces of the polymers before and after removing trithiocarbonate end groups indicate that the molecular weight distribution was not affected by the endgroup cleavage, as shown in Figure 7.3a and Figure 7.3b. The ^{1}H NMR spectra also demonstrated that the CTA endgroup was cleaved successfully, as the peak of dodecyl group disappears after cleavage (Figure 7.4). Additionally, the endgroup cleavage was characterized by UV-vis spectroscopy, using dichloromethane as the solvent, as shown in Figure 7.5. It can be seen that the trithiocarbonate absorbance peak at 310 nm disappears after cleavage, indicating the trithiocarbonate group was completely broken. However, two small unexpected peaks appear at 263 and 300 nm for both 10k and 30k POEGMAs. It is suspected that the absorbance peaks are from some impurities introduced in the Michael addition step or purification. Further investigation will be needed. A simple test would be measuring and comparing the UV-vis spectra of the reaction mixture before and after Michael addition. Another test would be to increase the purification times or change the solvent type used in the purification process to see whether the two absorbance peaks are affected.

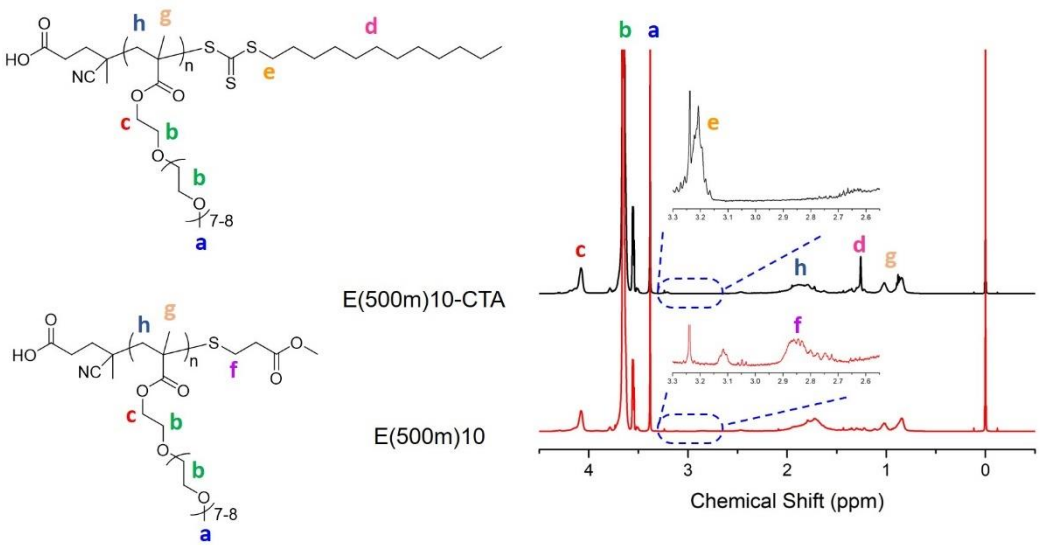

Figure 7.4. ^{1}H NMR spectra of E(500m)10 before and after removing trithiocarbonate endgroup.

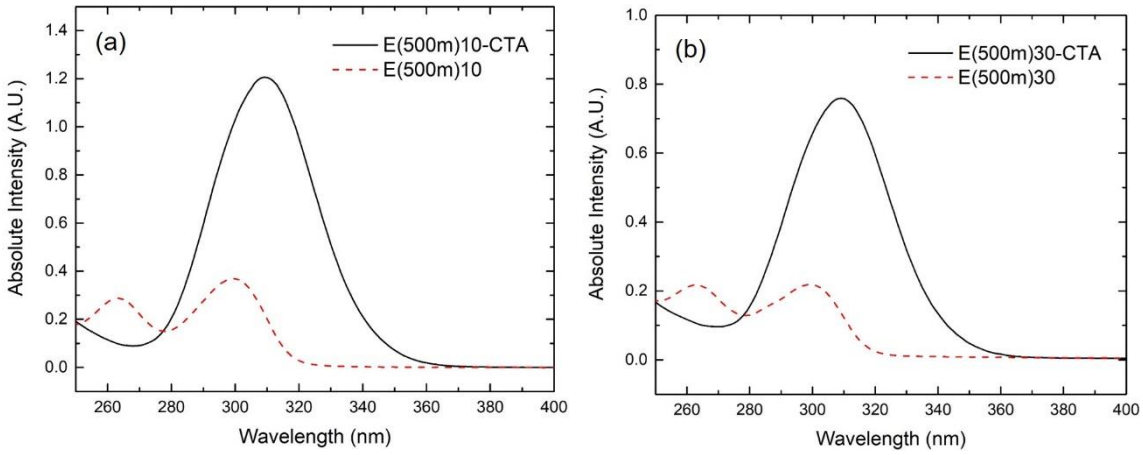

Figure 7.5. UV-vis spectra of (a) E(500m)10 and (b) E(500m)30 before and after removing trithiocarbonate endgroups.

7.3 Results and Discussion

7.3.1 POEGMA

First, the binding of two 10k POEGMAs with and without the trithiocarbonate endgroup at two different concentration was compared. The one with the CTA endgroup at high concentration (1 mg/mL) was not measured due to micelle formation. The other three conditions all show little binding since only the fast decays representing free polymer diffusion was observed, as shown in Figure 7.6. The binding of the 30k POEGMAs were also tested and the results are included in Figure 7.7. Similarly, all decay curves showed little binding as the second plateau was completely lost. The binding percentage of all POEGMAs was plotted as a histogram for direct comparison. As seen in Figure 7.8, all binding is less than 1%, indicating extremely weak interactions with the lipid bilayers regardless of the molecular weight or concentration of the POEGMAs. The binding of commercial linear PEO (M_n=8000 g/mol) was also included as reference. Comparing the linear PEO with E(500m)10, their binding is essentially the same within uncertainty. This suggests that the bottlebrush architecture does not enhance PEO binding to lipid bilayers compared to linear PEO with similar molecular weight. The binding percentage with uncertainty and the diffusion coefficients of free and bound polymers used for fitting are summarized in Table 7.2.

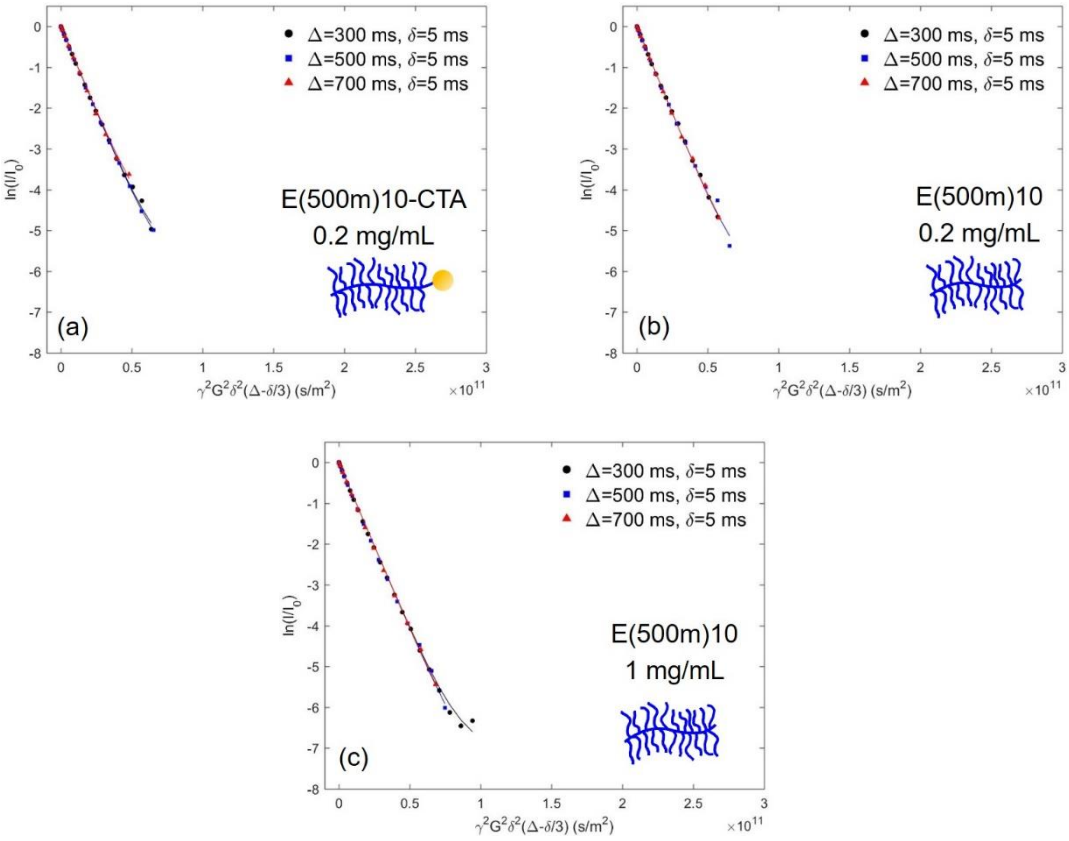

Figure 7.6. Experimental and fitted echo decay curves of the protons from OEG of (a) 0.2 mg/mL E(500m)10-CTA, (b) 0.2 mg/mL E(500m)10, and (c) 1 mg/mL E(500m)10 in 5 mM POPC liposome solution in D_2O at 27 °C with Δ = 300, 500, 700 ms and fixed δ = 5 ms. The data were fit to eq 2.4.

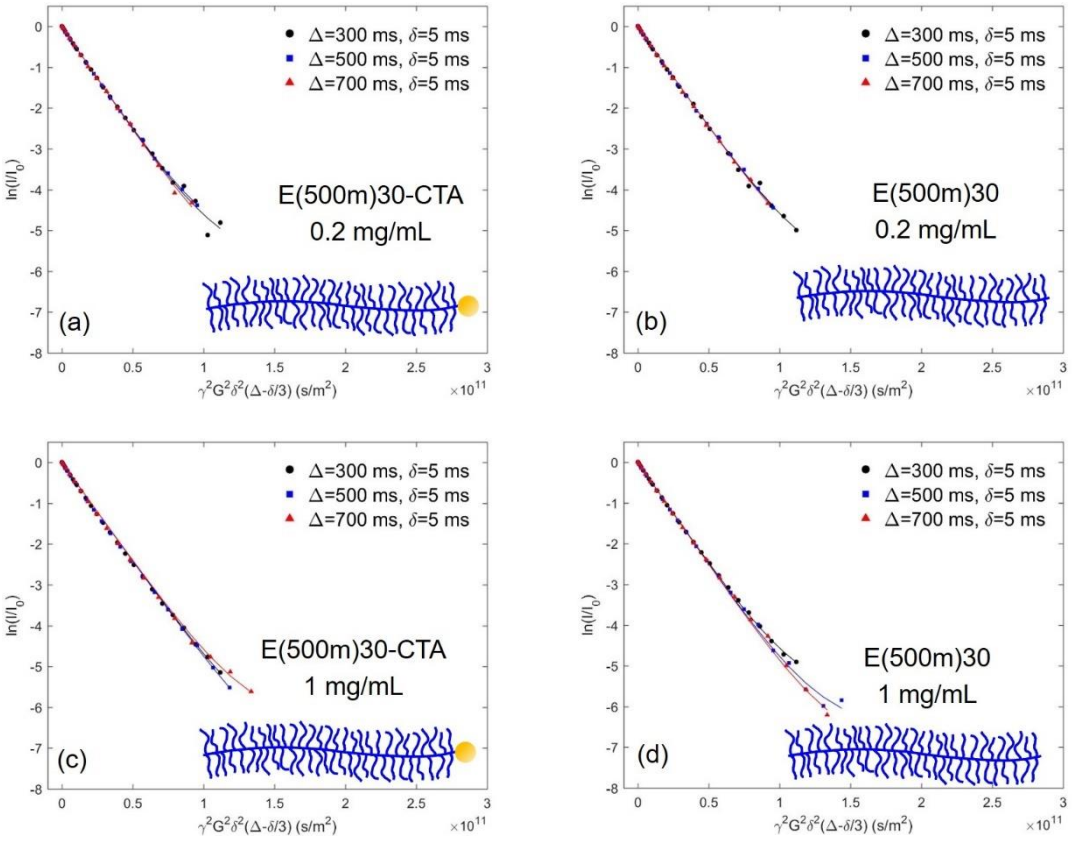

Figure 7.7. Experimental and fitted echo decay curves of the protons from OEG of (a) 0.2 mg/mL E(500m)30-CTA, (b) 0.2 mg/mL E(500m)30, (c) 1 mg/mL E(500m)30-CTA, and (d) 1 mg/mL E(500m)30 in 5 mM POPC liposome solution in D_2O at 27 °C with Δ = 300, 500, 700 ms and fixed δ = 5 ms. The data were fit to eq 2.4.

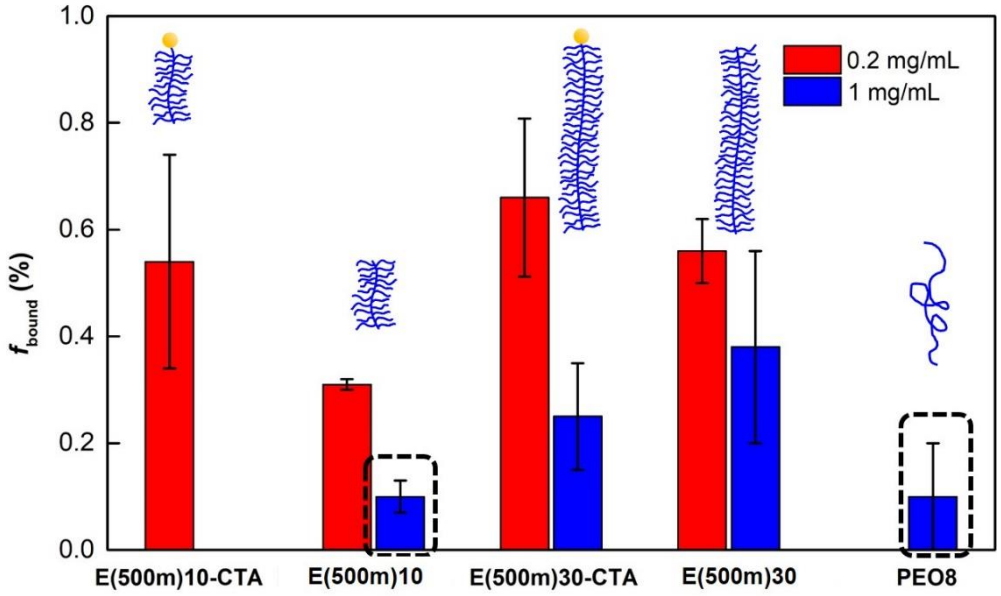

Figure 7.8. Binding summary of POEGMAs and PEO8.

Table 7.2. Summary of polymer binding with uncertainty and the diffusion coefficients used for fitting.

	c (mg/mL)	D_{bound} (10^{-11} m^2/s)	D_{free} (10^{-11} m^2/s)	f_{bound} (%)
E(500m)10-CTA	0.2	0.5	8.38	0.5±0.2
E(500m)10	0.2	0.51	8.55	0.31±0.01
E(500m)10	1	0.46	8.19	0.10±0.03
E(500m)30-CTA	0.2	0.5	5.13	0.7±0.1
E(500m)30-CTA	1	0.48	4.85	0.3±0.1
E(500m)30	0.2	0.54	4.98	0.6±0.1
E(500m)30	1	0.45	5.04	0.4±0.2
PEO8	1	0.5	6.5	0.1±0.1

Additionally, the protection efficacy of these POEGMAs was assessed by the lipid peroxidation assay. POPC liposomes extruded through 50 nm pore radius were used as model membranes. First, E(500m)10 with different polymer/lipid molar ratios was tested

to investigate the polymer concentration effect. The average scattered intensities and corresponding liposome size distributions at different polymer/lipid molar ratios are displayed in Figure 7.9. The liposome size distributions at the lowest polymer concentration (polymer/lipid = 2.5:1) could not be obtained due to the extremely low scattered intensity (close to negative control), indicating little protection at low polymer concentration. The protection efficacy increases upon increasing polymer concentration, as shown by the red columns in Figure 7.9a. At 10:1, polymer protection is most efficient as the scattered intensities of the liposome-polymer mixture before and after induced peroxidation are almost the same. Next, the polymer structure effect was investigated as shown in Figure 7.10. The endgroup effect was studied by comparing the protection efficacy of E(500m)10 with E(500m)10-CTA. With the dodecyl group of the CTA remaining on the polymer backbone, E(500m)10-CTA provides full protection to the liposomes, while its counterpart E(500m)10 can barely protect the liposomes. This demonstrates that the presence of the hydrophobic dodecyl group can significantly enhance polymer protection efficacy. The molecular weight effect was studied based on the comparison between E(500m)10 and E(500m)30. The protection efficacy significantly increases as the molecular weight triples. These conclusions on the influence of polymer concentration, endgroup, and molecular weight on polymer protection efficacy are consistent with those obtained from linear polymers (see Chapter 6). It indicates that PEO with bottlebrush architecture could be potentially used as membrane stabilizers as well.

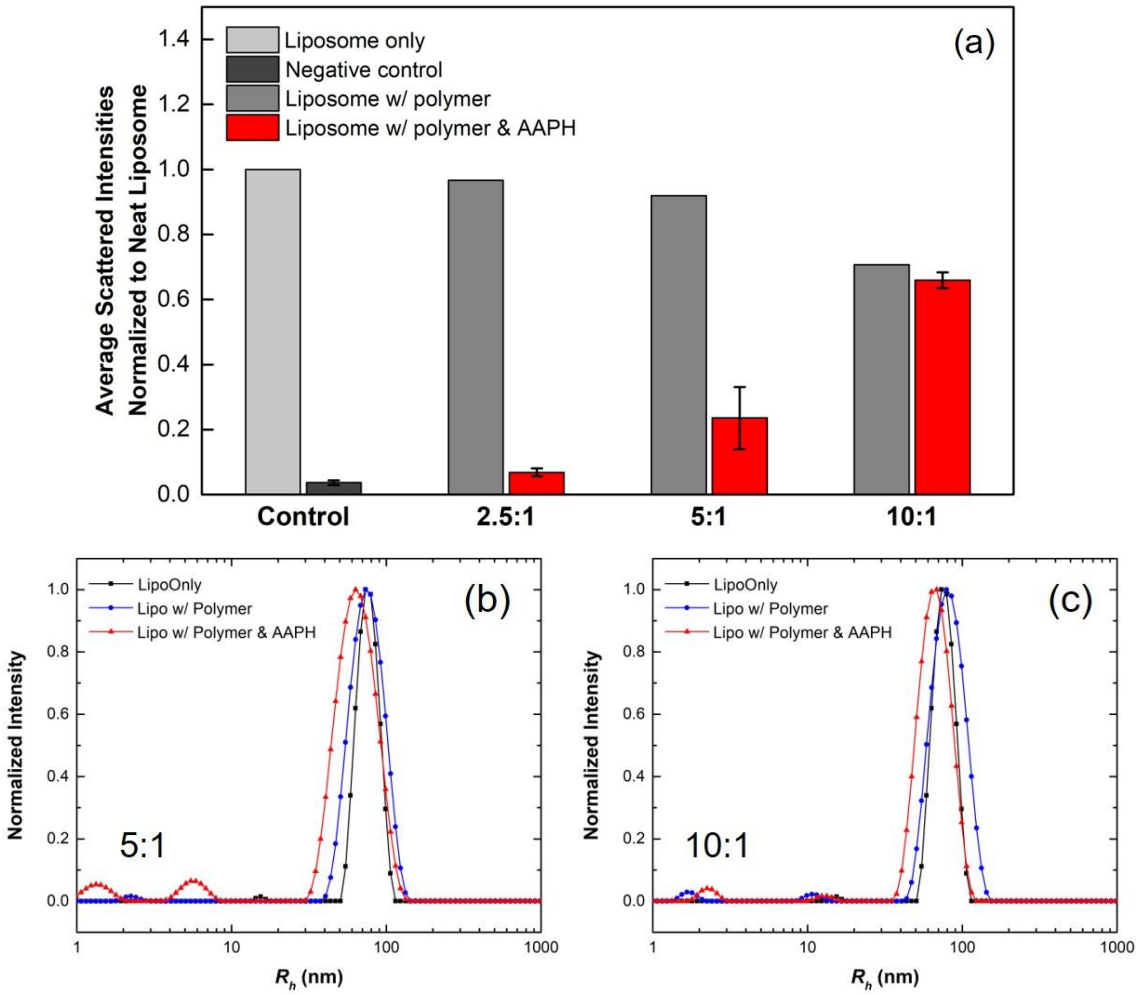

Figure 7.9. (a) Average scattered intensities of POPC liposomes with E(500m)10 at 2.5:1, 5:1 and 10:1 polymer/lipid molar ratios before and after lipid peroxidation. Error bars represent the data range for N = 3 replicates. R_h distributions at 90º of neat liposomes (black), liposomes with E(500m)10 at (b) 5:1 and (c) 10:1 polymer/lipid molar ratio before (blue) and after (red) lipid peroxidation.

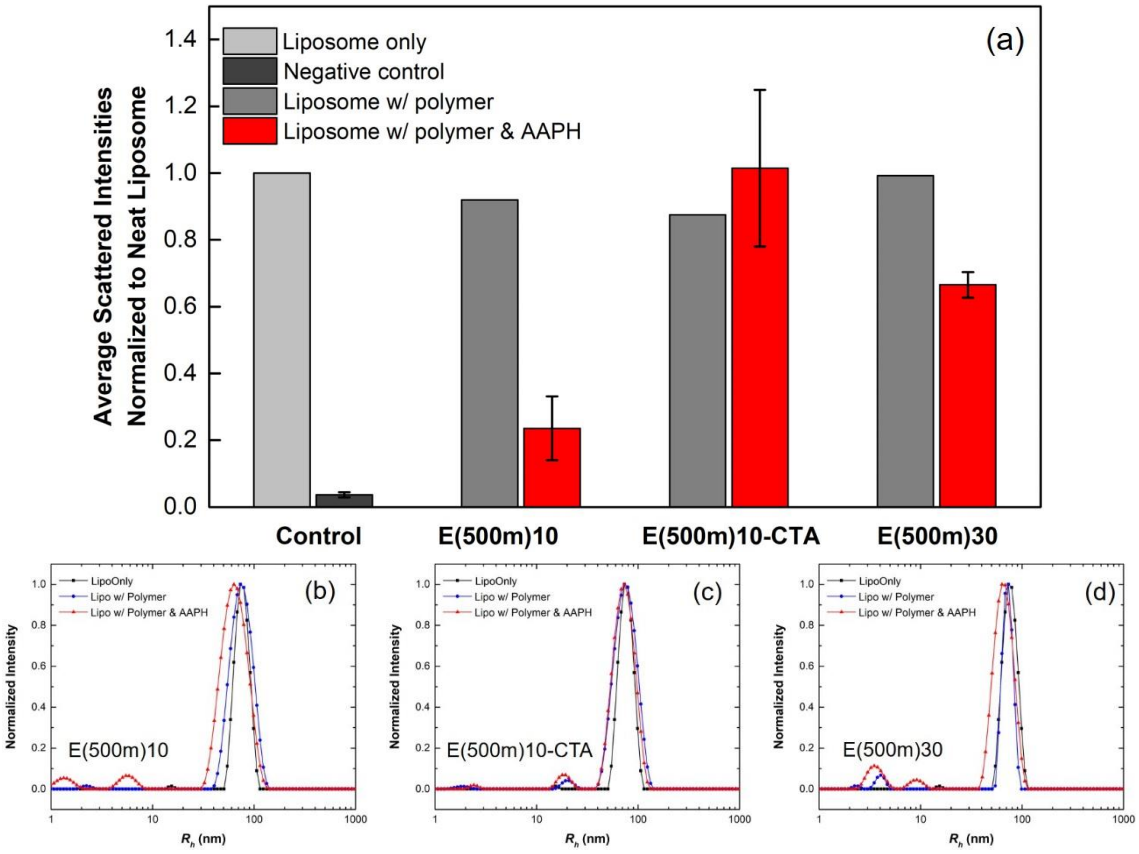

Figure 7.10. (a) Average scattered intensities of POPC liposomes with different polymers at 5:1 polymer/lipid molar ratio before and after lipid peroxidation. Error bars represent the data range for N = 3 replicates. R_h distributions at 90º of neat liposomes (black), liposomes with (b) E(500m)10, (c) E(500m)10-CTA, and (d) E(500m)30 at 5:1 polymer/lipid molar ratio before (blue) and after (red) lipid peroxidation.

7.3.2 POPGMA-*b*-POEGMA

Following the study of bottlebrush PEO, the PPO-PEO bottlebrush diblock was further investigated. The bottlebrush diblock E(500m)10-P(375h)4-CTA was characterized by DLS and PFG-NMR (Figure 7.11). The R_h was measured as 4 nm by both techniques, which demonstrates that the polymer does not micellize at a concentration of 0.2 mg/mL. Hence, this concentration was used for polymer binding measurements by PFG-NMR. The binding results are shown in Figure 7.12a, and compared to that of Pluronic F127 (M_n=13

kg/mol, 70 wt.% PEO) in Figure 7.12b. With similar molecular weight and hydrophilic-hydrophobic balance, the bottlebrush polymer, however, has much lower binding than linear F127 (6.6% vs 18.2%). It indicates that the bottlebrush architecture significantly weakened polymer association with lipid bilayers, compared to linear PPO-PEO block copolymers. This may be caused by the higher rigidity of the bottlebrush polymer due to the dense side chains. Therefore, future studies could modify the graft density of the side chains to investigate how the polymer binding is influenced. A combination of linear and bottlebrush diblock architectures is also worth investigating. Figure 7.13 shows an example of linear PPO with bottlebrush PEO and bottlebrush PPO with linear PEO, assuming they have similar molecular weight and PEO wt. % as E(500m)10-P(375h)4-CTA does. By comparing the binding of these two polymers with E(500m)10-P(375h)4-CTA, we can understand whether the reduction in binding of E(500m)10-P(375h)4-CTA is caused by the bottlebrush PPO portion or PEO portion. It will also indicate whether PPO or PEO plays the dominant role in polymer-membrane association. A synthetic scheme for preparing the polymers with combined architecture is shown in Figure 7.14, where DCC stands for dicyclohexylcarbodiimide, DMAP stands for 4-(dimethylamino)pyridine, and DCM stands for dichloromethane.[317,322,323]

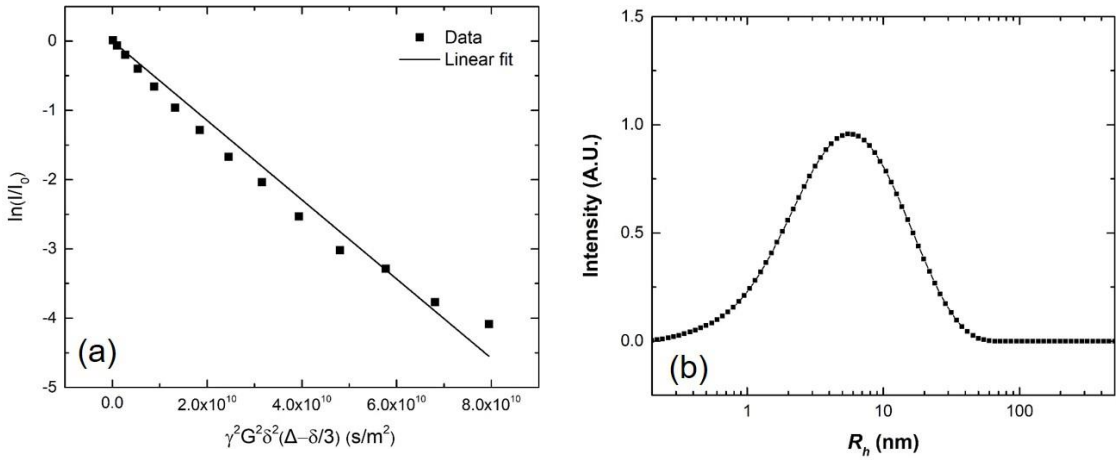

Figure 7.11. (a) Experimental and fitted echo decay curves of the protons from OEG of E(500m)10-P(375h)4-CTA at 0.2 mg/mL in D_2O at 27 °C with Δ = 700 ms and δ = 5 ms. The data were fit to eq 2.3. (b) R_h distribution of the polymers measured by DLS at 90º. The obtained R_h is 4 nm by both techniques, indicating free chains.

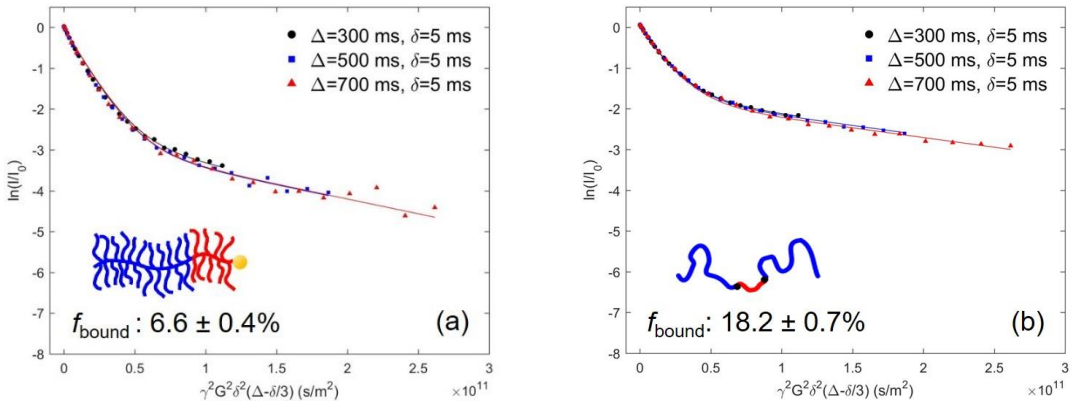

Figure 7.12. Experimental and fitted echo decay curves of the protons from (a) OEG of E(500m)10-P(375h)4-CTA, and (b) PEO of F127 at 0.2 mg/mL in 5 mM POPC liposome solution in D_2O at 27 °C with Δ = 300, 500, 700 ms and fixed δ = 5 ms. The data were fit to eq 2.4.

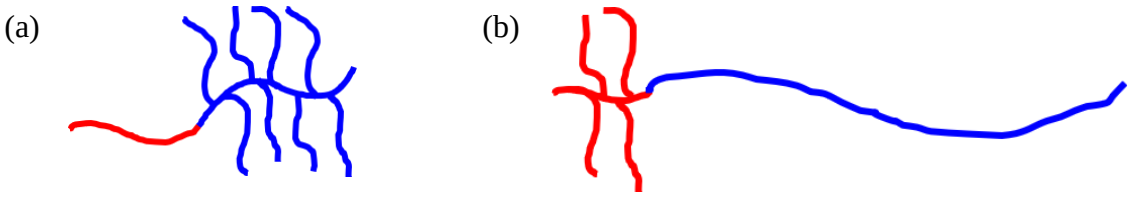

Figure 7.13. Chemical structures of (a) linear PPO with bottlebrush PEO, and (b) bottlebrush PPO with linear PEO.

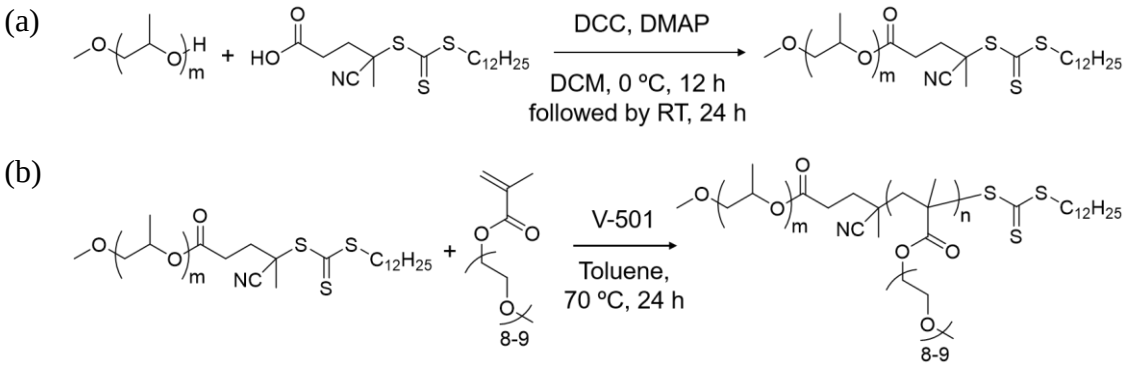

Figure 7.14. Synthetic scheme of PPO-POEGMA.

7.4 Conclusions

In this chapter, we have included some preliminary results of the binding and membrane protection efficacy of bottlebrush polymers. For the bottlebrush PEO (*i.e.*, POEGMA), the bottlebrush architecture does not show enhancement on polymer binding compared to linear PEO. The screening of polymer protection efficacy on damaged lipid membranes based on the lipid peroxidation assay indicates that POEGMA could be potentially used as membrane stabilizers. For the bottlebrush diblock POPGMA-*b*-POEGMA, the polymer binding is significantly lower than that of a linear triblock poloxamer with similar molecular weight and hydrophilic-hydrophobic balance. It could be due to higher rigidity of the bottlebrush polymer.

Chapter 8 – Conclusions and Outlook

8.1 Project Summary

The objective of this project was to gain an understanding of the fundamental mechanisms of the interactions between PPO-PEO block copolymers and cell membranes. The long term goal is to design polymers with optimized molecular architectures and structures that provide more effective stabilization of damaged cell membranes caused by DMD than P188, the only FDA approved commercially available poloxamer. Although the association of commercial Pluronics with cell or model membranes and their related biomedical applications have been widely studied over the past two decades, there is a lack of in-depth quantitative investigation of how polymer structure influences their interactions with membranes. The uniqueness of this research project stems from the following two features. The first is the synthesis of diblock analogues to commercial triblock Pluronics.

The use of diblock analogues significantly increases the diversity of polymer structures within the Pluronic family and enables the exploration of various polymer chemistries systematically. The second unique feature is the development of a quantitative, high resolution technique to characterize the relatively weak binding between the block copolymers and vesicular lipid bilayers, using PFG-NMR. This method provides direct evidence regarding how polymer structure dictates interactions between the block copolymers and lipid bilayers. Also, this is the first time that PFG-NMR has been employed to quantify polymer binding to lipid membranes in the literature to our knowledge. The key findings of this project are summarized as follows.

Chapter 3 describes how polymer molecular weight, individual block length of PPO and PEO, endgroup chemistry, and polymer concentration affect binding with lipid bilayers. Large unilamellar vesicles composed of pure POPC were used as model membranes. PFG-NMR was employed to probe polymer diffusion in the absence and presence of liposomes. The binding percentage of polymer to the liposome was quantified by fitting echo decay curves to a biexponential model. It was found that increasing the total molecular weight and hydrophobicity of the polymer can significantly enhance the polymer−lipid bilayer association, as the binding percentage and liposome surface coverage both increase. We hypothesize that the hydrophobic PPO block inserts into the lipid bilayer due to the fact that little molecular exchange between bound and free polymers occurs on the time scale of the diffusion experiments. Additionally, as polymer concentration increases, the liposome surface coverage increases and approaches a limiting value.

In Chapter 4, we investigated how cholesterol content in the bilayer and bilayer curvature affect polymer binding. Cholesterol concentration was manipulated by varying the molar percentage of this sterol in the POPC bilayer preparation. The membrane curvature was varied by adjusting the liposome size through a conventional pore extrusion technique. Although the PPO content significantly influences the overall amount of block copolymer adsorbed to the liposome as demonstrated in Chapter 3, we found that polymer binding decreases dramatically with increasing cholesterol concentration in a universal fashion, with the fraction of bound polymer dropping 10-fold between 0 and 30 mol % cholesterol relative to the total content of POPC and cholesterol. Increasing the bilayer curvature (decreasing the radius of the liposome) in the absence of cholesterol increases polymer binding between 2- and 4-fold over the range of liposome sizes studied. These results demonstrate that cholesterol plays a dominant role, and bilayer curvature has a less significant impact as the curvature decreases, on polymer−membrane association.

Chapter 5 explores how lipid headgroup and the degree of unsaturation of lipid alkyl chains affect polymer binding to the lipid bilayers. Headgroup composition was manipulated by the molar ratio of POPG to POPC in the lipid bilayers. Polymer binding was observed to increase substantially upon increasing the POPG content in the bilayer, which is likely due to hydrogen bonding between the glycerol headgroup of POPG and the ether oxygen moities of the polymers. The degree of unsaturation of lipid alkyl chains were investigated by comparing polymer binding to POPC, DOPC, PLPC, and DPPC/POPC bi-component liposomes. The results indicated that polymer binding to the liposomes composed of lipids with two mono-unsaturated hydrocarbon chains (*i.e.,* DOPC) is higher

by about 25% than that with one saturated chain and one mono- (*i.e.*, POPC) or poly-unsaturated chain (*i.e.*, PLPC). Also, polymer binding fluctuates as DPPC molar percentage increases in the DPPC/POPC bi-component liposomes, which could be partially related to a phase transition in the lipid bilayer.

After exploring how polymer-membrane association is affected by polymer structure and membrane composition and curvature, we further developed a screening assay to assess the protection efficacy of polymers with different architecture and structure on damaged lipid membranes in Chapter 6. Following earlier work by Wang et al. and Haman,[6,107] lipid peroxidation was introduced as model stress imposed on the vesicular lipid bilayers, which aims to mimic the damage on cell membranes. The polymer protective effect was evaluated based on the resulting membrane integrity after inducing peroxidation, using the scattered intensity and size distribution of the lipid vesicles measured by DLS. It was found that diblock architecture can protect the membrane as effectively as commercial triblock poloxamers. The diblock with 80 wt.% PEO turned out to be the most efficient polymer to protect the liposomes against peroxidation, compared to the ones with 70 and 90 wt.% PEO. Also, the *tert*-butyl ended diblock showed more effective protection than the one with a methyl endgroup at the same PPO/PEO composition. Additionally, the stabilization efficacy increases as polymer molecular weight increases. These screening results were compared with polymer stabilization efficacy *in vitro* and *in vivo*, and most of the results are consistent.

In Chapter 7, some preliminary results of bottlebrush polymers are included. For bottlebrush PEO (POEGMA), the bottlebrush architecture showed little improvement on

polymer binding compared to a linear PEO with similar molecular weight. The binding of the diblock bottlebrush polymer POPGMA-*b*-POEGMA is significantly lower than that of a linear commercial poloxamer with similar molecular weight and PEO wt.%. In terms of the polymer stabilization efficacy tested by the lipid peroxidation assay, POEGMA at higher concentration, with larger molecular weight, and with a hydrophobic endgroup on the backbone showed more efficient protection on damaged liposomes.

Overall, this project provided insights into the molecular interactions of PPO-PEO block copolymers with model membranes and built up the connection between the fundamental work of the mechanism of polymer−lipid bilayer association to the *in vivo* work of identifying effective therapies for DMD.

8.2 Project Outlook

In this final section, potential future research directions will be discussed. First, more polymer architectures, structures, and chemistries (*e.g.*, bottlebrush polymer, star polymer, endgroup chemistry) could be investigated since we have demonstrated through this thesis that these factors play a significant role on polymer interactions with lipid membranes. Second, mechanistic studies on polymer-membrane association should continue. SANS and neutron reflectometry could be employed to investigate the polymer configuration in the lipid membranes. Neutron spin echo and AFM could be applied to study how membrane rigidity is affected by polymer insertion.

8.2.1. Variation of Polymer Architecture, Structure, and Chemistry

Based on the preliminary results shown in Chapter 7, the bottlebrush architecture (Figure 8.1a) needs further investigation, especially the side chain length and graft density, as they could be the dominant factors that affect polymer binding with lipid bilayers. Another class of polymers that deserves further investigation is the mikto-arm star architecture (Figure 8.1b). Following what we learned from the endgroup anchoring effect with *tert*-butyl endgroup, the two PPO blocks in $PEO(PPO)_2$ may function as an amplified anchor, which is hypothesized to favor the insertion into the membranes. The other mikto-arm star architecture, $(PEO)_2PPO$, could be compared with the linear triblock with the same PPO/PEO composition to study whether the placement of two PEO arms onto the same end of the PPO block makes any difference. In addition to the polymer architecture, different chemistry could also be applied. Leiske *et al.* have shown that PBO-PEO diblock copolymers have a similar lipid insertion mechanism as PPO-PEO diblocks.[103] Hence, PBO which provides higher hydrophobicity could be potentially used as a substitute for PPO. Also, the endgroup chemistry on the PPO block could be manipulated and explored as another possible direction. So far, we have only investigated the *tert*-butyl endgroup compared to methyl and hydroxyl endgroups. This endgroup was incorporated by the use of potassium *tert*-butoxide as the initiator in the anionic polymerization of the PPO block. In the future, the endgroup chemistry could be intentionally modified to the chemical structures of interest, such as a short alkyl chain, which mimics the chemistry of lipid tails and thereby could possibly enhance polymer-membrane association.

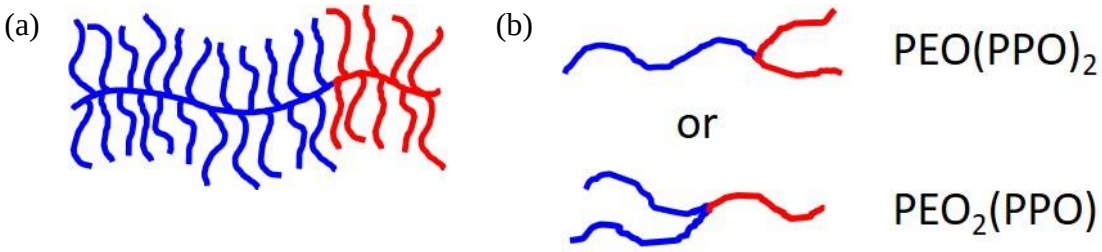

Figure 8.1. Schematics of (a) a bottlebrush polymer, and (b) two possible structures of mikto-arm star polymers. The hydrophobic PPO blocks are shown in red, while the hydrophilic PEO blocks are shown in blue.

8.2.2 Mechanistic Investigation of Polymer-Membrane Association

The olymer configuration when interacting with lipid bilayers is not fully understood. It is still controversial whether PEO blocks can insert into the membrane interior or only adsorb on the membrane surface. One technique to examine this is SANS. One benefit of SANS compared to other scattering techniques is contrast matching.[324–326] The large difference between the scattering length of hydrogen ($b_H = -0.374\times10^{-12}$ cm) and that of deuterium ($b_D = 0.667\times10^{-12}$ cm) can be employed to create contrast among different chemical species or different parts of the species. For example, tail-deuterated phospholipids could be used to increase the contrast between the liposomes and hydrogenated polymers. The contrast of the background solvent can be adjusted by tuning the ratio of H_2O to D_2O and enables contrast matching to selectively suppress scattering contributions from specific components of the solution. At certain ratios, the contrast of the solvent is equal to that of the polymer and the polymer scattering cannot be differentiated from the background. Therefore, the SANS profile only contains the structural information of liposome scattering as the polymer is rendered “invisible” via

contrast matching, by which we can directly compare the SANS profiles of the liposomes before and after polymer addition to see if the polymer induces any structural changes of the liposomes. Previously, we have measured the interaction of P188 with d54-DMPC liposomes by SANS using two different solvent contrast factors. As shown in Figure 8.2, the SANS profiles of liposomes measured in both cases indicate P188 has little interaction with the liposomes. Our PFG-NMR studies in Chapter 3 further provided direct evidence that P188 indeed has little binding (~0.1%) to liposomes. Since we learned from Chapter 3 that the commercial Pluronic with the strongest binding is F127 (~26% liposome surface coverage), with such relatively high liposome surface coverage, it might be worth comparing the liposome structure before and after introducing F127 using SANS, which might provide insights into the polymer adsorption/insertion mechanism.

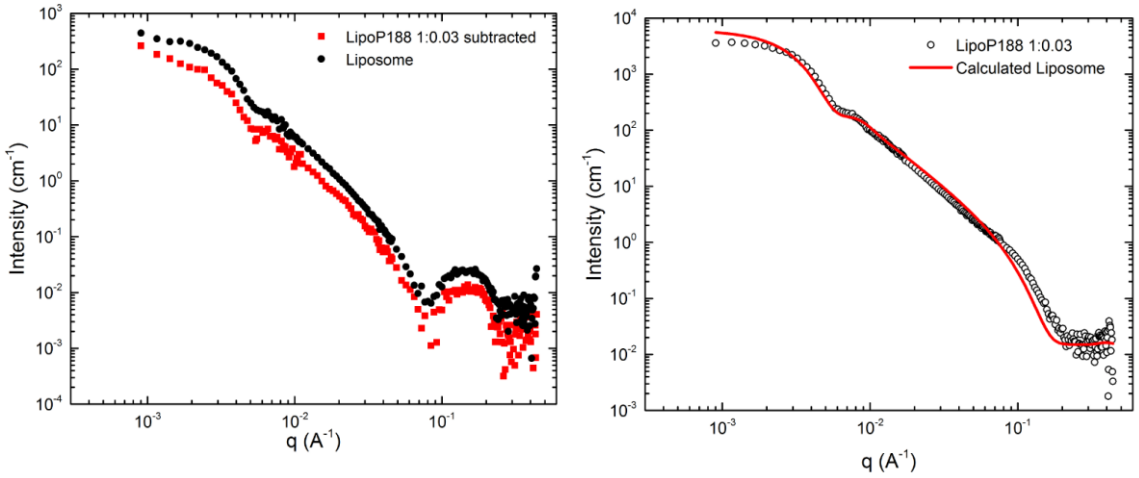

Figure 8.2. SANS profiles of liposome incubation with low polymer concentration (lipid/polymer molar ratio = 1:0.03) at 37 °C in (a) pure D_2O: the black dots are neat liposome scattering and the red dots are the liposome scattering in the presence of P188 wherein the scattering contribution of P188 was subtracted. (b) 84% H_2O/16% D_2O: the open circles are the liposome scattering in the presence of P188 and the red curve is the theoretical scattering profile of neat liposomes. Data were collected and analyzed in collaboration with Dr. Mihee Kim.

Another potential technique to characterize polymer-membrane association is neutron reflectometry. The reflectometry profile of a flat surface provides structural information about the thin films layered on the surface, such as the thickness and density of each layer (*e.g.*, lipid headgroup layer, tail layer). Comparing the structural information of lipid bilayers before and after introducing polymers, we can further deduce the polymer configuration in the bilayer. Recently, Hayden *et al.* have successfully employed this technique to investigate the penetration of Pluronic F98 into surface supported DMPC bilayers.[183] The preliminary results obtained by Dr. Mihee Kim on Pl88 also indicate that neutron reflectometry is a promising technique for mechanistic studies of polymer association with lipid bilayers.

Additionally, membrane dynamics could be used as a measure of their interaction with polymers. Neutron spin echo (NSE) spectroscopy can be applied to observe relaxation and diffusion in the membrane.[327–331] A study by Woodka *et al*. used NSE to examine the bending modulus and thickness fluctuations of neat lipid bilayers.[332] Polymer introduction to the system would disturb the membrane dynamics due to the interactions between the polymers and lipid bilayers. We hypothesize that the membrane fluctuations would be suppressed by the polymer-lipid bilayer association, resulting in higher rigidity (*i.e.*, higher bending modulus) of the lipid bilayers. AFM could be employed to measure membrane rigidity as well. Recently, Takechi-Haraya and coworkers investigated the dependence of membrane rigidity on the membrane phase by measuring the bending modulus of immobilized liposomes with various composition on glass surface in aqueous medium.[165]

This method could potentially be applied to probe the change of liposome membrane rigidity with and without polymers.

Bibliography

(1) Pacifico, C. R.; Lundsted, L. G.; Vaughn, T. H. Flake Form Nonionic Detergents. *Soap Sanit. Chem.* **1950**, *26*, 40–43.

(2) Vaughn, T. H.; Suter, H. R.; Lundsted, L. G.; Kramer, M. G. Properties of Some Newly Developed Nonionic Detergents. *J. Am. Oil Chem. Soc.* **1951**, *28*, 294–299.

(3) Lundsted, L. G. Polyoxyalkylene Compounds. US2674619, 1954.

(4) Schmolka, I. R. Artificial Skin I. Preparation and Properties of Pluronic F-127 Gels for Treatment of Burns. *J. Biomed. Mater. Res.* **1972**, *6*, 571–582.

(5) Schmolka, I. R. A Review of Block Polymer Surfactants. *J. Am. Oil Chem. Soc.* **1977**, *54*, 110–116.

(6) Haman, K. J. Development of Model Diblock Copolymer Surfactants for Mechanistic Investigations of Cell Membrane Stabilization, PhD Thesis, University of Minnesota, 2015.

(7) Alexandridis, P.; Hatton, T. A. Poly(Ethylene Oxide)-Poly(Propylene Oxide)-Poly(Ethylene Oxide) Block Copolymer Surfactants in Aqueous Solutions and at Interfaces: Thermodynamics, Structure, Dynamics, and Modeling. *Colloids Surfaces A Physicochem. Eng. Asp.* **1995**, *96*, 1–46.

(8) Batrakova, E.; Lee, S.; Li, S.; Venne, A.; Alakhov, V.; Kabanov, A. Fundamental Relationships between the Composition of Pluronic Block Copolymers and Their Hypersensitization Effect in MDR Cancer Cells. *Pharm. Res.* **1999**, *16*, 1373–

1379.

(9) Krupka, T. M.; Exner, A. A. Structural Parameters Governing Activity of Pluronic Triblock Copolymers in Hyperthermia Cancer Therapy. *Int. J. Hyperth.* **2011**, *27*, 663–671.

(10) Kozlov, M. Y.; Melik-Nubarov, N. S.; Batrakova, E. V.; Kabanov, A. V. Relationship between Pluronic Block Copolymer Structure, Critical Micellization Concentration and Partitioning Coefficients of Low Molecular Mass Solutes. *Macromolecules* **2000**, *33*, 3305–3313.

(11) Hiemenz, P. C.; Lodge, T. P. *Polymer Chemistry*, 2nd ed.; CRC Press: Boca Raton, FL, 2007.

(12) Alexandridis, P.; Athanassiou, V.; Fukuda, S.; Hatton, T. A. Surface Activity of Poly(Ethylene Oxide)-Block-Poly(Propylene Oxide)-Block-Poly(Ethylene Oxide) Copolymers. *Langmuir* **1994**, *10*, 2604–2612.

(13) Alexandridis, P; Holzwarth, J. F.; Hatton, T. A. Micellization of Poly(Ethylene Oxide)-Poly(Propylene Oxide)-Poly(Ethylene Oxide) Triblock Copolymers in Aqueous Solutions: Thermodynamics of Copolymer Association. *Macromolecules* **1994**, *27*, 2414–2425.

(14) Zhou, Z.; Chu, B. Light-Scattering Study on the Association Behavior of Triblock Polymers of Ethylene Oxide and Propylene Oxide in Aqueous Solution. *J. Colloid Interface Sci.* **1988**, *126*, 171–180.

(15) Liang, X.; Guo, C.; Ma, J.; Wang, J.; Chen, S.; Liu, H. Temperature-Dependent

Aggregation and Disaggregation of Poly(Ethylene Oxide)-Poly(Propylene Oxide)-Poly(Ethylene Oxide) Block Copolymer in Aqueous Solution. *J. Phys. Chem. B* **2007**, *111*, 13217–13220.

(16) Mortensen, K. Structural Studies of Aqueous Solutions of PEO–PPO–PEO Triblock Copolymers, Their Micellar Aggregates and Mesophases; a Small-Angle Neutron Scattering Study. *J. Phys. Condens. Matter* **1996**, *8*, A103–A124.

(17) Holland, R. J.; Parker, E. J.; Guiney, K.; Zeld, F. R. Fluorescence Probe Studies of Ethylene Oxide/Propylene Oxide Block Copolymers in Aqueous Solution. *J. Phys. Chem.* **1995**, *99*, 11981–11988.

(18) Altinok, H.; Nixon, S. K.; Gorry, P. A.; Attwood, D.; Booth, C.; Kelarakis, A.; Havredaki, V. Micellisation and Gelation of Diblock Copolymers of Ethylene Oxide and Propylene Oxide in Aqueous Solution, the Effect of P-Block Length. *Colloids Surfaces B Biointerfaces* **1999**, *16*, 73–91.

(19) Alexandridis, P. Poly(Ethylene Oxide)/Poly(Propylene Oxide) Block Copolymer Surfactants. *Curr. Opin. Colloid Interface Sci.* **1997**, *2*, 478–489.

(20) Matsuyama, A.; Tanaka, F. Theory of Solvation-Induced Reentrant Phase Separation in Polymer Solutions. *Phys. Rev. Lett.* **1990**, *65*, 341–344.

(21) Bekiranov, S.; Bruinsma, R.; Pincus, P. Solution Behavior of Polyethylene Oxide in Water as a Function of Temperature and Pressure. *Phys. Rev. E* **1997**, *55*, 577–585.

(22) Dormidontova, E. E. Role of Competitive PEO−Water and Water−Water

Hydrogen Bonding in Aqueous Solution PEO Behavior. *Macromolecules* **2002**, *35*, 987–1001.

(23) Kjellander, R.; Florin, E. Water Structure and Changes in Thermal Stability of the System Poly(Ethylene Oxide)–Water. *J. Chem. Soc. Faraday Trans. 1 Phys. Chem. Condens. Phases* **1981**, *77*, 2053.

(24) Ashbaugh, H. S.; Paulaitis, M. E. Monomer Hydrophobicity as a Mechanism for the LCST Behavior of Poly(Ethylene Oxide) in Water. *Ind. Eng. Chem. Res.* **2006**, *45*, 5531–5537.

(25) Steinschulte, A. A.; Schulte, B.; Rütten, S.; Eckert, T.; Okuda, J.; Möller, M.; Schneider, S.; Borisov, O. V.; Plamper, F. A. Effects of Architecture on the Stability of Thermosensitive Unimolecular Micelles. *Phys. Chem. Chem. Phys.* **2014**, *16*, 4917.

(26) Lau, B. K.; Wang, Q.; Sun, W.; Li, L. Micellization to Gelation of a Triblock Copolymer in Water: Thermoreversibility and Scaling. *J. Polym. Sci. Part B Polym. Phys.* **2004**, *42*, 2014–2025.

(27) Cabana, A.; Aït-Kadi, A.; Juhász, J. Study of the Gelation Process of Polyethylene Oxide–Polypropylene Oxide–Polyethylene Oxide Copolymer (Poloxamer 407) Aqueous Solutions. *J. Colloid Interface Sci.* **1997**, *190*, 307–312.

(28) Barba, A. A.; D'Amore, M.; Grassi, M.; Chirico, S.; Lamberti, G.; Titomanlio, G. Investigation of Pluronic F127-Water Solutions Phase Transitions by DSC and Dielectric Spectroscopy. *J. Appl. Polym. Sci.* **2009**, *114*, 688–695.

(29) Armstrong, J. K.; Parsonage, J.; Chowdhry, B.; Leharne, S.; Mitchell, J.; Beezer, A.; Loehner, K.; Laggner, P. Scanning Densitometric and Calorimetric Studies of Poly(Ethylene Oxide)/Poly(Propylene Oxide)/Poly(Ethylene Oxide) Triblock Copolymers (Poloxamers) in Dilute Aqueous Solution. *J. Phys. Chem.* **1993**, *97*, 3904–3909.

(30) Mata, J. P.; Majhi, P. R.; Guo, C.; Liu, H. Z.; Bahadur, P. Concentration, Temperature, and Salt-Induced Micellization of a Triblock Copolymer Pluronic L64 in Aqueous Media. *J. Colloid Interface Sci.* **2005**, *292*, 548–556.

(31) Armstrong, J. K.; Chowdhry, B. Z.; Snowden, M. J.; Leharne, S. A. Effect of Sodium Chloride upon Micellization and Phase Separation Transitions in Aqueous Solutions of Triblock Copolymers: A High-Sensitivity Differential Scanning Calorimetry Study. *Langmuir* **1998**, *14*, 2004–2010.

(32) Alexandridis, P.; Holzwarth, J. F. Differential Scanning Calorimetry Investigation of the Effect of Salts on Aqueous Solution Properties of an Amphiphilic Block Copolymer (Poloxamer). *Langmuir* **1997**, *13*, 6074–6082.

(33) Wanka, G.; Hoffmann, H.; Ulbricht, W. The Aggregation Behavior of Poly-(Oxyethylene)-Poly-(Oxypropylene)-Poly-(Oxyethylene)-Block-Copolymers in Aqueous Solution. *Colloid Polym. Sci.* **1990**, *268*, 101–117.

(34) Alexandridis, P.; Nivaggioli, T.; Hatton, T. A. Temperature Effects on Structural Properties of Pluronic P104 and F108 PEO-PPO-PEO Block Copolymer Solutions. *Langmuir* **1995**, *11*, 1468–1476.

(35) Ma, J.; Guo, C.; Tang, Y.; Xiang, J.; Chen, S.; Wang, J.; Liu, H. Micellization in

Aqueous Solution of an Ethylene Oxide–Propylene Oxide Triblock Copolymer, Investigated with 1H NMR Spectroscopy, Pulsed-Field Gradient NMR, and NMR Relaxation. *J. Colloid Interface Sci.* **2007**, *312*, 390–396.

(36) Hunter, R. J. *Foundations of Colloid Science*; Oxford University Press: New York, 1987.

(37) Hiemenz, P. C. *Principles of Colloid and Surface Chemistry*, 2nd ed.; Marcel Dekker: New York, 1986.

(38) Ben-Naim, A. *Hydrophobic Interactions*; Plenum: New York, 1980.

(39) Atkins, P; de Paula, J. *Physical Chemistry for the Life Sciences*; Oxford University Press: Oxford, UK, 2006.

(40) Chang, R. *Physical Chemistry for the Biosciences*; Edwards Brothers, Inc.: Sausalito, CA, 2005.

(41) Garrett, R. H.; Grisham, C. M. *Biochemistry*; Thomas Brooks/Cole: Belmont, CA, 2005.

(42) Schmolka, I. R. A Comparison of Block Copolymer Surfactant Gels. *J. Am. Oil Chem. Soc.* **1991**, *68*, 206–209.

(43) Deng, N.-J.; Luo, Y.-Z.; Tanodekaew, S.; Bingham, N.; Attwood, D.; Booth, C. Gelation of Micellar Solutions of Diblock-Copoly (Oxyethylene/Oxybutylene) in Aqueous K_2SO_4. An Investigation of Excluded Volume Effects. *J. Polym. Sci. Part B Polym. Phys.* **1995**, *33*, 1085–1096.

(44) Mortensen, K.; Brown, W.; Nordén, B. Inverse Melting Transition and Evidence

of Three-Dimensional Cubatic Structure in a Block-Copolymer Micellar System. *Phys. Rev. Lett.* **1992**, *68*, 2340–2343.

(45) Alexandridis, P.; Zhou, D.; Khan, A. Lyotropic Liquid Crystallinity in Amphiphilic Block Copolymers: Temperature Effects on Phase Behavior and Structure for Poly(Ethylene Oxide)- b -Poly(Propylene Oxide)- b -Poly(Ethylene Oxide) Copolymers of Different Composition. *Langmuir* **1996**, *12*, 2690–2700.

(46) Wanka, G.; Hoffmann, H.; Ulbricht, W. Phase Diagrams and Aggregation Behavior of Poly(Oxyethylene)-Poly(Oxypropylene)-Poly(Oxyethylene) Triblock Copolymers in Aqueous Solutions. *Macromolecules* **1994**, *27*, 4145–4159.

(47) Wu, Y. L.; Sprik, R.; Poon, W. C. K.; Eiser, E. Effect of Salt on the Phase Behaviour of F68 Triblock PEO/PPO/PEO Copolymer. *J. Phys. Condens. Matter* **2006**, *18*, 4461–4470.

(48) Ma, J.; Guo, C.; Tang, Y.; Liu, H. 1 H NMR Spectroscopic Investigations on the Micellization and Gelation of PEO−PPO−PEO Block Copolymers in Aqueous Solutions. *Langmuir* **2007**, *23*, 9596–9605.

(49) Armstrong, J.; Chowdhry, B.; Mitchell, J.; Beezer, A.; Leharne, S. Effect of Cosolvents and Cosolutes upon Aggregation Transitions in Aqueous Solutions of the Poloxamer F87 (Poloxamer P237): A High Sensitivity Differential Scanning Calorimetry Study. *J. Phys. Chem.* **1996**, *100*, 1738–1745.

(50) Cheng, Y.; Jolicoeur, C. Cosolvent Effects on Thermally-Induced Transitions of a Block Copolymer: Poly(Ethylene Oxide)-Poly(Propylene Oxide) in Aqueous Solutions. *Macromolecules* **1995**, *28*, 2665–2672.

(51) Bharatiya, B.; Guo, C.; Ma, J. H.; Hassan, P. A.; Bahadur, P. Aggregation and Clouding Behavior of Aqueous Solution of EO–PO Block Copolymer in Presence of n-Alkanols. *Eur. Polym. J.* **2007**, *43*, 1883–1891.

(52) Yang, B.; Guo, C.; Chen, S.; Ma, J.; Wang, J.; Liang, X.; Zheng, L.; Liu, H. Effect of Acid on the Aggregation of Poly(Ethylene Oxide)−Poly(Propylene Oxide)−Poly(Ethylene Oxide) Block Copolymers. *J. Phys. Chem. B* **2006**, *110*, 23068–23074.

(53) Pandit, N. Loss of Gelation Ability of Pluronic® F127 in the Presence of Some Salts. *Int. J. Pharm.* **1996**, *145*, 129–136.

(54) Desai, M.; Jain, N. J.; Sharma, R.; Bahadur, P. Temperature and Salt-Induced Micellization of Some Block Copolymers in Aqueous Solution. *J. Surfactants Deterg.* **2000**, *3*, 193–199.

(55) Alexandridis, P.; Athanassiou, V.; Hatton, T. A. Pluronic-P105 PEO-PPO-PEO Block Copolymer in Aqueous Urea Solutions: Micelle Formation, Structure, and Microenvironment. *Langmuir* **1995**, *11*, 2442–2450.

(56) Patel, K.; Bahadur, P.; Guo, C.; Ma, J. H.; Liu, H. Z.; Yamashita, Y.; Khanal, A.; Nakashima, K. Salt Induced Micellization of Very Hydrophilic PEO–PPO–PEO Block Copolymers in Aqueous Solutions. *Eur. Polym. J.* **2007**, *43*, 1699–1708.

(57) Jain, N. J.; George, A.; Bahadur, P. Effect of Salt on the Micellization of Pluronic P65 in Aqueous Solution. *Colloids Surfaces A Physicochem. Eng. Asp.* **1999**, *157*, 275–283.

(58) Ma, J.; Guo, C.; Tang, Y.; Wang, J.; Zheng, L.; Liang, X.; Chen, S.; Liu, H. Salt-Induced Micellization of a Triblock Copolymer in Aqueous Solution: A ^{1}H Nuclear Magnetic Resonance Spectroscopy Study. *Langmuir* **2007**, *23*, 3075–3083.

(59) Pandit, N.; Trygstad, T.; Croy, S.; Bohorquez, M.; Koch, C. Effect of Salts on the Micellization, Clouding, and Solubilization Behavior of Pluronic F127 Solutions. *J. Colloid Interface Sci.* **2000**, *222*, 213–220.

(60) Jain, N. J.; Aswal, V. K.; Goyal, P. S.; Bahadur, P. Salt Induced Micellization and Micelle Structures of' PEO/PPO/PEO Block Copolymers in Aqueous Solution. *Colloids Surfaces A Physicochem. Eng. Asp.* **2000**, *173*, 85–94.

(61) Zhou, D.; Alexandridis, P.; Khan, A. Self-Assembly in a Mixture of Two Poly(Ethylene Oxide)-b-Poly(Propylene Oxide)-b-Poly(Ethylene Oxide) Copolymers in Water. *J. Colloid Interface Sci.* **1996**, *183*, 339–350.

(62) Zhang, K.; Lindman, B.; Coppola, L. Melting of Block Copolymer Self-Assemblies Induced by a Hydrophilic Surfactant. *Langmuir* **1995**, *11*, 538–542.

(63) Hecht, E.; Mortensen, K.; Gradzielski, M.; Hoffmann, H. Interaction of ABA Block Copolymers with Ionic Surfactants: Influence on Micellization and Gelation. *J. Phys. Chem.* **1995**, *99*, 4866–4874.

(64) Lad, K; Bahadur, A; Pandya, K; Bahadur, P. Clouding and Aggregation Behaviour of Ethylene Oxide/Propylene Oxide/Ethylene Oxide Block Copolymers in Aqueous Media in the Presence of Sodium Dodecyl Sulphate. *Indian J. Chem. A* **1995**, *34*, 938–945.

(65) Lad, K; Bahadur, A; Bahadur, P. Clouding Behaviour of an Ethylene Oxide-Propylene Oxide Block Copolymer. *Tenside Surf. Det.* **1997**, *34*, 37–42.

(66) Li, Y.; Xu, R.; Couderc, S.; Bloor, M.; Wyn-Jones, E.; Holzwarth, J. F. Binding of Sodium Dodecyl Sulfate (SDS) to the ABA Block Copolymer Pluronic F127 (EO 97 PO 69 EO 97): F127 Aggregation Induced by SDS. *Langmuir* **2001**, *17*, 183–188.

(67) Yasuda, S.; Townsend, D.; Michele, D. E.; Favre, E. G.; Day, S. M.; Metzger, J. M. Dystrophic Heart Failure Blocked by Membrane Sealant Poloxamer. *Nature* **2005**, *436*, 1025–1029.

(68) Houang, E. M.; Haman, K. J.; Filareto, A.; Perlingeiro, R. C.; Bates, F. S.; Lowe, D. A.; Metzger, J. M. Membrane-Stabilizing Copolymers Confer Marked Protection to Dystrophic Skeletal Muscle in Vivo. *Mol. Ther. Methods Clin. Dev.* **2015**, *2*, 15042.

(69) Bartos, J. A.; Matsuura, T. R.; Tsangaris, A.; Olson, M.; McKnite, S. H.; Rees, J. N.; Haman, K.; Shekar, K. C.; Riess, M. L.; Bates, F. S.; Metzger, J. M. Yannopoulos D. Intracoronary Poloxamer 188 Prevents Reperfusion Injury in a Porcine Model of ST-Segment Elevation Myocardial Infarction. *JACC Basic to Transl. Sci.* **2016**, *1*, 224–234.

(70) Lee, C. A. A.; Seo, H. S.; Armien, A. G.; Bates, F. S.; Tolar, J.; Azarin, S. M. Modeling and Rescue of Defective Blood–Brain Barrier Function of Induced Brain Microvascular Endothelial Cells from Childhood Cerebral Adrenoleukodystrophy Patients. *Fluids Barriers CNS* **2018**, *15*, 9.

(71) Bao, H.-J.; Wang, T.; Zhang, M.-Y.; Liu, R.; Dai, D.-K.; Wang, Y.-Q.; Wang, L.; Zhang, L.; Gao, Y.-Z.; Qin, Z.-H.; Chen, X.-P.; Tao, L.-Y. Poloxamer-188 Attenuates TBI-Induced Blood–Brain Barrier Damage Leading to Decreased Brain Edema and Reduced Cellular Death. *Neurochem. Res.* **2012**, *37*, 2856–2867.

(72) Gu, J.-H.; Ge, J.-B.; Li, M.; Xu, H.-D.; Wu, F.; Qin, Z.-H. Poloxamer 188 Protects Neurons against Ischemia/Reperfusion Injury through Preserving Integrity of Cell Membranes and Blood Brain Barrier. *PLoS One* **2013**, *8*, e61641.

(73) Wang, T.; Chen, X.; Wang, Z.; Zhang, M.; Meng, H.; Gao, Y.; Luo, B.; Tao, L.; Chen, Y. Poloxamer-188 Can Attenuate Blood–Brain Barrier Damage to Exert Neuroprotective Effect in Mice Intracerebral Hemorrhage Model. *J. Mol. Neurosci.* **2015**, *55*, 240–250.

(74) Venne, A.; Li, S.; Mandeville, R.; Kabanov, A.; Alakhov, V. Hypersensitizing Effect of Pluronic L61 on Cytotoxic Activity, Transport, and Subcellular Distribution of Doxorubicin in Multiple Drug-Resistant Cells. *Cancer Res.* **1996**, *56*, 3626–3629.

(75) Valle, J. W.; Lawrance, J.; Brewer, J.; Clayton, A.; Corrie, P.; Alakhov, V.; Ranson, M. A Phase II, Window Study of SP1049C as First-Line Therapy in Inoperable Metastatic Adenocarcinoma of the Oesophagus. *J. Clin. Oncol.* **2004**, *22*, 4195–4195.

(76) Batrakova, E. V.; Kabanov, A. V. Pluronic Block Copolymers: Evolution of Drug Delivery Concept from Inert Nanocarriers to Biological Response Modifiers. *J. Control. Release* **2008**, *130*, 98–106.

(77) Kabanov, A. V; Batrakova, E. V; Alakhov, V. Y. Pluronic® Block Copolymers as Novel Polymer Therapeutics for Drug and Gene Delivery. *J. Control. Release* **2002**, *82*, 189–212.

(78) Alakhov, V.; Klinski, E.; Li, S.; Pietrzynski, G.; Venne, A.; Batrakova, E.; Bronitch, T.; Kabanov, A. Block Copolymer-Based Formulation of Doxorubicin. From Cell Screen to Clinical Trials. *Colloids Surfaces B Biointerfaces* **1999**, *16*, 113–134.

(79) Pavlov, D. N.; Dorodnykh, T. Y.; Zaborova, O. V.; Melik-Nubarov, N. S. Interaction of Copolymers of Dimethylsiloxane and Ethylene Oxide with Model Membranes and Cancerous Cells. *Polym. Sci. Ser. A* **2009**, *51*, 295–301.

(80) Zhirnov, A. E.; Pavlov, D. N.; Demina, T. V.; Badun, G. A.; Grozdova, I. D.; Melik-Nubarov, N. S. Effect of the Structure of Ethylene Oxide-Propylene Oxide Block Copolymers on Their Interaction with Biological Membranes. *Polym. Sci. Ser. A* **2006**, *48*, 1202–1210.

(81) Townsend, D.; Yasuda, S.; Metzger, J. Cardiomyopathy of Duchenne Muscular Dystrophy: Pathogenesis and Prospect of Membrane Sealants as a New Therapeutic Approach. *Expert Rev. Cardiovasc. Ther.* **2007**, *5*, 99–109.

(82) Townsend, D.; Yasuda, S.; Chamberlain, J.; Metzger, J. M. Cardiac Consequences to Skeletal Muscle-Centric Therapeutics for Duchenne Muscular Dystrophy. *Trends Cardiovasc. Med.* **2009**, *19*, 49–54.

(83) Le, S.; Yu, M.; Hovan, L.; Zhao, Z.; Ervasti, J.; Yan, J. Dystrophin As a Molecular Shock Absorber. *ACS Nano* **2018**, *12*, 12140–12148.

(84) Petrof, B. J.; Shrager, J. B.; Stedman, H. H.; Kelly, A. M.; Sweeney, H. L. Dystrophin Protects the Sarcolemma from Stresses Developed during Muscle Contraction. *Proc. Natl. Acad. Sci.* **1993**, *90*, 3710–3714.

(85) Emery, A. E. H.; Muntoni, F.; Quinlivan, R. C. *Duchenne Muscular Dystrophy*, 4th ed.; Oxford University Press: Oxford, 2015.

(86) Sarkis, J.; Vié, V.; Winder, S. J.; Renault, A.; Le Rumeur, E.; Hubert, J.-F. Resisting Sarcolemmal Rupture: Dystrophin Repeats Increase Membrane-Actin Stiffness. *FASEB J.* **2013**, *27*, 359–367.

(87) Gissel, H. The Role of Ca2+ in Muscle Cell Damage. *Ann. N. Y. Acad. Sci.* **2006**, *1066*, 166–180.

(88) Townsend, D.; Yasuda, S.; Metzger, J. Cardiomyopathy of Duchenne Muscular Dystrophy: Pathogenesis and Prospect of Membrane Sealants as a New Therapeutic Approach. *Expert Rev. Cardiovasc. Ther.* **2007**, *5*, 99–109.

(89) Bushby, K.; Bourke, J.; Bullock, R.; Eagle, M.; Gibson, M.; Quinby, J. The Multidisciplinary Management of Duchenne Muscular Dystrophy. *Curr. Paediatr.* **2005**, *15*, 292–300.

(90) Eagle, M.; Bourke, J.; Bullock, R.; Gibson, M.; Mehta, J.; Giddings, D.; Straub, V.; Bushby, K. Managing Duchenne Muscular Dystrophy–the Additive Effect of Spinal Surgery and Home Nocturnal Ventilation in Improving Survival. *Neuromuscul. Disord.* **2007**, *17*, 470–475.

(91) Goyenvalle, A.; Seto, J. T.; Davies, K. E.; Chamberlain, J. Therapeutic

Approaches to Muscular Dystrophy. *Hum. Mol. Genet.* **2011**, *20*, R69–R78.

(92) Hoffman, E. P.; McNally, E. M. Exon-Skipping Therapy for Muscular Dystrophy: A Roadblock, Detour, or Bump in the Road? *Sci Transl Med* **2014**, *6*, 230fs14.

(93) Lu, Q.; Cirak, S.; Partridge, T. What Can We Learn from Clinical Trials of Exon Skipping for DMD? *Mol. Ther. Nucleic Acids* **2014**, *3*, e152.

(94) McNally, E. M. New Approaches in the Therapy of Cardiomyopathy in Muscular Dystrophy. *Annu. Rev. Med.* **2007**, *58*, 75–88.

(95) Avioli, L. V. Glucocorticoid Effects on Statural Growth. *Rheumatology* **1993**, *32*, 27–30.

(96) Manzur, A. Y.; Kuntzer, T.; Pike, M.; Swan, A. V. Glucocorticoid Corticosteroids for Duchenne Muscular Dystrophy. *Cochrane Libr.* **2004**, No. 2.

(97) Wolthers, O. D.; Pedersen, S. Short Term Linear Growth in Asthmatic Children during Treatment with Prednisolone. *BMJ Br. Med. J.* **1990**, *301*, 145.

(98) Muntoni, F. Cardiomyopathy in Muscular Dystrophies. *Curr. Opin. Neurol.* **2003**, *16*, 577–583.

(99) Houang, E. M. Copolymer-Based Membrane Stabilizers for Duchenne Muscular Dystrophy, PhD Thesis, University of Minnesota, 2016.

(100) Kim, M.; Haman, K. J.; Houang, E. M.; Zhang, W.; Yannopoulos, D.; Metzger, J. M.; Bates, F. S.; Hackel, B. J. PEO–PPO Diblock Copolymers Protect Myoblasts from Hypo-Osmotic Stress In Vitro Dependent on Copolymer Size, Composition, and Architecture. *Biomacromolecules* **2017**, *18*, 2090–2101.

(101) Houang, E. M.; Haman, K. J.; Kim, M.; Zhang, W.; Lowe, D. A.; Sham, Y. Y.; Lodge, T. P.; Hackel, B. J.; Bates, F. S.; Metzger, J. M. Chemical End Group Modified Diblock Copolymers Elucidate Anchor and Chain Mechanism of Membrane Stabilization. *Mol. Pharm.* **2017**, *14*, 2333–2339.

(102) Firestone, M. A.; Seifert, S. Interaction of Nonionic PEO−PPO Diblock Copolymers with Lipid Bilayers. *Biomacromolecules* **2005**, *6*, 2678–2687.

(103) Leiske, D. L.; Meckes, B.; Miller, C. E.; Wu, C.; Walker, T. W.; Lin, B.; Meron, M.; Ketelson, H. A.; Toney, M. F.; Fuller, G. G. Insertion Mechanism of a Poly (Ethylene Oxide)-Poly (Butylene Oxide) Block Copolymer into a DPPC Monolayer. *Langmuir* **2011**, *27*, 11444–11450.

(104) Frey, S. L.; Zhang, D.; Carignano, M. A.; Szleifer, I.; Lee, K. Y. C. Effects of Block Copolymer's Architecture on Its Association with Lipid Membranes: Experiments and Simulations. *J. Chem. Phys.* **2007**, *127*, 114904.

(105) Maskarinec, S. A.; Wu, G.; Lee, K. Y. C. Membrane Sealing by Polymers. *Ann. N. Y. Acad. Sci.* **2006**, *1066*, 310–320.

(106) Cheng, C.-Y.; Wang, J.-Y.; Kausik, R.; Lee, K. Y. C.; Han, S. Nature of Interactions between PEO-PPO-PEO Triblock Copolymers and Lipid Membranes: (II) Role of Hydration Dynamics Revealed by Dynamic Nuclear Polarization. *Biomacromolecules* **2012**, *13*, 2624–2633.

(107) Wang, J.-Y.; Marks, J.; Lee, K. Y. C. Nature of Interactions between PEO-PPO-PEO Triblock Copolymers and Lipid Membranes: (I) Effect of Polymer Hydrophobicity on Its Ability to Protect Liposomes from Peroxidation.

Biomacromolecules **2012**, *13*, 2616–2623.

(108) Wang, J.; Segatori, L.; Biswal, S. L. Probing the Association of Triblock Copolymers with Supported Lipid Membranes Using Microcantilevers. *Soft Matter* **2014**, *10*, 6417.

(109) Lee, R. C.; Hannig, J.; Matthews, K. L.; Myerov, A.; Chen, C.-T. Pharmaceutical Therapies for Sealing of Permeabilized Cell Membranes in Electrical Injuries. *Ann. N. Y. Acad. Sci.* **1999**, *888*, 266–273.

(110) Agarwal, J.; Walsh, A.; Lee, R. C. Multimodal Strategies for Resuscitating Injured Cells. *Ann. N. Y. Acad. Sci.* **2006**, *1066*, 295–309.

(111) Rubinsky, B.; Arav, A.; Devries, A. L. The Cryoprotective Effect of Antifreeze Glycopeptides from Antarctic Fishes. *Cryobiology* **1992**, *29*, 69–79.

(112) Palmer, J. S.; Cromie, W. J.; Lee, R. C. Surfactant Administration Reduces Testicular Ischemia-Reperfusion Injury. *J. Urol.* **1998**, *159*, 2136–2139.

(113) McNeil, P. L.; Steinhardt, R. A. Loss, Restoration, and Maintenance of Plasma Membrane Integrity. *J. Cell Biol.* **1997**, *137*, 1–4.

(114) Fischer, T. A.; McNeil, P. L.; Khakee, R.; Finn, P.; Kelly, R. A.; Pfeffer, M. A.; Pfeffer, J. M. Cardiac Myocyte Membrane Wounding in the Abruptly Pressure-Overloaded Rat Heart under High Wall Stress. *Hypertension* **1997**, *30*, 1041–1046.

(115) Gaylor, D. C.; Prakah-Asante, K.; Lee, R. C. Significance of Cell Size and Tissue Structure in Electrical Trauma. *J. Theor. Biol.* **1988**, *133*, 223–237.

(116) Tsong, T. Y.; Su, Z. Biological Effects of Electric Shock and Heat Denaturation

and Oxidation of Molecules, Membranes, and Cellular Functions. *Ann. N. Y. Acad. Sci.* **1999**, *888*, 211–232.

(117) McNeil, P. L.; Vogel, S. S.; Miyake, K.; Terasaki, M. Patching Plasma Membrane Disruptions with Cytoplasmic Membrane. *J. Cell Sci.* **2000**, *113*, 1891–1902.

(118) Anno, G. H.; Young, R. W.; Bloom, R. M.; Mercier, J. R. Dose Response Relationships for Acute Ionizing-Radiation Lethality. *Health Phys.* **2003**, *84*, 565–575.

(119) Shi, R.; Borgens, R. B.; Blight, A. R. Functional Reconnection of Severed Mammalian Spinal Cord Axons with Polyethylene Glycol. *J. Neurotrauma* **1999**, *16*, 727–738.

(120) Togo, T.; Krasieva, T. B.; Steinhardt, R. A. A Decrease in Membrane Tension Precedes Successful Cell-Membrane Repair. *Mol. Biol. Cell* **2000**, *11*, 4339–4346.

(121) McNeil, P. L.; Steinhardt, R. A. Plasma Membrane Disruption: Repair, Prevention, Adaptation. *Annu. Rev. Cell Dev. Biol.* **2003**, *19*, 697–731.

(122) Brockman, H. Lipid Monolayers: Why Use Half a Membrane to Characterize Protein-Membrane Interactions? *Curr. Opin. Struct. Biol.* **1999**, *9*, 438–443.

(123) Maskarinec, S. A.; Hannig, J.; Lee, R. C.; Lee, K. Y. C. Direct Observation of Poloxamer 188 Insertion into Lipid Monolayers. *Biophys. J.* **2002**, *82*, 1453–1459.

(124) Maskarinec, S. A.; Lee, K. Y. C. Comparative Study of Poloxamer Insertion into Lipid Monolayers. *Langmuir* **2003**, *19*, 1809–1815.

(125) Frey, S. L.; Lee, K. Y. C. Temperature Dependence of Poloxamer Insertion Into

and Squeeze-Out from Lipid Monolayers. *Langmuir* **2007**, *23*, 2631–2637.

(126) Hädicke, A.; Blume, A. Interactions of Pluronic Block Copolymers with Lipid Vesicles Depend on Lipid Phase and Pluronic Aggregation State. *Colloid Polym. Sci.* **2015**, *293*, 267–276.

(127) Sandez-Macho, I.; Casas, M.; Lage, E. V.; Rial-Hermida, M. I.; Concheiro, A.; Alvarez-Lorenzo, C. Interaction of Poloxamine Block Copolymers with Lipid Membranes: Role of Copolymer Structure and Membrane Cholesterol Content. *Colloids Surfaces B Biointerfaces* **2015**, *133*, 270–277.

(128) Chang, L.-C.; Chang, Y.-Y.; Gau, C.-S. Interfacial Properties of Pluronics and the Interactions between Pluronics and Cholesterol/DPPC Mixed Monolayers. *J. Colloid Interface Sci.* **2008**, *322*, 263–273.

(129) Wu, G.; Majewski, J.; Ege, C.; Kjaer, K.; Weygand, M. J.; Lee, K. Y. C. Lipid Corralling and Poloxamer Squeeze-Out in Membranes. *Phys. Rev. Lett.* **2004**, *93*, 028101.

(130) Ziblat, R.; Leiserowitz, L.; Addadi, L. Crystalline Domain Structure and Cholesterol Crystal Nucleation in Single Hydrated DPPC:Cholesterol:POPC Bilayers. *J. Am. Chem. Soc.* **2010**, *132*, 9920–9927.

(131) Wu, G.; Majewski, J.; Ege, C.; Kjaer, K.; Weygand, M. J.; Lee, K. Y. C. Interaction between Lipid Monolayers and Poloxamer 188: An X-Ray Reflectivity and Diffraction Study. *Biophys. J.* **2005**, *89*, 3159–3173.

(132) Ratajczak, M. K.; Chi, E. Y.; Frey, S. L.; Cao, K. D.; Luther, L. M.; Lee, K. Y. C.;

Majewski, J.; Kjaer, K. Ordered Nanoclusters in Lipid-Cholesterol Membranes. *Phys. Rev. Lett.* **2009**, *103*, 028103.

(133) Espinosa, G.; Lopez-Montero, I.; Monroy, F.; Langevin, D. Shear Rheology of Lipid Monolayers and Insights on Membrane Fluidity. *Proc. Natl. Acad. Sci.* **2011**, *108*, 6008–6013.

(134) Langevin, D. Rheology of Adsorbed Surfactant Monolayers at Fluid Surfaces. *Annu. Rev. Fluid Mech.* **2014**, *46*, 47–65.

(135) Alvares, D. S.; dos Santos Cabrera, M. P.; Ruggiero Neto, J. Strategies for Exploring Electrostatic and Nonelectrostatic Contributions to the Interaction of Helical Antimicrobial Peptides with Model Membranes. In *Advances in Biomembranes and Lipid Self-Assembly*; 2016; pp 43–73.

(136) Risselada, H. J.; Marrink, S. J. Curvature Effects on Lipid Packing and Dynamics in Liposomes Revealed by Coarse Grained Molecular Dynamics Simulations. *Phys. Chem. Chem. Phys.* **2009**, *11*, 2056.

(137) Middleton, E. R.; Rhoades, E. Effects of Curvature and Composition on α-Synuclein Binding to Lipid Vesicles. *Biophys. J.* **2010**, *99*, 2279–2288.

(138) Ladokhin, A. S.; Jayasinghe, S.; White, S. H. How to Measure and Analyze Tryptophan Fluorescence in Membranes Properly, and Why Bother? *Anal. Biochem.* **2000**, *285*, 235–245.

(139) Zhao, H.; Mattila, J.-P.; Holopainen, J. M.; Kinnunen, P. K. J. Comparison of the Membrane Association of Two Antimicrobial Peptides, Magainin 2 and

Indolicidin. *Biophys. J.* **2001**, *81*, 2979–2991.

(140) Matos, P. M.; Franquelim, H. G.; Castanho, M. A. R. B.; Santos, N. C. Quantitative Assessment of Peptide–Lipid Interactions. *Biochim. Biophys. Acta - Biomembr.* **2010**, *1798*, 1999–2012.

(141) Leite, N. B.; dos Santos Alvares, D.; de Souza, B. M.; Palma, M. S.; Ruggiero Neto, J. Effect of the Aspartic Acid D2 on the Affinity of Polybia-MP1 to Anionic Lipid Vesicles. *Eur. Biophys. J.* **2014**.

(142) Klocek, G.; Schulthess, T.; Shai, Y.; Seelig, J. Thermodynamics of Melittin Binding to Lipid Bilayers. Aggregation and Pore Formation. *Biochemistry* **2009**, *48*, 2586–2596.

(143) Fernández-Vidal, M.; White, S. H.; Ladokhin, A. S. Membrane Partitioning: "Classical" and "Nonclassical" Hydrophobic Effects. *J. Membr. Biol.* **2011**, *239*, 5–14.

(144) Freire, J. M.; Domingues, M. M.; Matos, J.; Melo, M. N.; Veiga, A. S.; Santos, N. C.; Castanho, M. A. R. B. Using Zeta-Potential Measurements to Quantify Peptide Partition to Lipid Membranes. *Eur. Biophys. J.* **2011**, *40*, 481–487.

(145) Seelig, J. Thermodynamics of Lipid–Peptide Interactions. *Biochim. Biophys. Acta - Biomembr.* **2004**, *1666*, 40–50.

(146) Wu, G.; Khant, H. A.; Chiu, W.; Lee, K. Y. C. Effects of Bilayer Phases on Phospholipid-Poloxamer Interactions. *Soft Matter* **2009**, *5*, 1496.

(147) Wu, G.; Lee, K. Y. C. Interaction of Poloxamers with Liposomes: An Isothermal

Titration Calorimetry Study. *J. Phys. Chem. B* **2009**, *113*, 15522–15531.

(148) Svetlovics, J. A.; Wheaten, S. A.; Almeida, P. F. Phase Separation and Fluctuations in Mixtures of a Saturated and an Unsaturated Phospholipid. *Biophys. J.* **2012**, *102*, 2526–2535.

(149) Zhao, J.; Wu, J.; Shao, H.; Kong, F.; Jain, N.; Hunt, G.; Feigenson, G. Phase Studies of Model Biomembranes: Macroscopic Coexistence of Lα+Lβ, with Light-Induced Coexistence of Lα+Lo Phases. *Biochim. Biophys. Acta - Biomembr.* **2007**, *1768*, 2777–2786.

(150) Haluska, C. K.; Baptista, M. S.; Fernandes, A. U.; Schroder, A. P.; Marques, C. M.; Itri, R. Photo-Activated Phase Separation in Giant Vesicles Made from Different Lipid Mixtures. *Biochim. Biophys. Acta - Biomembr.* **2012**, *1818*, 666–672.

(151) Veatch, S. L.; Keller, S. L. Seeing Spots: Complex Phase Behavior in Simple Membranes. *Biochim. Biophys. Acta - Mol. Cell Res.* **2005**, *1746*, 172–185.

(152) Veatch, S. L.; Keller, S. L. Miscibility Phase Diagrams of Giant Vesicles Containing Sphingomyelin. *Phys. Rev. Lett.* **2005**, *94*, 148101.

(153) Veatch, S. L.; Gawrisch, K.; Keller, S. L. Closed-Loop Miscibility Gap and Quantitative Tie-Lines in Ternary Membranes Containing Diphytanoyl PC. *Biophys. J.* **2006**, *90*, 4428–4436.

(154) Veatch, S. L.; Keller, S. L. Separation of Liquid Phases in Giant Vesicles of Ternary Mixtures of Phospholipids and Cholesterol. *Biophys. J.* **2003**, *85*, 3074–

3083.

(155) Dua, J.S.; Rana, A.C.; Bhandari, A. K. Liposome: Methods of Preparation and Applications. *Int. J. Pharm. Stud. Res.* **2012**, *3*, 14–20.

(156) Olson, F.; Hunt, C. A. A.; Szoka, F. C. C.; Vail, W. J. J.; Papahadjopoulos, D. Preparation of Liposomes of Defined Size Distribution by Extrusion through Polycarbonate Membranes. *Biochim. Biophys. Acta - Biomembr.* **1979**, *557*, 9–23.

(157) Hope, M. J.; Bally, M. B.; Webb, G.; Cullis, P. R. Production of Large Unilamellar Vesicles by a Rapid Extrusion Procedure. Characterization of Size Distribution, Trapped Volume and Ability to Maintain a Membrane Potential. *Biochim. Biophys. Acta - Biomembr.* **1985**, *812*, 55–65.

(158) Huang, C.-H. Phosphatidylcholine Vesicles. Formation and Physical Characteristics. *Biochemistry* **1969**, *8*, 344–352.

(159) Mayer, L. D.; Hope, M. J.; Cullis, P. R.; Janoff, A. S. Solute Distributions and Trapping Efficiencies Observed in Freeze-Thawed Multilamellar Vesicles. *Biochim. Biophys. Acta - Biomembr.* **1985**, *817*, 193–196.

(160) Mayer, L. D.; Hope, M. J.; Cullis, P. R. Vesicles of Variable Sizes Produced by a Rapid Extrusion Procedure. *Biochim. Biophys. Acta - Biomembr.* **1986**, *858*, 161–168.

(161) Ong, S.; Chitneni, M.; Lee, K.; Ming, L.; Yuen, K. Evaluation of Extrusion Technique for Nanosizing Liposomes. *Pharmaceutics* **2016**, *8*, 36.

(162) Hope, M. J.; Bally, M. B.; Mayer, L. D.; Janoff, A. S.; Cullis, P. R. Generation of

Multilamellar and Unilamellar Phospholipid Vesicles. *Chem. Phys. Lipids* **1986**, *40*, 89–107.

(163) Parente, R. A.; Lentz, B. R. Phase Behavior of Large Unilamellar Vesicles Composed of Synthetic Phospholipids. *Biochemistry* **1984**, *23*, 2353–2362.

(164) Pick, U. Liposomes with a Large Trapping Capacity Prepared by Freezing and Thawing of Sonicated Phospholipid Mixtures. *Arch. Biochem. Biophys.* **1981**, *212*, 186–194.

(165) Takechi-Haraya, Y.; Sakai-Kato, K.; Abe, Y.; Kawanishi, T.; Okuda, H.; Goda, Y. Atomic Force Microscopic Analysis of the Effect of Lipid Composition on Liposome Membrane Rigidity. *Langmuir* **2016**, *32*, 6074–6082.

(166) Arriaga, L. R.; López-Montero, I.; Monroy, F.; Orts-Gil, G.; Farago, B.; Hellweg, T. Stiffening Effect of Cholesterol on Disordered Lipid Phases: A Combined Neutron Spin Echo + Dynamic Light Scattering Analysis of the Bending Elasticity of Large Unilamellar Vesicles. *Biophys. J.* **2009**, *96*, 3629–3637.

(167) Arriaga, L. R.; López-Montero, I.; Orts-Gil, G.; Farago, B.; Hellweg, T.; Monroy, F. Fluctuation Dynamics of Spherical Vesicles: Frustration of Regular Bulk Dissipation into Subdiffusive Relaxation. *Phys. Rev. E* **2009**, *80*, 031908.

(168) Zhirnov, A. E.; Demina, T. V.; Krylova, O. O.; Grozdova, I. D.; Melik-Nubarov, N. S. Lipid Composition Determines Interaction of Liposome Membranes with Pluronic L61. *Biochim. Biophys. Acta - Biomembr.* **2005**, *1720*, 73–83.

(169) Krylova, O. O.; Pohl, P. Ionophoric Activity of Pluronic Block Copolymers.

Biochemistry **2004**, *43*, 3696–3703.

(170) Krylova, O. O.; Melik-Nubarov, N. S.; Badun, G. A.; Ksenofontov, A. L.; Menger, F. M.; Yaroslavov, A. A. Pluronic L61 Accelerates Flip–Flop and Transbilayer Doxorubicin Permeation. *Chem. - A Eur. J.* **2003**, *9*, 3930–3936.

(171) Strömstedt, A. A.; Wessman, P.; Ringstad, L.; Edwards, K.; Malmsten, M. Effect of Lipid Headgroup Composition on the Interaction between Melittin and Lipid Bilayers. *J. Colloid Interface Sci.* **2007**, *311*, 59–69.

(172) Reeves, J. P.; Dowben, R. M. Formation and Properties of Thin-Walled Phospholipid Vesicles. *J. Cell. Physiol.* **1969**, *73*, 49–60.

(173) Akashi, K.; Miyata, H.; Itoh, H.; Kinosita, K. Preparation of Giant Liposomes in Physiological Conditions and Their Characterization under an Optical Microscope. *Biophys. J.* **1996**, *71*, 3242–3250.

(174) Tanaka, T.; Tamba, Y.; Masum, S. M.; Yamashita, Y.; Yamazaki, M. La^{3+} and Gd^{3+} Induce Shape Change of Giant Unilamellar Vesicles of Phosphatidylcholine. *Biochim. Biophys. Acta - Biomembr.* **2002**, *1564*, 173–182.

(175) Angelova, M. I.; Dimitrov, D. S. Liposome Electroformation. *Faraday Discuss. Chem. Soc.* **1986**, *81*, 303.

(176) Riske, K. A.; Dimova, R. Electro-Deformation and Poration of Giant Vesicles Viewed with High Temporal Resolution. *Biophys. J.* **2005**, *88*, 1143–1155.

(177) Li, W.; Wang, Q.; Yang, Z.; Wang, W.; Cao, Y.; Hu, N.; Luo, H.; Liao, Y.; Yang, J. Impacts of Electrical Parameters on the Electroformation of Giant Vesicles on

ITO Glass Chips. *Colloids Surfaces B Biointerfaces* **2016**, *140*, 560–566.

(178) Menger, F. M.; Angelova, M. I. Giant Vesicles: Imitating the Cytological Processes of Cell Membranes. *Acc. Chem. Res.* **1998**, *31*, 789–797.

(179) Wang, J.-Y.; Chin, J.; Marks, J. D.; Lee, K. Y. C. Effects of PEO−PPO−PEO Triblock Copolymers on Phospholipid Membrane Integrity under Osmotic Stress. *Langmuir* **2010**, *26*, 12953–12961.

(180) Tharad, S.; Promdonkoy, B.; Toca-Herrera, J. L. Lipid Phase Influences the Binding of Bacillus Thuringiensis Cyt2Aa2 Toxin on Model Lipid Membranes. *Biochem. Biophys. Res. Commun.* **2019**, *511*, 409–415.

(181) Åkesson, A.; Lind, T.; Ehrlich, N.; Stamou, D.; Wacklin, H.; Cárdenas, M. Composition and Structure of Mixed Phospholipid Supported Bilayers Formed by POPC and DPPC. *Soft Matter* **2012**, *8*, 5658.

(182) Kim, M.; Vala, M.; Ertsgaard, C. T.; Oh, S.-H.; Lodge, T. P.; Bates, F. S.; Hackel, B. J. Surface Plasmon Resonance Study of the Binding of PEO–PPO–PEO Triblock Copolymer and PEO Homopolymer to Supported Lipid Bilayers. *Langmuir* **2018**, *34*, 6703–6712.

(183) Hayden, S. C.; Junghans, A.; Majewski, J.; Firestone, M. A. Reversible Lifting of Surface Supported Lipid Bilayers with a Membrane-Spanning Nonionic Triblock Copolymer. *Biomacromolecules* **2017**, *18*, 1097–1107.

(184) Rahimi, M.; Regan, D.; Arroyo, M.; Subramaniam, A. B.; Stone, H. A.; Staykova, M. Shape Transformations of Lipid Bilayers Following Rapid Cholesterol Uptake.

Biophys. J. **2016**, *111*, 2651–2657.

(185) Tristram-Nagle, S.; Zhang, R.; Suter, R. M.; Worthington, C. R.; Sun, W. J.; Nagle, J. F. Measurement of Chain Tilt Angle in Fully Hydrated Bilayers of Gel Phase Lecithins. *Biophys. J.* **1993**, *64*, 1097–1109.

(186) Ahmed, S.; Nikolov, Z.; Wunder, S. L. Effect of Curvature on Nanoparticle Supported Lipid Bilayers Investigated by Raman Spectroscopy. *J. Phys. Chem. B* **2011**, *115*, 13181–13190.

(187) Beltramo, P. J.; Van Hooghten, R.; Vermant, J. Millimeter-Area, Free Standing, Phospholipid Bilayers. *Soft Matter* **2016**, *12*, 4324–4331.

(188) Adhikari, U.; Goliaei, A.; Tsereteli, L.; Berkowitz, M. L. Properties of Poloxamer Molecules and Poloxamer Micelles Dissolved in Water and Next to Lipid Bilayers: Results from Computer Simulations. *J. Phys. Chem. B* **2016**, *120*, 5823–5830.

(189) Goliaei, A.; Lau, E. Y.; Adhikari, U.; Schwegler, E.; Berkowitz, M. L. Behavior of P85 and P188 Poloxamer Molecules: Computer Simulations Using United-Atom Force-Field. *J. Phys. Chem. B* **2016**, *120*, 8631–8641.

(190) Wu, G.; Lee, K. Y. C. Effects of Poloxamer 188 on Phospholipid Monolayer Morphology: An Atomic Force Microscopy Study. *Langmuir* **2009**, *25*, 2133–2139.

(191) Amado, E.; Kerth, A.; Blume, A.; Kressler, J. Infrared Reflection Absorption Spectroscopy Coupled with Brewster Angle Microscopy for Studying Interactions of Amphiphilic Triblock Copolymers with Phospholipid Monolayers. *Langmuir*

2008, *24*, 10041–10053.

(192) Amado, E.; Kerth, A.; Blume, A.; Kressler, J. Phospholipid Crystalline Clusters Induced by Adsorption of Novel Amphiphilic Triblock Copolymers to Monolayers. *Soft Matter* **2009**, *5*, 669–675.

(193) Kostarelos, K.; Luckham, P. F.; Tadros, T. F. Steric Stabilization of Phospholipid Vesicles by Block Copolymers Vesicle Flocculation and Osmotic Swelling Caused by Monovalent and Divalent Cations. *J. Chem. Soc. Faraday Trans.* **1998**, *94*, 2159–2168.

(194) Kostarelos, K.; Tadros, T. F.; Luckham, P. F. Physical Conjugation of (Tri-) Block Copolymers to Liposomes toward the Construction of Sterically Stabilized Vesicle Systems. *Langmuir* **1999**, *15*, 369–376.

(195) Kostarelos, K.; Kipps, M.; Tadros, T. F.; Luckham, P. F. Molecular Structure and Conformation in Phospholipid Vesicles Sterically Stabilized by (Tri)-Block Copolymers Investigated by Multi-Nuclear Magnetic Resonance Techniques. *Colloids Surfaces A Physicochem. Eng. Asp.* **1998**, *136*, 1–9.

(196) Kostarelos, K.; Luckham, P. F.; Tadros, T. F. Addition of (Tri-)Block Copolymers to Phospholipid Vesicles: A Study of the Molecular Morphology and Structure by Using Hydrophobic Dye Molecules as Bilayer Probes. *J. Colloid Interface Sci.* **1997**, *191*, 341–348.

(197) Kostarelos, K.; Luckham, P. F.; Tadros, T. F. Addition of Block Copolymers to Liposomes Prepared Using Soybean Lecithin. Effects on Formation, Stability and the Specific Localization of the Incorporated Surfactants Investigated. *J. Liposome*

Res. **1995**, *5*, 117–130.

(198) Johnsson, M.; Bergstrand, N.; Edwards, K.; Stålgren, J. J. R. Adsorption of a PEO−PPO−PEO Triblock Copolymer on Small Unilamellar Vesicles: Equilibrium and Kinetic Properties and Correlation with Membrane Permeability. *Langmuir* **2001**, *17*, 3902–3911.

(199) Ileri Ercan, N.; Stroeve, P.; Tringe, J. W.; Faller, R. Understanding the Interaction of Pluronics L61 and L64 with a DOPC Lipid Bilayer: An Atomistic Molecular Dynamics Study. *Langmuir* **2016**, *32*, 10026–10033.

(200) Wood, I.; Martini, M. F.; Albano, J. M. R.; Cuestas, M. L.; Mathet, V. L.; Pickholz, M. Coarse Grained Study of Pluronic F127: Comparison with Shorter Co-Polymers in Its Interaction with Lipid Bilayers and Self-Aggregation in Water. *J. Mol. Struct.* **2016**, *1109*, 106–113.

(201) Firestone, M. A.; Wolf, A. C.; Seifert, S. Small-Angle X-Ray Scattering Study of the Interaction of Poly (Ethylene Oxide)-b-Poly (Propylene Oxide)-b-Poly (Ethylene Oxide) Triblock Copolymers with Lipid Bilayers. *Biomacromolecules* **2003**, *4*, 1539–1549.

(202) Lee, B.; Firestone, M. A. Electron Density Mapping of Triblock Copolymers Associated with Model Biomembranes: Insights into Conformational States and Effect on Bilayer Structure. *Biomacromolecules* **2008**, *9*, 1541–1550.

(203) Hezaveh, S.; Samanta, S.; De Nicola, A.; Milano, G.; Roccatano, D. Understanding the Interaction of Block Copolymers with DMPC Lipid Bilayer Using Coarse-Grained Molecular Dynamics Simulations. *J. Phys. Chem. B* **2012**,

116, 14333–14345.

(204) Samanta, S.; Hezaveh, S.; Roccatano, D. Theoretical Study of Binding and Permeation of Ether-Based Polymers through Interfaces. *J. Phys. Chem. B* **2013**, *117*, 14723–14731.

(205) Rabbel, H.; Werner, M.; Sommer, J.-U. Interactions of Amphiphilic Triblock Copolymers with Lipid Membranes: Modes of Interaction and Effect on Permeability Examined by Generic Monte Carlo Simulations. *Macromolecules* **2015**, *48*, 4724–4732.

(206) Liang, X.; Mao, G.; Ng, K. Y. S. Effect of Chain Lengths of PEO–PPO–PEO on Small Unilamellar Liposome Morphology and Stability: An AFM Investigation. *J. Colloid Interface Sci.* **2005**, *285*, 360–372.

(207) Johnsson, M.; Silvander, M.; Karlsson, G.; Edwards, K. Effect of PEO−PPO−PEO Triblock Copolymers on Structure and Stability of Phosphatidylcholine Liposomes. *Langmuir* **1999**, *15*, 6314–6325.

(208) Nawaz, S.; Redhead, M.; Mantovani, G.; Alexander, C.; Bosquillon, C.; Carbone, P. Interactions of PEO–PPO–PEO Block Copolymers with Lipid Membranes: A Computational and Experimental Study Linking Membrane Lysis with Polymer Structure. *Soft Matter* **2012**, *8*, 6744.

(209) Erukova, V. Y.; Krylova, O. O.; Antonenko, Y. N.; Melik-Nubarov, N. S. Effect of Ethylene Oxide and Propylene Oxide Block Copolymers on the Permeability of Bilayer Lipid Membranes to Small Solutes Including Doxorubicin. *Biochim. Biophys. Acta - Biomembr.* **2000**, *1468*, 73–86.

(210) Demina, T.; Grozdova, I.; Krylova, O.; Zhirnov, A.; Istratov, V.; Frey, H.; Kautz, H.; Melik-Nubarov, N. Relationship between the Structure of Amphiphilic Copolymers and Their Ability To Disturb Lipid Bilayers. *Biochemistry* **2005**, *44*, 4042–4054.

(211) Yaroslavov, A. A.; Melik-Nubarov, N. S.; Menger, F. M. Polymer-Induced Flip-Flop in Biomembranes. *Acc. Chem. Res.* **2006**, *39*, 702–710.

(212) Zaki, A. M.; Carbone, P. How the Incorporation of Pluronic Block Copolymers Modulates the Response of Lipid Membranes to Mechanical Stress. *Langmuir* **2017**, *33*, 13284–13294.

(213) Castile, J. D.; Taylor, K. M. G.; Buckton, G. The Influence of Incubation Temperature and Surfactant Concentration on the Interaction between Dimyristoylphosphatidylcholine Liposomes and Poloxamer Surfactants. *Int. J. Pharm.* **2001**, *221*, 197–209.

(214) Chieng, Y. Y.; Chen, S. B. Interaction and Complexation of Phospholipid Vesicles and Triblock Copolymers. *J. Phys. Chem. B* **2009**, *113*, 14934–14942.

(215) Redhead, M.; Mantovani, G.; Nawaz, S.; Carbone, P.; Gorecki, D. C.; Alexander, C.; Bosquillon, C. Relationship between the Affinity of PEO-PPO-PEO Block Copolymers for Biological Membranes and Their Cellular Effects. *Pharm. Res.* **2012**, *29*, 1908–1918.

(216) Pal, S.; Milano, G.; Roccatano, D. Synthetic Polymers and Biomembranes. How Do They Interact?: Atomistic Molecular Dynamics Simulation Study of PEO in Contact with a DMPC Lipid Bilayer. *J. Phys. Chem. B* **2006**, *110*, 26170–26179.

(217) Grozdova, I. D.; Badun, G. A.; Chernysheva, M. G.; Orlov, V. N.; Romanyuk, A. V.; Melik-Nubarov, N. S. Increase in the Length of Poly(Ethylene Oxide) Blocks in Amphiphilic Copolymers Facilitates Their Cellular Uptake. *J. Appl. Polym. Sci.* **2017**, *134*, 45492.

(218) Ding, J.; Price, C.; Booth, C. Use of Crown Ether in the Anionic Polymerization of Propylene Oxide—1. Rate of Polymerization. *Eur. Polym. J.* **1991**, *27*, 891–894.

(219) Ndoni, S.; Papadakis, C. M.; Bates, F. S.; Almdal, K. Laboratory-scale Setup for Anionic Polymerization under Inert Atmosphere. *Rev. Sci. Instrum.* **1995**, *66*, 1090–1095.

(220) Hillmyer, M. A.; Bates, F. S. Synthesis and Characterization of Model Polyalkane−Poly(Ethylene Oxide) Block Copolymers. *Macromolecules* **1996**, *29*, 6994–7002.

(221) Allgaier, J.; Willbold, S.; Chang, T. Synthesis of Hydrophobic Poly (Alkylene Oxide)s and Amphiphilic Poly (Alkylene Oxide) Block Copolymers. *Macromolecules* **2007**, *40*, 518–525.

(222) Ding, J.; Heatley, F.; Price, C.; Booth, C. Use of Crown Ether in the Anionic Polymerization of Propylene Oxide—2. Molecular Weight and Molecular Weight Distribution. *Eur. Polym. J.* **1991**, *27*, 895–899.

(223) Ding, J.; Attwood, D.; Price, C.; Booth, C. Use of Crown Ether in the Anionic Polymerization of Propylene Oxide—3. Preparation and Micellization of Diblock-Copoly(Oxypropylene/Oxyethylene). *Eur. Polym. J.* **1991**, *27*, 901–905.

(224) Van Krevelen, D. W.; Te Nijenhuis, K. *Properties of Polymers: Their Correlation with Chemical Structure; Their Numerical Estimation and Prediction from Additive Group Contributions*, 4th ed.; Elsevier, 2009.

(225) Brandrup, J.; Immergut, E. H.; Grulke, E. A. *Polymer Handbook*, 4th ed.; Wiley, Ed.; 1999.

(226) MacDonald, R. C.; MacDonald, R. I.; Menco, B. P. M.; Takeshita, K.; Subbarao, N. K.; Hu, L. R. Small-Volume Extrusion Apparatus for Preparation of Large, Unilamellar Vesicles. *Biochim. Biophys. Acta* **1991**, *1061*, 297–303.

(227) Wu, D. H.; Chen, A. D.; Johnson, C. S. An Improved Diffusion-Ordered Spectroscopy Experiment Incorporating Bipolar-Gradient Pulses. *J. Magn. Reson. Ser. A.* **1995**, *115*, 260–264.

(228) Momot, K. I.; Kuchel, P. W. Pulsed Field Gradient Nuclear Magnetic Resonance as a Tool for Studying Drug Delivery Systems. *Concepts Magn. Reson.* **2003**, *19A*, 51–64.

(229) Ross, R. The Pathogenesis of Atherosclerosis: A Perspective for the 1990s. *Nature* **1993**, *362*, 801–809.

(230) Halliwell, B. Free Radicals, Reactive Oxygen Species and Human Disease: A Critical Evaluation with Special Reference to Atherosclerosis. *Br. J. Exp. Pathol.* **1989**, *70*, 737.

(231) Girotti, A. W. Photodynamic Lipid Peroxidation in Biological Systems. *Photochem. Photobiol.* **1990**, *51*, 497–509.

(232) Girotti, A. W.; Kriska, T. Role of Lipid Hydroperoxides in Photo-Oxidative Stress Signaling. *Antioxidants Redox Signal.* **2004**, *6*, 301–310.

(233) Packer, L. *Understanding the Process of Aging: The Roles of Mitochondria: Free Radicals, and Antioxidants*; CRC Press, 1999.

(234) Heuvingh, J.; Bonneau, S. Asymmetric Oxidation of Giant Vesicles Triggers Curvature-Associated Shape Transition and Permeabilization. *Biophys. J.* **2009**, *97*, 2904–2912.

(235) Tirosh, O.; Kohen, R.; Katzhendler, J.; Gorodetsky, R.; Barenholz, Y. Novel Synthetic Phospholipid Protects Lipid Bilayers against Oxidationdamage: Role of Hydration Layer and Bound Water. *J. Chem. Soc., Perkin Trans. 2* **1997**, No. 2, 383–390.

(236) Niki, E. Free Radicals Initiators as Source of Water- or Lipid-Soluble Peroxyl Radicals. *Methods Enzymol.* **1990**, *186*, 100–108.

(237) Reis, A.; Spickett, C. M. Chemistry of Phospholipid Oxidation. *Biochim. Biophys. Acta (BBA)-Biomembranes* **2012**, *1818*, 2374–2387.

(238) Culbertson, S. M.; Porter, N. A. Unsymmetrical Azo Initiators Increase Efficiency of Radical Generation in Aqueous Dispersions, Liposomal Membranes, and Lipoproteins. *J. Am. Chem. Soc.* **2000**, *122*, 4032–4038.

(239) Krasowska, A.; Rosiak, D.; Szkapiak, K.; Oswiecimska, M.; Witek, S.; Lukaszewicz, M. The Antioxidant Activity of BHT and New Phenolic Compounds PYA and PPA Measured by Chemiluminescence. *Cell. Mol. Biol. Lett.* **2001**, *6*,

71–82.

(240) Vitrac, H.; Courrègelongue, M.; Couturier, M.; Collin, F.; Thérond, P.; Rémita, S.; Peretti, P.; Jore, D.; Gardès-Albert, M. Radiation-Induced Peroxidation of Small Unilamellar Vesicles of Phosphatidylcholine Generated by Sonication. *Can. J. Physiol. Pharmacol.* **2004**, *82*, 153–160.

(241) Domingues, M. R. M.; Reis, A.; Domingues, P. Mass Spectrometry Analysis of Oxidized Phospholipids. *Chem. Phys. Lipids* **2008**, *156*, 1–12.

(242) Güven, A.; Ortiz, M.; Constanti, M.; O'Sullivan, C. K. Rapid and Efficient Method for the Size Separation of Homogeneous Fluorescein-Encapsulating Liposomes. *J. Liposome Res.* **2009**, *19*, 148–154.

(243) Dave, P. C.; Tiburu, E. K.; Damodaran, K.; Lorigan, G. A. Investigating Structural Changes in the Lipid Bilayer upon Insertion of the Transmembrane Domain of the Membrane-Bound Protein Phospholamban Utilizing ^{31}P and ^{2}H Solid-State NMR Spectroscopy. *Biophys. J.* **2004**, *86*, 1564–1573.

(244) Huber, T.; Rajamoorthi, K.; Kurze, V. F.; Beyer, K.; Brown, M. F. Structure of Docosahexaenoic Acid-Containing Phospholipid Bilayers as Studied by ^{2}H NMR and Molecular Dynamics Simulations. *J. Am. Chem. Soc.* **2002**, *124*, 298–309.

(245) Kučerka, N.; Tristram-Nagle, S.; Nagle, J. F. Structure of Fully Hydrated Fluid Phase Lipid Bilayers with Monounsaturated Chains. *J. Membr. Biol.* **2006**, *208*, 193–202.

(246) Leson, A.; Hauschild, S.; Rank, A.; Neub, A.; Schubert, R.; Förster, S.; Mayer, C.

Molecular Exchange through Membranes of Poly(2-Vinylpyridine-Block-Ethylene Oxide) Vesicles. *Small* **2007**, *3*, 1074–1083.

(247) Kärger, J. NMR Self-Diffusion Studies in Heterogeneous Systems. *Adv. Colloid Interface Sci.* **1985**, *23*, 129–148.

(248) So, S.; Lodge, T. P. Rate of Molecular Exchange through the Membranes of Ionic Liquid Filled Polymersomes Dispersed in Water. *J. Phys. Chem. C* **2014**, *118*, 21140–21147.

(249) So, S.; Yao, L. J.; Lodge, T. P. Permeability of Rubbery and Glassy Membranes of Ionic Liquid Filled Polymersome Nanoreactors in Water. *J. Phys. Chem. B* **2015**, *119*, 15054–15062.

(250) Zhang, W.; Coughlin, M. L.; Metzger, J. M.; Hackel, B. J.; Bates, F. S.; Lodge, T. P. Influence of Cholesterol and Bilayer Curvature on the Interaction of PPO–PEO Block Copolymers with Liposomes. *Langmuir* **2019**, *35*, 7231–7241.

(251) van Meer, G. Lipid Traffic in Animal Cells. *Annu. Rev. Cell Biol.* **1989**, *5*, 247−275.

(252) Shrestha, R.; Anderson, C. M.; Cardenas, A. E.; Elber, R.; Webb, L. J. Direct Measurement of the Effect of Cholesterol and 6-Ketocholestanol on the Membrane Dipole Electric Field Using Vibrational Stark Effect Spectroscopy Coupled with Molecular Dynamics Simulations. *J. Phys. Chem. B* **2017**, *121*, 3424–3436.

(253) Chiu, S. W.; Jakobsson, E.; Scott, H. L. Combined Monte Carlo and Molecular Dynamics Simulation of Hydrated Lipid-Cholesterol Lipid Bilayers at Low

Cholesterol Concentration. *Biophys. J.* **2001**, *80*, 1104–1114.

(254) Huang, C.-H. Roles of Carbonyl Oxygens at the Bilayer Interface in Phospholipid–Sterol Interaction. *Nature* **1976**, *259*, 242–244.

(255) Yeagle, P. L. Cholesterol and Related Sterols. In *The Membranes of Cells*; Elsevier, 2016; pp 189–218.

(256) Presti, F. T. The Role of Cholesterol in Regulating Membrane Fluidity. In *Membrane Fluidity in Biology*; Aloia, R. C., Boggs, J. M., Eds.; Academic Press: Orlando, 1985; pp 97–146.

(257) *Cholesterol in Membrane Models*; Finegold, L., Ed.; CRC Press: Boca Raton, 1993.

(258) Mouritsen, O. G.; Jørgensen, K. Dynamical Order and Disorder in Lipid Bilayers. *Chem. Phys. Lipids* **1994**, *73*, 3–25.

(259) Khelashvili, G.; Pabst, G.; Harries, D. Cholesterol Orientation and Tilt Modulus in DMPC Bilayers. *J. Phys. Chem. B* **2010**, *114*, 7524–7534.

(260) Kučerka, N.; Nieh, M.-P.; Katsaras, J. Fluid Phase Lipid Areas and Bilayer Thicknesses of Commonly Used Phosphatidylcholines as a Function of Temperature. *Biochim. Biophys. Acta - Biomembr.* **2011**, *1808*, 2761–2771.

(261) Henriksen, J.; Rowat, A. C.; Brief, E.; Hsueh, Y. W.; Thewalt, J. L.; Zuckermann, M. J.; Ipsen, J. H. Universal Behavior of Membranes with Sterols. *Biophys. J.* **2006**, *90*, 1639–1649.

(262) Smaby, J. M.; Momsen, M. M.; Brockman, H. L.; Brown, R. E.

Phosphatidylcholine Acyl Unsaturation Modulates the Decrease in Interfacial Elasticity Induced by Cholesterol. *Biophys. J.* **1997**, *73*, 1492–1505.

(263) Róg, T.; Pasenkiewicz-Gierula, M. Cholesterol Effects on the Phosphatidylcholine Bilayer Nonpolar Region: A Molecular Simulation Study. *Biophys. J.* **2001**, *81*, 2190–2202.

(264) Jedlovszky, P.; Mezei, M. Effect of Cholesterol on the Properties of Phospholipid Membranes. 1. Structural Features. *J. Phys. Chem. B* **2003**, *107*, 5311–5321.

(265) Marsh, D.; Smith, I. C. P. Interacting Spin Labels as Probes of Molecular Separation within Phospholipid Bilayers. *Biochem. Biophys. Res. Commun.* **1972**, *49*, 916–922.

(266) Kusumi, A.; Tsuda, M.; Akino, T.; Ohnishi, S.; Terayama, Y. Protein-Phospholipid-Cholesterol Interaction in the Photolysis of Invertebrate Rhodopsin. *Biochemistry* **1983**, *22*, 1165–1170.

(267) Lingwood, D.; Simons, K. Lipid Rafts As a Membrane-Organizing Principle. *Science.* **2010**, *327*, 46–50.

(268) Simons, K.; Ikonen, E. Functional Rafts in Cell Membranes. *Nature* **1997**, *387*, 569–572.

(269) Holz, M.; Heil, S. R.; Sacco, A. Temperature-Dependent Self-Diffusion Coefficients of Water and Six Selected Molecular Liquids for Calibration in Accurate ^{1}H NMR PFG Measurements. *Phys. Chem. Chem. Phys.* **2000**, *2*, 4740–4742.

(270) Li, Z.; Johnson, L. M.; Ricarte, R. G.; Yao, L. J.; Hillmyer, M. A.; Bates, F. S.; Lodge, T. P. Enhanced Performance of Blended Polymer Excipients in Delivering a Hydrophobic Drug through the Synergistic Action of Micelles and HPMCAS. *Langmuir* **2017**, *33*, 2837–2848.

(271) Li, Z.; Lenk, T. I.; Yao, L. J.; Bates, F. S.; Lodge, T. P. Maintaining Hydrophobic Drug Supersaturation in a Micelle Corona Reservoir. *Macromolecules* **2018**, *51*, 540–551.

(272) Li, Z.; Van Zee, N. J.; Bates, F. S.; Lodge, T. P. Polymer Nanogels as Reservoirs To Inhibit Hydrophobic Drug Crystallization. *ACS Nano* **2019**, *13*, 1232–1243.

(273) Coldren, B.; Van Zanten, R.; Mackel, M. J.; Zasadzinski, J. A.; Jung, H. T. From Vesicle Size Distributions to Bilayer Elasticity via Cryo-Transmission and Freeze-Fracture Electron Microscopy. *Langmuir* **2003**, *19*, 5632–5639.

(274) Pan, J.; Mills, T. T.; Tristram-Nagle, S.; Nagle, J. F. Cholesterol Perturbs Lipid Bilayers Nonuniversally. *Phys. Rev. Lett.* **2008**, *100*, 198103.

(275) Zhang, W.; Haman, K. J.; Metzger, J. M.; Hackel, B. J.; Bates, F. S.; Lodge, T. P. Quantifying Binding of Ethylene Oxide–Propylene Oxide Block Copolymers with Lipid Bilayers. *Langmuir* **2017**, *33*, 12624–12634.

(276) Yeagle, P. L. The Lipids of Biological Membranes. In *The Membranes of Cells*; Elsevier, 2016; pp 27–56.

(277) Starke-Peterkovic, T.; Clarke, R. J. Effect of Headgroup on the Dipole Potential of Phospholipid Vesicles. *Eur. Biophys. J.* **2009**, *39*, 103–110.

(278) Yeagle, P. L.; Hutton, W. C.; Huang, C.-H.; Martin, R. B. Phospholipid Head-Group Conformations; Intermolecular Interactions and Cholesterol Effects. *Biochemistry* **1977**, *16*, 4344–4349.

(279) Garidel, P.; Blume, A. Miscibility of Phospholipids with Identical Headgroups and Acyl Chain Lengths Differing by Two Methylene Units: Effects of Headgroup Structure and Headgroup Charge. *Biochim. Biophys. Acta - Biomembr.* **1998**, *1371*, 83–95.

(280) Cevc, G. Effect of Lipid Headgroups and (Nonelectrolyte) Solution on the Structural and Phase Properties of Bilayer Membranes. *Berichte der Bunsengesellschaft für Phys. Chemie* **1988**, *92*, 953A – 961.

(281) Nagle, J. F. Theory of Lipid Monolayer and Bilayer Phase Transitions: Effect of Headgroup Interactions. *J. Membr. Biol.* **1976**, *27*, 233–250.

(282) Bakht, O.; Pathak, P.; London, E. Effect of the Structure of Lipids Favoring Disordered Domain Formation on the Stability of Cholesterol-Containing Ordered Domains (Lipid Rafts): Identification of Multiple Raft-Stabilization Mechanisms. *Biophys. J.* **2007**, *93*, 4307–4318.

(283) Niu, S.-L.; Litman, B. J. Determination of Membrane Cholesterol Partition Coefficient Using a Lipid Vesicle–Cyclodextrin Binary System: Effect of Phospholipid Acyl Chain Unsaturation and Headgroup Composition. *Biophys. J.* **2002**, *83*, 3408–3415.

(284) Zhao, L.; Feng, S.-S. Effects of Lipid Chain Unsaturation and Headgroup Type on Molecular Interactions between Paclitaxel and Phospholipid within Model

Biomembrane. *J. Colloid Interface Sci.* **2005**, *285*, 326–335.

(285) Ding, L.; Chi, E. Y.; Schanze, K. S.; Lopez, G. P.; Whitten, D. G. Insight into the Mechanism of Antimicrobial Conjugated Polyelectrolytes: Lipid Headgroup Charge and Membrane Fluidity Effects. *Langmuir* **2010**, *26*, 5544–5550.

(286) Hädicke, A.; Blume, A. Binding of the Cationic Peptide (KL) 4 K to Lipid Monolayers at the Air–Water Interface: Effect of Lipid Headgroup Charge, Acyl Chain Length, and Acyl Chain Saturation. *J. Phys. Chem. B* **2016**, *120*, 3880–3887.

(287) Ishitsuka, Y.; Pham, D. S.; Waring, A. J.; Lehrer, R. I.; Lee, K. Y. C. Insertion Selectivity of Antimicrobial Peptide Protegrin-1 into Lipid Monolayers: Effect of Head Group Electrostatics and Tail Group Packing. *Biochim. Biophys. Acta - Biomembr.* **2006**, *1758*, 1450–1460.

(288) Heller, W. T.; He, K.; Ludtke, S. J.; Harroun, T. A.; Huang, H. W. Effect of Changing the Size of Lipid Headgroup on Peptide Insertion into Membranes. *Biophys. J.* **1997**, *73*, 239–244.

(289) Elmore, D. E.; Dougherty, D. A. Investigating Lipid Composition Effects on the Mechanosensitive Channel of Large Conductance (MscL) Using Molecular Dynamics Simulations. *Biophys. J.* **2003**, *85*, 1512–1524.

(290) Yeagle, P. L. Lipid Dynamics in Membranes. In *The Membranes of Cells*; Elsevier, 2016; pp 155–188.

(291) Dowhan, W. Molecular Basis for Mmebrane Phospholipid Diversity: Why Are

There So Many Lipids? *Annu. Rev. Biochem.* **1997**, *66*, 199–232.

(292) Elmore, D. E. Molecular Dynamics Simulation of a Phosphatidylglycerol Membrane. *FEBS Lett.* **2006**, *580*, 144–148.

(293) Dickey, A.; Faller, R. Examining the Contributions of Lipid Shape and Headgroup Charge on Bilayer Behavior. *Biophys. J.* **2008**, *95*, 2636–2646.

(294) Zhao, W.; Róg, T.; Gurtovenko, A. A.; Vattulainen, I.; Karttunen, M. Atomic-Scale Structure and Electrostatics of Anionic Palmitoyloleoylphosphatidylglycerol Lipid Bilayers with Na+ Counterions. *Biophys. J.* **2007**, *92*, 1114–1124.

(295) Kučerka, N.; Holland, B. W.; Gray, C. G.; Tomberli, B.; Katsaras, J. Scattering Density Profile Model of POPG Bilayers As Determined by Molecular Dynamics Simulations and Small-Angle Neutron and X-Ray Scattering Experiments. *J. Phys. Chem. B* **2012**, *116*, 232–239.

(296) Yeagle, P. L. Lipid–Protein Interactions in Membranes. In *The Membranes of Cells*; Elsevier, 2016; pp 291–334.

(297) Mpofu, P.; Addai-Mensah, J.; Ralston, J. Investigation of the Effect of Polymer Structure Type on Flocculation, Rheology and Dewatering Behaviour of Kaolinite Dispersions. *Int. J. Miner. Process.* **2003**, *71*, 247–268.

(298) Spitzer, M.; Sabadini, E.; Loh, W. Entropically Driven Partitioning of Ethylene Oxide Oligomers and Polymers in Aqueous/Organic Biphasic Systems. *J. Phys. Chem. B* **2002**, *106*, 12448–12452.

(299) Blandamer, M. J.; Fox, M. F.; Powell, E.; Stafford, J. W. A Viscometric Study of

Poly(Ethylene Oxide) in t-Butyl Alcohol/Water Mixtures. *Die Makromol. Chemie* **1969**, *124*, 222–231.

(300) Anselmo, A. G.; Sassonia, R. C.; Loh, W. Thermodynamics of the Partitioning of Poly(Propylene Oxide) between Aqueous and Chlorinated Organic Phases Compared to Poly(Ethylene Oxide) and Other Hydrophilic Polymers. *J. Phys. Org. Chem.* **2006**, *19*, 780–785.

(301) Papke, B. L.; Ratner, M. A.; Shriver, D. F. Vibrational Spectroscopy and Structure of Polymer Electrolytes, Poly(Ethylene Oxide) Complexes of Alkali Metal Salts. *J. Phys. Chem. Solids* **1981**, *42*, 493–500.

(302) Chaurasia, S. K.; Singh, R. K.; Chandra, S. Ion–Polymer Complexation and Ion-Pair Formation in a Polymer Electrolyte PEO:LiPF6 Containing an Ionic Liquid Having Same Anion: A Raman Study. *Vib. Spectrosc.* **2013**, *68*, 190–195.

(303) Matsui, Y.; Kubota, T.; Tadokoro, H.; Yoshihara, T. Raman Spectra of Polyethers. *J. Polym. Sci. Part A Gen. Pap.* **1965**, *3*, 2275–2288.

(304) Yoshihara, T.; Tadokoro, H.; Murahashi, S. Normal Vibrations of the Polymer Molecules of Helical Conformation. IV. Polyethylene Oxide and Polyethylene- d_4 Oxide. *J. Chem. Phys.* **1964**, *41*, 2902–2911.

(305) Machida, K.; Miyazawa, T. Infrared and Raman Spectra of Polyethyleneglycol Dimethylethers in the Liquid State. *Spectrochim. Acta* **1964**, *20*, 1865–1873.

(306) Carrier, D.; Pézolet, M. Raman Spectroscopic Study of the Interaction of Poly-L-Lysine with Dipalmitoylphosphatidylglycerol Bilayers. *Biophys. J.* **1984**, *46*, 497–

506.

(307) Spiker, R. C.; Levin, I. W. Raman Spectra and Vibrational Assignments for Dipalmitoyl Phosphatidylcholine and Structurally Related Molecules. *Biochim. Biophys. Acta - Lipids Lipid Metab.* **1975**, *388*, 361–373.

(308) Lis, L. J.; Kauffman, J. W.; Shriver, D. F. Raman Spectroscopic Detection and Examination of the Interaction of Amino Acids, Polypeptides and Proteins with the Phosphatidylcholine Lamellar Structure. *Biochim. Biophys. Acta - Biomembr.* **1976**, *436*, 513–522.

(309) Lippert, J. L.; Peticolas, W. L. Raman Active Vibrations in Long-Chain Fatty Acids and Phospholipid Sonicates. *Biochim. Biophys. Acta - Biomembr.* **1972**, *282*, 8–17.

(310) Claessens, M. M. A. E.; Leermakers, F. A. M.; Hoekstra, F. A.; Cohen Stuart, M. A. Opposing Effects of Cation Binding and Hydration on the Bending Rigidity of Anionic Lipid Bilayers. *J. Phys. Chem. B* **2007**, *111*, 7127–7132.

(311) Yang, H.; Xu, Y.; Gao, Z.; Mao, Y.; Du, Y.; Jiang, H. Effects of Na^+ , K^+, and Ca^{2+} on the Structures of Anionic Lipid Bilayers and Biological Implication. *J. Phys. Chem. B* **2010**, *114*, 16978–16988.

(312) Mao, Y.; Du, Y.; Cang, X.; Wang, J.; Chen, Z.; Yang, H.; Jiang, H. Binding Competition to the POPG Lipid Bilayer of Ca^{2+}, Mg^{2+}, Na^+, and K^+ in Different Ion Mixtures and Biological Implication. *J. Phys. Chem. B* **2013**, *117*, 850–858.

(313) Fenton, D. E.; Parker, J. M.; Wright, P. V. Complexes of Alkali Metal Ions with

Poly(Ethylene Oxide). *Polymer*. **1973**, *14*, 589.

(314) Curatolo, W.; Sears, B.; Neuringer, L. J. A Calorimetry and Deuterium NMR Study of Mixed Model Membranes of 1-Palmitoyl-2-Oleylphosphatidylcholine and Saturated Phosphatidylcholines. *Biochim. Biophys. Acta - Biomembr.* **1985**, *817*, 261–270.

(315) Davis, P. J.; Coolbear, K. P.; Keough, K. M. W. Differential Scanning Calorimetric Studies of the Thermotropic Phase Behaviour of Membranes Composed of Dipalmitoyllecithin and Mixed-Acid Unsaturated Lecithins. *Can. J. Biochem.* **1980**, *58*, 851–858.

(316) Marsh, D. Cholesterol-Induced Fluid Membrane Domains: A Compendium of Lipid-Raft Ternary Phase Diagrams. *Biochim. Biophys. Acta - Biomembr.* **2009**, *1788*, 2114–2123.

(317) Jung, S.; Lodge, T. P.; Reineke, T. M. Structures and Protonation States of Hydrophilic–Cationic Diblock Copolymers and Their Binding with Plasmid DNA. *J. Phys. Chem. B* **2018**, *122*, 2449–2461.

(318) Laaser, J. E.; Lohmann, E.; Jiang, Y.; Reineke, T. M.; Lodge, T. P. Architecture-Dependent Stabilization of Polyelectrolyte Complexes between Polyanions and Cationic Triblock Terpolymer Micelles. *Macromolecules* **2016**, *49*, 6644–6654.

(319) Zhou, C.; Hillmyer, M. A.; Lodge, T. P. Micellization and Micellar Aggregation of Poly(Ethylene- alt -Propylene)- b -Poly(Ethylene Oxide)- b -Poly(N -Isopropylacrylamide) Triblock Terpolymers in Water. *Macromolecules* **2011**, *44*, 1635–1641.

(320) Qiu, X.-P.; Winnik, F. M. Facile and Efficient One-Pot Transformation of RAFT Polymer End Groups via a Mild Aminolysis/Michael Addition Sequence. *Macromol. Rapid Commun.* **2006**, *27*, 1648–1653.

(321) Trzebicka, B.; Szweda, D.; Rangelov, S.; Kowalczuk, A.; Mendrek, B.; Utrata-Wesołek, A.; Dworak, A. (Co)Polymers of Oligo(Ethylene Glycol) Methacrylates-Temperature-Induced Aggregation in Aqueous Solution. *J. Polym. Sci. Part A Polym. Chem.* **2013**, *51*, 614–623.

(322) Jiang, Y.; Lodge, T. P.; Reineke, T. M. Packaging PDNA by Polymeric ABC Micelles Simultaneously Achieves Colloidal Stability and Structural Control. *J. Am. Chem. Soc.* **2018**, *140*, 11101–11111.

(323) Xu, X.; Smith, A. E.; Kirkland, S. E.; McCormick, C. L. Aqueous RAFT Synthesis of PH-Responsive Triblock Copolymer MPEO−PAPMA−PDPAEMA and Formation of Shell Cross-Linked Micelles. *Macromolecules* **2008**, *41*, 8429–8435.

(324) Imae, T.; Kanaya, T.; Furusaka, M.; Torikai, N. *Neutrons in Soft Matter*; John Wiley & Sons, 2011.

(325) Higgins, J. S.; Benoit, H. C. *Polymers and Neutron Scattering*. Clarendon: Oxford 1994.

(326) Sköld, K.; Price, D. L. *Methods of Experimental Physics*; Academic Press, 1987; Vol. 23.

(327) Farago, B.; Monkenbusch, M.; Goecking, K. D.; Richter, D.; Huang, J. S. Dynamics of Microemulsions as Seen by Neutron Spin Echo. *Phys. B Condens.*

Matter **1995**, *213*, 712–717.

(328) Farago, B. Spin Echo Studies of Microemulsions. *Phys. B Condens. Matter* **1996**, *226*, 51–55.

(329) Nagao, M. Observation of Local Thickness Fluctuations in Surfactant Membranes Using Neutron Spin Echo. *Phys. Rev. E* **2009**, *80*, 31606.

(330) Callaway, D. J. E.; Farago, B.; Bu, Z. Nanoscale Protein Dynamics: A New Frontier for Neutron Spin Echo Spectroscopy. *Eur. Phys. J. E* **2013**, *36*, 1–8.

(331) Farago, B. Neutron Spin Echo Study of Well Organized Soft Matter Systems. *Phys. B Condens. Matter* **2006**, *385*, 688–691.

(332) Woodka, A. C.; Butler, P. D.; Porcar, L.; Farago, B.; Nagao, M. Lipid Bilayers and Membrane Dynamics: Insight into Thickness Fluctuations. *Phys. Rev. Lett.* **2012**, *109*, 58102.